Verticillium wilt of olive, caused by the soil-borne fungus *Verticillium dahliae* Kleb., is the most limiting disease of this crop worldwide. Currently, no control measure applied singly is fully effective for the management of Verticillium wilt of olive. However, the detection of Verticillium wilt-affected trees patches within fields at early stages of disease development would be the most effective way to conduct an integrated disease management strategy in order to mitigate the spread of the pathogen through the field. Thus, the main objective of this Doctoral Thesis was to evaluate the use of high-resolution thermal and hyperspectral remote sensing imagery as a tool to early detect Verticillium wilt infection and severity in olive orchards and larger areas, assessing temperature and physiological indices from leaf to canopy scale. In addition, very little is known about the influence of the physical environment on Verticillium wilt development, therefore, the second objective was to assess the effect of soil temperature on Verticillium wilt development taking into account different *V. dahliae* pathotypes and olive cultivars.

Detection of Verticillium wilt in olive using high-resolution hyperspectral and thermal remote sensing imagery

Rocío Calderón Madrid

2015

Doctoral Thesis

Detection of Verticillium wilt in olive using high-resolution hyperspectral and thermal remote sensing imagery

Detección de Verticilosis en olivar mediante teledetección hiperespectral y térmica de alta resolución

PhD Candidate
Rocío Calderón Madrid

Supervisors
Pablo J. Zarco Tejada
Juan A. Navas Cortés

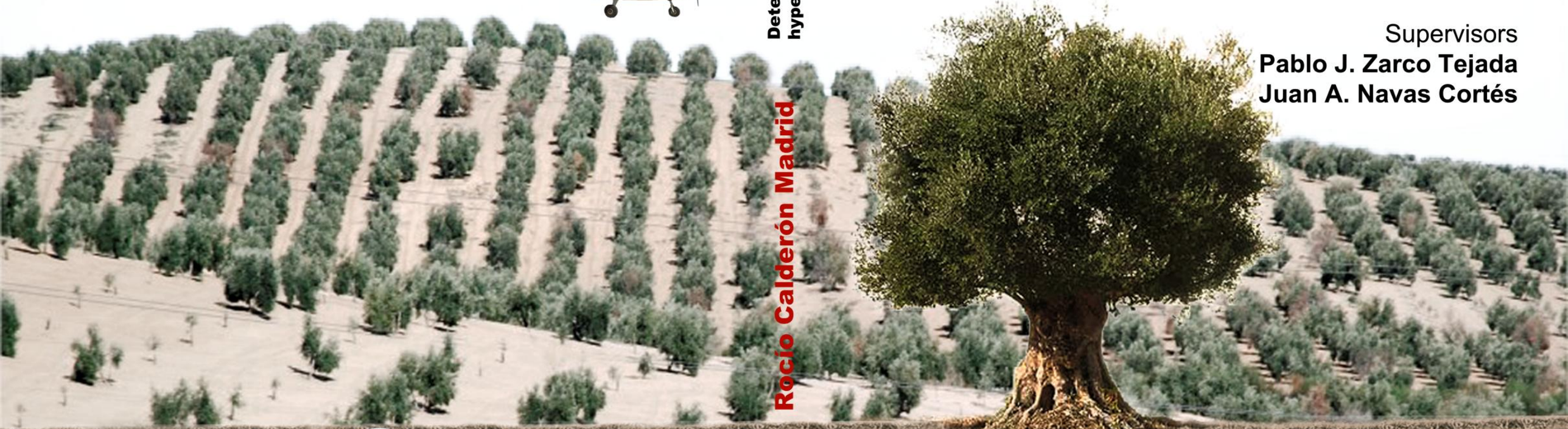

CSIC
Consejo Superior de Investigaciones Científicas

Instituto de Agricultura Sostenible IAS

UNIVERSIDAD DE CÓRDOBA

DEPARTAMENTO DE AGRONOMÍA

Programa de Doctorado

Biociencias y ciencias agroalimentarias

TESIS DOCTORAL

POR COMPENDIO DE PUBLICACIONES

Detección de Verticilosis en olivar mediante teledetección hiperespectral y térmica de alta resolución

Detection of Verticillium wilt in olive using high-resolution hyperspectral and thermal remote sensing imagery

Autora
Rocío Calderón Madrid

Dirigida por
Dr. Pablo J. Zarco Tejada
Dr. Juan A. Navas Cortés

Instituto de Agricultura Sostenible

CONSEJO SUPERIOR DE INVESTIGACIONES CIENTÍFICAS

Córdoba, Mayo 2015

UNIVERSIDAD D CÓRDOBA

DEPARTAMENTO DE AGRONOMÍA

TESIS DOCTORAL

Detección de Verticilosis en olivar mediante teledetección hiperespectral y térmica de alta resolución

presentada por ROCÍO CALDERÓN MADRID en satisfacción de los requisitos necesarios para la obtención del grado de DOCTOR INGENIERO AGRÓNOMO

Los Directores,

Dr. Pablo J. Zarco Tejada

Investigador Científico
Dpto. Agronomía
Instituto de Agricultura Sostenible (CSIC)

Dr. Juan A. Navas Cortés

Investigador Científico
Dpto. Protección de cultivos
Instituto de Agricultura Sostenible (CSIC)

CSIC
CONSEJO SUPERIOR DE INVESTIGACIONES CIENTÍFICAS

INSTITUTO DE AGRICULTURA SOSTENIBLE IAS

Córdoba, Mayo 2015

TÍTULO DE LA TESIS: DETECCIÓN DE VERTICILOSIS EN OLIVAR MEDIANTE TELEDETECCIÓN HIPERESPECTRAL Y TÉRMICA DE ALTA RESOLUCIÓN

DOCTORANDO/A: ROCÍO CALDERÓN MADRID

INFORME RAZONADO DEL DIRECTOR DE LA TESIS

(se hará mención a la evolución y desarrollo de la tesis, así como a trabajos y publicaciones derivados de la misma)

D. PABLO J. ZARCO TEJADA, Investigador Científico del Departamento de Agronomía, Instituto de Agricultura Sostenible, CSIC, y **D. JUAN A. NAVAS CORTÉS**, Investigador Científico del Departamento de Protección de Cultivos, Instituto de Agricultura Sostenible, CSIC, directores de la presente Tesis Doctoral

INFORMAN:

Que en la Tesis Doctoral titulada **"Detección de Verticilosis en olivar mediante teledetección hiperespectral y térmica de alta resolución"** que ha llevado a cabo la Ingeniera Agrónoma por la Escuela Técnica Superior de Ingenieros Agrónomos y de Montes de la Universidad de Córdoba **Dª. Rocío Calderón Madrid** bajo nuestra dirección, ha completado con éxito todos los objetivos planteados en dicho trabajo de investigación.

Que dicha Tesis Doctoral se va a presentar como compendio de publicaciones donde se recogen los objetivos perseguidos y cumple con todos los requisitos y obligaciones dispuestos en el **Real Decreto 1393/2007, de 29 de octubre**, y la **Normativa Reguladora de los Estudios de Doctorado adaptada al EEES de la Universidad de Córdoba propuesta por la Comisión de Másteres y Doctorado de 14.12.2011 y aprobada por Consejo de Gobierno de 21.12.11 y modificada por el mismo órgano el 29.05.13 y 23.07.13.** En cumplimiento del Art. 24 de dicha Normativa, se presentan tres artículos científicos correspondientes a los Capítulos tercero, cuarto y quinto de la presente Tesis Doctoral:

Calderón, R., Lucena, C., Trapero-Casas, J.L., Zarco-Tejada, P.J., and Navas-Cortés, J.A. (2014). **Soil Temperature Determines the Reaction of Olive Cultivars to**

Verticillium dahliae Pathotypes. *PLoS ONE* 9(10):e110664. DOI: 10.1371/journal.pone.0110664.

Calderón, R., Navas-Cortés, J.A., Lucena, C., and Zarco-Tejada, P.J. (2013). **High-resolution airborne hyperspectral and thermal imagery for early detection of Verticillium wilt of olive using fluorescence, temperature and narrow-band spectral indices**. *Remote Sensing of Environment* 139:231-245.

Calderón, R., Navas-Cortés, J.A., & Zarco-Tejada, P.J. (2015). **Early detection and quantification of Verticillium wilt in olive using hyperspectral and thermal imagery over large areas**. *Remote Sensing* 7(5):5584-5610. DOI: 10.3390/rs70505584.

Estas revistas presentan un reconocido prestigio internacional en su ámbito. **PLoS ONE** es una revista internacional de temática Multidisciplinar editada por la Public Library of Science con un índice de impacto de 3,534 ocupando la posición 8/55 (Primer Cuartil) en el descriptor "Multidisciplinary Sciences" del ISI-JCR. **Remote Sensing of Environment** es una revista internacional de Teledetección editada por Elsevier con un índice de impacto de 4,769 ocupando la posición 1/27 (Primer Cuartil) en el descriptor "Remote Sensing" del ISI-JCR. Por último, **Remote Sensing** es una revista internacional de Teledetección editada por Molecular Diversity Preservation International (MDPI) con un índice de impacto de 2,623 ocupando la posición 6/27 (Primer Cuartil) en el descriptor "Remote Sensing" del ISI-JCR.

Otras aportaciones destacables que han surgido de la presente Tesis Doctoral son cinco contribuciones a congresos tanto de ámbito internacional como nacional:

<u>Contribuciones a Congresos Internacionales</u>

Calderón, R., Navas-Cortés, J.A., Lucena, C. and Zarco-Tejada, P.J. (2013). High-resolution hyperspectral and thermal imagery acquired from UAV platforms for early detection of Verticillium wilt using fluorescence, temperature and narrow-band indices. Tipo de participación: Panel. Congreso: **Workshop on UAV-based Remote Sensing Methods for Monitoring Vegetation.** Colonia, Alemania, Septiembre 9-10, 2013. Publicación: Proceedings pp. 7-14.

Calderón, R., Navas-Cortés, J.A., Montes-Borrego, M., Landa, B.B., Lucena, C., and Zarco-Tejada, P.J. (2014). Detection of Verticillium wilt of olive trees and downy mildew of opium poppy using hyperspectral and thermal UAV imagery. Tipo de participación: Comunicación oral. Congreso: **European Geosciences Union General Assembly 2014.** Viena, Austria, Abril 27 - Mayo 4, 2014.

Calderón, R., Navas-Cortés, J.A., and Zarco-Tejada, P.J. (2014). Early detection and quantification of Verticillium wilt in olive using UAV and manned platforms to acquire hyperspectral and thermal imagery at local and regional scale. Tipo de participación: Comunicación oral. Congreso: **2nd International Conference on Robotics, Associated**

High-Technologies and Equipment for Agriculture and Forestry. Madrid, España, Mayo 21-23, 2014. Publicación: Proceedings pp. 309-318.

Calderón, R., Navas-Cortés, J.A., and Zarco-Tejada, P.J. (2014). Early detection and quantification of Verticillium wilt in olive using hyperspectral and thermal imagery acquired by manned platforms at regional scale. Tipo de participación: Comunicación oral. Congreso: **4th International Symposium: Recent Advances in Quantitative Remote Sensing.** Torrent (Valencia), España, Septiembre 22-26, 2014. Publicación: Abstract Book pp. 70-71.

Contribuciones a Congresos Nacionales

Calderón, R., Navas-Cortés, J.A., Lucena, C. and Zarco-Tejada, P.J. (2013). Teledetección aerotransportada hiperespectral y térmica de alta resolución para la detección temprana de Verticilosis en olivar usando fluorescencia, temperatura e índices espectrales. Tipo de participación: Comunicación Oral. Congreso: **XV Congreso de la Asociación Española de Teledetección.** INTA, Torrejón de Ardoz (Madrid), España, Octubre 22-23, 2013. Publicación: Libro de Actas pp. 414-417.

Por todo ello, consideramos finalizada dicha Tesis Doctoral, y creemos que puede ser presentada y tramitada para su exposición y defensa en la Comisión de Doctorado de la Universidad de Córdoba, autorizando la presentación de la misma.

Córdoba, 15 de Mayo de 2015

Firma de los directores

Fdo.: Pablo J. Zarco Tejada

Fdo.: Juan A. Navas Cortés

TÍTULO DE LA TESIS: DETECCIÓN DE VERTICILOSIS EN OLIVAR MEDIANTE TELEDETECCIÓN HIPERESPECTRAL Y TÉRMICA DE ALTA RESOLUCIÓN

DOCTORANDO/A: ROCÍO CALDERÓN MADRID

ESCRITO RAZONADO DEL TUTOR Y RESPONSABLE DE LA LÍNEA DE INVESTIGACIÓN

(Ratificando el informe favorable del director. Sólo cuando el director no pertenezca a la Universidad de Córdoba).

D. RAFAEL M. JIMÉNEZ DÍAZ, Catedrático de Patología Vegetal del Departamento de Agronomía de la Universidad de Córdoba

INFORMA:

Que la investigación sobre **"Detección de Verticilosis en olivar mediante teledetección hiperespectral y térmica de alta resolución"** que ha llevado a cabo la Ingeniero Agrónomo **Dña. Rocío Calderón Madrid,** bajo la dirección de los Drs. Pablo J. Zarco Tejada y Juan A. Navas Cortés, Investigadores Científicos, respectivamente, de los Departamentos de Agronomía y Protección de Cultivos del Instituto de Agricultura Sostenible, CSIC, y la tutoría del que subscribe, ha sido desarrollada con éxito y alcanzado los objetivos inicialmente propuestos. Los resultados de la investigación realizada constituyen una aportación científica innovadora y relevante para el manejo integrado de la Verticilosis del olivo, lo cual queda adecuadamente reflejado en los artículos publicados en revistas del JCR que satisfacen los requisitos de indicios de calidad. En consecuencia, como tutor de la Tesis Doctoral que comprende dicha investigación, considero que puede ser presentada para su exposición y defensa públicas en la Universidad de Córdoba y ratifico la consideración favorable emitida por los Directores de la Tesis Doctoral a tal efecto.

Por todo ello, se autoriza la presentación de la presente Tesis Doctoral.

Córdoba, 16 de Mayo de 2015

Firma del tutor y responsable de la línea de investigación

Fdo.: Rafael M. Jiménez Díaz

Financiación

Esta Tesis se trata de un trabajo de carácter interdepartamental entre el Grupo PAIDI AGR-136 'Sanidad Vegetal' del Departamento de Protección de Cultivos del Instituto de Agricultura Sostenible, CSIC, y el Grupo PAIDI AGR-119 'Relaciones Suelo – Agua – Planta' del Departamento de Agronomía del Instituto de Agricultura Sostenible, CSIC, gracias a la concesión de la beca predoctoral **BES-2010-035511** en el marco del programa de "Formación de Personal Investigador" (FPI) del Ministerio de Ciencia e Innovación adscrita al Proyecto de Investigación AGL2009-13105-C03-01 **"Teledetección hiperespectral y térmica para detección de estrés y monitorización de parámetros fisiológicos en vid y olivar"** financiado por el Ministerio de Ciencia e Innovación y fondos FEDER de la UE.

Además, los trabajos incluidos en esta Tesis Doctoral han sido parcialmente subvencionados por los proyectos AGL2012-37521 **"Desarrollo de un sistema de apoyo a la toma de decisiones para mitigar el impacto de patógenos de suelo en olivar y promover la microbiota beneficiosa en condiciones de clima actual y de cambio climático"** y AGL2012-40053-C03-01 **"Métodos de estimación de fluorescencia clorofílica en olivar, naranjo y vid a partir de microsensores hiperespectrales a bordo de UAVs"** del Ministerio de Economía y Competitividad (cofinanciado con fondos FEDER de la UE), y el proyecto P08-AGR-03528 **"Impacto del cambio climático en las enfermedades de cultivos. La Verticilosis del olivo y sus interacciones con la microbiota del suelo y nematodos fitoparásitos, e identificación temprana por teledetección"** de la Consejería de Economía, Innovación y Ciencia, Junta de Andalucía (cofinanciado con fondos FEDER de la UE).

Tesis por compendio de artículos

Esta tesis cumple el requisito establecido por la Universidad de Córdoba para su presentación como compendio de artículos, consistente en un mínimo de 3 artículos publicados o aceptados en revistas incluidas en los tres primeros cuartiles de la relación de revistas del ámbito de la especialidad y referenciadas en la última relación publicada por el Journal Citations Report (SCI):

1. **Calderón, R.**, Lucena, C., Trapero-Casas, J.L., Zarco-Tejada, P.J., & Navas-Cortés, J.A. (2014). Soil Temperature Determines the Reaction of Olive Cultivars to *Verticillium dahliae* Pathotypes. *PLoS ONE* 9(10):e110664, DOI: 10.1371/journal.pone.0110664

   Datos de 2013 (JCR): índice de impacto 3.534, índice de impacto de los últimos 5 años 4.015, posición 8/55 y 1º cuartil en el área temática de *Multidisciplinary Sciences*.

2. **Calderón, R.**, Navas-Cortés, J.A., Lucena, C., & Zarco-Tejada, P.J. (2013). High-resolution airborne hyperspectral and thermal imagery for early detection of Verticillium wilt of olive using fluorescence, temperature and narrow-band spectral indices. *Remote Sensing of Environment* 139:231-245.

   Datos de 2013 (JCR): índice de impacto 4.769, índice de impacto de los últimos 5 años 6.065, posición 1/27 y 1º cuartil en el área temática de *Remote Sensing*.

3. **Calderón, R.**, Navas-Cortés, J.A., & Zarco-Tejada, P.J. (2015). Early detection and quantification of Verticillium wilt in olive using hyperspectral and thermal imagery over large areas. *Remote Sensing* 7(5):5584-5610, DOI: 10.3390/rs70505584

   Datos de 2013 (JCR): índice de impacto 2.623, índice de impacto de los últimos 5 años 2.729, posición 6/27 y 1º cuartil en el área temática de *Remote Sensing*.

La Doctoranda

Fdo.: Rocío Calderón Madrid

Agradecimientos

Una vez acabada esta travesía de esfuerzo y dedicación de algo más de cuatros años, quisiera agradecer la ayuda de un gran número de personas, sin los cuales hubiera sido imposible llevar a cabo la realización de esta Tesis Doctoral.

En primer lugar me gustaría agradecer de forma especial a Pablo J. Zarco Tejada, mi maestro y ejemplo a seguir dentro del mundo de la investigación. Gracias por darme la oportunidad de realizar esta Tesis en tu grupo de trabajo y de establecer los cimientos para cumplir uno de mis sueños: *dedicarme a la Ciencia*. Agradecerte también tus ánimos en todo momento que me han hecho tener claras mis limitaciones y potenciar mis talentos, claves para rentabilizar al máximo el tiempo y el esfuerzo invertidos en realizar esta Tesis.

Quiero continuar agradeciendo a Juan A. Navas Cortés, quien ha sido un apoyo fundamental en esta aventura. Gracias por inocularme el virus de la fitopatología y la estadística, y enseñarme en poco tiempo lo que en otras circunstancias me hubiera llevado años de dedicación. Resaltar mi admiración por tu forma de aplicar la perfección a la Ciencia, sin que nunca se te escape detalle.

Gracias a ambos por haber hecho que dos disciplinas como la Teledetección y la Fitopatología sean a día de hoy dos de mis grandes pasiones. Estoy muy orgullosa de haberos tenido como directores de esta Tesis Doctoral.

Tampoco habría sido posible esta Tesis sin la ayuda del resto de miembros de Quantalab: Alberto Hornero, Alberto Vera, Alfredo, David y Rafa. Gracias por las horas dedicadas, la eficiencia y rapidez en el procesamiento de imágenes, por arrimar el hombro en las campañas de campo en verano y las risas en nuestro tiempo libre. Hacéis un trabajo brillante.

También quiero agradecer al equipo de Juan A.: José Luis, Carlos, Blanca, Miguel, Guille y Efrén por su apoyo y tiempo invertido en mi aprendizaje sobre la Verticilosis a nivel de campo y laboratorio. No tengo palabras para agradeceros la cantidad de conocimientos que he adquirido de cada uno de vosotros.

Agradecer también a Elías Fereres por sus consejos de ámbito multidisciplinar y su gran apoyo durante mi estancia en el IAS, y a Hava por ayudarme a mejorar el inglés y por sus conversaciones durante el desayuno.

A los chic@s de Agronomía: a Manuela por estar siempre a mi lado, a Mari Luz por hacerme sentir como en casa cuando todo era extraño para mí, a Kiki por su valentía, a Carmen por su sonrisa, a Marga por su nobleza, a Vicky por sus sabios consejos, a

Mónica por su fuerza, a Manuel *"niño Lama"* por enseñarme a vivir la vida, a McMolder por su juventud y ganas de comerse el mundo, a Manolo por su inteligencia y seguir siempre las bromas, a Álvaro por su bondad y alegría, a Omar por amenizar los peroles y sus *"potensiales"*, a Rafa por ser el guía del departamento en los eventos lúdicos y a Marcos por su generosidad.

A los chicos de estancia, que en algún periodo de este camino han compartido imborrables momentos conmigo: a Pablo Elorza por saber lo que pienso y siento sin necesidad de mediar palabra, a Luis por su bondad, nobleza y alegría, a Facundo por su paciencia en el último tramo de esta Tesis y a Inian por ayudarme a salir del cascarón.

A Cristinita, por estar siempre ahí y demostrarme que la amistad está por encima de todo.

A los IAS buddies, en especial a Carlos, Liz, Carmen, Mercedes, Héctor, Thais e Inma, por los momentos vividos.

A mis *"Agromonas"*: Esther, Elena, Maribel, Marisa, Tere y Vero, porque a pesar de que cada una siga su camino siempre nos tendremos las unas a las otras.

A mis norieg@s: Mari Ángeles, Trini, Sonia, Lorena, Marisa, Noelia, Fátima, Rosa, Ricardo, Paco, Edu, Polas, Samu, por ayudarme a desconectar los fines de semana.

A Rafa por tus años de apoyo desinteresado y paciencia. Gracias por creer en mí cuando más lo necesitaba.

A María, mi compañera de viaje, mi *Rigodón*, nada hubiera sido igual sin ti, sin nuestras risas, nuestras riñas, nuestras aventuras,… Porque juntas hemos aprendido que por muchas piedras que encontremos por el camino, hay que levantarse y seguir caminando.

A mi hermana Elena por complementarme y ponerme los pies en la tierra cuando mi mente divaga sin rumbo.

A mi familia, en especial a mi abuela Maravilla, por estar unidos cuando la vida nos sacude y celebrarlo cuando la tormenta queda atrás.

Finalmente, quiero dedicar este trabajo a mis padres, Augusto y Toñi, por la educación que me han brindado y creer siempre en mí. Gracias por apoyarme y acompañarme en el punto de inflexión de mi vida, a partir del cual me hice más fuerte y aprendí a disfrutar del más mínimo detalle. Sólo vosotros sabéis que tras la tempestad, por muy larga que sea, siempre llega la calma. Gracias por vuestra confianza y por dejarme volar.

Table of Contents

List of Figures i
List of Tables v
List of Symbols vii
List of Abbreviations ix
Resumen xiii
Abstract xvii

Chapter 1: Introduction 1

1.1 Olive crop 4
1.2. Verticillium wilt of olive 4
1.3. Remote sensing for the detection of soil-borne plant pathogens 7
1.4. Early detection of wilting stress using remote sensing 13
Literature cited 16

Chapter 2: Objectives 27

2.1. Outline of the thesis 29

Chapter 3: Soil temperature determines the reaction of olive cultivars to *Verticillium dahliae* pathotypes 33

Resumen 35
Abstract 36
3.1. Introduction 36
3.2. Materials and Methods 40
3.2.1. Verticillium dahliae isolates, olive plants, inoculation, and growth conditions 40
3.2.2. Disease assessment 41
3.2.3. Disease, stress, plant growth-related parameters, and data analyses 41
3.3. Results 45
3.3.1. Verticillium wilt development 45
3.3.2. Relationship between leaf-level measurements of stress-related parameters and soil temperature 47
3.3.3. Relationships between experimental treatments and parameters related to disease, stress, and plant growth 52
3.3.4. Relationship between stress-related parameters and Verticillium wilt severity classes 53
3.3.5. Identification of stress-related parameter thresholds 57
3.4. Discussion 58
Acknowledgments 63
References 64

Chapter 4: High-resolution airborne hyperspectral and thermal imagery for early detection of Verticillium wilt of olive using fluorescence, temperature andices 71

Resumen 73
Abstract 74
4.1. Introduction 75
4.2. Materials and Methods 78
4.2.1. Study site description 78
4.2.2. Verticillium wilt assessment 79
4.2.3. Field measurements 79
4.2.4. Airborne campaigns and remote sensing indices 80
4.3. Results and Discussion 87
4.3.1. Verticillium wilt symptom development 87
4.3.2. Field measurement results 88
4.3.3. Airborne hyperspectral, multispectral and thermal imagery results 91
4.4. Conclusions 97
Acknowledgments 99
References 100

Chapter 5: Early detection and quantification of Verticillium wilt using hyperspectral and thermal imagery over large areas 111

Resumen 113
Abstract 113
5.1. Introduction 114
5.2. Material and Methods 117
5.2.1. Study site description 117
5.2.2. Verticillium wilt assessment 119
5.2.3. Airborne hyperspectral and thermal imagery acquisition 119
5.2.4. Data analyses 124
5.3. Results 127
5.4. Discussion 135
5.5. Conclusions 138
Acknowledgments 139
References 140

Chapter 6: Conclusions 147

6.1. Conclusions of the Research Published Papers 149
6.2. General Conclusions 151

Appendix: Scientific production 153

List of Figures

Chapter 1: Introduction 1

Figure 1.1. (a) Olive-producing countries in the world. (b) Olive area in Spain by provinces. (c) Olive distribution in Andalucía 5
Figure 1.2. Biological cycle of the soil-borne fungus *Verticillium dahliae* in olive trees 6
Figure 1.3. (a) Intense defoliation and large amount of fallen green leaves associated with infection by D *V. dahliae*. (b) Symptoms associated with infection by ND *V. dahliae*. Note olive branches with dried, necrotic leaves that remain attached to the symptomatic branch. (c) Death of a 3-years-old irrigated olive cv. Arbequina infected by *V. dahliae*. (d) Sectorial necrosis of branches and shoots in a 15-years-old rainfed olive cv. Picual infected by *V. dahliae*. (e) Verticillium wilt affected olive orchard located next to a cotton field. Note the patchy occurrence of symptoms due to the low mobility in the field of *V. dahliae*. (f) Olive orchard with Verticillium wilt infected trees showing nonrandom distribution 8
Figure 1.4. Leaf reflectance of olive trees infected by *Verticillium dahliae* 9

Chapter 2: Objectives 27

Chapter 3: Soil temperature determines the reaction of olive cultivars to *Verticillium dahliae* pathotypes 33

Figure 3.1. Relationship between Verticillium wilt-related parameters and soil temperature 46
Figure 3.2. Verticillium wilt disease progress at different soil temperatures 48
Figure 3.3. Relationship between stress-related parameters and soil temperature 50
Figure 3.4. Relationship between stress-related parameters and soil temperature 51
Figure 3.5. Relationship between plant growth-related parameters and soil temperature 52
Figure 3.6. Dendrogram showing results of cluster analyses and heat map representation of disease, stress, and plant growth parameters 54
Figure 3.7. Predicted probabilities according to the multinomial logistic regression model with Verticillium wilt severity as the response variable and stress-related parameters as explanatory variables using healthy plants as the reference category 57
Figure 3.8. Classification tree to discriminate among Verticillium wilt severity classes based on stress-related parameters 58

Chapter 4: High-resolution airborne hyperspectral and thermal imagery for early detection of Verticillium wilt of olive using fluorescence, temperature andices 71

Figure 4.1. Overview of the two study sites in southern Spain used in this study: (a) 7 ha commercial olive orchard in Castro del Rio (Cordoba province); (b) 10-ha commercial olive orchard in Utrera (Seville province). 78
Figure 4.2. Multispectral scene (a) obtained with the multispectral camera on board the UAV platform at 20-cm resolution, showing the Castro del Rio orchard study site (Córdoba province). (b) Automatic object-based crown detection applied to the multispectral imagery to identify pure olive crowns. Yellow square (a) shown in detail in (b). 81
Figure 4.3. Hyperspectral scene (a) obtained with the hyperspectral imager on board the UAV platform at 40-cm resolution. Automatic object-based crown detection applied to the hyperspectral imagery to identify pure olive crowns (b). The methodology enabled the separation of pure olive crowns from shaded and sunlit soil reflectance, observing the effects of pixel aggregation (c). Yellow square (a) shown in detail in (b). 83
Figure 4.4. Thermal scene (a) of the Castro del Rio site (Córdoba province) obtained with the thermal camera on board the UAV platform at 20-cm resolution, enabling pure olive crown identification (b). Automatic object-based crown detection applied to the thermal imagery to identify pure olive crowns (c). Yellow square (a) shown in detail in (b; c). 85
Figure 4.5. Frequency (%) of olive trees showing Verticillium wilt (VW) symptoms at the different severity values in Castro del Rio (Córdoba province) (a,b) and Utrera (Seville province) (c,d) study sites assessed in May and July of 2009 (a,c) and 2010 (b,d). VW severity was assessed by visual inspection of each individual tree using a 0-4 rating scale according to percentage of foliage with disease symptoms, where: 0 = 0%, IS=initial symptoms, 1 = 1 to 33%, 2 = 34 to 66%, 3 = 67 to 100% and 4 = dead plant. Severity of disease symptoms were grouped in asymptomatic (DS=0), initial ($0.2 \leq DS \leq 0.5$), low ($1 \leq DS \leq 1.5$), moderate ($2 \leq DS \leq 2.5$) and severe ($3 \leq DS \leq 4$) disease symptoms. 88
Figure 4.6. Diurnal mean crown temperature (Tc-Ta) measured from 7:00 to 17:00 GMT at 5-minute intervals and obtained with the IRT sensors from trees showing different Verticillium wilt severity levels in the Castro del Rio site (Córdoba province) in the summer of 2011..... 89
Figure 4.7. Diurnal mean leaf stomatal conductance G measured from 7:00 to 17:00 GMT at 2-hour intervals and obtained with the leaf porometer from trees showing different Verticillium wilt severity levels (n=5 per tree at each measuring time) in the Castro del Rio site (Córdoba province) in the summer of 2011. 89
Figure 4.8. Mean measurements of crown temperature (Tc-Ta) (a), leaf stomatal conductance (G) (b), leaf PRI_{570} (c) and leaf Fs (d) for every Verticillium wilt severity level. Analysis of variance of each index was conducted and asterisks

indicate significant differences from the asymptomatic plants according to Dunnett's two-tailed test at $P < 0.05$. Error bars indicate standard errors. 90

Figure 4.9. Relationship between crown temperature extracted from the thermal imagery and leaf stomatal conductance (G) (a) and leaf PRI_{570} measurements (b) taken on olive trees showing different Verticillium wilt severity levels, and relationship between leaf G and leaf PRI_{570} (c). Thermal imagery was obtained at 11:00 GMT on 15 June 2011 and leaf measurements were obtained between 10:00 and 13:00 GMT on 27 and 28 July 2011 from crowns with different VW severity levels in the Castro del Rio study site (Córdoba province). Error bars indicate standard errors. 92

Figure 4.10. Mean measurements of crown temperature (Tc-Ta) for every Verticillium wilt severity level. Tc-Ta was calculated from thermal imagery obtained in summer of two consecutive years (2009 and 2010) for the two study sites, Castro del Rio (Córdoba province) (a, c) and Utrera (Seville province) (b, d). Analysis of variance was conducted and asterisks indicate significant differences from the asymptomatic plants according to Dunnett's two-tailed test at $P < 0.05$. Error bars indicate standard errors. 93

Figure 4.11. (a) Mean values of Crop Water Stress Index (CWSI) for every Verticillium wilt severity level on 2 June 2011 in the Castro del Rio study site (Córdoba province). Analysis of variance was conducted and asterisks indicate significant differences from the asymptomatic plants according to Dunnett's two-tailed test at $P < 0.05$. Error bars indicate standard errors. (b) Relationship between leaf stomatal conductance (G) and the CWSI in trees with different VW severity levels. Leaf stomatal conductance measurements were obtained between 10:00 and 13:00 GMT on 27 and 28 July 2011 and the CWSI was calculated from the thermal imagery obtained at 11:00 GMT on 15 June 2011 in the Castro del Rio study site. Error bars indicate standard errors. 94

Figure 4.12. Mean measurements of NDVI (a), PRI_{570} (b), PRI_{515} (c), TCARI (d), Blue index (B) (e), B/R index (BR1) (f), chlorophyll fluorescence FLD3 (g) and healthy-index (HI) (h) for every Verticillium wilt severity level. Analysis of variance of each index was conducted and asterisks indicate significant differences from the asymptomatic plants according to Dunnett's two-tailed test at $P < 0.05$. Error bars indicate standard errors. 98

Chapter 5: Early detection and quantification of Verticillium wilt using hyperspectral and thermal imagery over large areas 111

Figure 5.1. Overview of the olive area flown with the manned platform located in Écija (Seville province). Verticillium wilt severity was assessed in the plots which are shown in yellow. High-resolution detail of each individual olive plot assessed in

this study was shown with lettering (a-i) in agreement with the plot lettering (a-i) in central image. Note differences in soil and crop management among plots. 118
Figure 5.2. RGB images showing olive trees with the five different Verticillium wilt severity classes: (a) asymptomatic, (b) initial, (c) low, (d) moderate and (e) severe disease symptoms 120
Figure 5.3. Thermal mosaic (a) obtained with the thermal camera on board the manned platform at 63-cm resolution, enabling pure olive crown identification (b). Pure olive crowns were identified using automatic object-based crown detection. Mean crown normalized temperature (Tc-Ta) calculated from thermal imagery is shown for every Verticillium wilt severity class in (c). Mean values of Tc-Ta were supported by the data of the 9 plots, consisting of 510, 98, 64, 46 and 38 olive trees which correspond to asymptomatic, initial, low, moderate and severe severity classes, respectively. Error bars indicate standard errors. Red square (a) is shown in detail in (b). 124
Figure 5.4. Hyperspectral mosaic (a) obtained with the hyperspectral sensor on board the manned platform at 50-cm resolution. Pure olive crowns were identified using automatic object-based crown detection (b). Sample crown reflectance obtained by the hyperspectral imagery from Verticillium wilt asymptomatic, initially symptomatic and severely symptomatic olive trees is shown in (c). Red square (a) is shown in detail in (b). 125
Figure 5.5. Classification of 756 olive trees assessed in Ecija into five Verticillium wilt severity classes based on (a) the first and second canonical variates and (b) the first and third canonical variates, from the canonical discriminant analysis. 131
Figure 5.6. Spatial distribution of Verticillium wilt severity classes assessed at field level (a, d, g) and the severity classes predicted by the linear discriminant analysis (LDA) (b, e, h) and support vector machine (SVM) methods (c, f, i) in three different plots 133

Chapter 6: Conclusions 147

Appendix: Scientific production 153

List of Tables

Chapter 1: Introduction **1**

Chapter 2: Objectives **27**

Chapter 3: Soil temperature determines the reaction of olive cultivars to *Verticillium dahliae* pathotypes **33**

Table 3.1. Results of the multinomial logistic regression models fitted for each variable separately and the multivariate multinomial logistic regression model fitted with a stepwise method. 55

Chapter 4: High-resolution airborne hyperspectral and thermal imagery for early detection of Verticillium wilt of olive using fluorescence, temperature and narrow-band indices **71**

Table 4.1. Overview of the vegetation indices used in this study and their formulations. 84

Table 4.2. Inputs used to calculate the Crop Water Stress Index (CWSI) from high resolution airborne thermal imagery acquired in June 2011 in the Castro del Rio site. The CWSI was calculated as described in Berni *et al.* (2009a). 86

Chapter 5: Early detection and quantification of Verticillium wilt using hyperspectral and thermal imagery over large areas **111**

Table 5.1. Agronomic characteristics of olive plots assessed in this study. 118

Table 5.2. Overview of the vegetation indices that contribute most to the model conducted in this study and their formulations. 122

Table 5.3. Local atmospheric conditions measured by a portable weather station during the flight at 30-min interval. 123

Table 5.4. Variables selected from normalized canopy temperature (Tc-Ta) and vegetation indices in the forward stepwise discriminant analysis to determine the severity of *Verticillium dahliae* infection in olive trees. 128

Table 5.5. Confusion matrix for Verticillium wilt severity classes using the linear discriminant classification based on the indices selected by the forward stepwise discriminant analysis. 128

Table 5.6. Squared Mahalanobis distances for Verticillium wilt severity classes obtained in a forward stepwise discriminant analysis. 129

Table 5.7. Standardized canonical coefficients (SCCs) and correlation coefficients (CCCs) of discriminant canonical functions of canopy normalized canopy temperature (Tc-Ta) and vegetation indices selected by the forward stepwise discriminant analysis that determine Verticillium wilt severity levels. 129

Table 5.8. Confusion matrix for Verticillium wilt severity classes using the support vector machine classification based on the indices selected by the forward stepwise discriminant analysis. 132
Table 5.9. Overall accuracy and kappa obtained from the linear discriminant analysis (LDA) and the support vector machine (SVM) classification methods to detect Verticillium wilt severity levels for the individual olive plots assessed and for the all the plots together. 132
Table 5.10. Variables selected in the forward stepwise discriminant analysis to distinguish among Verticillium wilt severity levels for each individual plot assessed. . 134

Chapter 6: Conclusions..... 147

Appendix: Scientific production 153

List of Symbols

a	Maximum asymptote used in sigmoid function
a,b,c	Parameters that control the shape of Type I combined exponential and power curve
B	Constant of integration in Gompertz equation
$\mathbf{C_{a+b}}$	Chlorophyll a+b
F	*F* statistic from ANOVA
G	Maximum response used in the modified beta function
G	Stomatal conductance
H	Shape parameter used in the modified beta function
K	Asymptote parameter in Gompertz equation
k	Half maximum parameter used in sigmoid function
L	Radiance
$\mathbf{O_2}$**-A**	Oxygen A-band around 760 nm
$\mathbf{O_2}$**-B**	Oxygen B-band around 687 nm
P	Probability
R	Reflectance
r	Relative rate of disease increase
$\boldsymbol{R^2}$	Determination coefficient
rho	Intrinsic rate of disease increase
T	Soil temperature used in sigmoid function
t	Time of disease assessment in days after inoculation
$\boldsymbol{T_{max}}$	Maximum temperature for growth of *Verticillium dahliae* isolates used in the modified beta function
$\boldsymbol{T_{min}}$	Minimum temperature for growth of *Verticillium dahliae* isolates used in the modified beta function
$\boldsymbol{T_{opt}}$	Optimal soil temperature used in the modified beta function
$\mathbf{Y_T}$	Response of the measured variable to soil temperature
ε	Emissivity
κ	Kappa coefficient

List of Abbreviations

AGL	Above Ground Level
ANOVA	ANalysis Of VAriance
B	Blue index
BGI1	Blue/Green Index 1
BGI2	Blue/Green Index 2
BRI1	Blue/Red Index 1
BRI2	Blue/Red Index 2
CFU	Colony-Forming Unit
CMS	Cornmeal Sand
cv.	Olive cultivar
CWSI	Crop Water Stress Index
D	Defoliating *Verticillium dahliae* pathotype
DOY	Day Of Year
DS	Disease Severity
FLD3	Chlorophyll fluorescence based on FLD principle using three bands (747, 762, 780)
FOV	Field Of View
FPA	Focal Plane Array
Fs	Steady-state chlorophyll fluorescence
FWHM	Full Width at Half-Maximum bandwidth
G	Greenness index
GLM	General Linear Model
GM1	Gitelson and Merzlyak Index 1
GM2	Gitelson and Merzlyak Index 2
GMT	Greenwich Mean Time
HI	Healthy Index
IFOV	Instantaneous Field Of View
IMU	Inertial Measurement Unit
IP	Incubation Period
IP_R	Reciprocal Incubation Period
IR	Infrared region of the electromagnetic spectrum
IRT	Infrared Temperature
LAI	Leaf Area Index
LDA	Linear Discriminant Analysis
LDCM	Landsat Data Continuity Mission
LIC3	Lichtenhaler Index
LRA	Logistic Regression Analysis
LRT	Likelihood Ratio Test
mCAI	Modified Chlorophyll-Absorption-Integral

MODTRAN	MODerate resolution atmospheric TRANsmission model
MSR	Modified Simple Ratio
MTVI	Modified Triangular Vegetation Index
ND	Non-Defoliating *Verticillium dahliae* pathotype
NDVI	Normalized Difference Vegetation Index
NIR	Near-Infrared region of the electromagnetic spectrum
NN	Artificial Neural Network
NUC	Non-Uniformity Correction
OSAVI	Optimized Soil-Adjusted Vegetation Index
PAM	Pulse Amplitude Modulated
PCA	Principal Component Analysis
PCR	Polymerase Chain Reaction
PDA	Potato Dextrose Agar
PRI_{515}	Photochemical Reflectance Index using R_{515} as reference band
PRI_{570}	Photochemical Reflectance Index using R_{570} as reference band
PSSRa	Pigment Specific Simple Ratio Chlorophyll a
PSSRb	Pigment Specific Simple Ratio Chlorophyll b
PSSRc	Pigment Specific Simple Ratio Carotenoids
R	Redness index
RDVI	Renormalized Difference Vegetation Index
RH	Relative Humidity
RMSE	Root Mean Square Error
SAUDPC	Standardized Area Under Disease Progress Curve
SIPI	Structure-Intensive Pigment Index
SMARTS	Simple Model of the Atmospheric Radiative Transfer of Sunshine
SPAD	Portable chlorophyll meter
SR	Simple Ratio
SVM	Support Vector Machine
Ta	Air Temperature
Tc	Canopy Temperature
TCARI	Transformed Chlorophyll Absorption in Reflectance Index
TCARI/OSAVI	Transformed Chlorophyll Absorption in Reflectance Index / Optimized Soil-Adjusted Vegetation Index
Tc − Ta	Normalized canopy temperature
TIR	Thermal-Infrared region of the electromagnetic spectrum
Tl	Leaf Temperature
Tl − Ta	Normalized leaf temperature
TOW	Take-Off Weight
TVI	Triangular Vegetation Index

UAS	Unmanned Aerial System
UAV	Unmanned Aerial Vehicle
VIS	Visible region of the electromagnetic spectrum
VNIR	Visible and Near-Infrared region of the electromagnetic spectrum
VOG1	Vogelmann Index
VPD	Vapor Pressure Deficit
VW	Verticillium Wilt
ZM	Red edge

Resumen

El olivo (*Olea europaea* L.) es el cultivo leñoso no tropical que ocupa mayor superficie en todo el mundo, con el 95% de la producción mundial localizada en la cuenca Mediterránea. España es el país con mayor superficie de olivar del mundo con 2.5 MHa y aproximadamente el 39% de la producción mundial. Durante las últimas décadas, la Verticilosis, causada por el hongo de suelo *Verticillium dahliae* Kleb., ha ocasionado severas pérdidas de rendimiento en el olivar, convirtiéndose en la enfermedad más limitante causada por patógenos de suelo de este cultivo a nivel mundial. Este patógeno coloniza el sistema vascular de la planta, bloqueando el flujo del agua y finalmente induciendo estrés hídrico. El desarrollo de la Verticilosis en el olivo puede estar influenciado por factores bióticos y abióticos, sin embargo, poco se sabe sobre la influencia del medio físico en él. Actualmente, ninguna medida de control aplicada individualmente es completamente efectiva para el tratamiento de la Verticilosis del olivo, no obstante, una estrategia de control integrado es la mejor forma de manejar la enfermedad, combinando el uso de medidas de control previas y posteriores a la plantación. Las medidas de control posteriores a la plantación serían más efectivas si las zonas del terreno con árboles afectados por Verticilosis fueran identificadas en etapas tempranas del desarrollo de la enfermedad con el objetivo de disminuir la expansión del patógeno y sucesivas infecciones a árboles o plantaciones vecinas. Sin embargo, la inspección visual en campo de síntomas de la enfermedad en estadios tempranos de su desarrollo es costosa en tiempo y recursos. Por lo tanto, la teledetección puede ser una herramienta muy útil para detectar el estrés hídrico inducido por la infección de *V. dahliae* en olivos en etapas tempranas del desarrollo de la enfermedad.

Los principales objetivos de la presente Tesis Doctoral fueron: (i) evaluar el efecto de la temperatura del suelo en el desarrollo de la Verticilosis teniendo en cuanta diferentes patotipos de *V. dahliae* y cultivares de olivo; (ii) valorar el uso de la teledetección térmica e hiperespectral de alta resolución como herramienta para detectar la infección y severidad por Verticilosis en parcelas de olivar y áreas de mayor extensión, evaluando la temperatura e índices fisiológicos desde escala foliar a escala de cubierta.

El primer objetivo se llevó a cabo con plantas de olivo de los cultivares (cv.) Arbequina y Picual que crecieron en suelo infestado con los patotipos defoliante (D) y no defoliante (ND) de *V. dahliae* bajo condiciones climáticas controladas en tanques de suelo con temperaturas de 16 a 32ºC. El desarrollo de la Verticilosis en plantas infectadas por el patotipo D fue más rápido y severo en cv. Picual que en cv. Arbequina. La temperatura de suelo óptima para el desarrollo de la infección del patotipo D fue de 16 a 24ºC para cv. Picual y de 20 a 24ºC para cv. Arbequina. Para el patotipo ND el rango de temperatura más favorable para la infección por *V. dahliae* fue de 16 a 20ºC. Estos resultados permiten

un mejor conocimiento de la distribución geográfica diferencial de los patotipos de *V. dahliae* así como evaluar el efecto potencial del cambio climático en el desarrollo de la enfermedad.

En una siguiente fase de esta serie de experimentos, el segundo objetivo de la Tesis Doctoral fue abordado a escala foliar. Para ello, se estimaron periódicamente a nivel foliar diversos parámetros relacionados con el estrés de la planta (i.e., temperatura, fluorescencia clorofílica en estado estacionario Fs, Photochemical Reflectance Index PRI, contenido de clorofila y producción de etileno) para estimar su relación con la infección por *V. dahliae* y el desarrollo de la enfermedad en plantas de olivo que crecieron a diferentes temperaturas de suelo. Esta relación se determinó por regresión logística multinomial y árboles de clasificación, identificando el contenido de clorofila, Fs y temperatura foliar como los mejores indicadores de la Verticilosis en etapas tempranas del desarrollo de la enfermedad, mientras que la producción de etileno y PRI sólo la detectaron en etapas avanzadas de su desarrollo.

Para estudiar la detección de la Verticilosis a escala de cubierta, se realizaron vuelos durante tres años consecutivos con vehículos aéreos no tripulados (UAVs) usando cámaras térmicas, multiespectrales e hiperespectrales sobre dos parcelas de olivar. Las imágenes obtenidas se relacionaron con la severidad de la Verticilosis evaluada en campo al mismo tiempo que los vuelos. Además, se realizaron medidas en campo a nivel foliar y de copa en una de las parcelas con el fin de apoyar los resultados obtenidos de las imágenes y corroborar que éstos se debían a la infección y colonización de los tejidos vasculares por *V. dahliae* y no sólo a los cambios estructurales causados por el estrés hídrico inducido por la enfermedad. Estos vuelos permitieron la detección temprana de la Verticilosis a partir de la temperatura de cubierta derivada de las imágenes térmicas, el Crop Water Stress Index (CWSI) calculado de las imágenes térmicas, los ratios azul/azul-verde/azul-rojo y la fluorescencia clorofílica (FLD3), confirmando los resultados obtenidos en las medidas de campo. Los índices estructurales (i.e., NDVI), índices fisiológicos como PRI, el índice de enfermedad HI, los índices de clorofila y carotenos y los ratios rojo/verde fueron buenos indicadores para detectar la presencia de daño de moderado a severo.

Posteriormente, este método para la detección de la Verticilosis a escala de parcela fue validado para vuelos en áreas de mayor extensión que constaban de varias parcelas de olivar que diferían en diversas características agronómicas. Se evaluó una metodología para la clasificación automática de la infección y severidad por *V. dahliae* usando imágenes térmicas e hiperespectrales de alta resolución adquiridas en un solo vuelo con una plataforma tripulada sobre una región olivarera de 3,000-ha. Los métodos de clasificación, análisis discriminante lineal (LDA) y support vector machines (SVM), se aplicaron para discriminar entre niveles de severidad de la Verticilosis, explotando la

información combinada de la temperatura de cubierta e índices fisiológicos calculados a partir de las imágenes. LDA alcanzó una precisión en la clasificación global del 59.0% y un coeficiente kappa (κ) de 0.487, mientras que con SVM se obtuvo una mayor precisión en la clasificación, 79.2% con un κ similar 0.495. Sin embargo, LDA clasificó mejor árboles con niveles de severidad iniciales y bajos, alcanzando precisiones de 71.4 y 75.0%, respectivamente, en comparación con el 14.3 y 40.6% obtenido por SVM. La temperatura de cubierta, fluorescencia clorofílica FLD3, los índices estructurales, de xantofilas, clorofila, carotenos y de enfermedad fueron los mejores indicadores para detectar etapas tempranas y avanzadas de la infección por Verticilosis. Comparando con los resultados obtenidos a escala de parcela, la temperatura de cubierta y FLD3 permitieron identificar olivos en etapas tempranas del desarrollo de la enfermedad tanto a escala de parcela como a mayor escala, no estando influenciados por la variación en características agronómicas dentro del área de estudio. Los índices estructurales, de xantofilas, clorofila, carotenos y de enfermedad y los ratios azul/verde/rojo fueron buenos indicadores para detectar la presencia de daño de moderado a severo a ambas escalas.

Este trabajo demuestra el potencial de usar la teledetección térmica e hiperespectral de alta resolución para la detección temprana de olivos infectados por *V. dahliae* con el fin de diseñar estrategias de control de la enfermedad a escala de parcela y regional.

Abstract

Olive (*Olea europaea* L.) is the most cultivated non-tropical fruit tree in the world, with 95% of the world production located in the Mediterranean Basin. Spain is the leading olive-producing country with 2.5 MHa and nearly 39% of the world production. During the last few decades, Verticillium wilt, caused by the soil-borne fungus *Verticillium dahliae* Kleb., has caused severe olive yield losses, becoming the most limiting soil-borne disease of this crop worldwide. This pathogen colonizes the vascular system of plants, blocking water flow and eventually inducing water stress. Development of Verticillium wilt in olive can be influenced by biotic and abiotic factors, nevertheless, little is known about the influence of the physical environment on it. Currently, no control measure applied singly is fully effective for the management of Verticillium wilt of olive; therefore an integrated disease management strategy is needed to manage the disease, combining the use of pre-planting and post-planting control measures. Post-planting control measures would be more efficient if Verticillium wilt-affected trees patches within fields are identified at early stages of disease development in order to mitigate the spread of the pathogen and successive infections to neighboring trees. However, visual inspection of disease symptoms at early stages of development in the field is time-consuming and expensive. Thus, remote sensing is thought to be a useful tool to detect water stress induced by *V. dahliae* infection in olive trees at early stages of disease development.

The main objectives of this PhD Thesis were: (i) to assess the effect of soil temperature on Verticillium wilt development taking into account different *V. dahliae* pathotypes and olive cultivars; and (ii) to evaluate the use of high-resolution thermal and hyperspectral remote sensing imagery as a tool to detect Verticillium wilt infection and severity in olive orchards and larger areas, assessing temperature and physiological indices from leaf to canopy scale.

The first objective was conducted with olive plants of cultivar (cv.) Arbequina and cv. Picual grown in soil infested with the defoliating (D) or non-defoliating (ND) pathotype of *V. dahliae* under controlled climatic conditions in soil tanks with a range of soil temperatures from 16 to 32ºC. Verticillium wilt development in plants infected by the D pathotype was faster and more severe on cv. Picual than on cv. Arbequina. Models estimated that infection by the D pathotype was promoted by soil temperature in a range of 16 to 24°C for cv. Picual and of 20 to 24ºC for cv. Arbequina. For the ND pathotype a range of 16 to 20ºC was estimated as the most favorable for infection. These results provide a better understanding of the differential geographic distribution of *V. dahliae* pathotypes and assess the potential effect of climate change on Verticillium wilt development.

In a next step of this PhD Thesis, the second objective at leaf level was approached. For that, several parameters related with plant stress (i.e., temperature, steady-state chlorophyll fluorescence Fs, Photochemical Reflectance Index PRI, chlorophyll content and ethylene production) were periodically measured at leaf level to assess their relationship with *V. dahliae* infection and disease development in olive plants growing at different soil temperatures. This relationship was determined by multinomial logistic regression and classification trees, identifying chlorophyll content, Fs and leaf temperature as the best indicators of Verticillium wilt at early stages of disease development, while ethylene production and PRI only detected Verticillium wilt at advanced stages.

To study the detection of Verticillium wilt at canopy scale, time series of airborne thermal, multispectral and hyperspectral imagery were acquired with unmanned aerial vehicles (UAVs) in three consecutive years over two olive orchards and related to Verticillium wilt severity at the time of the flights. In addition, field measurements at leaf and tree-crown levels were conducted in one of the olive orchards to support the results obtained from imagery and to confirm that these results were due to the infection and colonization of vascular tissues by *V. dahliae* and not simply due to structural effects driven by the water stress induced by the disease. The airborne flights enabled the early detection of Verticillium wilt by using canopy-level image-derived airborne canopy temperature, Crop Water Stress Index (CWSI) calculated from the thermal imagery, blue/blue-green/blue-red ratios and chlorophyll fluorescence quantification from the hyperspectral imagery (FLD3), confirming the results obtained in the field. The structural indices (i.e., NDVI), physiological indices such as PRI, disease index HI, chlorophyll and carotenoid indices, and the red/green ratios were good indicators to detect the presence of moderate to severe damage.

Furthermore, this methodology for Verticillium wilt detection at orchard scale was validated on flights conducted over larger areas comprising several olive orchards differing in agronomic characteristics. A methodology for the automatic classification of *V. dahliae* infection and severity was assessed using high-resolution thermal and hyperspectral imagery acquired with a manned platform over a 3,000-ha commercial olive area in one single flight. Linear discriminant analysis (LDA) and support vector machine (SVM) classification methods were applied to discriminate among Verticillium wilt severity levels exploiting the combined information of the canopy temperature and physiological indices calculated from the imagery. LDA reached an overall accuracy of 59.0% and a kappa coefficient (κ) of 0.487, while SVM obtained a higher overall accuracy, 79.2%, with a similar κ, 0.495. However, LDA better classified trees at initial and low severity levels, reaching accuracies of 71.4 and 75.0%, respectively, in comparison with the 14.3 and 40.6% obtained by SVM. Canopy temperature, FLD3, structural, xanthophyll, chlorophyll, carotenoid and disease indices were found to be the

best indicators for early and advanced stage infection by Verticillium wilt. Comparing with the results obtained at orchard scale, canopy temperature and chlorophyll fluorescence FLD3 allowed identifying olive trees at the early stages of disease development as much at orchard scale as at larger scale, being not influenced by the variation of agronomic characteristics within the study area. Structural indices, xanthophyll, chlorophyll, carotenoid and disease indices and blue/green/red ratios proved to be good indicators to detect the presence of moderate to severe damage caused by Verticillium wilt at both scales.

This work proved the potentials for the early detection of *V. dahliae* infection in olive trees using thermal and hyperspectral airborne imagery in order to design focalized Verticillium wilt control strategies at orchard level and at larger scales.

CHAPTER 1

INTRODUCTION

CHAPTER 1: Introduction

Contemporary agriculture faces an enormous challenge: *a rising demand of crop production that guarantee future food security* (Fereres *et al.*, 2011). By 2050, crop production need to be increased by 70-110% (FAO, 2011; Tilman *et al.*, 2011) to meet this increasing demand caused by the population growth, dietary changes (especially meat consumption) and increasing bioenergy use (Godfray *et al*., 2010; Foley *et al.*, 2011). Numerous authors have suggested that increasing crop yields, rather than clearing more land for food production, is the most sustainable path for food security (Godfray *et al*,. 2010; Foley *et al.*, 2011; Phalan *et al.*, 2011). In this sense, crop protection plays a very important role in the reduction of yield losses caused by pests (weeds, animal pests and pathogens), which are responsible for losses ranging between 20 and 40% of global agricultural productivity (Teng, 1987; Oerke, 2006). The impacts of pests on yield are well known, however, the appearance of climate change on scene has made the study of these impacts be more complex and important than ever (Newton *et al.*, 2011). Higher temperatures, increasing levels of carbon dioxide, water limitation and quality may all affect existing pests, increasing the incidence of some of them and reducing the incidence of others (Gregory *et al.*, 2009; Newton *et al.*, 2011).

Precise disease control is a demanding challenge within precision agriculture in order to achieve high yields in agricultural crop systems while reducing the costs and the environmental impact of pesticide use. Therefore, the early detection of plant diseases in the field (before the onset of disease symptoms) could be a valuable source of information for executing proper disease management strategies and disease control measures to prevent the development and the spread of plant pathogens (Bock *et al.*, 2010; Mahlein *et al.*, 2012). However, conventional methods of detection rely on visual inspection of disease symptoms in the field, which is time-consuming and expensive and often results in detection after the optimum time for control has passed (Steiner *et al.*, 2008). Furthermore, diseases as well as abiotic stress conditions are commonly heterogeneous in time and space in a production field. Thus, site-specific disease management has to be assessed by detailed recording of spatial distribution and disease development, requiring large-scale and geo-referenced monitoring of diseases in the crop for precise timing and application of control measures (Nutter *et al.*, 2010). Consequently, precise and time-saving methods are essential for disease monitoring (detection, identification and quantification). Therefore, in the last decade remote sensing methods have made progress in order to provide useful tools to detect disease symptoms at early stages of development and spatial heterogeneities due to pathogens at canopy scale (Bock *et al.*, 2010; Nutter *et al.*, 2010; Mahlein *et al.*, 2012). The early detection of within-field differences in crop status or growth conditions caused by diseases would enable the farmer to streamline input factors thereby optimizing his profit margin, while simultaneously improving the overall stability of the agro-system.

1.1 Olive crop

Olive (*Olea europaea* L.) is the most cultivated non-tropical fruit tree in the world, with an estimation of 865 million trees in production (IOC, 2013). Olive trees grow in a cultivated area of 10 million ha and produce an annual average of 14 million t of olives, which has increased during the last decade at an annual average rate of 4% (FAO, 2012; IOC, 2013). Olive oil is the main commodity of this crop with the 90% of total production, while the other 10% is assigned to table olives. Olive is one of the most important crops in the Mediterranean Basin that represents the 95% of the world production (Figure 1.1). Spain is the leading olive-producing country, comprising in 2012 the 24% of the world olive area, 44% of the olive oil production and 21% of the table olives production (FAO, 2012; IOC, 2013) (Figure 1.1). Andalucía, at southern Spain accounts for the 60% of the Spanish olive area and the 80% of the Spanish olive oil production (Consejería de Agricultura y Pesca, 2012) (Figure 1.1).

Due to the easy vegetative propagation of this species, most olive cultivars were selected many centuries ago in the same area as they are grown nowadays, probably starting by crosses between local wild olives and newly introduced cultivars from the Near East (Berlaj *et al.*, 2010; Besnard *et al.*, 2013). Therefore, high cultivar diversity is common in traditional olive producing countries (Rallo, 2005). The olive cultivars currently cultivated were selected mainly for their high oil content, high productivity and large fruit size (Rallo, 2005). In Spain, 262 different cultivars were identified (Barranco, 1995) but only 24 were classified as major cultivars due to the large portion of the acreage or the predomination in one or more olive districts (Barranco and Rallo, 2000). Most of the major cultivars are used for olive oil, highlighting cv. 'Picual', 'Hojiblanca' and 'Arbequina' which comprised the 37.7, 9.5 and 3.1% of the Spanish olive surface, respectively (Barranco, 2008). 'Picual' is the main cultivar because of its many favorable agronomic characteristics, such as early bearing, high yield, low fruit removal force facilitating mechanical harvesting, and high adaptability to different environmental conditions (Barranco, 2008). 'Hojiblanca' is characterized by high yield, late bearing, large fruit size, tolerance to chalky soils and drought and high oil quality (Barranco, 2008). 'Arbequina' is increasing in acreage in intensive plantings, due to its low vigor, very early bearing, high productivity and high oil content and quality (Barranco, 2008).

1.2. Verticillium wilt of olive

Verticillium wilt of olive trees is the most limiting disease of this crop worldwide and is caused by the soil-borne fungus *Verticillium dahliae* Kleb (Tsror, 2011; Jiménez-Díaz *et al.*, 2012). This pathogen is able to infect more than 200 plant species, including most vegetables, flowers, fruit trees, field crops and shade and forest trees (Pegg and

Brady, 2002; Klosterman *et al.*, 2009). In Spain, *V. dahliae* was firstly detected infecting cotton in the Guadalquivir valley (Blanco-López *et al.*, 1984) in the early 1980s, but during the following decades it spread to affect newly established irrigated crops (Sánchez-Hernández *et al.*, 1998; Jiménez-Díaz *et al.*, 2011). Thus, this pathogen is currently a problem on a wide range of crops in several areas of Spain, but olive is the most affected host (López-Escudero and Mercado-Blanco, 2011; Jiménez-Díaz *et al.*, 2012). In 2014, Verticillium wilt of olive accounted for a mean incidence of 0.3%, but in some provinces it reached more than 0.6% with more than 40% of affected orchards (Ruiz Torres, 2015). In the last decade, the spread of Verticillium wilt in olive trees has been associated with the expansion of olive cultivation and changes in cropping practices aimed at increasing yields (Jiménez-Díaz *et al.*, 2011). Such changes include the use of self-rooted planting stocks to establish high-density plantings, drip irrigation, reduced or no tillage, and high inputs of fertilizer in newly cultivated soils or fertile soils (Villalobos *et al.*, 2006) previously cropped with plants susceptible to *V. dahliae*, such as cotton (Jiménez-Díaz *et al.*, 2011).

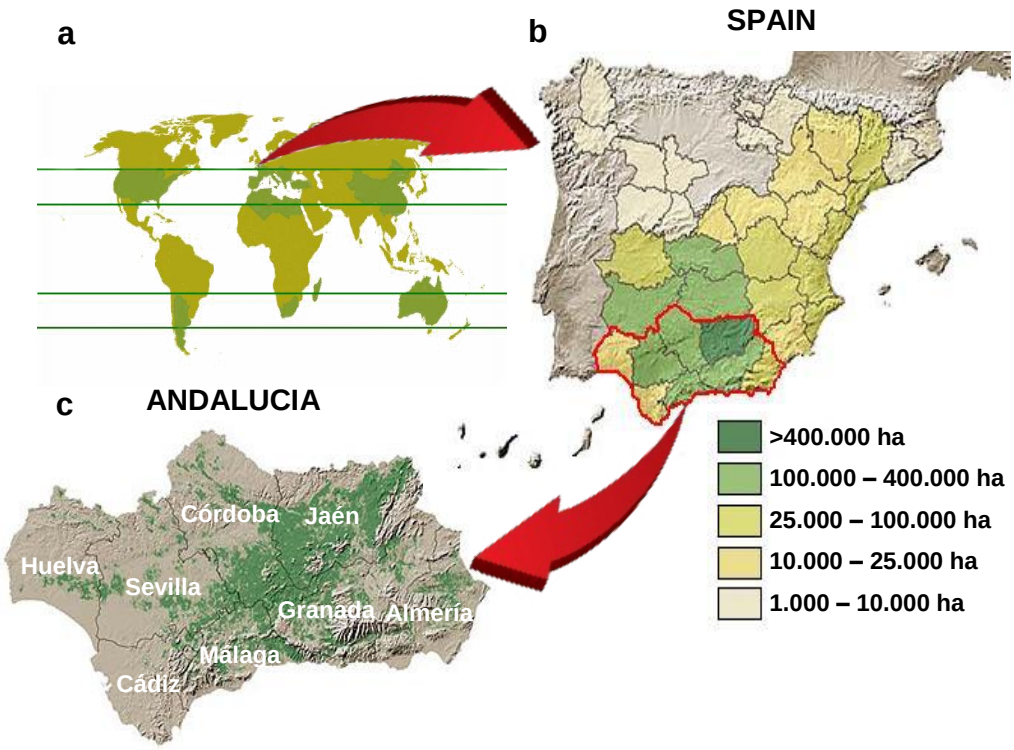

Figure 1.1. (a) Olive-producing countries in the world. (b) Olive area in Spain by provinces. (c) Olive distribution in Andalucía (Picture source: R. Calderón).

V. dahliae can be found in agricultural soils as long-lasting surviving structures called 'microsclerotia', which can survive for up to 15 years (DeVay *et al.*, 1974) (Figure 1.2). These structures germinate multiple times in response to root exudates (Schreiber and Green, 1963) and favorable soil environmental conditions, forming hyphae that penetrate into the plant roots and grow into the root cortex until reach the xylem vessels (Figure 1.2). The rapid upward spread of the pathogen in vascular tissues occurs primarily through conidia transported with the transpiration stream (Talboys, 1962) (Figure 1.2). As a result of xylem colonization, water flow decreases inducing water stress which is mainly responsible for the vascular wilt syndrome caused by *V. dahliae* (Ayres, 1978). The first Verticillium wilt symptoms in irrigated olive trees growing in *V. dahliae*-infested orchards develop 18-24 months after plantation, depending on the density of pathogen propagules in the soil, the *V. dahliae* pathotype prevailing in the soil, the olive cultivar susceptibility and the environmental conditions (Navas-Cortés *et al.*, 2008). In the Mediterranean region, over an annual cropping season, disease incidence and symptom severity typically increase from late autumn-early winter to spring and sharply decrease in summer, with no further development until the next autumn (Navas-Cortés *et al.*, 2008).

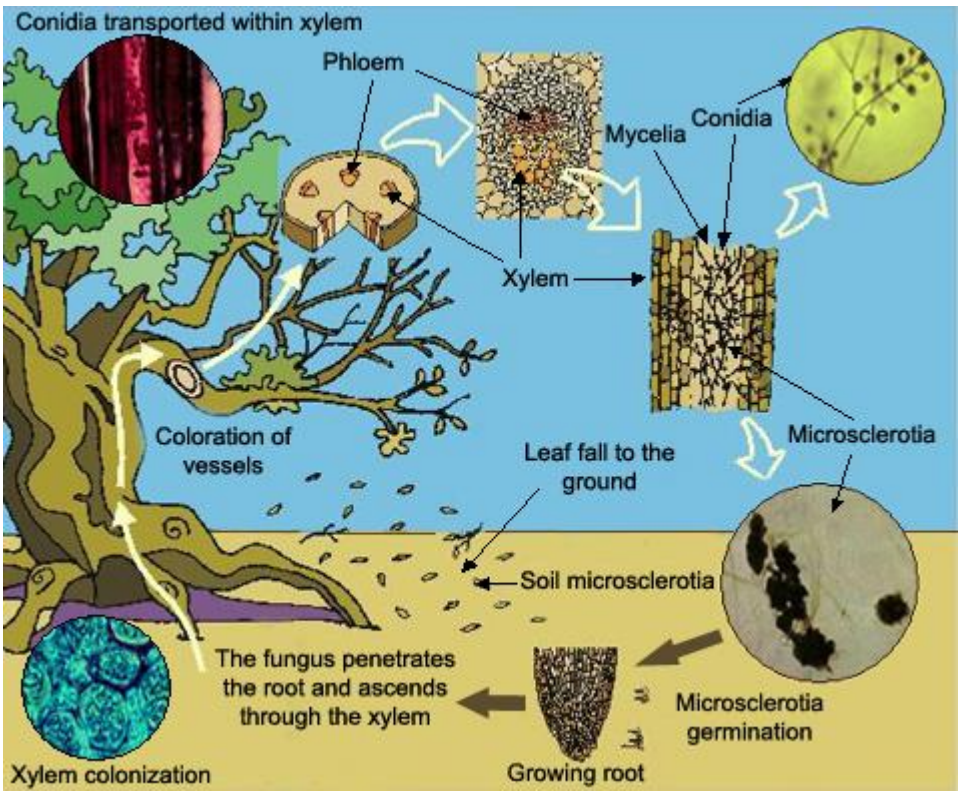

Figure 1.2. Biological cycle of the soil-borne fungus *Verticillium dahliae* in olive trees (Composition: R. Calderón, pictures: R.M. Jiménez-Díaz).

Severity of attacks by *V. dahliae* depends on the virulence of pathogen isolates, which can be classified into defoliating (D) and non-defoliating (ND) based on their ability to cause defoliation or no defoliation of green leaves from shoots and twigs (Navas-Cortés *et al.*, 2008; Jiménez-Díaz *et al.*, 2012). The D pathotype is highly virulent and able to completely kill an olive tree, especially when it is young (López-Escudero and Mercado-Blanco, 2011) (Figure 1.3a). The ND pathotype is moderate or low virulent, although it has also been associated with wilting and death of olive trees (López-Escudero and Mercado-Blanco, 2011) (Figure 1.3b). The success of the pathogen colonization and the subsequent symptom development depends on the genetic resistance level of the host plant (Yadeta and Thomma, 2013). Therefore, planting resistant cultivars of olive is the most effective measure for controlling and limiting the spread of Verticillium wilt (Jiménez-Díaz *et al.*, 2012). However, the most widely used olive cultivars in Spain (i.e., Picual and Arbequina) have been found to be highly susceptible and susceptible to D pathotype, respectively, and susceptible and moderately resistant to ND pathotype, respectively, under controlled conditions in artificial inoculation tests (López-Escudero *et al.*, 2004) (Figure 1.3c, d).

Current importance of Verticillium wilt is due to the severity of the infections, the long-term persistence in the field, the easy spread of the pathogen within and among orchards and the inefficacy of chemical compounds in controlling the disease (López-Escudero and Mercado-Blanco, 2011). Therefore, an integrated disease management strategy is the best way to manage the disease, combining the use of preplanting and postplanting control measures (Tjamos and Jiménez-Díaz, 1998). Preplanting disease control measures include: (i) site selection to avoid planting into high risk soils (Figure 1.3e, f); (ii) use of *V. dahliae*–free planting material; (iii) reduction or elimination of *V. dahliae* inoculum in soil; (iv) protection of healthy planting material from infection by residual inoculum in soil; and (v) use of resistant cultivars and rootstocks. Postplanting control measures are: (vi) cultural practices; (vii) soil solarization; and (viii) organic or biological amendments.

1.3. Remote sensing for the detection of soil-borne plant pathogens

Remote sensing has been used to detect, monitor and quantify a range of diseases in different crops. Comprehensive reviews on the application of remote sensing to the detection of plant diseases are available (e.g., Nilsson, 1995; Bock *et al.*, 2010; Sankaran *et al.*, 2010; Mahlein *et al.*, 2012). Most studies have focused on foliar pathogens in annual crops, where disease symptoms are mainly characterized by distinct color changes

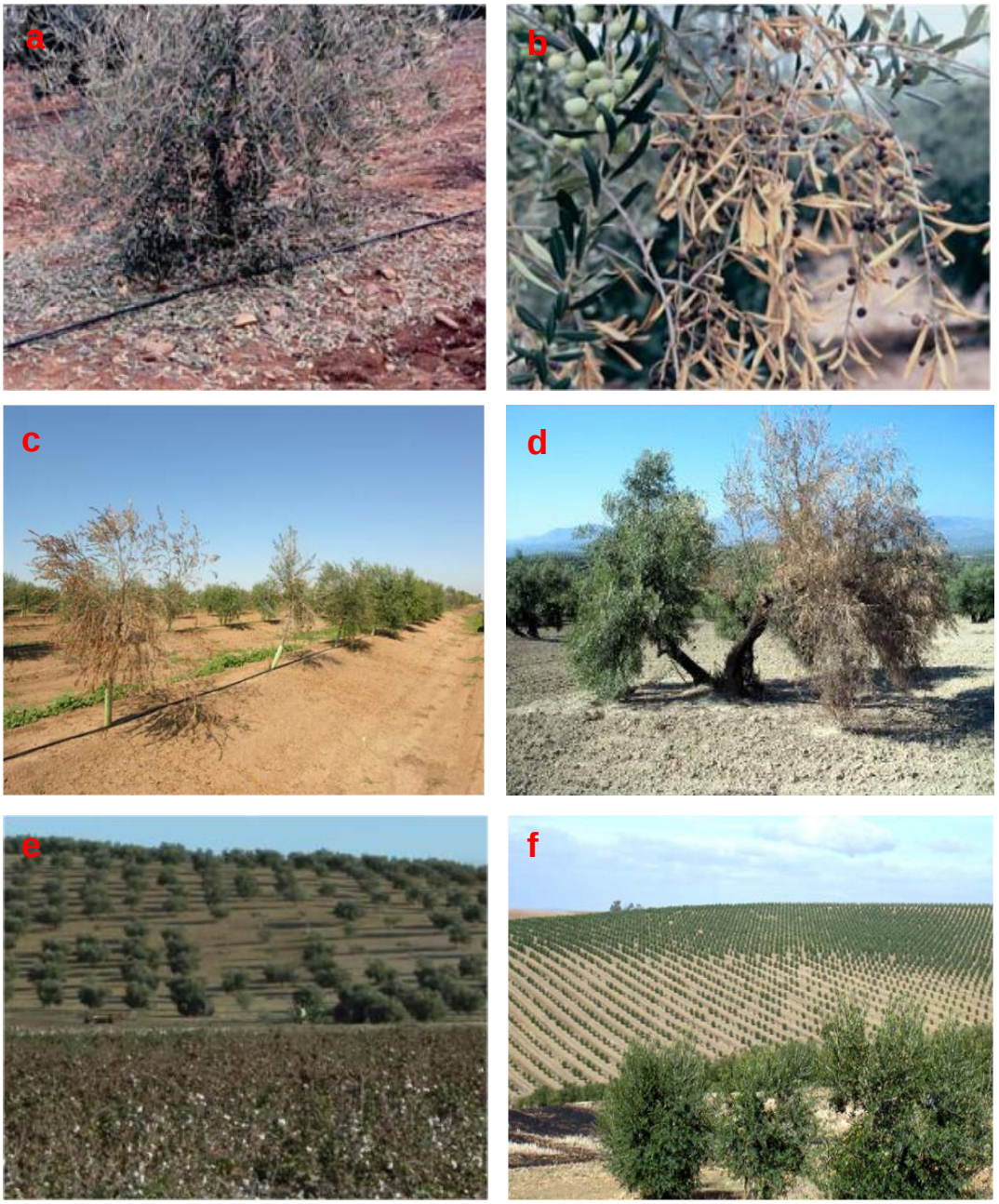

Figure 1.3. (a) Intense defoliation and large amount of fallen green leaves associated with infection by D *V. dahliae*. (b) Symptoms associated with infection by ND *V. dahliae*. Note olive branches with dried, necrotic leaves that remain attached to the symptomatic branch. (c) Death of a 3-years-old irrigated olive cv. Arbequina infected by *V. dahliae*. (d) Sectorial necrosis of branches and shoots in a 15-years-old rainfed olive cv. Picual infected by *V. dahliae*. (e) Verticillium wilt affected olive orchard located next to a cotton field. Note the patchy occurrence of symptoms due to the low mobility in the field of *V. dahliae*. (f) Olive orchard with Verticillium wilt infected trees showing nonrandom distribution (Picture source: (a,b) Navas-Cortés *et al.* 2008, (c,d,e,f) Lucena *et al.* 2009).

in the aerial parts of the plant. However, this technology is still poorly developed for detection of soil-borne plant pathogens.

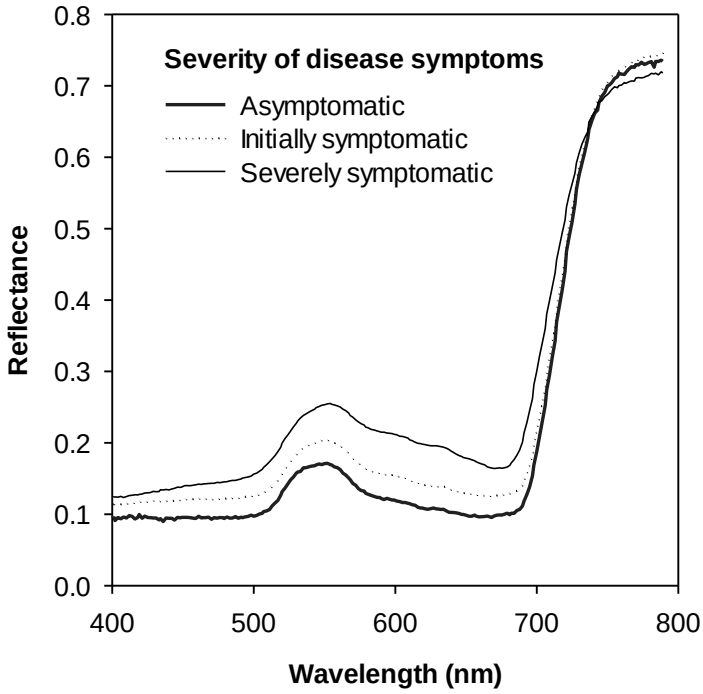

Figure 1.4. Leaf reflectance of olive trees infected by *Verticillium dahliae* (Source: Calderón *et al.*, 2014).

Remote sensing for the detection of damage caused by soil-borne plant pathogens is the best-fit technology for optimization of integrated disease management (Bock *et al.*, 2010; Hillnhüter *et al.*, 2010; Sankaran *et al.*, 2010; Mahlein *et al.*, 2012). Soil-borne pathogens parasitize the plant roots, disrupting the xylem vessels and reducing nutrient and water uptake. Therefore, this damage results in a change of spectral reflectance due to a significant reduction in leaf transpiration rate which leads to a decline characterized by leaf chlorosis and defoliation (Hillnhüter *et al.*, 2010) (Figure 1.4). Chlorophyll content tends to decrease in infected plants, showing a higher reflectance in the visible (VIS) green (550 nm) and red-edge (650-720 nm) regions that is correlated with the severity of symptoms (Figure 1.4). Stressed plants also show a drop in canopy density and leaf area that leads to a decrease of spectral reflectance in the near-infrared (NIR) range (680-800 nm) (Figure 1.4). In addition, thermal-infrared (TIR) region (8000-15000 nm) is highly suitable for the detection of soil-borne pathogen infection due to the decrease in transpiration rate that increases canopy temperature. Considering these changes in the spectrum of infected plants, disease symptoms could be detected remotely in the VIS, red edge, NIR and TIR regions. In addition, these symptoms usually appear in long-term

stable and clearly delineated patches in the field which makes the use of remote sensing even more suitable for site-specific disease management to prevent yield losses (Hillnhütter *et al.*, 2010; Mahlein *et al.*, 2012).

Nowadays, remote sensing has several platforms which are able to provide information of the vegetation, such as satellites, manned and unmanned airborne platforms. However, the choice of the platform will influence the spatial, spectral and temporal resolution of the imagery acquired. Therefore, due to the high spatial and spectral resolution required for crop management (e.g., disease detection), the selection of the platform is of vital importance. Current satellite-based imagery has limited application in crop management due to the low spatial and spectral resolutions provided and the lack of high resolution satellite thermal imagery. In particular, high spatial resolution imagery acquired in the visible and near infrared regions is relatively feasible with current airborne and satellite sensors. By contrast, thermal imaging is still limited to medium-resolution sensors due to the technical limitations of micro-bolometer technology (Berni *et al.*, 2009a). As an example, the Landsat Data Continuity Mission (LDCM) launched in February 2013 delivers two thermal infrared bands at 100 m resolution. Although it is useful for certain global monitoring studies, the low resolution of the thermal bands is a clear limitation for precision agriculture applications, such as disease detection and monitoring. Alternatives based on manned airborne platforms have demonstrated capabilities for vegetation condition monitoring due to the high spatial resolution used (0.5-2 m pixel sizes). However, their use is limited because of their high operational costs in some cases (Berni *et al.*, 2009b). Remote sensors on board unmanned aerial vehicle (UAV) platforms provide sub-meter spatial resolution (Herwitz *et al.*, 2004; Sugiura *et al.*, 2005; Berni *et al.*, 2009b). This allows retrieving of pure canopy temperature and reflectance, thus minimizing background and shadow effects.

Sensors installed on board the different platforms are able to measure the electromagnetic radiance reflected (spectral sensors) and/or emitted (thermal sensors) by the earth's surface. The first aerial images of damage caused by a soil-borne plant disease were made in 1927 when Taubenhaus *et al.* (1929) took pictures from an US Army airplane to detect symptom development of cotton root rot caused by *Phymatotrichum omnivorum*. Once the use of aerial photography was established as a technique, infrared (IR) cameras were developed and available for experimentation. The first use of IR imagery for detection of soil-borne plant diseases was conducted in the early 1960s by Norman and Fritz (1965) to detect the nematode *Radophoulus similis* in citrus trees before visible symptom development. Heald *et al.* (1972) took IR aerial images of cotton fields to detect the nematode *Rotylenchulus reniformis* as well as early symptoms of *Phym. omnivorum* root rot. A sugar beet field study using IR picture was conducted by Schmitz *et al.* (2003) to detect infection of the nematode *Heterodera schachtii* by supervised classification methods. The use of airborne multispectral sensors in the detection of

diseases caused by soil-borne pathogens was firstly assessed by Brodrick *et al.* (1971) who identified avocado trees infected with *Phytophthora cinnamomi* root rot with an accuracy of 100%, even at initial disease severity level, while IR film only showed an accuracy of 80%. Multispectral sensors have a combination of three or more spectroradiometers so that each sensor record one scene of a small band which are then combined to obtain the multispectral image. Other examples of the use of multispectral imagery for the detection and evaluation of diseases caused by soil-borne pathogens include creeping bentgrass affected by Rhizoctonia blight infected by *Rhizoctonia solani* (Raikes and Burpe, 1998); interaction between the root-knot nematode *Meloidogyne incognita* and root rot due to *Phym. omnivorum* in kenaf (Cook *et al.*, 1999); the nematode *Heterodera glycines* in soybean fields (Nutter *et al.*, 2002); soybean root rot caused by *Fusarium* spp. (Wang *et al.*, 2004); and Fusarium head blight in winter wheat (Dammer *et al.*, 2011).

In the last decade, technological advances in spectral sensors development, in particular progress from multispectral broadband sensors to hyperspectral narrowband sensors, have drastically increased the quantity and quality of information on the spectral characteristics of the canopy surface that can be used to detect and quantify disease symptoms (Schowengerdt, 1997). These devices provide information over a wide spectral range (350-2500 nm), obtaining a spectral resolution up to <1 nm (Bock *et al.*, 2010). Typically, hyperspectral images consist of hundreds of registered and contiguous spectral bands such that for each pixel it is possible to derive a complete reflectance spectrum. Hyperspectral reflectance enabled the detection of disease symptoms of the nematodes *Globodera pallida* and *Globodera rostochinensis* in potato plants (Heath *et al.*, 2000), root rot caused by *Rhizoctonia solani* in sugar beet at field conditions (Laudien *et al.*, 2004; Reynolds *et al.*, 2012) and the co-infection of sugar beet with this pathogen and the plant parasitic nematode *Heterodera schachatii* (Hillnhütter *et al.*, 2011, 2012), *Verticillium dahliae* (Chen *et al.*, 2008, 2011) and the nematode *Rotylenchulus reniformis* (Lawrence *et al.*, 2004) infecting cotton at field conditions as well as Fusarium head blight in wheat (Bauriegel *et al.*, 2011). Nevertheless, only relatively recently have hyperspectral sensors been explored for the detection and quantification of diseases caused by soil-borne pathogens, especially at the near-range scale (leaf, plants or small quadrats) (Heath *et al.*, 2000; Chen *et al.*, 2008, 2011; Bauriegel *et al.*, 2011; Hillnhütter *et al.*, 2012; Reynolds *et al.*, 2012). Up to now, few studies have successfully detected and quantified these plant diseases at canopy level using airborne hyperspectral sensors (Laudien *et al.*, 2004; Lawrence *et al.*, 2004; Hillnhütter *et al.*, 2011).

Leaf temperature results from the incoming radiation, the water status of the plant and the functionality of the epidermal layer (cuticle and stomata) to regulate the transpiration of leaves, as well as from environmental conditions like air temperature, relative humidity and wind speed (Jones, 1992). As leaf temperature is negatively

correlated to transpiration rate form the canopy surface (Inoue *et al.*, 1990), TIR sensing of the canopy temperature can be used to monitor the transpiration rate of plants (Jones, 1999). Infections by soil-borne pathogens causing vascular wilt diseases affect the water uptake of plants, inducing the stomatal closure which reduces the transpiration rate. In turn, this decreases evaporative cooling and increases leaf temperature (Jones, 2004). Therefore, thermal imagery has shown to be particularly useful to detect root infection and vascular colonization by soil-borne pathogens that lead to water stress symptoms. Thermal imagery has potential for use in early disease detection, even prior to the appearance of visual symptoms, which is very important for efficient and environmentally friendly disease control methods that can be used to reduce the quantity and quality of yield losses (Oerke and Steiner, 2010). Thermal sensors are used to quantify the temperature, being able to measure the radiance emitted by a surface in the TIR range of the spectrum between 8 and 15 μm. The first experiment using IR thermometry on the detection of biological stress in plants infected by soil-borne pathogens was conducted by Pinter *et al.* (1979), who found foliar temperatures 3-5 ºC higher than those of healthy plants in sugar beet and cotton infected by *Pythium aphanidermatum* and *Phym. omnivorum*, respectively. Other examples of the use of leaf temperature include beans infected by *Fussarium solani*, *Pythium ultimum* or *R. solani* (Tu and Tan, 1985); soybeans affected by brown stem rot caused by *Phialophora gregata* (Mengistu *et al.*, 1987); wheat with moderate take-all symptoms caused by *Gaeumannomyces graminis* var. *tritici* (Nilsson, 1991); the flag leaf temperature of cereals with root and vascular diseases, such as barley infected by *Pyrenophora graminea* and wheat infected by *Cephalosporium gramineum* (Nilsson, 1995); and oil seed rape plants infected by *V. dahliae*, which exhibited leaf temperatures 5-8 ºC higher than non-infected plants (Nilsson, 1995). The use of hand-held thermometers in the previous examples provide no spatial information, so their use is limited because of influences of environmental conditions like sunlight, wind, soil, etc. Thus, the development of thermal imaging systems has increased considerably the potential of IR thermography in plant stress detection due to the assessment of spatial heterogeneities on various scales, from the leaf level to canopies (Oerke and Steiner, 2010). Thermal imagery was used to detect significantly higher canopy temperatures in wheat soils moderately infested by *Heterodera avenae* as compared to low infestations (Nicolas *et al.*, 1991). Schmitz *et al.* (2004) were able to differentiate between sugar beet varieties susceptible and resistant to the nematode *H. schachtii* by using aerial thermal imagery.

However, as occurred with hyperspectral sensors, most of the studies of detection of diseases caused by soil-borne pathogens with thermal sensors were conducted in terms of near remote sensing with ground based-equipment at leaf and quadrat level (Pinter *et al.*, 1979; Tu and Tan, 1985; Mengistu *et al.*, 1987; Nicolas *et al.*, 1991; Nilsson, 1991, 1995). Yet, to the best of our knowledge, airborne thermal cameras have been only used

to detect temperature differences in sugar beet infected by *H. schachtii* (Schmitz *et al.*, 2004).

The ability to identify diseases at early stages and to quantify severity accurately is crucial in plant disease assessment and management. Spectral remote sensing has been extensively used to early detect diseases caused by soil-borne pathogens as much at near-range scale as at canopy scale (i.e., Chen *et al.*, 2008, 2011; Hillnhütter *et al.*, 2011). Nevertheless, TIR remote sensing only has been employed to early detect and quantify root rot in bean at leaf level with IR-thermometers (Tu and Tan, 1985). Despite that, thermal imagery has been widely used to early detect water stress in different crops (Leinonen and Jones, 2004; Cohen *et al.*, 2005; Sepulcre-Cantó *et al.*, 2006, 2007; Berni *et al.*, 2009a; Zarco-Tejada *et al.*, 2012). Thus, taking into account the water stress induced by soil-borne pathogen infection, thermal imagery has poorly taken advantage of the early detection of this kind of diseases. Up to now, no studies have been conducted to study olive tree diseases using spectral and thermal remote sensing.

1.4. Early detection of wilting stress using remote sensing

Verticllium dahliae penetrates into the plant roots, bloquing water flow and reducing the transpiration rate which eventually induced water stress (Ayres, 1978). The early detection of water stress is a key issue to avoid yield losses due to plant pathogens (Hsiao *et al.*, 1976). It is well known that severe water deficits affect many physiological processes and have a strong impact on crop yield (Hsiao *et al.*, 1976). However, even moderate water deficits, which are not easy to detect, can also have important negative effects on yield (Hsiao and Bradford, 1983). Water stress in plants caused by either infection by soil-borne wilting pathogens or drought-induced stomatal closure reduces the transpiration rate. In turn, this decreases evaporative cooling and increases leaf temperature. Remote sensing has successfully proved the early detection of water stress in the past using TIR radiation (Jackson *et al.*, 1977, 1981; Idso *et al.*, 1978, 1981; Jackson and Pinter, 1981). Thermal remote sensing of water stress has been fulfilled using spectrometers at ground level (Jackson *et al.*, 1977, 1981; Idso *et al.*, 1978, 1981), thermal sensors at image level (Leinonen and Jones, 2004; Cohen *et al.*, 2005; Sepulcre-Cantó *et al.*, 2006, 2007; Berni *et al.*, 2009a; Zarco-Tejada *et al.*, 2012) and satellite thermal imagery (Sepulcre-Cantó *et al.*, 2009). Working with hand-held infrared thermometers on herbaceous crops, Jackson and co-workers (Idso *et al.*, 1978; Jackson *et al.*, 1981) developed the Crop Water Stress Index (CWSI), which became a standard thermal-based stress indicator. The CWSI is based on the normalization of differences between canopy (Tc) and air temperature (Ta) with evaporative demand (by means of the vapor pressure deficit of the air).

Apart from the progress made in water-stress detection using the thermal region, the VIS part of the spectrum has also been useful for early water stress detection. This involves using indices focused on bands located at specific wavelengths where photosynthetic pigments are affected by stress conditions. In the past, several indicators related with structural changes in the vegetation such as wilt or loss of foliar area (Broadford and Hsiao, 1982; Wolfe *et al.*, 1983) and the estimation of the decrease in biochemical components such as chlorophyll (Björkman and Powles, 1982) or water (Peñuelas *et al.*, 1993, 1997; Gao, 1996) only detected water stress at advanced stages when the symptoms were visible. On the other hand, nowadays two spectral indicators of water stress, spanning from initial through severe symptoms, are widely used. One is the *Photochemical Reflectance Index* (PRI) (Gamon *et al.*, 1992). This index is sensitive to the epoxidation state of the xanthophyll cycle pigments and to photosynthetic efficiency, serving as a proxy for water stress detection (Thenot *et al.*, 2002; Peguero-Pina *et al.*, 2008; Suárez *et al.*, 2008, 2009, 2010). The PRI has been used to assess pre-visual water stress al leaf level (Thenot *et al.*, 2002; Winkel *et al.*, 2002), at canopy level (Evain *et al.*, 2004; Dobrowsky *et al.*, 2005; Peguero-Pina *et al.*, 2008; Sun *et al.*, 2008) and using airborne imaging spectroscopy (Suárez *et al.*, 2008, 2009, 2010). Despite the successful results obtained with PRI as a proxy for photosynthesis, some studies have shown that this index is highly affected by the canopy structure, leaf pigments and background (Suarez *et al.*, 2008, 2009).

Another indicator of water stress is solar-induced chlorophyll fluorescence emission (Flexas *et al.*, 1999, 2000, 2002; Zarco-Tejada *et al.*, 2009, 2012), because of the strong relationship found between *steady-state chlorophyll fluorescence* (Fs) and the reduced assimilation caused by water stress conditions. Chlorophyll fluorescence is associated with photosynthesis and other physiological processes, as demonstrated consistently in laboratory studies (e.g., Papageorgiu, 1975; Krause and Weis, 1984). Water-stressed plants dissipate a fraction of the excess of intercepted radiation as heat while the other fraction is re-emitted as fluorescence light with well-defined wavelength characteristics. Fs is emitted in two broad and overlapping bands with peaks at 690 and 740 nm. At early stages of water stress, the plant increases the dissipation of energy as heat, reducing Fs (Yahyaoui *et al.*, 1998). Thus, the detection of the decrease in Fs could be useful to determine the level of stress. Over the last few years, scientific interest in Fs obtained under natural outdoor conditions has increased due to its potential development using remote sensing methods (Soukupová *et al.*, 2008). The main problem for the detection of Fs relies on the small contribution of fluorescence to the vegetation's radiance signal (2-3% of the radiance), its mixture with the surface reflectance and the influence of atmospheric effects. It results in a light increase of the detected radiance and, therefore, of the canopy reflectance. One approach for the detection of Fs is based on the observation of those regions of the spectrum which shows a high atmospheric absorption. In these bands, known as Fraunhofer lines, the incoming solar radiation reaching the Earth surface

is minor, so that the reflected radiance is mainly caused by the fluorescence. The Fraunhofer lines are: the Hα line at 656.3 nm is due to the hydrogen absorption by the solar atmosphere whereas two bands at 687nm (O_2-B) and 760 nm (O_2-A) are due to the molecular oxygen absorption by the terrestrial atmosphere. Specially the O_2-A and O_2-B bands overlap with the chlorophyll fluorescence emission spectrum and are wide enough to allow quantifying fluorescence at the leaf and canopy levels with very narrow spectral bands (Meroni *et al.*, 2008a, 2008b, 2009; Pérez-Priego *et al.*, 2005). This method is called "*in-filling*" and recent studies (Zarco-Tejada *et al.*, 2009) used 1 nm FWHM (full-width at half-maximum) airborne multispectral imagery acquired over crops for early stress detection, showing the feasibility of mapping fluorescence at 40 cm resolution using micro-hyperspectral imager on board an UAV (Zarco-Tejada *et al.*, 2012). The modeling study conducted by Zarco-Tejada *et al.* (2009) showed that the fluorescence using in-filling methods were little affected by structural changes of the canopy such as leaf area density.

According to these advances obtained in the early detection of water stress, canopy temperature, PRI and Fs may be useful indicators for the early detection of the water stress induced by *V. dahliae* infection in olive trees.

Literature cited

Ayres, P.G. (1978). Water relations of diseased plants. In Kozlowski, T.T. (Eds.), *Water Deficits and Plant Growth*, (vol. 5, pp. 1-60). London, United Kingdom: Academic Press.

Barranco, D. (1995). La elección varietal en España. *Olivae* 59:54-58.

Barranco, D. (2008). Variedades y patrones. In Barranco, D., Fernández-Escobar, R., & Rallo, L. (Eds.), *El cultivo del olivo*, 6th edition (pp. 63-92). Madrid, Spain: Mundi-Prensa and Junta de Andalucía.

Barranco, D., & Rallo, L. (2000). Olive cultivars in Spain. *HortTechnology* 10(1):107-110.

Bauriegel E., Giebel A., Geyer M., Schmidt, U., & Herppich, W.B. (2011). Early detection of *Fusarium* infection in wheat using hyper-spectral imaging. *Comput. Electron. Agr.* 75:304-312.

Belaj, A., Muñoz-Diez, C., Baldoni, L., Satovic, Z., & Barranco, D. (2010). Genetic diversity and relationships of wild and cultivated olives at regional level in Spain. *Sci. Hortic-Amsterdam.* 124:323-330.

Berni, J.A.J., Zarco-Tejada, P.J., Sepulcre-Cantó, G., Fereres, E., & Villalobos, F.J. (2009a). Mapping canopy conductance and CWSI in olive orchards using high resolution thermal remote sensing imagery. *Remote Sens. Environ.* 113:2380-2388.

Berni, J.A.J., Zarco-Tejada, P.J., Suárez, L., & Fereres, E. (2009b). Thermal and narrow-band multispectral remote sensing for vegetation monitoring from an unmanned aerial vehicle. *IEEE T. Geosci. Remote*. 47:722-738.

Besnard, G., Khadari, B., Navascués, M., Fernández-Mazuecos, M., El Bakkali, A., *et al.* (2013). The complex history of the olive tree: from Late Quaternary diversification of Mediterranean lineages to primary domestication in the northern Levant. *P. Roy. Soc. B-Biol.* 280:20122833.

Björkman, O., & Powles, S.B. (1982). Inhibition of photosynthetic reactions under water stress: Interaction with light level. *Planta* 161:490-504.

Blanco-López, M.A., Jiménez-Díaz, R.M., & Caballero, J.M. (1984). Symptomatology, incidence and distribution of Verticillium wilt of olive trees in Andalucia. *Phytopathol. Mediterr.* 23:1-8.

Bock, C.H., Poole, G.H., Parker, P.E., & Gottwald, T.R. (2010). Plant disease severity estimated visually, by digital photography and image analysis, and hyperspectral imaging. *Crit. Rew. Plant Sci.* 29:59-107.

Brodrick, H.T., Gilbertson, B., & Kreitzer, M.H. (1971). Advances in aerial photography. *SA Citrus J.* 449:9-13.

Bradford, K.J., & Hsiao, T.C. (1982). Physiological responses to moderate water stress. In Lange, O.L., Nobel, P.S., Osmond, C.B., & Ziegler, H. (Eds.), *Physiological plant ecology II: Water relations and carbon assimilation* (pp. 263-324). Berlin, Germany: Springer.

Calderón, R., Navas-Cortés, J.A., & Zarco-Tejada, P.J. (2014). Early detection and quantification of Verticillium wilt in olive using UAV and manned platforms to acquire hyperspectral and thermal imagery at local and regional scale. In *Proceedings of the 2nd International Conference on Robotics, Associated High-Technologies and Equipment for Agriculture and Forestry* (pp. 309-318). Madrid, Spain: RHEA Consortium.

Chen, B., Wang, K., Li, S., Wang, J., Bai, J., Xiao, C., & Lai, J. (2008). Spectrum characteristics of cotton canopy infected with Verticillium wilt and inversion of severity level. In Li, D. (Ed.), *Computer and Computing Technologies in Agriculture* (vol. 2, pp. 1169-1180). New York, NY, USA: Springer.

Chen, B., Li, S., Wang, K., Zhou, G., & Bai, J. (2011). Evaluating the severity level of cotton Verticillium using spectral signature analysis. *Int. J. Remote Sens.* 33:2706-2724.

Cohen, Y., Alchanatis, V., Meron, M., Saranga, Y., & Tsipris, J. (2005). Estimation of leaf potential by thermal imagery and spatial analysis. *J. Exp. Bot.* 56:1843-1852.

Consejería de Agricultura y Pesca (2012). Estudios y Estadísticas de la Consejería de Agricultura y Pesca, Sevilla. http://www.juntadeandalucia.es/agriculturaypesca/.

Cook, C.G., Escobar., D.E., Everitt, J.H., Cavazos, I., Robinson, A.F., *et al.* (1999). Utilizing airborne video imagery in kenaf management and production. *Ind. Crop Prod.* 19:205-210.

Dammer, K.H., Möller, B., Rodemann, B., & Heppner, D. (2011). Detection of head blight (*Fusarium* ssp.) in winter wheat by color and multispectral image analyses. *Crop Prot.* 30:420-428.

DeVay, J.E., Forrester, L.L., Garber, R.H., & Butterfield, E.J. (1974). Characteristics and concentration of propágulos of *Verticillium dahliae* in air-dried field soils in relation to the prevalence of Verticillium wilt in cotton. *Phytopathology* 64:22-29.

Dobrowsky, S.Z., Pushnik, J., Zarco-Tejada, P.J., & Ustin, S.L. (2005). Simple reflectance indices track heat and water stress induced changes in steady-state chlorophyll fluorescence at the canopy scale. *Remote Sens. Environ.* 9:403-414.

Evain, S., Flexas, J., & Moya, I. (2004). A new instrument for passive remote sensing: 2. Measurement of leaf and canopy reflectance changes at 531 mm and their relationship with photosynthesis and chlorophyll fluorescence. *Remote Sens. Environ.* 91:175-185.

FAO (2011). *FAO in the 21st Century: Ensuring Food Security in a Changing World*. Rome, Italy: Food and Agriculture Organization of the United Nations.

FAO (2012). The Statistical Database (FAOSTAT), Rome. http://faostat.fao.org.

Fereres, E., Orgaz, F., & González-Dugo, V. (2011). Reflection on food security under water scarcity. *J. Exp. Bot.* 62:4079-4086.

Flexas, J., Briantais, J.M., Cerovic, Z., Medrano, H., & Moya, I. (2000). Steady-state and maximum chlorophyll fluorescence responses to water stress in grapevine leaves: A new remote sensing system. *Remote Sens. Environ.* 73:282-297.

Flexas, J., Escalona, J.M., & Medrano, H. (1999). Water stress induces different levels of photosynthesis and electron transport rate regulation in grapevine. *Plant Cell Environ.* 22:39-48.

Flexas, J., Escalona, J.M., Evain, S., Gulias, J., Moya, I., Osmond, C.B., & Medrano, H. (2002). Steady-state chlorophyll fluorescence (Fs) measurements as a tool to follow variations of net CO_2 assimilation and stomatal conductance during water-stress in C-3 plants. *Physiol. Plantarum* 114(2):231-240.

Foley, J.A., Ramankutty, N., Brauman, K.A., Cassidy, E.S., Gerber, J.S., *et al.* (2011). Solutions for a cultivated planet. *Nature* 478:337-342.

Gamon, J.A., Peñuelas, J., & Field, C.B. (1992). A narrow-wave band spectral index that tracks diurnal changes in photosynthetic efficiency. *Remote Sens. Environ.* 41:35-44.

Gao, B.C. (1996). NDWI - A normalized difference water index for remote sensing f vegetation liquid water from space. *Remote Sens. Environ*. 58:257-266.

Godfray, H.C.J., Beddington, J.R., Crute, I.R., Haddad, L., Lawrence, D., *et al.* (2010). Food security: The challenge of feeding 9 billion people. *Science* 327:812-818.

Gregory, P.J., Johnson, S.N., Newton, A.C. & Ingram S.L. (2009). Integrating pest and pathogens into de climate change/ food security debate. *J. Exp. Bot.* 60:2827-2838.

Heald, C.M., Thames, W.H., & Wiegand, C.L. (1972). Detection of *Rotylenchulus reniformis* infestations by aerial infrared photography. *J. Nematol.* 4:298-300.

Heath, W.L., Haydock, P.P.J., Wilcox, A., & Evans, K. (2000). The potential use of spectral reflectance from the potato crop for remote sensing of infection by potato cyst nematodes. *Asp. Appl. Biol.* 60:185-188.

Herwitz, S.R., Johnson, L.F., Dunagan, S.E., Higgins, R.G., Sullivan, D.V., *et al.* (2004). Imaging from an unmanned aerial vehicle: Agricultural surveillance and decision support. *Comput. Electron. Agr.* 44:49-61.

Hillnhütter, C., Mahlein, A.-K., Sikora, R.A., & Oerke, E.-C. (2011). Remote sensing to detect plant stress induced by *Heterodera schachtii* and *Rhizoctonia solani* in sugar beet fields. *Field Crops Res.* 122:70-77.

Hillnhütter, C., Mahlein, A.-K., Sikora, R.A., & Oerke, E.-C. (2012). Use of imaging spectroscopy to discriminate symptoms caused by *Heterodera schachtii* and *Rhizoctonia solani* on sugar beet. *Precis. Agric.* 13(1):17-32.

Hillnhütter, C., Schweizer, A., Kühnhold, V., & Sikora, R.A. (2010). Remote sensing for the detection of soil-borne plant parasitic nematodes and fungal pathogens. In Oerke, E.-C., Gerhards, R., Menz, G., & Sikora, R.A. (Eds.), *Precision Crop Protection – the Challenge and Use of Heterogeneity* (pp.151-165). New York, NY, USA: Springer.

Hsiao, T.C., & Bradford, K.J. (1983). Physiological consequences of cellular water deficits. In Taylor, H.M., Jordan, W.R., & Sinclair, T.R. (Eds.), *Limitations to efficient water use in crop production* (pp. 227-265). Madison, WI, USA: ASA, CSSA, SSSA.

Hsiao, T.C., Fereres, E., Acevedo, E., & Henderson, D.W. (1976). Water stress and dynamics of growth and yield of crops. In Lange, O.L., Kappen, L., & Schulze, E.-D. (Eds.), *Water and plant life: Problems and modern approaches* (pp. 281-305). Berlin, Germany: Springer-Verlag.

Idso, S.B., Jackson, R.D., & Reginato, R. (1978). Extending the "degree day" concept of phenomenological development to include water stress effects. *Ecology* 59:431-433.

Idso, S.B., Jackson, R.D., Pinter, P.J., Reginato, R.J., & Hatfield, J.L. (1981). Normalizing the stress-degree-day parameter for environment variability. *Agric. Forest Meteorol.* 24:45-55.

Inoue, Y., Kimball, B.A., Jackson, R.D., Pinter, P.J., & Reginato, R.J. (1990). Remote estimation of leaf transpiration rate and stomatal resistence based on infrared thermometry. *Agric. Forest Meteorol.* 51:21-33.

IOC (2013). International Olive Council, Madrid. http://www.internationaloliveoil.org.

Jackson, R.D., & Pinter, P.J., Jr. (1981). Detection of water stress in wheat by measurement of reflected solar and emitted thermal IR radiation. In *Proc. Intern. Colloquium on spectral signatures of objects in remote sensing* (pp. 399-406). Versalle, France: Institut National de la Reserche Agronomique.

Jackson, R.D., Idso, S.B., Reginato, R.J., & Ehrler, W.L. (1977). Crop temperature reveals stress. *Crop Soils* 29:10-13.

Jackson, R.D., Idso, S.B., Reginato, R.J., & Pinter, P.J., Jr. (1981). Canopy temperature as a crop water stress indicator. *Water Resour. Res.* 17:1133-1138.

Jiménez-Díaz, R.M., Cirulli, M., Bubici, G., Jiménez-Gasco, L.M., Antoniou, P.P., & Tjamos E.C. (2012). Verticillium wilt, a major threat to olive production: Current status and future prospects for its management. *Plant Dis.* 96(3):304-329.

Jiménez-Díaz, R.M., Olivares-García, C., Landa, B.B., Jiménez-Gasco, M.M., & Navas-Cortés, J.A. (2011). Region-wide analysis of genetic diversity in *Verticillium dahliae* populations infecting olive in southern Spain and agricultural factors influencing the distribution and prevalence of vegetative compatibility groups and pathotypes. *Phytopathology* 101:304-315.

Jones, H.G. (1992*). Plant and microclimate*, 2nd edition. Cambridge, United Kingdom: Cambridge University Press.

Jones, H.G. (1999). Use of infrared thermography for estimation of stomatal conductance in irrigation scheduling. *Agric. Forest Meteorol.* 95:135-149.

Jones, H.G. (2004). Application of thermal imaging and infrared sensing in plant physiology and Ecophysiology. *Adv. Bot. Res.* 41:107-163.

Klosterman, S.J., Atallah, Z.K., Vallad, G.E., & Subbarao, K.V. (2009). Diversity, pathogenicity, and management of Verticillium species. *Annu. Rev. Phytopathol.* 47:39-62.

Krause, G.H., & Weis, E. (1984). Chlorophyll fluorescence as a tool in plant physiology. II. Interpretation of fluorescence signals. *Photosynth. Res.* 5:139-157.

Laudien, R., Bareth, G., & Doluschitz, R. (2004). Comparison of remote sensing based analysis of crop diseases by using high resolution multispectral and hyperspectral data – case study: *Rhizoctonia solani* in sugar beet. In Brandt, S.A. (Eds.), *Proceedings of 12th International Conference on Geoinfromatics* (pp. 670-676). Gävle, Sweden: Gävle University Press.

Lawrence, G.W., Kelley, A.T., King, R.L., Vickery, J., Lee, H.K., & McLean, K.S. (2004). Remote sensing and precision nematicide applications for *Rotylenchulus reniformis* management in cotton. In Cook, R., & Hunt, D.J. (Eds.), *Nematology monographs and perspectives* (vol. 2, pp. 13-21). Leiden, the Netherlands: Brill Academic Publishers.

Leinonen, I., & Jones, H.G. (2004). Combining thermal and visible imagery for stimulating canopy temperature and identifying plant stress. *J. Exp. Bot.* 55:1423-1431.

López-Escudero, F.J., & Mercado-Blanco, J. (2011). Verticillium wilt of olive: A case study to implement an integrated strategy to control a soil-borne pathogen. *Plant Soil* 344:1-50.

López-Escudero, F.J., del Rio, C., Caballero, J.M., & Blanco-López, M.A. (2004). Evaluation of olive cultivars for resistance to *Verticillium dahliae*. *Eur. J. Plant Pathol.* 110:79-85.

Lucena, C., Berni, J.A.J., Montes-Borrego, M., Trapero-Casas, J.L., Landa, B.B., Zarco-Tejada, P.J., & Navas-Cortés, J.A. (2009). High resolution thermal remote Sensing imagery for Verticillium wilt detection in olive. In *10th International Verticillium Symposium*, Corfu Island, Greece, 16-20 November, 2009.

Mahlein, A.-K., Oerke, E.-C., Steiner, U., & Dehne, H.-W. (2012). Recent advances in sensing plant diseases for precision crop protection. *Eur. J. Plant Pathol.* 133:197-209.

Mengistu, A., Tachibana, H., Epstein, A.H., Bidne, K.G., & Hatfield, J.D. (1987). Use of leaf temperature to measure the effect of brown stem rot and soil moisture stress and its relation to yields of soybeans. *Plant Dis.* 71:632-634.

Meroni, M., Picchi, V., Rossini, M., Cogliati, S., Panigada, C., *et al.* (2008a). Leaf level early assessment of ozone injuries by passive fluorescence and PRI. *Int. J. Remote Sens.* 29(17-18):5409-5422.

Meroni, M., Rossini, M., Guanter, L., Alonso, L., Rascher, U., Colombo, R., & Moreno, J. (2009). Remote sensing of solar-induced chlorophyll fluorescence: Review of methods and applications. *Remote Sens. Environ.* 113:2037-2051.

Meroni, M., Rossini, M., Picchi, V., Panigada, C., Cogliati, S., Nali, C., & Colombo, R. (2008b). Assessing steady-state fluorescence and PRI from hyperspectral proximal sensing as early indicators of plant stress: The case of ozone exposure. *Sensors* 8:1740-1754.

Navas-Cortés, J.A., Landa, B.B., Mercado-Blanco, J., Trapero-Casas, J.L., Rodríguez-Jurado, D., & Jiménez-Díaz, R.M. (2008). Spatiotemporal analysis of spread of infections by *Verticillium dahliae* pathotypes within a high tree density olive orchard in southern Spain. *Phytopathology* 98:167-180.

Newton, A.C., Johnson, S.N., & Gregory, P.J. (2011). Implications of climate change for diseases, crop yields and food security. *Euphytica* 179:3-18.

Nicolas, H., Rivoal, R., Duchesne, J., & Lili, Z. (1991). Detection of *Heterodera avenae* infestations on winter wheat by radiothermometry. *Rev. Nematol.* 14:285-290.

Nilsson, H.E. (1991). Hand-held radiometry and IR-thermography of plant diseases in field plot experiments. *Int. J. Remote Sens.* 12:545-557.

Nilsson, H.E. (1995). Remote sensing and image analysis in plant pathology. *Annu. Rev. Phytopathol.* 15:489-527.

Norman, G.G., & Fritz, N.L. (1965). Infrared photography as an indicator of disease and decline in citrus trees. *Proc. Florida State Hort. Soc.* 78:59-63.

Nutter, F.W., Tylka, G.L., Guan, J., Moreira, A.J.D., Marett, C.C., *et al.* (2002). Use of remote sensing to detect soybean cyst nematode-induced plant stress. *J. Namatol.* 34:222-231.

Nutter, F.W., Van Rij, N., Eggenberger, S.K., & Holah, N. (2010). Spatial & temporal dynamics of plant pathogens. In Oerke, E.-C., Gerhards, R., Menz, G., & Sikora, R.A. (Eds.), *Precision Crop Protection – the Challenge and Use of Heterogenety* (pp. 27-50). New York, NY, USA: Springer.

Oerke, E.-C, & Steiner, U. (2010). Potential of Digital Thermography for Disease Control. In Oerke, E.-C., Gerhards, R., Menz, G., & Sikora, R.A. (Eds.),

Precision Crop Protection – the Challenge and Use of Heterogeneity (pp.167-182). New York, NY, USA: Springer.

Oerke, E.-C. (2006). Crop losses to pests. *J. Agr. Sci.* 144:31-43.

Papageorgiu, G. (1975). Chlorophyll fluorescence; an intrinsic probe of photosynthesis. In Govindjee (Eds.), *Bioenergetics of photosynthesis* (pp. 319-371). New York, NY, USA: Academic Press.

Pegg, G.F., & Brady, B.L. (2002). *Verticillium Wilts*. Wallingford, United Kingdom: CABI Publishing.

Peguero-Pina, J.J., Morales, F., Flexas, J., Gil-Pelegrín, E., & Moya, I. (2008). Photochemistry, remotely sensed physiological reflectance index and de-epoxidation state of the xanthophyll cycle in *Quercus coccifera* under intense drought. *Oecologia* 156(1):1-11.

Peñuelas, J., Filella, I., Biel, C., Serrano, L., & Save, R. (1993). The reflectance at the 950-970 nm region as an indicator of plant water status. *Int. J. Remote Sens.* 14:1887-1905.

Peñuelas, J., Llusia, J., Piñol, J., & Filella, I. (1997). Photochemical reflectance index and leaf photosynthetic radiation use-efficiency assessment in Mediterranean trees. *Int. J. Remote Sens.* 18:2863-2868.

Pérez-Priego, O., Zarco-Tejada, P.J., Sepulcre-Cantó, G., Miller, J.R., & Fereres, E. (2005). Detection of water stress in orchard trees with a high-resolution spectrometer through chlorophyll fluorescence in-filling of the O_2-A band. *IEEE T. Geosci. Remote* 43:2860-2869.

Phalan, B., Balmford, A., Green, R.E., & Scharlemann, J.P.W. (2011). Minimising the harm to biodiversity of producing more food globally. *Food Policy* 36:S62-S71.

Pinter, P.J., Stanghellini, M.E., Reginato, R.J., Idso, S.B., Jenkins, A.D., & Jackson, R.D. (1979). Remote detection of biological stresses in plants with infrared thermometry. *Science* 205:585-587.

Raikes, C., & Burpee, L.L. (1998). Use of multispectral radiometry for assessment of Rhizoctonia blight in creeping bentgrass. *Phytopathology* 88:446-449.

Rallo, L. (2005). Variedades de olivo en España: una aproximación cronológica. In Rallo, L., Barranco, D., Caballero, J.M., del Río, C., Martín, A., Tous, J., & Trujillo, I. (Eds.), *Variedades de olivo en España* (pp. 17-44). Madrid, Spain: Junta de Andalucía, MAPA and Mundi-Prensa.

Reynolds, G.J., Windels, C.E., MacRae, I.V., & Laguette, S. (2012). Remote sensing for assessing Rhizoctonia crown and root rot severity in sugar beet. *Plant Dis.* 96:497-505.

Ruiz Torres, M.J. (2015). Balance fitosanitario del olivar andaluz en el año 2014. *Vida Rural* 392:36-42.

Sánchez Hernández, M.E., Ruiz Dávila, A., Pérez De Algaba, A., Blanco López, M.A., & Trapero Casas, A. (1998). Occurrence and etiology of death of young olive trees in southern Spain. *Eur. J. Plant Pathol.* 104:347-357.

Sankaran, S., Mishra, A., Ehsani, R., & Davis, C. (2010). A review of advanced techniques for detecting plant diseases. *Comput. Electro. Agr.* 72:1-13.

Schmitz, A., Kiewnik, S., Schlang, J., Schmidt, K., & Sikora, R.A. (2003). Use of remote sensing to identify the spatial distribution of sugar beet cyst nematode *Heterodera schachtii*. In Werner, A., & Jarfe, A. (Eds.), *Programme book of the joint conference of ECPA-ECPLF*. Wageningen, The Netherlands: Wageningen Academic Publishers.

Schmitz, A., Kiewnik, S., Schlang, J., & Sikora, R.A. (2004). Use of high resolution digital thermography to detect *Heterodera schachtii* infestation in sugar beets. *Comm. Appl. Biol. Sci.* 69:359-363.

Schowengerdt, R.A. (1997). *Remote sensing, models and methods for image processing*. San Diego, CA, USA: Elsevier.

Schreiber, L.R., & Green, R.J., Jr. (1963). Effect of root exudates on germination of conidia and microsc1erotia of *Verticillium albo-atrum* inhibited by the soil fungistatic principle. *Phytopathology* 53:260-264.

Sepulcre-Cantó, G., Zarco-Tejada, P.J., Jiménez-Muñoz, J.C., Sobrino, J.A., de Miguel, E., *et al.* (2006). Within-field thermal variability detection as function of water stress in *Olea europea* L. orchards with high resolution spatial remote sensing imagery. *Agric. Forest Meteorol.* 136:31-44.

Sepulcre-Cantó, G., Zarco-Tejada, P.J., Jiménez-Muñoz, J.C., Sobrino, J.A., Soriano, M.A., *et al.* (2007). Monitoring yield and fruit quality parameters in open-canopy tree crops under water stress. Implications for ASTER. *Remote Sens. Environ.* 107:455-470.

Sepulcre-Cantó, G., Zarco-Tejada, P.J., Sobrino, J.A., Berni, J.A.J., Jiménez-Muñoz, J. C., & Gastellu-Etchegorry, J.P. (2009). Discriminating irrigated and rainfed olive

orchards with thermal ASTER imagery and DART 3D simulations. *Agric. Forest Meteorol.* 149:962-975.

Soukupová, J., Cséfalvay, L., Urban, O., Kosvancová, M., Marek, M., Rascher, U., & Nedbal, L. (2008). Annual variation of the steady-state chlorophyll fluorescence emission of evergreen plants in temperate zone. *Funct. Plant Biol.* 35:63-76.

Steiner, U., Buerling, K., & Oerke, E.-C. (2008). Sensor use in plant protection. *Gesunde Pflanz.* 60(4):131-141.

Suárez, L., Zarco-Tejada, P.J., Berni, J.A.J., González-Dugo, V., & Fereres, E. (2009). Modelling PRI for water stress detection using radiative transfer models. *Remote Sens. Environ*. 113:730-740.

Suárez, L., Zarco-Tejada, P.J., González-Dugo, V., Berni, J.A.J., Sagardoy, R., Morales, F., & Fereres, E. (2010). Detecting water stress effects on fruit quality in orchards with time-series PRI airborne imagery. *Remote Sens. Environ.* 114:286-298.

Suárez, L., Zarco-Tejada, P.J., Sepulcre-Cantó, G., Pérez-Priego, O., Miller, J.R., Jiménez-Muñoz. J.C., & Sobrino, J. (2008). Assessing canopy PRI for water stress detection with diurnal airborne imagery. *Remote Sens. Environ.* 112:560-575.

Sugiura, R., Noguchi, N., & Ishii, K. (2005). Remote-sensing technology for vegetation monitoring using an unmanned helicopter. *Biosyst. Eng.* 90:369-379.

Sun, P., Grignetti, A, Liu, S., Casacchia, R., Salvatori, R., Pietrini, F., Loreto, F., & Centritto, M. (2008). Associated changes in physiological parameters and spectral reflectance indices in olive (*Olea europaea* L.) leaves in response to different levels of water stress. *Int. J. Remote Sens.* 29(6):1725-1743.

Talboys, P.W. (1962). Systemic movement of some vascular pathogens. *T. Brit. Mycol. Soc.* 45:280-281.

Taubenhaus, J.J., Ezekiel, W.N., & Neblette, C.B. (1929). Airplane photography in the study of cotton root rot. *Phytopathology* 19:1025-1029.

Teng, P.S. (1987). *Crop loss assessment and pest management*. St. Paul, MN, USA: APS Press.

Thenot, F., Méthy, M., & Winkel, T. (2002). The photochemical reflectance index (PRI) as a water-stress index. *Int. J. Remote Sens.* 23(23):5135-5139.

Tilman, D., Balzer, C., Hill, J., & Befort, B.L. (2011). Global food demand and the sustainable intensification of agriculture. *P. Natl. Acad. Sci. USA*. 108:20260-20264.

Tjamos, E.C., & Jiménez-Díaz, R.M. (1998). Management of disease. In Hiemstra, J.A., & Harris, D.C. (Eds.), *A compendium of Verticillium wilts in tree species* (pp. 55-57). Wageningen, The Netherlands: Ponsen and Looijen.

Tsror, L. (Lahkim) (2011). Review: Epidemiology and control of *Verticillium* wilt on olive. *Israel J. Plant Sci.* 59:59-69.

Tu, J.C., & Tan, C.S. (1985). Infrared thermometry for determination of root rot severity in bean. *Phytopathology* 75:840-844.

Villalobos, F.J., Testi, L., Hidalgo, J., Pastor, M., & Orgaz, F. (2006). Modelling potential growth and yield of olive (*Olea europaea* L.) canopies. *Eur. J. Agron.* 24:296-303.

Wang, D., Kurle, J.E., Estevez de Jensen, C., & Percich, J.A. (2004). Radiometric assessment of tillage and seed treatment effect on soybean root rot caused by *Fusarium* spp. in central Minnesota. *Plant Soil* 258:319-331.

Winkel, T., Méthy, M., & Thénot, F. (2002). Radiation use efficiency, chlorophyll fluorescence, and reflectance indices associated with ontogenic changes in water-limited *Chenopodium quinoa* leaves. *Photosynthetica* 40(2):227-232.

Wolfe, D.W., Fereres, E., & Voss, R.E. (1983). Growth and yield response of two potato cultivars to various levels of water applied. *Irrigation Sci.* 3:211-222.

Yadeta, K.A., & Thomma, B.P.H.J. (2013). The xylem as battleground for plant hosts and vascular wilt pathogens. *Front. Plant Sci.* 4:97.

Yahyaoui, W., Harnois, J., & Carpentier, R. (1998). Demonstration of thermal dissipation of absorbed quanta during energy-dependent quenching of chlorophyll fluorescence in photosynthetic membranes. *FEBS Letters* 440(1-2):59-63.

Zarco-Tejada, P.J., Berni, J.A.J., Suárez, L., Sepulcre-Cantó, G., Morales, F., & Miller, J.R. (2009). Imaging chlorophyll fluorescence from an airborne narrow-band multispectral camera for vegetation stress detection. *Remote Sens. Environ.* 113:1262-1275.

Zarco-Tejada, P.J., González-Dugo, V., & Berni, J.A.J. (2012). Fluorescence, temperature and narrow-band indices acquired from a UAV for water stress detection using a hyperspectral imager and a thermal camera. *Remote Sens. Environ.* 117:322-337.

CHAPTER 2

OBJECTIVES

CHAPTER 2: Objectives

Due to the reasons explained in Chapter 1, the early detection of *Verticillium dahliae* infection in olive would help to avoid the spread of the pathogen into new areas, especially if they are free of *V. dahliae*, and to improve the efficiency of available control measures. Therefore, the main objective of this Thesis was to evaluate the use of high-resolution thermal and hyperspectral remote sensing imagery as a tool to detect Verticillium wilt infection and severity in olive orchards and larger areas. In addition, the effect of soil temperature on Verticillium wilt development was assessed in order to determine the effects of this environmental factor on disease development and the feasibility of related stress parameters used in the remote sensing studies to detect *V. dahliae* infection in a range of biological combinations of pathogen and plant genotypes interactions. These results could be of use to better understanding the differential geographic distribution of *V. dahliae* pathotypes and to assess the potential effect of climate change on the development of Verticillium wilt of olive under future climate change scenarios.

Thus, the following specific objectives were identified:

1. To quantify the combined effects of biotic factors (*Verticillium dahliae*-pathotype virulence and olive-cultivar susceptibility) and abiotic factors (soil temperature) on the development of Verticillium wilt and olive tree growth.

2. To determine the relationship between stress indicators including several remote sensing parameters and Verticillium wilt severity at leaf level.

3. To evaluate the use of high-resolution thermal imagery and physiological indices calculated from hyperspectral imagery as indicators of Verticillium wilt infection and severity in olive orchards.

4. To develop a robust and accurate method for the automatic detection of *V. dahliae* infection and severity in olive growing areas using remote sensing at large scale.

2.1. Outline of the thesis

This Thesis is presented as chapters, each one dealing with the objectives previously described.

Chapter 3 approaches objectives 1 and 2. In a first phase, the effect of soil temperature on Verticillium wilt development caused by defoliating (D) and non-defoliating (ND) *V. dahliae* pathotypes in olive cultivars (cv.) Picual and Arbequina was explored. In a second stage, several parameters related with stress (i.e., temperature, steady-state chlorophyll fluorescence Fs, photochemical reflectance index PRI, chlorophyll content and ethylene production) were periodically measured at leaf level to assess the stress caused by *V. dahliae* in olive plants at different soil temperatures and the relationship between such parameters and disease severity. To achieve this, olive plants of cv. Arbequina and cv. Picual grew in soil infested by the D or ND pathotypes of *V. dahliae* under controlled conditions in soil tanks with a range of soil temperatures from 16 to 32 ºC. This chapter has been published in the research journal *PLoS ONE*:

> **Calderón, R.**, Lucena, C., Trapero-Casas, J. L., Zarco-Tejada, P. J., & Navas-Cortés, J. A. (2014). **Soil Temperature Determines the Reaction of Olive Cultivars to *Verticillium dahliae* Pathotypes**. *PLoS ONE* 9(10):e110664, DOI: 10.1371/journal.pone.0110664

Chapter 4 attends to objective 3, focusing on the evaluation of canopy temperature and physiological indices (chlorophyll fluorescence, structural, xanthophyll, chlorophyll a+b, carotenoids and blue/green/red indices) calculated from high-resolution thermal, multispectral and hyperspectral imagery for the early detection of water stress caused by *Verticillium dahliae* infection and disease severity in two olive orchards with different agronomic characteristics. To attain this, time series of airborne thermal, multispectral and hyperspectral imagery was acquired with unmanned aerial vehicles (UAVs) in three consecutive years and related to Verticillium wilt severity at the time of the flights. In addition, field measurements at leaf and tree-crown levels were conducted in one of the olive orchards to support the results obtained from imagery and to confirm that these results are due to Verticillium wilt and not simply influences by structural effects driven by the water stress induced by *V. dahliae* infection. This chapter has been published in the research journal *Remote Sensing of Environment*:

> **Calderón, R.**, Navas-Cortés, J. A., Lucena, C., & Zarco-Tejada, P. J. (2013). **High-resolution airborne hyperspectral and thermal imagery for early detection of *Verticillium* wilt of olive using fluorescence, temperature and narrow-band spectral indices**. *Remote Sensing of Environment* 139:231-245.

Chapter 5 addresses objective 4 and proposes a methodology for the automatic classification of *V. dahliae* infection and severity of disease symptoms using high-resolution thermal and hyperspectral imagery acquired with a manned platform over a 3,000-ha commercial olive area. Linear discriminant analysis (LDA) and support vector

machine (SVM) classification methods were assessed to discriminate among Verticillium wilt severity levels exploiting the combined information of the canopy temperature and physiological indices calculated from the imagery. This work completed the previous one conducted in Chapter 4 at orchard scale, extrapolating the methods to larger areas comprising several olive orchards differing in soil and crop management characteristics. This chapter has been published for publication in the research journal *Remote Sensing*:

> **Calderón, R.**, Navas-Cortés, J. A., & Zarco-Tejada, P. J. (2015). **Early detection and quantification of Verticillium wilt in olive using hyperspectral and thermal imagery acquired by manned platforms at large scale**. *Remote Sensing* 7(5):5584-5610, DOI: 10.3390/rs70505584.

Chapter 6 summarizes the conclusions of each chapter and the general conclusions of this Thesis.

CHAPTER 3

Soil temperature determines the reaction of olive cultivars to *Verticillium dahliae* pathotypes

Authors: Calderón, R., Lucena, C., Trapero-Casas, J.L., Zarco-Tejada, P.J., & Navas-Cortés, J.A.

Instituto de Agricultura Sostenible (IAS), Consejo Superior de Investigaciones Científicas (CSIC), Apartado 4084, Campus de Excelencia Internacional Agroalimentario, Córdoba, Spain.

Published in: *PLoS ONE* 9(10):e110664

DOI: 10.1371/journal.pone.0110664

CHAPTER 3: Soil temperature determines the reaction of olive cultivars to *Verticillium dahliae* pathotypes

Resumen

Antecedentes: El desarrollo de la Verticilosis en olivo, causada por el hongo de suelo *Verticillium dahliae*, puede estar influenciado por factores bióticos y abióticos. En este estudio se demostraron i) los efectos combinados de los factores bióticos (i.e., virulencia de patotipo y susceptibilidad de cultivar) y abióticos (i.e., temperatura de suelo) en el desarrollo de la enfermedad y ii) la relación entre la severidad de la enfermedad y varios parámetros de teledetección e indicadores de estrés de la planta.

Metodología: Las plantas de olivo de los cultivares Arbequina y Picual se inocularon con aislados de los patotipos de *V. dahliae* defoliante y no defoliante y se cultivaron en tanques de suelo con temperaturas de 16 a 32ºC. La evolución de la enfermedad se correlacionó con parámetros de estrés de la planta (i.e., temperatura foliar, fluorescencia clorofílica en estado estacionario, photochemical reflectance index, contenido de clorofila, y producción de etileno) y parámetros relacionados con el crecimiento de la planta (i.e., longitud de cubierta y peso seco).

Resultados: El desarrollo de la enfermedad en plantas infectadas por el patotipo defoliante fue más rápido y severo en Picual. Los modelos estimaron que la infección por el patotipo defoliante fue favorecida por temperaturas de suelo de 16 a 24ºC en cv. Picual y de 20 a 24ºC en cv. Arbequina. En el patotipo no defoliante, temperaturas de suelo de 16 a 20ºC fueron las más favorables para la infección. La relación entre los parámetros relacionados con el estrés y la severidad de la enfermedad determinada por regresión logística multinomial y árboles de clasificación fue capaz de detectar los efectos de la infección por *V. dahliae* y la colonización del flujo de agua que finalmente causa estrés hídrico.

Conclusiones: El contenido de clorofila, la fluorescencia clorofílica en estado estacionario, y la temperatura foliar fueron los mejores indicadores para la detección de la Verticilosis en etapas tempranas del desarrollo de la enfermedad, mientras que la producción de etileno y el photochemical reflectance index fueron indicadores para la detección de la enfermedad en etapas avanzadas. Estos resultados aportan una mejor comprensión de la distribución geográfica diferencial de los patotipos de *V. dahliae* y evalúan el efecto potencial del cambio climático en el desarrollo de la Verticilosis.

Abstract

Background: Development of Verticillium wilt in olive, caused by the soil-borne fungus *Verticillium dahliae*, can be influenced by biotic and environmental factors. In this study we modeled i) the combined effects of biotic factors (i.e., pathotype virulence and cultivar susceptibility) and abiotic factors (i.e., soil temperature) on disease development and ii) the relationship between disease severity and several remote sensing parameters and plant stress indicators.

Methodology: Plants of Arbequina and Picual olive cultivars inoculated with isolates of defoliating and non-defoliating *V. dahliae* pathotypes were grown in soil tanks with a range of soil temperatures from 16 to 32ºC. Disease progression was correlated with plant stress parameters (i.e., leaf temperature, steady-state chlorophyll fluorescence, photochemical reflectance index, chlorophyll content, and ethylene production) and plant growth-related parameters (i.e., canopy length and dry weight).

Findings: Disease development in plants infected with the defoliating pathotype was faster and more severe in Picual. Models estimated that infection with the defoliating pathotype was promoted by soil temperatures in a range of 16 to 24ºC in cv. Picual and of 20 to 24ºC in cv. Arbequina. In the non-defoliating pathotype, soil temperatures ranging from 16 to 20ºC were estimated to be most favorable for infection. The relationship between stress-related parameters and disease severity determined by multinomial logistic regression and classification trees was able to detect the effects of *V. dahliae* infection and colonization on water flow that eventually cause water stress.

Conclusions: Chlorophyll content, steady-state chlorophyll fluorescence, and leaf temperature were the best indicators for Verticillium wilt detection at early stages of disease development, while ethylene production and photochemical reflectance index were indicators for disease detection at advanced stages. These results provide a better understanding of the differential geographic distribution of *V. dahliae* pathotypes and to assess the potential effect of climate change on Verticillium wilt development.

Received: 19 April 2014 / Accepted: 24 September 2014 / Published: 17 October 2014

3.1. Introduction

Verticillium wilt (VW) of olive (*Olea europaea* L.), caused by the fungus *Verticillium dahliae* Kleb., is the most important soil-borne disease affecting olive trees worldwide (Tsror, 2011; Jiménez-Díaz *et al.*, 2012) and can cause severe yield losses and plant death (Levin *et al.*, 2003). The disease was first observed in Italy in 1946 (Ruggieri, 1946) and is now present in many Mediterranean countries and in California, USA

(Jiménez-Díaz *et al.*, 2012). In Spain, the spread of Verticillium wilt in olive trees has been associated with the expansion of olive cultivation and changes in cropping practices aimed at increasing yields (Jiménez-Díaz *et al.*, 2011). Such changes include the use of self-rooted planting stocks to establish high-density plantings, drip irrigation, reduced or no tillage, and high inputs of fertilizer in newly cultivated soils or fertile soils (Villalobos *et al.*, 2006) previously cropped with plants susceptible to *V. dahliae*, such as cotton (Jiménez-Díaz *et al.*, 2011).

Microsclerotia, the long-lasting surviving structures of *V. dahliae*, constitute the main potential infective inoculum of the pathogen in field soils, where it can survive for up to 15 years (Wilhelm, 1955). These structures germinate multiple times in response to root exudates (Schreiber and Green, 1963) and favorable soil environmental conditions, forming hyphae that penetrate the plant root, grow across the root cortex, and upon reaching the xylem vessels facilitate the rapid upward spread of the pathogen by conidia transported in the transpiration stream (Talboys, 1962). As a result of xylem colonization by the pathogen, water flow decreases, leading to water stress (Ayres, 1978). Infection with *V. dahliae* in olive trees has resulted in two main disease syndromes, namely defoliating (D) and non-defoliating (ND), which are induced by specific D and ND *V. dahliae* pathotypes, respectively (Navas-Cortés *et al.*, 2008; Jiménez-Díaz *et al.*, 2012). The D syndrome is characterized by early drop of asymptomatic green leaves from individual twigs and branches, eventually leading to complete defoliation and necrosis (Jiménez-Díaz *et al.*, 2012). These symptoms can develop from late fall to late spring (Navas-Cortés *et al.*, 2008). Conversely, the ND syndrome comprises two symptom complexes: (i) apoplexy, a rapid and extensive dieback of twigs and branches of olive trees without loss of leaves occurring in late winter, and (ii) slow decline, mainly characterized by flower mummification and necrosis of inflorescences along with leaf chlorosis and necrosis (Jiménez-Díaz *et al.*, 2012), which occurs during springtime (Navas-Cortés *et al.*, 2008). Infections with the D pathotype can be lethal to the plant, whereas ND-infected olive trees may eventually show remission from symptoms (Jiménez-Díaz *et al.*, 1998; Levin *et al.*, 2003). D and ND *V. dahliae* pathotypes also have different modes of dispersal and produce different spatial patterns of disease (Navas-Cortés *et al.*, 2008). Infections with the D pathotype are of greater concern because the pathogen can spread rapidly over short and relatively long distances through windblown infected leaves that fall early and in large numbers from diseased trees (Navas-Cortés *et al.*, 2008). Planting resistant cultivars is the most effective measure for controlling and limiting the spread of Verticillium wilt (Jiménez-Díaz *et al.*, 2012). However, the most widely used olive cultivars in Spain (i.e., Picual and Arbequina) have been found to be highly susceptible and susceptible to D *V. dahliae*, respectively, and susceptible and moderately resistant to ND *V. dahliae*, respectively, under controlled conditions in artificial inoculation tests (López-Escudero *et al.*, 2004).

A recent study on Verticillium wilt in olive trees has shown that overall disease incidence is related to initial inoculum density in the soil (López-Escudero and Blanco-López, 2007). However, the development of symptoms in relation to inoculum density is variable and strongly influenced by environmental and soil conditions (DeVay *et al.*, 1974). Soil temperature is a critical factor for the development of Verticillium wilt and fungal growth (Pegg and Brady, 2002). Using soil tanks, McKeen (1943) found that infection of potato by *V. albo-atrum* occurred between 12 and 32ºC, but symptom expression was greatest between 20 and 28ºC. In southern Spain, Bejarano-Alcázar *et al.* (1996) reported that the optimal temperature for in vitro growth of *V. dahliae* isolates from cotton ranged from 24 to 27ºC in the D pathotype and from 21 to 24ºC in the ND pathotype. In China, Xu *et al.* (2012) determined that the optimal growth temperature for *V. dahliae* isolates of the D and ND pathotype was 25ºC, although D pathotype isolates can adapt well to high temperatures and severely infect cotton at temperatures ranging from 25 to 30ºC. In olive plants, development of Verticillium wilt is favored by air and soil temperatures close to the optimal growth range of *V. dahliae* (Jiménez-Díaz *et al.*, 1998). In Mediterranean-type climates, severity of Verticillium wilt attacks is favored by moderate air temperatures during spring, but high summer temperatures suppress further development of the disease (Levin *et al.*, 2003; Navas-Cortés *et al.*, 2008). Nevertheless, very little is known about the influence of the physical environment on Verticillium wilt in olive trees, which limits our understanding of the disease (Jiménez-Díaz *et al.*, 2012).

In plants, water stress caused either by *V. dahliae* infection or drought induces stomatal closure, which reduces the transpiration rate (Ayres, 1978). As a result, evaporative cooling decreases and leaf temperature increases. In the past, this increase in leaf temperature has been detected early using thermal infrared radiation (Jackson and Pinter, 1981) recorded by spectrometers at ground level. The visible part of the spectrum has also been used for early water stress detection based on indices that use bands at specific wavelengths in which photosynthetic pigments are affected by stress. An example of such indices is the photochemical reflectance index (PRI), a narrowband spectral index (Gamon *et al.*, 1992) that is sensitive to the epoxidation state of xanthophyll-cycle pigments and to photosynthetic efficiency, serving as a proxy for water stress detection at leaf level (Thenot *et al.*, 2002). Another indicator of water stress is chlorophyll fluorescence emission, as shown by several laboratory studies that have found it to be strongly correlated with photosynthesis and other physiological processes (Papageorgiu, 1975). Over the last ten years, scientific interest in steady-state chlorophyll fluorescence (Fs) (i.e., fluorescence emitted under constant illumination without saturation flashes) has increased because measurements of Fs do not require high-energy sources and can be conducted remotely using active or passive methods (Flexas *et al.*, 2000). In particular, leaf-level Fs measurements obtained with instruments known as pulse amplitude modulating (PAM) fluorometers have been used successfully to detect plant water stress (Flexas *et al.*, 2000). In fact, Minolta Corporation developed a portable chlorophyll meter

(SPAD) in the 1990s to take rapid measurements of chlorophyll content in leaves. This instrument uses two light-emitting diodes (650 and 940 nm) and a photodiode detector to measure transmission of red and infrared light through plant leaves. Given that there is a close relationship between leaf chlorophyll content and the output of the SPAD meter (Fanizza *et al.*, 1991), such measurements have been used to assess stress in crops (Fanizza *et al.*, 1991; Hayat *et al.*, 2008), revealing that water stress levels decrease chlorophyll content in leaves and consequently SPAD readings.

Leaf-level remote sensing studies have been conducted to detect and assess diseases in various crops. Most of these studies have focused on foliar pathogens in annual crops. Leaf temperature has been shown to successfully detect water stress caused by soil-borne pathogens, as mentioned above. In fact, Pinter *et al.* (1979) recorded leaf temperatures 3-4ºC higher than those of healthy plants in sugar beet and cotton crops affected by *Pythium aphanidermatum* and *Pymatotrichum omnivorum*, respectively. Other examples of leaf temperature measurements for the detection of root diseases include beans infected by *Fusarium solani*, *Pythium ultimum*, and *Rhizoctonia solani* (Tu and Tan, 1985), soybeans affected by brown stem rot caused by *Phialophora solani* (Mengistu *et al.*, 1987), and wheat with moderate takeall symptoms caused by *Gaeumannomyces graminis* var. *tritici* (Nilsson, 1991). As regards *V. dahliae* infection, Nilsson (1995) reported that infected oilseed rape plants exhibited leaf temperatures 5-8ºC higher than those of non-infected plants. Calderón *et al.* (2013) found increases of 2ºC at early stages of Verticillium wilt development in olive trees under field conditions. Chlorophyll fluorescence was also found to be a good indicator for detecting Verticillium wilt at early stages of the disease, while the photochemical reflectance and chlorophyll indices were good indicators for detecting the disease at advanced stages (Calderón *et al.*, 2013).

The objectives of this study were (i) to quantify the combined effects of biotic factors (i.e., pathotype virulence and cultivar susceptibility) and abiotic factors (i.e., soil temperature) on the development of Verticillium wilt and olive tree growth and (ii) to determine the relationship between stress indicators including several remote sensing parameters and VW severity according to the hypothesis that thermal, reflectance, and fluorescence measurements are sensitive to physiological changes induced by infection and colonization by *V. dahliae* pathotypes.

3.2. Materials and Methods

3.2.1. *Verticillium dahliae* isolates, olive plants, inoculation, and growth conditions

Olive plants were inoculated with *V. dahliae* isolates V138 (D) and V176 (ND), which have been characterized in previous studies (Mercado-Blanco *et al.*, 2003) and are deposited in the culture collection of the *Departamento de Protección de Cultivos* (Crop Protection Department) of the *Instituto de Agricultura Sostenible* (IAS-CSIC) in Cordoba, Spain. Isolates were stored by covering cultures on plum extract agar with liquid paraffin and keeping them at 4ºC in the dark. Active cultures of isolates were obtained on chlortetracycline-amended water agar (1 l of distilled water, 20 g of agar, 30 mg of chlortetracycline) and were further subcultured on Potato Dextrose Agar (PDA; Difco Laboratories, Detroit, USA). Cultures on PDA were grown for 7 days at 24ºC in the dark.

Eight-month-old plants of olive cvs. Arbequina and Picual were used. Plants were obtained by micropropagation techniques and provided by Cotevisa (L'Alcudia, Valencia, Spain). Arbequina and Picual are olive cultivars grown extensively throughout Spain (Barranco *et al.*, 2004). Picual plants were inoculated with both *V. dahliae* pathotypes, while Arbequina plants were inoculated with the D isolate only.

Inocula of *V. dahliae* were produced in an autoclaved cornmealsand (CMS) mixture in flasks incubated at 24±1ºC in the dark for 6 weeks. Infested CMS substrate was mixed thoroughly with an autoclaved soil mixture (clay loam/sand/peat at 1:1:1 vol/vol/vol) at a rate of 1:10 (wt/wt) to reach an inoculum density of approximately $4x10^4$ CFU/g of soil for each of the *V. dahliae* isolates. Non-infested CMS mixed with the autoclaved soil mixture at the same rate explained above served as control. Plants were grown in soil tanks (Frisol S.A., Córdoba, Spain) placed inside a walk-in growth chamber adjusted to 24±1ºC, 40 to 70% relative humidity, and a 14-h photoperiod of fluorescent light at 360 $\mu E\ m^{-2} \cdot s^{-1}$ for 3 months. Pots with soil and plant roots were set inside the soil tanks at a constant temperature of 16, 20, 24, 28 and 32ºC, with a maximum variation of ±1ºC for each of temperatures. Plants were watered daily as needed and fertilized weekly with 100 ml of Hoagland's nutrient solution (Hoagland and Arnon, 1950).

The experiment consisted of a three-way factorial treatment design with pathotype of *V. dahliae*, olive cultivar, and soil temperature as factors. For each soil temperature there were ten and six replicated pots (one plant per pot) for inoculated and non-inoculated plants, respectively, in a completely randomized design. The full experiment was repeated twice.

3.2.2. Disease assessment

Incidence (0 = plant showing no disease symptoms; 1 = plant showing disease symptoms) and severity of symptoms were assessed at 2- to 3-day intervals throughout the duration of the experiment, 3 months after inoculation. Disease severity was assessed by visually observing foliar symptoms in each individual plant and rating them on a 0 to 4 scale according to the percentage of foliage with disease symptoms, where 0 = 0%, 1 = 1 to 33%, 2 = 34 to 66%, 3 = 67 to 100%, and 4 = dead plant (Mercado-Blanco *et al.*, 2003). Symptoms caused by the ND pathotype consisted on a dieback of twigs and branches where leaves turned light-brown, rolled back toward the abaxial side, dried up and remained attached to the symptomatic shoots; whereas, those caused by the D pathotype were characterized by early drop of green, infected leaves that eventually gave rise to complete defoliation and necrosis of branches. Upon termination of the experiments, colonization of plant tissues by *V. dahliae* was determined in each plant by isolating the fungus on water agar amended with Aureomycin (1 l of distilled water, 20 g of agar, 30 mg of aureomycin). For each plant, six 5-mm-long stem pieces representative of the lower, middle and upper parts were thoroughly washed under running tap water for 30 min. The surface of the samples was disinfested in 0.5% NaClO for 1.5 min; next, the samples were rinsed with sterile water, plated onto the medium, and incubated at 24ºC in the dark for 7 days (Mercado-Blanco *et al.*, 2003; Navas-Cortés *et al.*, 2008). Colonies of *V. dahliae* were identified by microscopic observation of verticillate conidiophores and formation of microsclerotia. Data from the stem isolations of the pathogen were used to calculate the intensity of stem vascular colonization, determined as the percentage of stem pieces from which the pathogen was isolated.

3.2.3. Disease, stress, plant growth-related parameters, and data analyses

3.2.3.1. Relationship between disease development and parameters associated with disease progress curves

Disease progress curves were obtained from accumulated disease severity scores over time in days from the date of inoculation. The nonlinear form of the Gompertz model was evaluated for goodness of fit to disease severity progress data using nonlinear regression analyses. In the Gompertz equation,

$$DS(t) = K \exp[-B \exp(-r\, t)] \qquad [3.1]$$

where DS = disease severity, K = asymptote parameter, B = constant of integration, r = relative rate of disease increase, and t = time of disease assessment in days after inoculation.

To further assess disease development, four additional variables associated with disease progression were explored. These variables included (i) the incubation period (IP), established as the time in days to first symptoms or its reciprocal ($IP_R = 1/IP$); (ii) the final disease incidence and severity assessed at the end of the experiment; (iii) the standardized area under the disease severity progress curve (SAUDPC), calculated using the trapezoidal integration method standardized by duration of disease development in days (Simko and Piepho, 2011); (iv) the intrinsic rate of disease increase (*rho*) parameter estimates of the Gompertz model fitted to the disease severity progress data; and (v) the intensity of stem vascular colonization determined as the percentage of stem pieces from which the pathogen was isolated.

3.2.3.2. Leaf-level stress-related parameters

In addition to disease-associated parameters, several stress-related parameters were measured in six leaves of each of ten (inoculated) and six (non-inoculated, control) plants for each soil temperature and olive cultivar-*V. dahliae* pathotype combination. All measurements were taken at 2-week intervals, starting 20 days after inoculation until the end of the experiment, and comprised (i) leaf temperature; (ii) leaf chlorophyll fluorescence; (iii) leaf photochemical reflectance index; (iv) leaf chlorophyll content (through SPAD readings); and (v) ethylene production. For each stress-related parameter, average daily increase was determined as the standardized area under the parameter value progress curve over the observation period, calculated with the trapezoidal method. Such increase was used to assess the relationship between stress-related parameters and soil temperature and differences between experimental treatments in such parameters. Leaf temperature and steady-state chlorophyll fluorescence measurements were conducted with the PAM-2100 pulse-amplitude modulated fluorometer (Heinz Walz GMBH, Effeltrich, Germany). Steady-state chlorophyll fluorescence was also assessed separately with a second instrument designed to measure chlorophyll fluorescence (FluorPen, Photon System Instruments, Brno, Czech Republic). In addition, measurements of the leaf photochemical reflectance index (Gamon *et al.*, 1992), calculated as $(R_{570}-R_{531})/(R_{570}+R_{531})$ (Suárez *et al.*, 2008, 2009; Zarco-Tejada *et al.*, 2012), were obtained with a custom-designed instrument to measure the R531 and R570 spectral bands with a bandwidth of 10 nm (PlantPen, Photon System Instrument, Brno, Czech Republic). Leaf chlorophyll content was obtained with the SPAD-502 chlorophyll meter (Minolta Corp., Ramsey, NJ, USA). This instrument was used preferentially because of the strong relationship between its digital readings and real leaf chlorophyll content, as demonstrated by several authors (e.g., Yadava, 1986; Marquard and Tipton, 1987). Ethylene production was determined in the two youngest fully expanded leaves in the upper part of the plant. Leaves were separated from the stem and enclosed in 3-ml test tubes containing 50 ml tap water. Tubes were sealed with rubber caps and incubated in the dark at 24ºC for 24 h. Before sampling, the test tubes were stirred to favor the diffusion of ethylene gas into the

water. Gas samples were withdrawn from the incubation tubes with a 1 ml gas-tight syringe and assayed with a Hewlett Packard gas chromatograph (Model 5890A), as previously described (Romera *et al.*, 1999).

3.2.3.3. Plant growth-related parameters

At the end of the experiments, plants were removed from the soil and their roots were washed free of soil. We measured the weight of fresh roots and dry and fresh aerial plant parts as well as the length of stems and shoots of individual plants. For this latter parameter, we calculated a daily growth rate relative to the initial values.

3.2.3.4. Relationship between disease, stress and plant growth-related parameters, and soil temperature

Three functions were used to describe the effects of soil temperature on disease, stress, and plant growth-related parameters for the different olive cultivar-pathogen pathotype combinations. We used the following reverse sigmoid function to determine the relationship between disease incidence, disease severity, and intensity of stem vascular colonization:

$$Y_T = f(T) = a\, k^n / (a^n + T^n) \qquad [3.2]$$

where Y_T is the response of disease-related parameters to soil temperature (T), a determines the maximum asymptote, and k is the half maximum parameter.

For the remaining disease-related parameters and leaf temperature measurements, we used the modified beta function (Hau, 1988):

$$Y_T = f(T) = G[(T - T_{min})/(T_{opt} - T_{min})]^{[H(Topt-Tmin)/(Tmax-Topt)]}[(T_{max} - T)/(T_{max} - T_{opt})^H] \qquad [3.3]$$

where Y_T is the response of disease-related parameters to soil temperature, and T_{max} and T_{min} are 36 and 8ºC, respectively, which are known maximum and minimum temperatures for growth of *V. dahliae* isolates (Bejarano-Alcázar *et al.*, 1996; Pegg and Brady, 2002; Xu *et al.*, 2012). The shape parameter (H) determines the soil temperature range near the optimal soil temperature (T_{opt}) at which the response values are close to the maximum response (G). For the remaining parameters, we used a Type I combined exponential and power model:

$$Y_T = f(T) = a\, T^b\, c^T \qquad [3.4]$$

where Y_T is the response of the measured variable to soil temperature, and a, b and c are parameters that closely interact to control the shape of the curve (Sit and Poulin-Costello, 1994).

All regression analyses were conducted using the Marquardt nonlinear least-squares iterative procedure for nonlinear models (NLIN) of SAS software (version 9.3; SAS Institute, Cary, NC, USA). The coefficient of determination (R^2), mean square error, standard errors associated with the parameter estimates, confident intervals of predicted values, and pattern of standardized residuals plotted against either predicted values or the response variable were used to evaluate the appropriateness of models to describe the data (Madden *et al.*, 2007).

3.2.3.5. Relationships between experimental treatments and disease, stress, and plant growth-related parameters

The overall response of experimental treatment combinations to disease, stress, and plant growth-related parameters was first explored by cluster analyses. To establish functional groups of correlated experimental treatments, agglomerative clustering based on the Spearman correlation matrix was performed using the Ward clustering method (Borcard *et al.*, 2011). The optimal number of clusters was estimated on the basis of the average silhouette width according to the Mantel statistic. The number of clusters in which the within-group mean intensity of the link between the objects (i.e., experimental treatments) and their groups was highest (i.e., with the largest average silhouette width) indicated the optimal cluster number. A dendrogram was then produced representing the treatment groups identified (Borcard *et al.*, 2011). A heat map was developed to visualize the values of the different treatments and parameters used in the analysis. All cluster analysis calculations were performed using R software, version 3.0.2 (R Foundation for Statistical Computing, http://www.R-project.org/) with the *cluster* (Maechler *et al.*, 2013), *gplots* (Warnes *et al.*, 2013) and *vegan* (Oksanen *et al.*, 2013) packages.

3.2.3.6. Relationship between disease severity classes and stress-related parameters

Two approaches were used to assess the ability to discriminate among disease severity classes and stress-related parameters: logistic regression models and classification trees. Logistic models are direct probability models that are stated in terms of the probability of occurrence of an event (i.e., disease severity class) under a given set of conditions (i.e., stress parameters) (Hosmer and Lemeshow, 2000). In this study, a multinomial logistic regression model was fitted to each stress parameter as an independent-explanatory variable and disease severity class as the dependent-response variable, using healthy plants as the reference category. Multinomial models with ordinal responses are an extension of standard (i.e., binary) logistic regression to regression with three or more ordered categories (Agresti, 2007). To assess the statistical significance of each independent variable, each model was compared to the null model using a likelihood ratio test. The proportion of the variance explained by each model was evaluated using the maximum rescaled R^2 determination coefficient, and classification accuracy. This was

done by using the LOGISTIC procedure of SAS software. To assess the combined effects of all stress-related variables, a multiple logistic regression model was fitted using the stepwise procedure. The developed model was externally validated by partitioning of individuals into two samples: the training sample containing 80% the data of each severity class selected at random and the testing or validation sample with the remaining 20%. The logistic model was fitted using the training sample and externally validated by using the testing sample to assess its classification accuracy.

Classification trees were used to determine the thresholds of stress parameters that discriminated between disease severity classes. The decision tree was obtained by recursive data partitioning, thereby splitting the data set into increasingly smaller subsets based on the predictive variables. The optimal tree was determined using the minimal estimate of cross-validated prediction error for different numbers of splits (Everitt and Hothorn, 2010). Residual mean deviance and misclassification error rates were used as a measure of goodness of fit of the selected tree. The analysis was conducted using the *rpart* package (Therneau *et al.*, 2013) in the R environment. The selected tree was validated by dividing the full data set into two parts and testing for classification accuracy, as described above for the logistic regression analyses.

3.3. Results

3.3.1. Verticillium wilt development

Treatment effects

Soil temperature, olive cultivar, and pathotype of *V. dahliae* were found to influence the development of Verticillium wilt in olive. Plants grown in soil infested with the D pathotype showed typical symptoms of the defoliating syndrome in the full range of soil temperatures tested, irrespective of the olive cultivar. Disease incidence, disease severity, and intensity of stem vascular colonization decreased with increasing soil temperature according to a reverse sigmoid model with asymptotic optimal values in the range of 16 to 28ºC and 16 to 24ºC for the interaction of the D pathotype with cvs. Picual and Arbequina, respectively (Fig. 3.1A-C). In these two cultivars, no significant differences ($P \geq 0.05$) existed between temperatures within the optimal range regarding levels of disease incidence or intensity of stem vascular colonization caused by the D pathotype (Fig. 3.1A-B). At 32ºC, the three disease parameters (i.e., disease incidence, disease severity, and intensity of stem vascular colonization) decreased markedly in both cultivars, reaching 40.0%, 1.00 (on a 0-4 scale), and 44.2% in cv. Picual and 15%, 0.23, and 13.3% in cv. Arbequina, respectively (Fig. 3.1A-C). Disease was scarce in cv. Picual

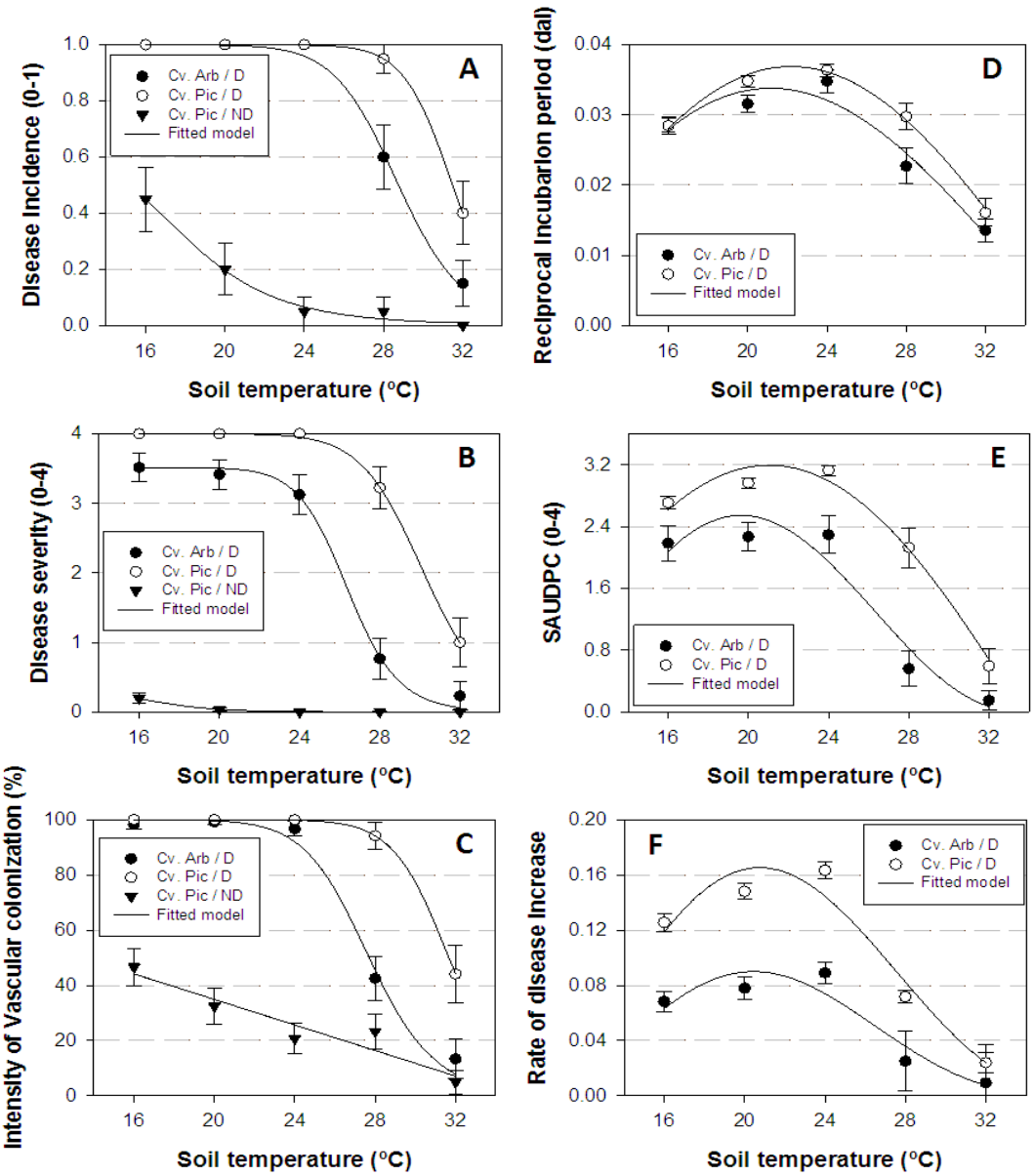

Figure 3.1. Relationship between Verticillium wilt-related parameters and soil temperature. Relationship between Verticillium wilt-related parameters and soil temperature in olive cvs. Arbequina (Arb) and Picual (Pic) grown in soil infested with the defoliating (D) or non-defoliating (ND) pathotype of *V. dahliae*. **A.** Final disease incidence; **B.** Overall disease severity (0-4 scale: 0 = no symptoms, 4 = dead plant); **C.** Intensity of stem vascular colonization determined at the end of the experiment by isolation in growth media; **D.** Reciprocal incubation period (time to initial symptoms); **E.** Standardized area under the disease severity progress curve (SAUDPC); **F.** Rate of disease increase parameter of the Gompertz function fitted to disease progress data. Each point represents the mean of data from two repeated experiments, each comprising 10 pots with one plant per pot. Vertical bars represent the standard error of the mean. Lines represent the predicted model calculated with a reverse sigmoid function (left panels) or a Beta function (right panels).

plants grown in soil infested with the ND pathotype and incubated at 16 to 28ºC, and no symptoms were observed at 32ºC (Fig. 3.1A-C). In this combination, disease incidence and intensity of stem vascular colonization was highest at 16ºC (i.e., 46.7 and 45%, respectively) and decreased steadily with increasing soil temperature to 5% of stem vascular colonization at 32ºC (Fig. 3.1C).

Time to symptom expression in olive plants was shortest at 24ºC in both cultivars grown in soil infested with D *V. dahliae*. Symptoms started to develop 27 to 29 days after planting in cv. Picual and about 3 days later in cv. Arbequina; yet, symptom appearance was delayed the most at 20ºC, followed by 16, 28, and 32ºC (Fig. 3.1D). Disease development over time was adequately described by the Gompertz model (R^2 > 0.97; RMSE < 0.7631) for all cultivar-soil temperature combinations involving the D pathotype (Fig. 3.2). The increase in disease severity (DS) became asymptotic (i.e., DS > 3 on a 0-4 scale) at all soil temperatures except for cv. Picual (DS = 1.0) at 32ºC and cv. Arbequina at 28 and 32ºC (DS = 0.77 and 0.23, respectively). Nevertheless, disease severity was always significantly greater (P < 0.05) in cv. Picual than in cv. Arbequina regardless of soil temperature (Fig. 3.1B, Fig. 3.2).

The beta function adequately described the effects of soil temperature on the reciprocal of the incubation period, the standardized area under the disease severity progress curve (SAUDPC), and the intrinsic rate of disease progression (*rho* parameter of the Gompertz model fitted to temporal disease severity progress). Those three disease-related parameters increased within the range of 16 to 24ºC and rapidly started to decrease at 28 and 32ºC (Fig. 3.1D-F). Values of those parameters were significantly lower (P < 0.05) in Arbequina plants compared to Picual plants infected with D *V. dahliae* at all soil temperatures, except for the incubation period at the extreme temperatures of 16 and 32ºC, for which values were similar in the two cultivars (Fig. 3.1D-F).

3.3.2. Relationship between leaf-level measurements of stress-related parameters and soil temperature

Similarly to the disease-related parameters described above and for all olive cultivar-*V. dahliae* pathotype combinations, leaf temperature (estimated as the difference between leaf and mean air temperature) increased with soil temperature according to a beta model. Leaf temperature increased in the range of 16 to 28ºC soil temperature and decreased at a soil temperature of 32ºC (Fig. 3.3A). Leaf temperature in Arbequina plants infected with the D pathotype was 0.03 to 0.64ºC higher than that of non-inoculated control plants at 20 to 32ºC soil temperature (Fig. 3.3A). Conversely, there were minor differences in the leaf temperature of Picual plants infected with D or ND *V. dahliae*, although leaf temperature was higher in the most susceptible interaction – cv. Picual/D pathotype (1.47 to 2.29ºC) –,

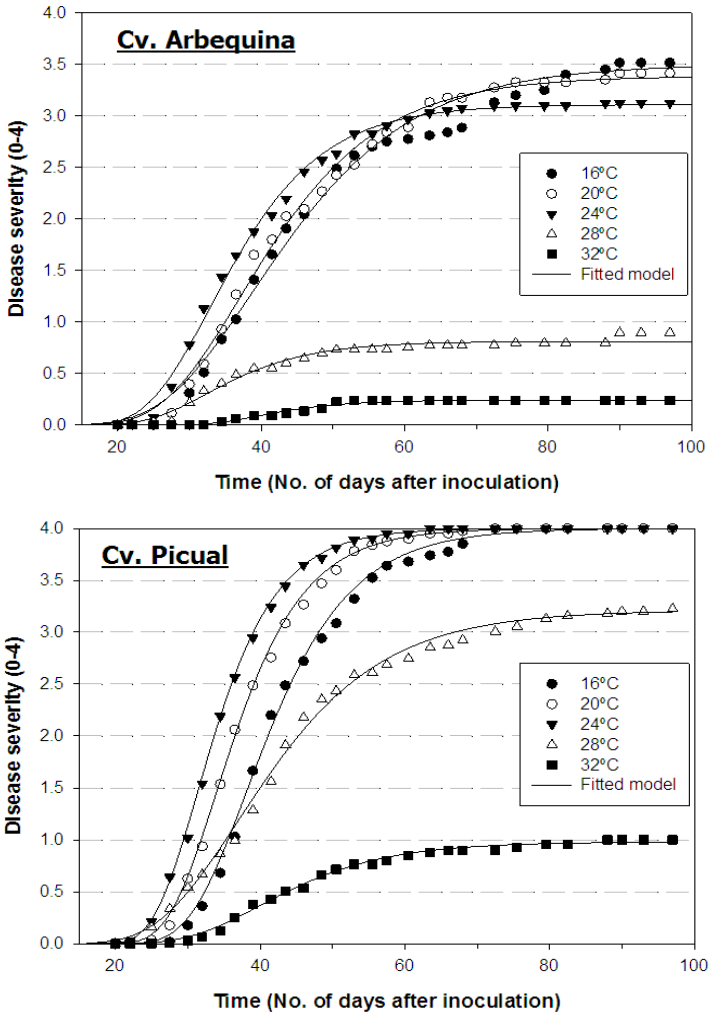

Figure 3.2. Verticillium wilt disease progress at different soil temperatures. Verticillium wilt disease progression in olive cvs. Arbequina and Picual grown in soil infested with the defoliating pathotype of *Verticillium dahliae* and incubated at different soil temperatures. Each point represents the mean disease severity (0-4 scale: 0 = healthy, 4 = dead plant) of data from two repeated experiments, each comprising 10 pots with one plant per pot, at 2-to-3-day intervals. Solid lines represent the predicted disease progress curve calculated with the Gompertz function.

decreased in plants infected with the ND pathotype (1.51 to 2.05ºC), and was the lowest in control plants (Fig. 3.3B). Progression of the remaining four stress-related parameters with soil temperature was well described by a Type I combined exponential and power function. The photochemical reflectance index showed different relationships with soil temperature depending on the olive cultivar infected with D *V. dahliae* (Fig. 3.3C-D). Specifically, minimum values were measured in Arbequina plants grown at 24 and 28ºC soil temperature, while the opposite occurred in Picual plants. Overall, however, both cultivars exhibited a similar range of PRI values: 0.03 to 0.04 (Fig. 3.3C-D). In the

remaining three experimental treatment combinations, PRI values were not greatly modified by soil temperature. Values were highest in Arbequina control plants (in a range of 0.031 to 0.034), decreased to a range of 0.025 to 0.031 in the cv. Picual/ND pathotype interaction, and were lowest (0.024 to 0.026) in Picual control plants (Fig. 3.3C-D). Steady-state fluorescence also exhibited a different relationship with soil temperature depending on the olive cultivar. In cv. Arbequina, steady-state chlorophyll fluorescence values increased with higher soil temperatures ranging from 16 to 24ºC and decreased at 28 and 32ºC in both D-pathotype-infected and control plants. Yet, steady-state chlorophyll fluorescence values were lower in the control treatment group regardless of soil temperature (Fig. 3.3E). In cv. Picual, the highest steady-state chlorophyll fluorescence values were reached at the extreme 16 and 32ºC soil temperatures. In this cultivar, at each soil temperature, steady-state chlorophyll fluorescence values were highest in control plants and tended to decrease in plants infected with *V. dahliae* regardless of the pathotype (Fig. 3.3F). Infection with the D pathotype had a strong effect on chlorophyll content estimated with SPAD readings. Specifically, in both olive cultivars, chlorophyll content was lowest in D *V. dahliae*-infected plants grown at 16 to 24ºC (42.4 to 48.0 SPAD units), increased at 28ºC (51.3 to 51.8 SPAD units), and reached the highest levels at 32ºC (60.9 to 61.5 SPAD units). Chlorophyll content values exhibited minor differences between control plants of both cultivars and Picual plants infected with the ND pathotype at soil temperatures ranging from 20 to 32ºC (59.7 to 66.0 SPAD units), but slightly lower values were recorded at 16ºC (56.7 to 60.4 SPAD units) (Fig. 3.4A-B). Similarly, high ethylene production was detected mostly in olive plants infected with the D pathotype and was particularly higher in plants grown at 20 to 24ºC, and in Picual plants (12.8 to 25.2 pmol g^{-1} root fresh weight h^{-1}) compared to Arbequina plants. Ethylene production was always lower and almost constant irrespective of soil temperature for the remaining treatment combinations, ranging from 7.4 to 10.4 pmol g^{-1} root fresh weight h^{-1} in the cv. Picual/D pathotype combination and from 4.2 to 9.8 pmol g^{-1} root fresh weight h^{-1} in control plants of both cultivars (Fig. 3.4C-D).

Plant growth, estimated by the relative rate of canopy growth and dry canopy weight, was also strongly affected by the experimental treatments. The lowest values for both growth measures were observed in plants infected with the D pathotype of *V. dahliae* at a soil temperature ranging from 16 to 24ºC. At these soil temperatures, based on measurements of canopy height at the beginning and the end of the experiments, Arbequina plants exhibited a 1.5 to 1.7 rate of canopy growth. The rate of canopy growth of Picual plants was 1.3 to 1.4 times lower than on Arbequina plants (Fig. 3.5A, B). At the same soil temperature levels, canopy dry weight values exhibited few differences, ranging from 2.4 to 2.8 g in cv. Arbequina and from 2.3 to 2.5 g in Picual plants; this parameter was about 75 to 82% lower than in non-infected control plants (Fig. 3.5C, D). At a soil temperature of 28ºC, both growth parameters increased by 3.4 cm/day and 7.4 g/day in cv. Arbequina, and by 2.4 cm/day and 3.4 g/day in cv. Picual. At 32ºC,

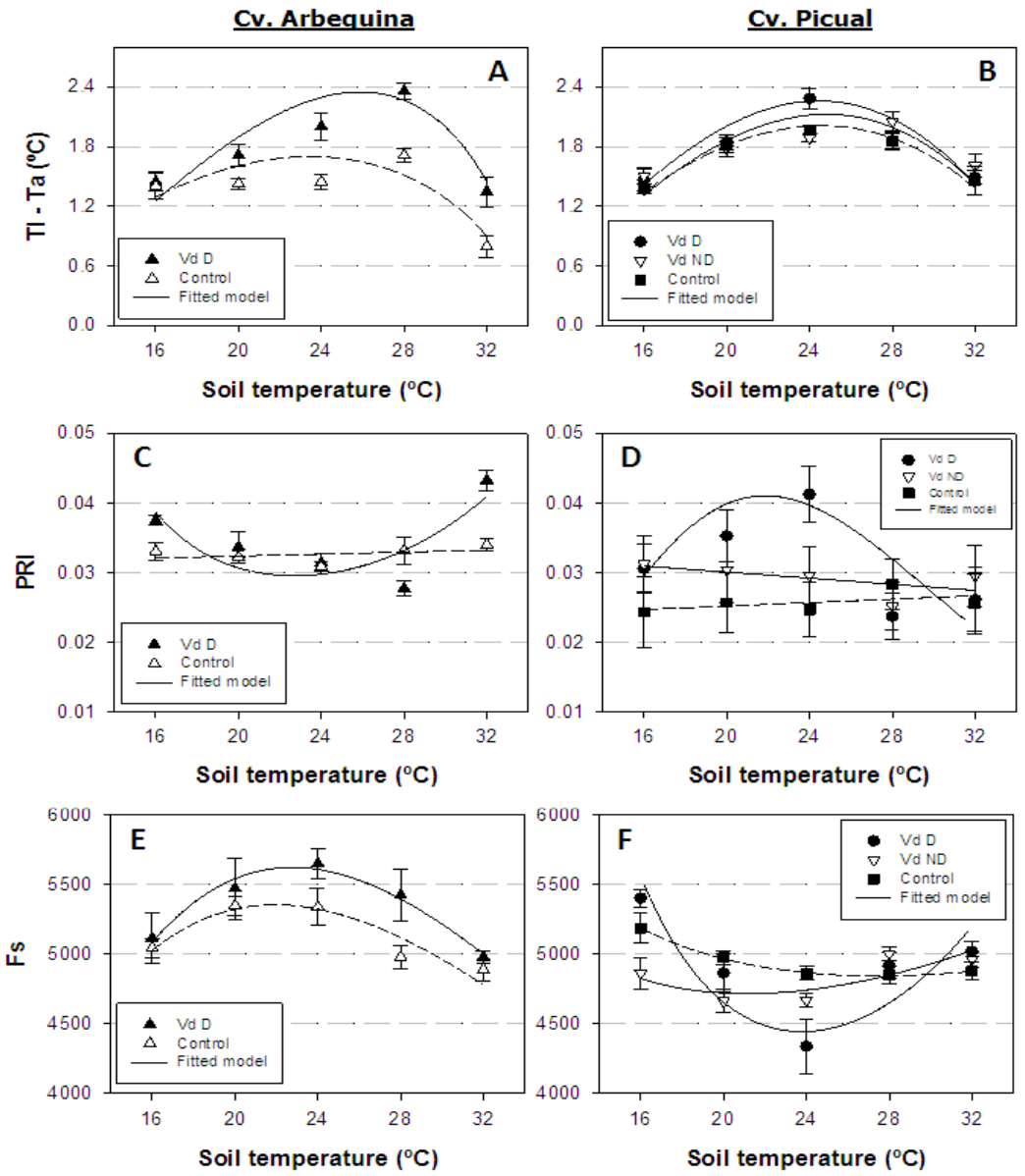

Figure 3.3. Relationship between stress-related parameters and soil temperature**.** Relationship between stress-related parameters and soil temperature in olive cvs. Arbequina (Arb) (left panels) and Picual (Pic) (right panels) grown in sterilized soil (control) or in soil infested with the defoliating (D) or the non-defoliating (ND) pathotype of *V. dahliae*. **A, B.** Leaf temperature minus air temperature (Tl-Ta); **C, D.** Photochemical reflectance index (PRI); **E, F.** Steady-state chlorophyll fluorescence (Fs). Each point represents the mean of data from two repeated experiments, each comprising 6 pots with one plant per pot, at 2-week intervals. For each parameter, the average daily increase was calculated as the standardized area under the parameter value progress curve over the observation period. Vertical bars represent the standard error of the mean. Lines represent the predicted model calculated with a Beta function (leaf temperature minus air temperature) or a Type I combined exponential and power function.

maximum growth values were observed in all treatments and both cultivars. Plant growth of Picual plants infected with the ND pathotype was about 24 to 36% lower than that of control plants at a soil temperature of 16 and 20ºC but minor differences were observed when plants grew at a soil temperature range of 24 to 32ºC. In control treatments, plant growth tended to increase with the increase in soil temperatures but did so at a lower rate than in infected plants. Specifically, soil temperature reduced plant growth only in the lower soil temperature range of 16 and 20ºC, and optimal maximum growth took place at 24 to 32ºC (Fig. 3.5).

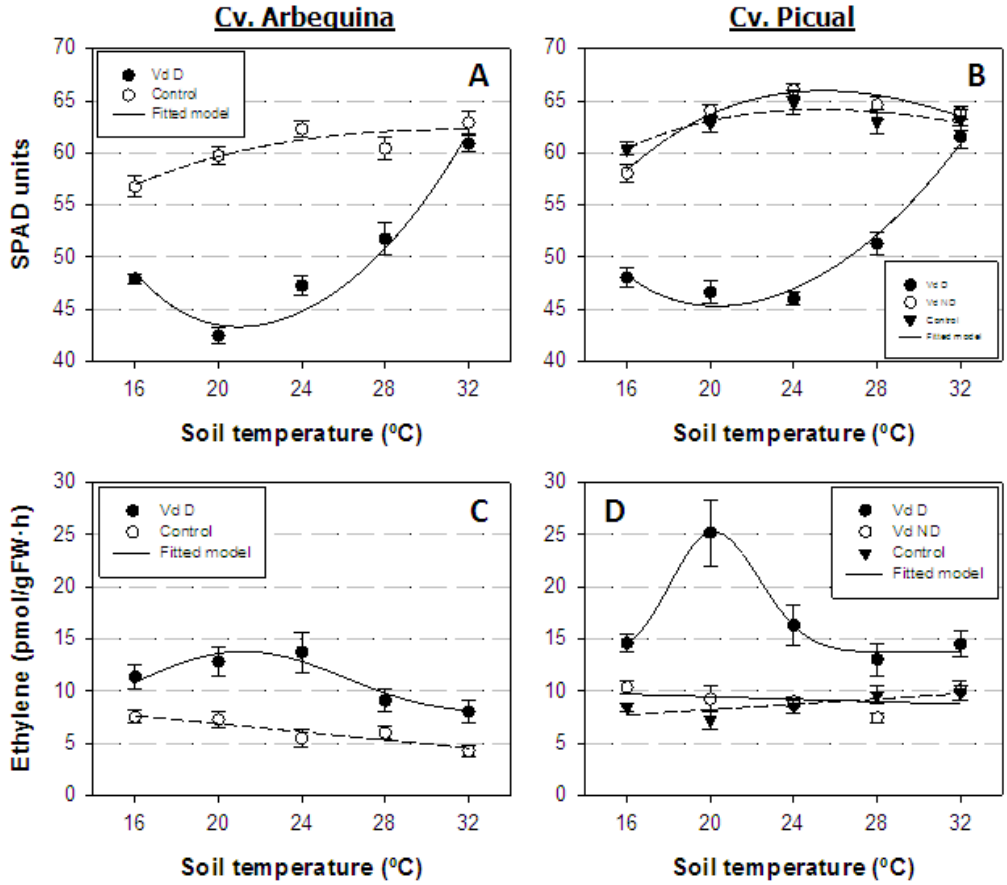

Figure 3.4. Relationship between stress-related parameters and soil temperature. Relationship between stress-related parameters and soil temperature in olive cvs. Arbequina (Arb) (left panels) and Picual (Pic) (right panels) grown in sterilized soil (control) or in soil infested with the defoliating (D) or the non-defoliating (ND) pathotype of *V. dahliae*. **A, B**. Chlorophyll content (SPAD readings); **C, D.** Ethylene production. Each point represents the mean of data from two repeated experiments, each comprising six pots with one plant per pot, at 2-week intervals. For each parameter, the average daily increase was calculated as the standardized area under the parameter value progress curve over the observation period. Vertical bars represent the standard error of the mean. Lines represent the predicted model calculated with a Type I combined exponential and power exponential function.

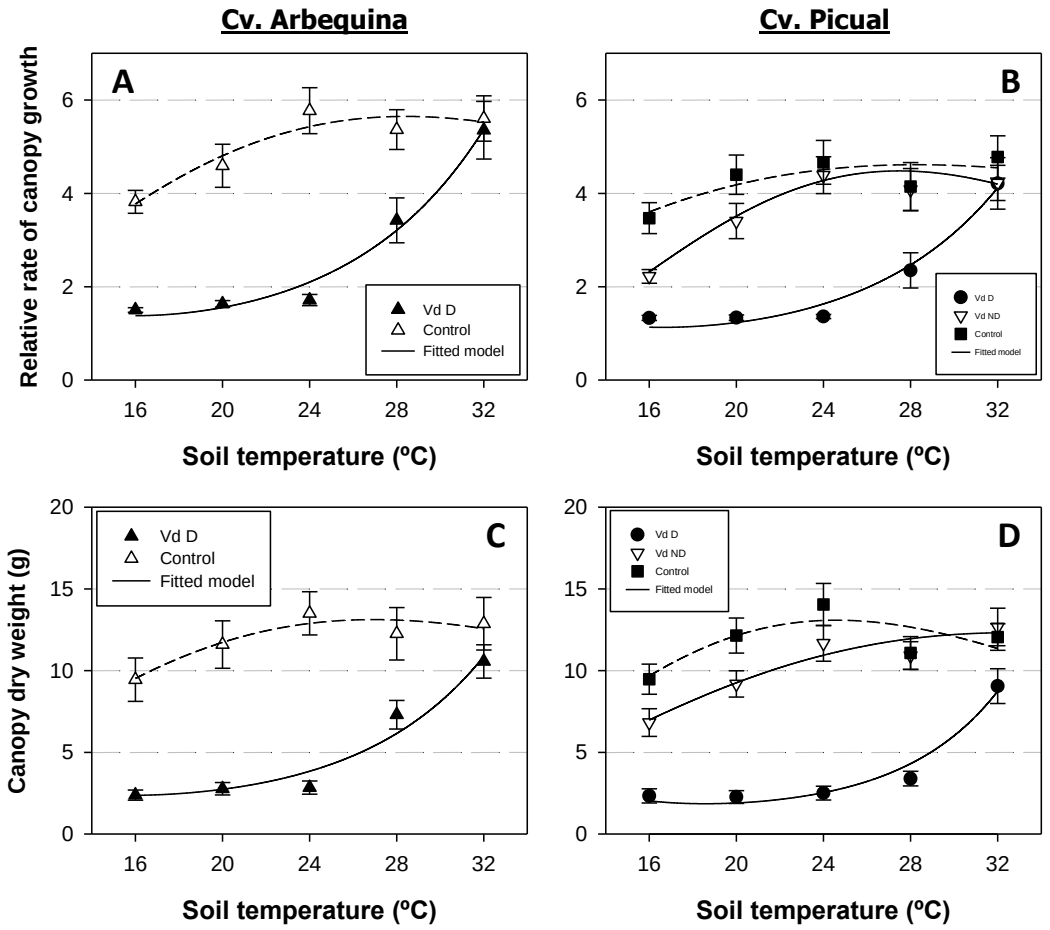

Figure 3.5. Relationship between plant growth-related parameters and soil temperature. Relationship between plant growth-related parameters and soil temperature in olive cvs. Arbequina (Arb) (left panels) and Picual (Pic) (right panels) grown in sterilized soil (control) or in soil infested with the defoliating (D) or the non-defoliating (ND) pathotype of *V. dahliae*. **A, B.** Relative rate of canopy growth; **C, D.** Dry weight of the canopy. Each point represents the mean of data from two repeated experiments, each comprising six pots with one plant per pot, at the end of the experiments. Vertical bars represent the standard error of the mean. Lines represent the predicted model calculated with a Type I power exponential function.

3.3.3. Relationships between experimental treatments and parameters related to disease, stress, and plant growth

To further analyze the interactions between *V. dahliae* pathotype, olive cultivar, and soil temperature, we performed a multivariate hierarchical cluster analysis, including all 12 parameters related to disease, stress, and growth as response variables. This analysis led to the creation of four functional groups – A to D – among the 25 experimental treatment combinations (Fig. 3.6). Group A included seven experimental treatments with a severe disease reaction, including plants infected with the highly virulent D pathotype

grown at optimal soil temperature for Verticillium wilt development (i.e., 16 to 28ºC for cv. Picual and of 16 to 24ºC for cv. Arbequina). Overall, high values of disease severity-related parameters were associated with high levels of leaf temperature and ethylene production and low levels of chlorophyll content and growth-related parameters. In this group, Arbequina plants also exhibited low and high levels in PRI and steady-state chlorophyll fluorescence parameters, respectively; Picual plants exhibited the opposite pattern. Group B comprised four experimental treatments with a moderate disease reaction. It included Arbequina and Picual plants infected with the D pathotype and grown at 28ºC and 32ºC, respectively, and plants in the cv. Picual/ND pathotype combination grown at 16 or 20ºC. This group of treatment combinations exhibited intermediate values in most of the parameters included in the study. Group C comprised three experimental treatments associated with a low level of disease. Specifically, plants in the cv. Arbequina/D pathotype combination grown at 32ºC, and plants in the cv. Picual/ND pathotype combination grown at 24 or 28ºC. The low Verticillium wilt development observed in treatment combinations within this group was associated with moderate values of stress and plant growth parameters. Group D comprised the remaining eleven treatments with healthy plants, including asymptomatic Picual plants inoculated with the ND pathotype grown at 32ºC and all non-inoculated control plants of both cultivars at all soil temperature levels tested (Fig. 3.6).

3.3.4. Relationship between stress-related parameters and Verticillium wilt severity classes

A multinomial logistic regression analysis was performed to determine the relationship between stress-related parameters and Verticillium wilt severity classes. Logistic regression models fitted for each variable (Table 3.1, Fig. 3.7) exhibited significant differences between Verticillium wilt severity classes in all stress-related parameters. When fitted individually, chlorophyll content, ethylene production, and leaf temperature were the most explanatory parameters and had the highest correct classification rate (i.e., the Verticillium wilt severity class matched the assigned class with the highest probability) (Table 3.1, Fig. 3.7A-E). Although the PRI and steady-state chlorophyll fluorescence values were also statistically significant ($P < 0.011$), their explanatory power and correct classification rate was lower (Table 3.1, Fig. 3.7D-E). In addition, we fitted a multiple logistic model using a stepwise procedure, selecting a model that included the four stress parameters with the highest explanatory power (i.e., chlorophyll content, ethylene production, leaf temperature, and steady-state chlorophyll fluorescence) but did not include the PRI. The model explained 98.75% of the total variability and correctly classified 73.40% of the cases (Table 3.1, Fig. 3.7F-I).

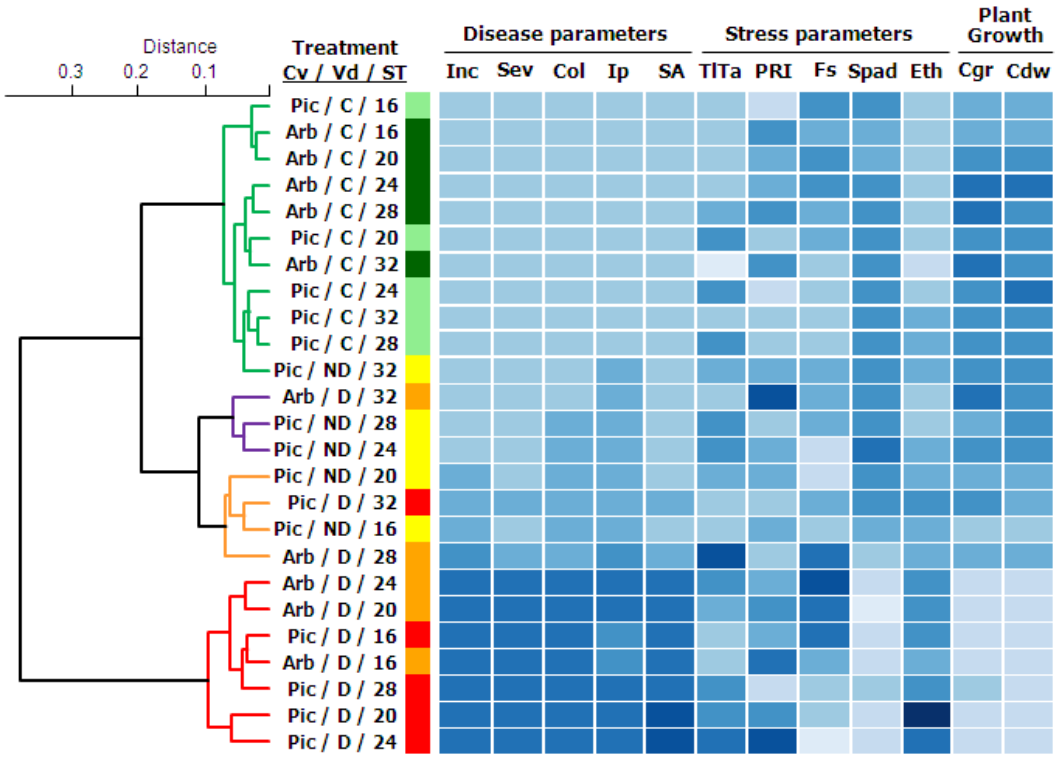

Figure 3.6. Dendrogram showing results of cluster analyses and heat map representation of disease, stress, and plant growth parameters. The 12 parameters selected for the heat map representation were related to Verticillium wilt reaction (5 parameters): Final disease incidence (Inc), Overall disease severity (Sev), Standardized area under disease severity progress curve (SA), Time to initial symptoms (Ip), and Intensity of stem vascular colonization (Col); related to stress (five parameters): Leaf temperature minus air temperature (Tl-Ta), Steady-state chlorophyll fluorescence (Fs), Photochemical reflectance index (PRI), Chlorophyll content (Spad), and Ethylene production (Eth); and related to plant growth (two parameters): Relative rate of canopy growth (Cgr) and Dry canopy weight (Cdw). Agglomerative cluster analyses were performed based on the Spearman correlation matrix calculated from values of the different parameters using the Ward method. Cluster groupings of experimental treatment combinations represented in different colors were estimated on the basis of the average silhouette width according to the Mantel statistic. In the heat map, for each column, cells represent the relative value of each parameter for each experimental treatment combination of soil temperature, olive cultivar, and non-inoculated control and Verticillium dahliae pathotypes of the study from two repeated experiments.

Interestingly, 76 (91.6%) of the 83 healthy plants were correctly classified; of the remaining seven plants, three were classified as asymptomatic and four were classified as plants with only minor symptoms (*data not shown*), demonstrating the ability of the model to discriminate between healthy and diseased plants. Overall, in the selected model the probability of increase of Verticillium wilt symptom severity increased with growing leaf temperature and ethylene production, but the opposite occurred for chlorophyll content and steady-state chlorophyll fluorescence values. Figures 3.7F to I show the predicted probability distribution curves for the stress parameters included in the model

keeping the remaining three stress parameters constant. The predicted probability distribution curves corresponding to Verticillium wilt severity classes from healthy to severely affected were distinct in all the parameters (Fig. 3.7). Moreover, chlorophyll content values showed distinct curves for all five severity classes (Fig. 3.7F), and ethylene production showed distinct probability curves for all Verticillium wilt severity classes except for asymptomatic and low symptom severity, which overlapped (Fig. 3.7G). Finally, leaf temperature (Fig. 3.7H) and steady-state chlorophyll fluorescence (Fig. 3.7I) showed distinct probability curves for healthy, asymptomatic, and low symptom severity classes, but overlapping curves for moderately or severely affected classes. The model was validated using a test data set containing 20% of the data of the original set that had a correct classification rate of 76.60% and explained 99.81% of the variation.

Table 3.1. Results of the multinomial logistic regression models fitted for each variable separately and the multivariate multinomial logistic regression model fitted with a stepwise method.

	LRT test[b]			
Predictor[a]	**Chi-square**	***P*>Chi-square**	**Max-rescaled R^2 [b]**	**Correct classification (%)[b]**
SPAD	423.05	<0.0001	0.8964	59.57
Ethylene	122.30	<0.0001	0.4854	56.38
Tl-Ta	26.65	<0.0001	0.1358	49.47
Fs	16.78	0.0021	0.0869	47.74
PRI	13.17	0.0105	0.0888	46.28
SPAD, Ethylene, Tl-Ta, Fs	819.35	<0.0001	0.9875	73.40

[a] A multinomial logistic regression model was fitted to each of the stress parameters as independent variable (predictor) and disease severity class as independent variable, using healthy plants as the reference category. To assess the combined effect of all stress related variables, a multiple logistic regression model was fitted using the stepwise procedure. SPAD: SPAD index; Ethylene: Ethylene production; Tl-Ta: Leaf temperature minus air temperature; Fs: Steady-state chlorophyll fluorescence.

[b] Likelihood ratio test (LRT), maximum rescaled R^2 determination coefficient and correct classification rate were obtained when using the models for prediction.

Predicted probabilities for single predictor effect

Predicted probabilities for combined effects of predictors for each predictor

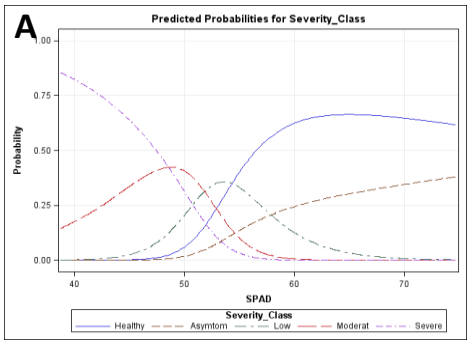

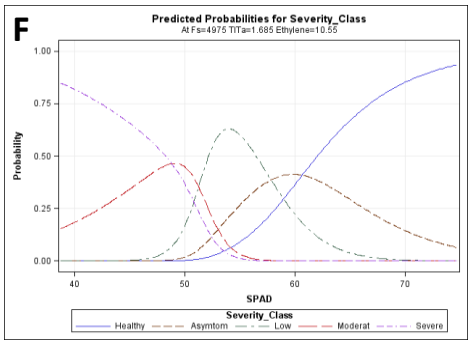

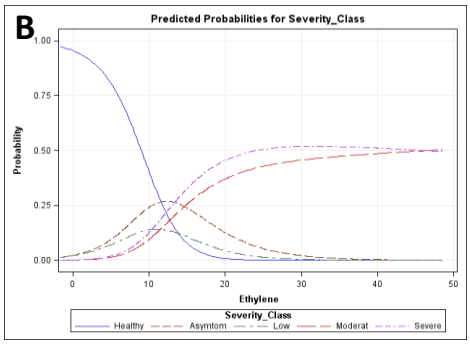

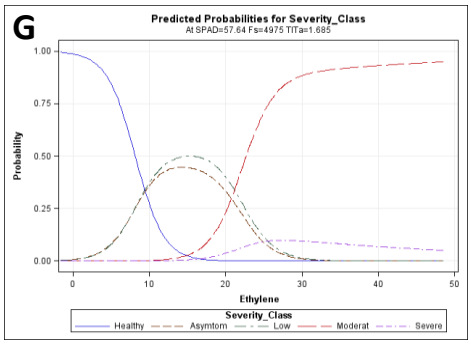

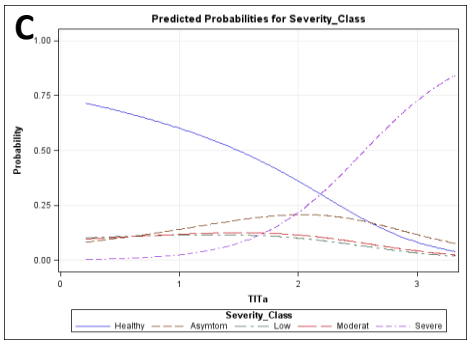

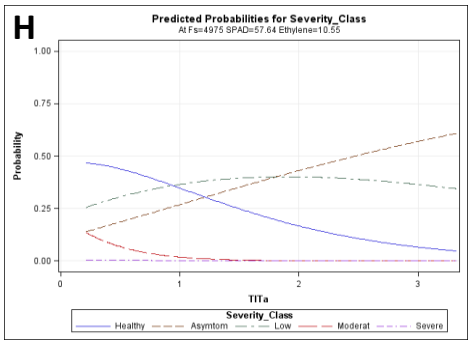

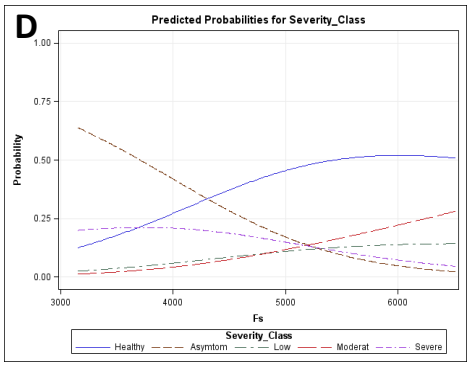

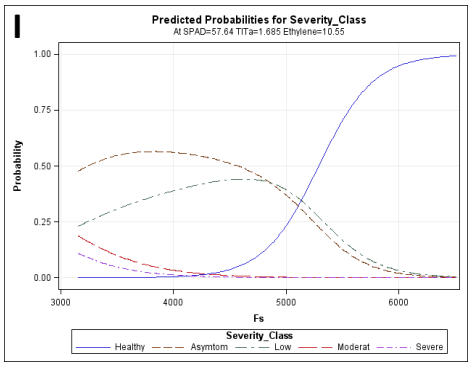

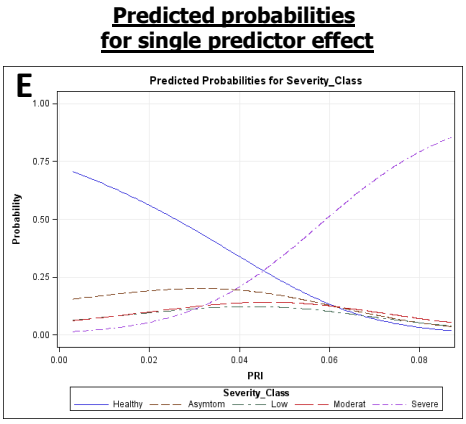

Figure 3.7. Predicted probabilities according to the multinomial logistic regression model with Verticillium wilt severity as the response variable and stress-related parameters as explanatory variables using healthy plants as the reference category. Left panels (A to E) represent the predicted probability distribution curves for each stress parameter fitted separately. Right panels (F to I) represent the predicted probability for each of the four stress parameters when the other three are fixed. **A, F.** Chlorophyll content (SPAD value); **B, G.** Ethylene production; **C, H.** Leaf temperature minus air temperature (Tl-Ta); **D, I.** Steady-state chlorophyll fluorescence (Fs); **E.** Photochemical reflectance index (PRI). Severity class indicates the severity of Verticillium wilt symptoms from Healthy control plants to Severe symptom development. Data include a training set of 188 plants selected at random from a total set of 235 plants in two repeated experiments comprising all experimental combinations of soil temperature, olive cultivars, and non-inoculated control and *Verticillium dahliae* pathotypes of the study.

3.3.5. Identification of stress-related parameter thresholds

The optimal classification tree fitted to the data had seven terminal nodes and a discrimination ability of 76.6% (Fig. 3.8). Chlorophyll content (44.7%), ethylene production (37.3%), and steady-state chlorophyll fluorescence (30.4%) were the most important parameters in the construction of the classification tree. Leaf temperature and the PRI accounted for a much lower importance (i.e., 18.5 and 17.7%, respectively). Chlorophyll content was the main factor (i.e., first splitting stress parameter) that differentiated between plants in the healthy and low symptom severity class and those in moderate to severely affected classes with a chlorophyll content value <53.8 SPAD units. At the second level, ethylene and leaf temperature differentiated between both groups. Specifically, healthy plants were separated from asymptomatic plants by an ethylene production threshold of 11.5 pmol g^{-1} root fresh weight h^{-1}. Plants below this threshold with a steady-state chlorophyll fluorescence >4658 were healthy, while plants with a lower fluorescence value were asymptomatic. In addition, plants with ethylene production above 11.5 pmol g^{-1} root fresh weight h^{-1} and a chlorophyll content value >58.5 SPAD units were asymptomatic and those with a lower chlorophyll content value exhibited mild symptoms. Moderate and severe Verticillium wilt classes separated by a chlorophyll

content value <53.8 SPAD units were divided into two groups by leaf temperature: plants with a leaf temperature >1.9ºC, which exhibited severe Verticillium wilt symptoms, and plants with a lower leaf temperature, which were in turn split in two new groups (i.e., plants with moderate Verticillium wilt symptoms and a steady-state chlorophyll fluorescence value <5670 and plants with severe Verticillium wilt symptoms and a steady-state chlorophyll fluorescence value above this threshold). The selected tree was validated using a test data set containing 20% of the data of the original set that was found to have a correct classification rate of 85.11%.

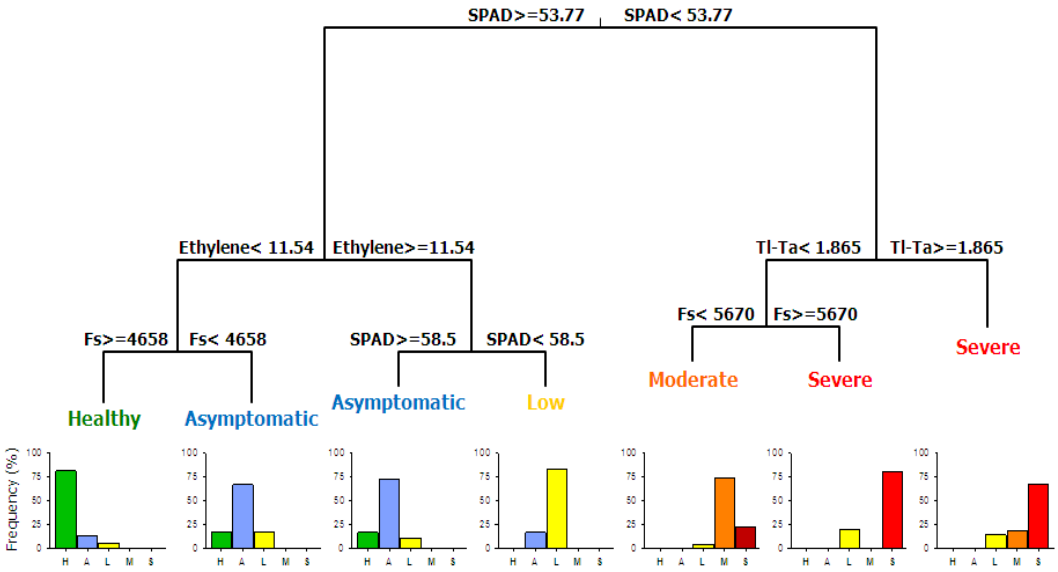

Figure 3.8. Classification tree to discriminate among Verticillium wilt severity classes based on stress-related parameters. Five stress-related parameters were used: Chlorophyll content (SPAD value), Ethylene production, Steady-state chlorophyll fluorescence (Fs), Leaf temperature minus air temperature (Tl-Ta), and Photochemical reflectance index (PRI). Severity class indicates the severity of Verticillium wilt symptoms from Healthy control plants to Severe symptom development. For each terminal node the most prevalent Verticillium wilt severity class is indicated. The histogram for each terminal node represents the percentage of plants in each severity class (where H = Healthy, A = Asymptomatic, L = Low, M = Moderate and S = Severe symptoms). Data include a training set of 188 plants selected at random from a total set of 235 plants in two repeated experiments comprising all experimental combinations of soil temperature, olive cultivars, and non-inoculated control and *Verticillium dahliae* pathotypes of the study.

3.4. Discussion

The development of Verticillium wilt in various crops has been related to environmental and soil conditions (Pegg and Brady, 2002). Soil temperature has been found to affect the development of diseases caused by *V. dahliae* in different crops (Pegg

and Brady, 2002). However, no studies have explored the relationship between Verticillium wilt development and soil temperature in olive trees. The main objective of this study was to explore the relationship between soil temperature and Verticillium wilt symptom development, considering the potential influence of the virulence of *V. dahliae* pathotypes and the susceptibility of the host cultivar. We also measured several parameters at leaf level to assess the stress caused by the pathogen in olive plants at different soil temperatures and the relationship between such parameters and disease severity.

In our study, the most favorable soil temperature for Verticillium wilt development caused by the *V. dahliae* D pathotype was 24ºC in both olive cultivars, showing the highest values in the five disease-related parameters measured (i.e., incubation period, final disease incidence and severity, standardized area under the disease severity progress curve, intrinsic rate of disease increase, and intensity of stem vascular colonization). At 16 and 20ºC soil temperatures, high values of these parameters were also observed, although they were lower than those reached at 24ºC. At 28 and 32ºC, such disease parameters decreased dramatically, reaching the lowest values at 32ºC. Our results are in close agreement with most studies on the effect of temperature on disease caused by *V. dahliae* in various host plants (Pegg and Brady, 2002). For example, studies conducted in cotton, tomato, and pepper infected by *V. dahliae* revealed that the optimal soil temperatures for *V dahliae* growth were close to 20ºC and temperatures higher than 28ºC greatly reduced the development of the disease (Pegg and Brady, 2002). Temperature also interacts with the expression level of resistance of host cultivars. Specifically, severe disease symptoms caused by a highly virulent isolate can be modified by a temperature of 28ºC and above to reach those of a moderately susceptible cotton cultivar (Pegg and Brady, 2002), as occurred in our experiments with Picual plants infected with D *V. dahliae*. High temperatures delay germination of microsclerotia and therefore impair the ability of *V. dahliae* to penetrate the plant and cause disease (Pullman *et al.*, 1981; Tjamos and Fravel, 1995). Values reached by disease-related parameters were higher in cv. Picual than in cv. Arbequina, as previously found by López-Escudero *et al.* (2004), who reported that cv. Picual was more susceptible than cv. Arbequina to the D pathotype. Moreover, stress-related parameters showed the highest differences between D-*V. dahliae*-infected plants and control plants at 24ºC. The reason for this was probably that 24ºC was the most favorable soil temperature for Verticillium wilt development and consequently that plants at this soil temperature suffered the highest level of stress. Leaf temperature was higher in infected plants than in control plants, and the lowest differences them were recorded at 16 and 32ºC soil temperatures. The higher leaf temperatures observed in infected plants than in control plants are consistent with the results of similar studies in oilseed rape plants infected by *V. dahliae* (Nilsson, 1995) and other soil-borne pathogens (Pinter *et al.*, 1979; Tu and Tan, 1985; Mengistu *et al.*, 1987; Nilsson, 1991, 1995; Hayat *et al.*, 2008). In potato, infection with *V. dahliae* has been found to cause lower stomatal conductance,

lower transpiration, and therefore higher leaf temperature (Bowden and Rouse, 1991). In sunflower plants, however, Sadras *et al.* (2000) did not observe changes in leaf temperature or stomatal conductance due to infection with *V. dahliae*.

The photochemical reflectance index was higher in infected plants than in control plants in the cv. Picual/D pathotype combination; by contrast, this only occurred at a soil temperature of 16 and 32ºC in the cv. Arbequina/D pathotype combination. These results are consistent with those obtained by Suárez *et al.* (2008, 2009) in trees subjected to water stress. Leaf chlorophyll fluorescence measurements estimated from steady-state chlorophyll fluorescence showed lower values in D pathotype infected plants of cv. Picual; in the cv. Arbequina/D pathotype combination, however, steady-state chlorophyll fluorescence values were higher in infected plants. The opposite trends observed in the two cultivars for the photochemical reflectance index and steady state fluorescence to soil temperature showed on Fig. 3.3C to F could be due to the differential response of both olive cultivars to infection by *V. dahliae* and soil temperature. Specifically, maximum disease severity and symptom expression is reached when Picual plants are grown at 20 to 28ºC, while at these same soil temperatures disease severity and symptom expression on Arbequina plants are moderate or low. This is also supported by the minor differences showed between cultivars for both stress parameters at extreme soil temperatures (i.e., 16 and 32ºC) where disease symptoms are low. The decrease in steady-state chlorophyll fluorescence in cv. Picual/D pathotype infected plants could be also expected according to previous results obtained with trees under water stress (Zarco-Tejada *et al.*, 2009, 2012). Depression in photosynthetic activity mainly due to drought in plants inoculated with wilting fungi has been described in several pathosystems, including potato infected with *V. dahliae* (Bowden and Rouse, 1991), tomato infected with *Verticillium albo-atrum* (Lorenzini *et al.*, 1997), and *Quercus ilex* infected with *Cryphonectria parasitica* (El Omari *et al.*, 2001). Chlorophyll content in leaves estimated by SPAD readings was inversely correlated with disease severity, as previously found in potato plants infected with *V. dahliae* (Gamliel *et al.*, 1997). Similarly, SPAD values related to chlorophyll content levels were able to indicate a reduction in photosynthetic activity in tomato plants (Fanizza *et al.*, 1991) and grapevines (Flexas *et al.*, 2000) under water stress.

Ethylene is a plant hormone that acts as a signaling molecule in basal plant defense responses (Fradin and Thomma, 2006) and is known to increase rapidly upon *V. albo-atrum* infection (Pegg and Gronshaw, 1976). In our study, ethylene production in leaf petioles was greater in infected plants of susceptible cv. Picual than in those of moderately susceptible cv. Arbequina. This agrees with the results of Birem *et al.* (2009), who reported higher levels of ethylene in cv. Picual than in resistant cv. Frantoio plants due to infection by D *V. dahliae*. These findings are also consistent with those of Pegg and Cronshaw (1976), who reported a significant production of ethylene in internodes of a

susceptible cultivar, but low or no ethylene production in a resistant tomato cultivar following infection with *V. albo-atrum*.

The most favorable soil temperature for Verticillium wilt development of the *V. dahliae* ND pathotype in cv. Picual was 16ºC. From that temperature upwards, values of disease incidence and severity and intensity of stem vascular colonization progressively decreased. These values were much lower than those reached by the D pathotype, as previously found by López-Escudero *et al.* (2004), who reported that cv. Picual was more susceptible to the D pathotype than to the ND pathotype. In agreement with such findings, the greatest differences in stress-related parameters between ND pathotype infected plants and control plants were found at 16ºC and decreased with rising soil temperatures. These differences were lower than those obtained in the D pathotype, confirming that the lower Verticillium wilt development in plants infected with the ND pathotype is related to a lower stress level. In plants infected with the ND pathotype, however, chlorophyll content and ethylene production showed similar values to those of control plants, revealing that photosynthesis and ethylene production were not affected by pathogen infection. In consequence, plant growth parameters of ND pathotype-infected plants showed almost no differences when compared to those of control plants.

According to our results, the optimal soil temperature for D pathotype infection was in a range of 16 to 24ºC in cv. Picual plants and 20 to 24ºC in cv. Arbequina plants. The optimal soil temperature for ND pathotype development was in a range of 16 to 20ºC. Differences found in the optimal temperature range for disease development for both *V. dahliae* pathotypes are in agreement with the optimal mycelial growth for isolates of the D and ND pathotypes. Indeed, in *V. dahliae* cotton isolates from southern Spain, Bejarano-Alcázar *et al.* (1996) estimated that the optimal temperature for in vitro growth (over a 21 to 30ºC range) was 24 to 27ºC for isolates of the D pathotype compared to 21 to 24ºC for the ND isolates. In addition, the lower temperature optimum for the ND pathotype may explain why this *V. dahliae* pathotype tends to be geographically restricted to cooler areas of southern Spain such as Granada and Huelva provinces, whereas the D pathotype is present in most olive growing areas but is particularly prevalent in the warmer areas of the Guadalquivir Valley (Jiménez-Díaz *et al.*, 2011).

The relationship between stress-related parameters and Verticillium wilt severity classes was determined by a multinomial logistic regression analysis and a tree classification. According to the multinomial regression models fitted for each parameter separately, significant differences were found among Verticillium wilt severity classes in all stress-related parameters. The parameters with the highest explanatory power were chlorophyll content, ethylene production, leaf temperature, and steady-state chlorophyll fluorescence. Predicted probability distribution curves corresponding to chlorophyll content values were different for all Verticillium wilt severity classes, which made it

possible to discriminate between each disease severity level, even at early stages of *V. dahliae* infection. However, ethylene production showed similar probability curves for asymptomatic and initial-low symptom development classes, while leaf temperature and steady-state chlorophyll fluorescence were similar in moderately and severely affected plants. In fact, ethylene production of plants at early stages of Verticillium wilt development did not differ significantly from that of plants in the asymptomatic class, while leaf temperature and steady-state chlorophyll fluorescence showed significant differences between plants in such classes. Based on the results of the multinomial regression models fitted for each parameter separately, we fitted a multiple logistic regression model including the four best stress parameters: chlorophyll content, ethylene production, leaf temperature, and steady-state chlorophyll fluorescence. The model explained 98.75% of the variance and correctly classified 73.40% of the cases. The optimal classification tree had a similar discrimination ability (76.6%), revealing that chlorophyll content, ethylene production, steady-state chlorophyll fluorescence, and leaf temperature were the most important parameters. As shown by the logistic regression analysis, chlorophyll content was the main factor that differentiated between asymptomatic and low Verticillium wilt severity classes, while ethylene production did not distinguish between them. Nevertheless, leaf temperature and steady-state chlorophyll fluorescence differentiated between moderate and severe Verticillium wilt classes; by contrast, in the logistic regression analysis, these two parameters distinguished between all Verticillium wilt severity classes except moderate and severe classes. The PRI was the parameter with the lowest explanatory power and classification rate in both classification methods. These results obtained at leaf level under controlled conditions confirmed those obtained at leaf and canopy levels under field conditions by Calderón *et al.* (2013), who proved the potential for early detection of *V. dahliae* infection and discrimination among Verticillium wilt severity levels in olive crops using thermal, multispectral, and hyperspectral imagery acquired with an unmanned aerial vehicle. In that study, temperature and chlorophyll fluorescence were identified as the best indicators to detect Verticillium wilt at initial stages of disease development, while the photochemical reflectance and chlorophyll indices proved to be good indicators to detect moderate and severe Verticillium wilt severity classes under field conditions.

In conclusion, the optimal soil temperatures for D and ND pathotype development were 20-24ºC and 16-20ºC, respectively, with a drastic reduction of Verticillium wilt symptom development at soil temperatures higher than 28ºC. Cv. Picual plants were more susceptible to the D than to the ND pathotype and were more affected by the D pathotype than Arbequina plants. Stress-related parameters were able to detect the effects of *V. dahliae* infection and colonization on water flow that eventually cause water stress effects. Results demonstrated that leaf temperature, physiological indices (i.e., photochemical reflectance, steady-state chlorophyll fluorescence, and chlorophyll content), and ethylene production are related to physiological stress caused by

Verticillium wilt. Chlorophyll content, steady-state chlorophyll fluorescence, and leaf temperature were identified as the best indicators to detect Verticillium wilt at early stages of disease development, while ethylene production and the photochemical reflectance index were good indicators to detect Verticillium wilt at advanced stages. In addition, chlorophyll content was the parameter with the highest explanatory power and correct classification rate in the classification models used in this study, followed by ethylene production, steady-state chlorophyll fluorescence, and leaf temperature. These results will be useful to better understand the differential geographic distribution of *V. dahliae* pathotypes in southern Spain found by Jiménez-Díaz *et al.* (2011) and to assess the potential effect of climate change on the development of Verticillium wilt of olive under different future climate change scenarios.

Acknowledgments

M. Medina is acknowledged for her support in remote sensing parameter measurements. We thank R.M. Jiménez-Díaz and B.B. Landa from IAS-CSIC for critically reading the manuscript and making valuable suggestions prior to submission.

Funding

Financial support for this research was provided by Project P08-AGR-03528 from ‘‘Consejería de Economía, Innovación y Ciencia’’ of Junta de Andalucía and the European Social Fund (JANC), and projects AGL-2012-37521 (JANC) and AGL2012-40053-C03-01 (PJZT) from the Spanish ‘‘Ministerio de Economía y Competitividad’’ and the European Social Fund. R. Calderón is a recipient of research fellowship BES-2010-035511 from the Spanish ‘‘Ministerio de Ciencia e Innovación’’ and C. Lucena was a recipient of a JAE-DOC postdoctoral contract from ‘‘Consejo Superior de Investigaciones Científicas’’ (CSIC) co-funded by the European Social Fund. The funders had no role in study design, data collection and analysis, decision to publish, or preparation of the manuscript.

Author Contributions

Conceived and designed the experiments: RC CL JLTC PJZT JANC. Performed the experiments: RC CL JLTC PJZT JANC. Analyzed the data: RC JANC. Contributed reagents/materials/analysis tools: JANC PJZT. Wrote the paper: RC PJZT JANC.

References

Agresti, A. (2007). *An Introduction to Categorical Data Analysis*, 2nd ed. Hoboken, NJ, USA: John Wiley & Sons, Inc.

Ayres, P.G. (1978). Water relations of diseased plants. In Kozlowski, T.T. (Eds.), *Water Deficits and Plant Growth* (vol.5, pp. 1-60). London, United Kingdom: Academic Press.

Barranco, D., Fernández-Escobar, R., & Rallo, L. (2004). *El cultivo del olivo*, 5th edition. Madrid, Spain: Ediciones Mundi-Prensa.

Bejarano-Alcázar, J., Blanco-López, M.A., Melero-Vara, J.M., & Jiménez-Díaz, R.M. (1996). Etiology, importance, and distribution of Verticillium wilt of cotton in southern Spain. *Plant Dis.* 80:1233-1238.

Birem, F., Alcántara, E., Blanco-López, M.A., & López-Escudero, F.J. (2009). Physiologycal differences expressed by susceptible and resistant olive cultivars inoculated with *Verticillium dahliae*. In *10th International Verticillium Symposium, Book of Abstracts* (p. 71). Corfu Island, Hellas.

Borcard, D., Gillet, F., & Legendre, P. (2011). *Numerical Ecology with R*. New York, NY, USA: Springer.

Bowden, R.L., & Rouse, D.L. (1991). Effects of *Verticillium dahliae* on gas exchange of potato. *Phytopathology* 81:293-301.

Calderón, R., Navas-Cortés, J.A., Lucena, C., & Zarco-Tejada, P.J. (2013). High-resolution airborne hyperspectral and thermal imagery for early detection of *Verticillium* wilt of olive using fluorescence, temperature and narrow-band spectral indices. *Remote Sens. Environ.* 139:231-245.

DeVay, J.E., Forrester, L.L., Garber, R.H., & Butterfield, E.J. (1974). Characteristics and concentration of propágulos of *Verticillium dahliae* in air-dried field soils in relation to the prevalence of Verticillium wilt in cotton. *Phytopathology* 64:22-29.

El Omari, B., Fleck, I., Aranda, X., Moret, A., & Nadal, M. (2001). Effect of fungal infection on leaf gas-exchange and chlorophyll fluorescence in *Quercus ilex*. *Ann. For. Sci.* 58:165-174.

Everitt, B.S., & Hothorn, T. (2010). *A Handbook of Statistical Analysis Using R*, 2nd ed. Boca Raton, FL, USA: Chapman and Hall/CRC Press.

Fanizza, G., Ricciardi, L., & Bagnulo, C. (1991). Leaf greenness measurements to evaluate water stressed genotypes in *Vitis vinifera*. *Euphytica* 55:27-31.

Flexas, J., Briantais, J.M., Cerovic, Z., Medrano, H., & Moya, I. (2000). Steady-state and maximum chlorophyll fluorescence responses to water stress in grapevine leaves: A new remote sensing system. *Remote Sens. Environ.* 73:282-297.

Fradin, E.F., & Thomma, B.P.H.J. (2006). Physiology and molecular aspects of Verticillium wilt diseases caused by *V. dahliae* and *V. albo-atrum*. *Mol. Plant Pathol.* 7:71-86.

Gamliel, A., Grinstein, A., Peretz, Y., Klein, L., Nachmias, A., Tsror, L., Livescu, L., & Katan, J. (1997). Reduced dosage of methyl bromide for controlling Verticillium wilt of potato in experimental and commercial plots. *Plant Dis.* 81:469-474.

Gamon, J.A., Peñuelas, J., & Field, C.B. (1992). A narrow-wave band spectral index that tracks diurnal changes in photosynthetic efficiency. *Remote Sens. Environ.* 41:35-44.

Hau, B. (1988). *Ein erweitertes analytisches modell für epidemien von pflanzenkrankheiten* (An extended analytical model for epidemics of plant diseases). Giessen, Germany: Justus-Liebig-Universität.

Hayat, S., Hasan, S.A., Fariduddin, Q., & Ahmad, A. (2008). Growth of tomato (*Lycopersicon esculentum*) in response to salicylic acid under water stress. *J. Plant Interact.* 3:297-304.

Hoagland, D.R., & Arnon, D.I. (1950). The water culture method for growing plants without soil. California Agricultural Experiment Station, Circular No. 347.

Hosmer, D.W., & Lemeshow, S. (2000). *Applied Logistic Regression*, 2nd ed. New York, NY, USA: John-Wiley & Sons, Inc.

Jackson, R.D., & Pinter, P.J., Jr. (1981). Detection of water stress in wheat by measurement of reflected solar and emitted thermal IR radiation. In *Proc. Intern. Colloquium on Spectral Signatures of Objects in Remote Sensing* (pp. 399-406). Versalles, France: Institut National de la Reserche Agronomique.

Jiménez-Díaz, R.M., Cirulli, M., Bubici, G., Jiménez-Gasco, L.M., Antoniou, P.P., & Tjamos, E.C. (2012). Verticillium wilt, a major threat to olive production: Current status and future prospects for its management. *Plant Dis.* 96:304-329.

Jiménez-Díaz, R.M., Olivares-García, C., Landa, B.B., Jiménez-Gasco, M.M., & Navas-Cortés, J.A. (2011). Region-Wide Analysis of genetic diversity in *Verticillium*

dahliae populations infecting olive in southern Spain and agricultural factors influencing the distribution and prevalence of vegetative compatibility groups and pathotypes. *Phytopathology* 101:304-315.

Jiménez-Díaz, R.M., Tjamos, E.C., & Cirulli, M. (1998). Verticillium wilt of major tree hosts: Olive. In Hiemstra, J.A., & Harris, D.C. (Eds.), *A Compendium of Verticillium Wilt in Tree Species* (pp. 13-16). Wageningen, The Netherlands: Ponsen and Looijen.

Levin, A.G., Lavee, S., & Tsror, L. (2003). Epidemiology of *Verticillium dahliae* on olive (cv. Picual) and its effects on yield under saline conditions. *Plant Pathol.* 52:212-218.

López-Escudero, F.J., & Blanco-López, M.A. (2007). Relationship between the inoculum density of *Verticillium dahliae* and the progress of Verticillium wilt of olive. *Plant Dis.* 91:1372-1378.

López-Escudero, F.J., del Río, C., Caballero, J.M., & Blanco-López, M.A. (2004). Evaluation of olive cultivars for resistance to *Verticillium dahliae*. *Eur. J. Plant Pathol.* 110:79-85.

Lorenzini, G., Guidi, L., Nali, C., Ciompi, S., & Soldatini, G.F. (1997). Photosynthetic response of tomato plants to vascular wilt diseases. *Plant Sci.* 124:143-152.

Madden, L.V., Hughes, G., & van den Bosch, F. (2007). *The Study of Plant Disease Epidemics*. St. Paul, MN, USA: APS Press, The American Phytopathological Society.

Maechler, M., Rousseeuw, P., Struyf, A., Hubert, M., & Hornik, K. (2013). *cluster: Cluster Analysis Basics and Extensions*. R package version 1.14.4.

Marquard, R.D., & Tipton, J.L. (1987). Relationship between extractable chlorophyll and an in situ method to estimate leaf greenness. *HortScience* 22:1327.

McKeen, C.D. (1943). A study of some factors affecting the pathogenicity of *Verticillium albo-atrum*. *R. & B. Can. J. Res.* 21:95-117.

Mengistu, A., Tachibana, H., Epstein, A.H., Bidne, K.G., & Hatfield, J.D. (1987). Use of leaf temperature to measure the effect of brown stem rot and soil moisture stress and its relation to yields of soybeans. *Plant Dis.* 71:632-634.

Mercado-Blanco, J., Rodríguez-Jurado, D., Parrilla-Araujo, S., & Jiménez-Díaz, R.M. (2003). Simultaneous detection of the defoliating and nondefoliating *Verticillium*

dahliae pathotypes in infected olive plants by duplex, nested polymerase chain reaction. *Plant Dis.* 87:1487-149.

Navas-Cortés, J.A., Landa, B.B., Mercado-Blanco, J., Trapero-Casas, J.L., Rodríguez-Jurado, D., & Jiménez-Díaz, R.M. (2008). Spatiotemporal analysis of spread of *Verticillium dahliae* pathotypes within a high tree density olive orchard in southern Spain. *Phytopathology* 98:167-180.

Nilsson, H.E. (1991). Hand-held radiometry and IR-thermography of plant diseases in field plot experiments. *Int. J. Remote Sens.* 12:545-557.

Nilsson, H.E. (1995). Remote sensing and image analysis in plant pathology. *Annu. Rev. Phytopathol.* 15:489-527.

Oksanen, J., Blanchet, F.G., Kindt, R., Legendre, P., Minchin, P.R., *et al.* (2013). *vegan: Community Ecology Package*. R package version 2.0-10.

Papageorgiu, G. (1975). Chlorophyll fluorescence; an intrinsic probe of photosynthesis. In Govindjee (Eds.), *Bioenergetics of photosynthesis* (pp. 319-371.). New York, NY, USA: Academic Press.

Pegg, G.F., & Brady, B.L. (2002). *Verticillium Wilts*. Wallingford, United Kingdom: CABI Publishing.

Pegg, G.F., & Cronshaw, D.K. (1976). Ethylene production in tomato plants infected by *Verticillium albo-atrum*. *Physiol. Plant Pathol.* 8:279-295.

Pinter, P.J., Stanghellini, M.E., Reginato, R.J., Idso, S.B., Jenkins, A.D., & Jackson, R.D. (1979). Remote detection of biological stresses in plants with infrared thermometry. *Science* 205:585-587.

Pullman, G.S., DeVay, J.E., Garber, R.H., & Weinhold, A.R. (1981). Soil Solarization: Effects on Verticillium Wilt of Cotton and Soilborne Populations of *Verticillium dahliae*, *Pythium* spp., *Rhizoctonia solani*, and *Thielaviopsis basicola*. *Phytopathology* 71:954-959.

Romera, F.J., Alcántara, E., & De la Guardia, M.D. (1999). Ethylene production by Fe-deficient roots and its involvement in the regulation of Fe-deficiency stress responses by strategy I plants. *Ann. Bot.* 83:51-55.

Ruggieri, G. (1946). A new disease of olive. *L'Italia Agricola* 83:369-372.

Sadras, V.O., Quiroz, F., Echarte, L., Escande, A., & Pereyra, V.R. (2000). Effect of *Verticillium dahliae* on photosynthesis, leaf expansion and senescence of field-grown sunflower. *Ann. Bot.* 86:1007-1015.

Schreiber, L.R., & Green, R.J., Jr. (1963). Effect of root exudates on germination of conidia and microsc1erotia of *Verticillium albo-atrum* inhibited by the soil fungistatic principle. *Phytopathology* 53:260-264.

Simko, I., & Piepho, H.-P. (2011). The area under the disease progress stairs: calculation, advantage, and application. *Phytopathology* 102:381-389.

Sit, V., & Poulin-Costello, M. (1994). *Catalogue of curves for curve fitting. Biometrics Information Handbook Series, 4*. Victoria, Canada: Forest Science Research Branch, Ministry of Forests.

Suárez, L., Zarco-Tejada, P.J., Berni, J.A.J., González-Dugo, V., & Fereres, E. (2009). Modelling PRI for water stress detection using radiative transfer models. *Remote Sens. Environ.* 113:730-740.

Suárez, L., Zarco-Tejada, P.J., Sepulcre-Cantó, G., Pérez-Priego, O., Miller, J.R., Jiménez-Múñoz, J.C., & Sobrino, J. (2008). Assessing canopy PRI for water stress detection with diurnal airborne imagery. *Remote Sens. Environ.* 112:560-575.

Talboys, P.W. (1962). Systemic movement of some vascular pathogens. *Trans. Br. Mycol. Soc.* 45:280-281.

Thenot, F., Méthy, M., & Winkel, T. (2002). The photochemical reflectance index (PRI) as a water-stress index. *Int. J. Remote Sens.* 23:5135-5139.

Therneau, T., Atkinson, B., & Ripley, B. (2013). *rpart: Recursive Partitioning*. R package version 4.1-4.

Tjamos, E.C., & Fravel, D.R. (1995). Detrimental Effects of Sublethal Heating and *Talaromyces flavus* on Microsclerotia of *Verticillium dahliae*. *Phytopathology* 85:388-392.

Tsror, L. (Lahkim) (2011). Review: Epidemiology and control of Verticillium wilt on olive. *Israel J. Plant Sci.* 59:59-69.

Tu, J.C., & Tan, C.S. (1985). Infrared thermometry for determination of root rot severity in bean. *Phytopathology* 75:840-844.

Villalobos, F.J., Testi, L., Hidalgo, J., Pastor, M., & Orgaz, F. (2006). Modelling potential growth and yield of olive (*Olea europaea* L.) canopies. *Eur. J. Agron.* 24:296-303.

Warnes, G.R., Bolker, B., Bonebakker, L., Gentleman, R., Liaw, W.H.A., *et al.* (2013). *gplots: Various R programming tools for plotting data*. R package version 2.12.1.

Wilhelm, S. (1955). Longevity of the Verticillium wilt fungus in the laboratory and field. *Phytopathology* 45:180-181.

Xu, F., Yang, L., Zhang, J., Guo, X., Zhang, X., & Li, G. (2012). Effect of temperature on conidial germination, mycelial growth and aggressiveness of the defoliating and nondefoliating pathotypes of *Verticillium dahliae* from cotton in China. *Phytoparasitica* 40:319-327.

Yadava, U.L. (1986). A rapid and nondestructive method to determine chlorophyll in intact leaves. *HortScience*, *21*, 1449-1450.

Zarco-Tejada, P.J., Berni, J.A.J., Suárez, L., Sepulcre-Cantó, G., Morales, F., & Miller, J. R. (2009). Imaging chlorophyll fluorescence from an airborne narrow-band multispectral camera for vegetation stress detection. *Remote Sens. Environ.* 113:1262-1275.

Zarco-Tejada, P.J., González-Dugo, V., & Berni, J.A.J. (2012). Fluorescence, temperature and narrow-band indices acquired from a UAV for water stress detection using a hyperspectral imager and a thermal camera. *Remote Sens. Environ.* 117:322-337.

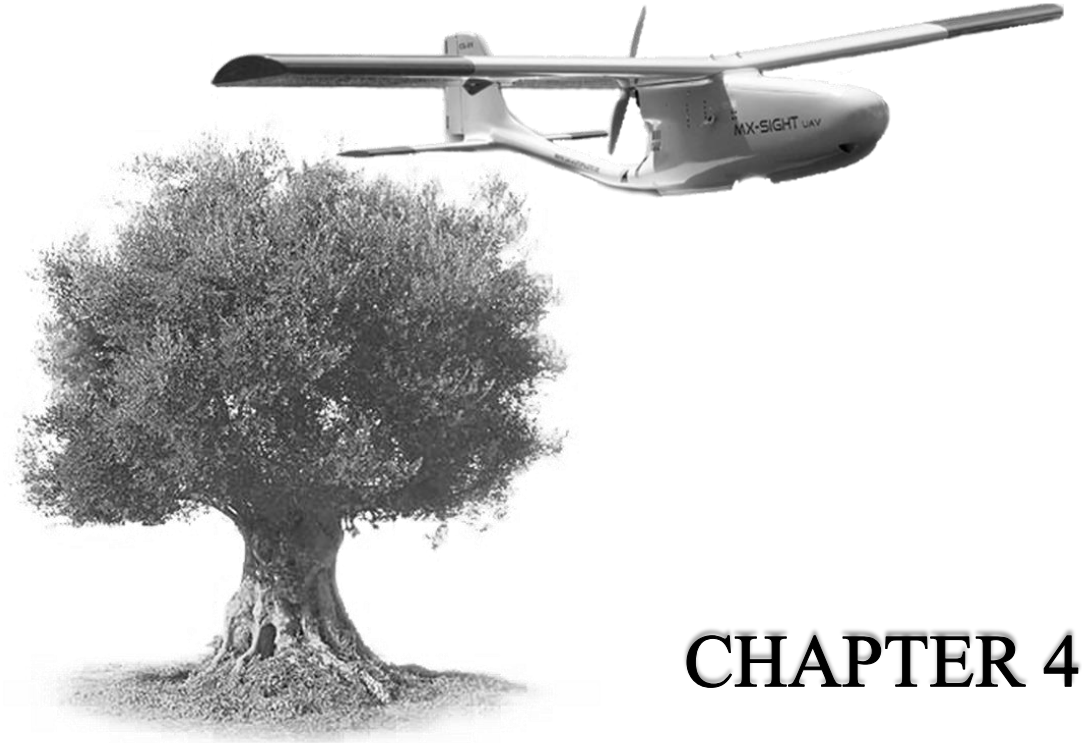

CHAPTER 4

High-resolution airborne hyperspectral and thermal imagery for early detection of Verticillium wilt of olive using fluorescence, temperature and narrow-band spectral indices

Authors: Calderón, R., Navas-Cortés, J.A., Lucena, C., & Zarco-Tejada, P.J.

Instituto de Agricultura Sostenible (IAS), Consejo Superior de Investigaciones Científicas (CSIC), Córdoba, Spain

Published in: *Remote Sensing of Environment* 139:231-245

dx.doi.org/10.1016/j.rse.2013.07.031

CHAPTER 4: High-resolution airborne hyperspectral and thermal imagery for early detection of Verticillium wilt of olive using fluorescence, temperature and narrow-band spectral indices

Resumen

La Verticilosis (VW) causada por el hongo de suelo *Verticillium dahliae* Kleb., es la enfermedad más limitante en todas las regiones olivareras tradicionales del mundo. Este patógeno coloniza el sistema vascular de las plantas, bloqueando el flujo del agua y finalmente induciendo estrés hídrico. El presente estudio exploró el uso de imágenes térmicas de alta resolución, fluorescencia clorofílica, índices estructurales y fisiológicos (índices de xantofilas, clorofila a+b, carotenos y azul/verde/rojo B/G/R) calculados a partir de imágenes multiespectrales e hiperespectrales como indicadores tempranos del estrés hídrico causado por la infección y severidad de la Verticilosis. El estudio se llevó a cabo en dos parcelas de olivar naturalmente infectadas por *V. dahliae*. Se adquirieron series temporales de imágenes térmicas, multiespectrales e hiperespectrales en tres años consecutivos y se relacionaron con la severidad de la enfermedad evaluada al mismo tiempo que los vuelos. Simultáneamente a las campañas de vuelo, las medidas de campo tomadas a nivel foliar y de copa mostraron un aumento significante en la temperatura de copa (Tc) menos la temperatura del aire (Ta) y un descenso de la conductancia estomática foliar (G) a lo largo de los niveles de severidad, identificando árboles infectados por la enfermedad en etapas tempranas del desarrollo de la misma. Elevados valores de Tc − Ta y bajos valores de G medidos en campo fueron asociados con niveles de severidad avanzados. A nivel de hoja, la reducción en G causada por la infección de la Verticilosis fue asociada con un aumento significante en el Photochemical Reflectance Index (PRI_{570}) y una disminución en la fluorescencia clorofílica (F). Los vuelos permitieron la detección temprana de la Verticilosis usando Tc − Ta derivada de las imágenes térmicas, el Crop Water Stress Index (CWSI) calculado a partir de las imágenes térmicas, los ratios azul/azul-verde/azul-rojo (índices B/BG/BR) y la fluorescencia clorofílica, confirmando los resultados obtenidos en campo. Tc − Ta obtenida de los vuelos mostró valores en aumento con un incremento significante de ~2 K en niveles de severidad bajos, y fue significantemente correlacionado con G (R^2 = 0.76, P = 0.002) y PRI_{570} (R^2 = 0.51, P = 0.032). Etapas tempranas del desarrollo de la enfermedad pudieron ser diferenciadas basándose en un aumento del CWSI a medida que la enfermedad progresaba, obteniendo una fuerte correlación con G (R^2 = 0.83, P < 0.001). Igualmente, la fluorescencia clorofílica obtenida a nivel de cubierta descendió en niveles de severidad avanzados, mostrando un aumento significante a medida que la

enfermedad progresaba. Estos resultados indican el potencial de una detección temprana de la infección por *V. dahliae* y la discriminación de los niveles de severidad usando teledetección. Los indicadores basados en temperatura de copa como CWSI, y ratios visibles B/BG/BR así como la fluorescencia fueron efectivos en detectar la Verticilosis en etapa tempranas del desarrollo de la enfermedad. En arboles afectados, los índices estructurales, PRI, índices de clorofila y carotenos, y los ratios R/G fueron buenos indicadores para evaluar el daño causado por la enfermedad.

Palabras clave: Detección de estrés, Hiperespectral, Térmico, Fluorescencia, Alta resolución, UAV, Índices fisiológicos, *Verticillium dahliae*.

Abstract

Verticillium wilt (VW) caused by the soil-borne fungus *Verticillium dahliae* Kleb, is the most limiting disease in all traditional olive-growing regions worldwide. This pathogen colonizes the vascular system of plants, blocking water flow and eventually inducing water stress. The present study explored the use of high-resolution thermal imagery, chlorophyll fluorescence, structural and physiological indices (xanthophyll, chlorophyll a+b, carotenoids and blue/green/red B/G/R indices) calculated from multispectral and hyperspectral imagery as early indicators of water stress caused by VW infection and severity. The study was conducted in two olive orchards naturally infected with *V. dahliae*. Time series of airborne thermal, multispectral and hyperspectral imagery was acquired in three consecutive years and related to VW severity at the time of the flights. Concurrently to the airborne campaigns, field measurements conducted at leaf and tree-crown levels showed a significant increase in crown temperature (Tc) minus air temperature (Ta) and a decrease in leaf stomatal conductance (G) across VW severity levels, identifying VW-infected trees at early stages of the disease. Higher Tc − Ta and lower G values measured in the field were associated with higher VW severity levels. At leaf level, the reduction in G caused by VW infection was associated with a significant increase in the Photochemical Reflectance Index (PRI_{570}) and a decrease in chlorophyll fluorescence (F). The airborne flights enabled the early detection of VW by using canopy-level image-derived airborne Tc − Ta, Crop Water Stress Index (CWSI) calculated from the thermal imagery, blue/blue–green/blue–red ratios (B/BG/BR indices) and chlorophyll fluorescence, confirming the results obtained in the field. Airborne Tc − Ta showed rising values with a significant increase of ~2 K at low VW severity levels, and was significantly correlated with G (R^2 = 0.76, P = 0.002) and PRI_{570} (R^2 = 0.51, P = 0.032). Early stages of disease development could be differentiated based on a CWSI increase as VW developed, obtaining a strong correlation with G (R^2 = 0.83, P < 0.001). Likewise, the canopy-level chlorophyll fluorescence dropped at high VW severity levels, showing a

significant increase as disease progressed. These results indicate the potentials of an early detection of *V. dahliae* infection and discrimination of VW severity levels using remote sensing. Indicators based on crown temperature such as CWSI, and visible ratios B/BG/BR as well as fluorescence were effective in detecting VW at early stages of disease development. In affected trees, the structural indices, PRI, chlorophyll and carotenoid indices, and the R/G ratio were good indicators to assess the damage caused by the disease.

Keywords: Stress detection, Hyperspectral, Thermal, Fluorescence, High resolution, UAV, Physiological indices, *Verticillium dahliae*.

Received: 27 July 2012 / Received in revised form: 24 July 2013 / Accepted: 27 July 2013 / Available online: 5 September 2013

4.1. Introduction

Verticillium wilt (VW) of olive (*Olea europaea* L.) trees, caused by the soil-borne fungus *Verticillium dahliae* Kleb., is the most limiting disease of this crop in all traditional olive-growing regions worldwide (Tsror, 2011; Jiménez-Díaz *et al.*, 2012) and causes severe yield losses and tree mortality (Levin *et al.*, 2003). In Spain, the first reports of the disease, which was found to affect olive crops in the Guadalquivir valley, were documented in the early 1980s (Blanco-López *et al.*, 1984). However, in the last 15-20 years the disease has spread to affect newly established irrigated crops (Sánchez-Hernández *et al.*, 1998; Jiménez-Díaz *et al.*, 2011). Under field conditions, the first VW symptoms in irrigated olive trees growing in *V. dahliae*-infested orchards develop 18-24 months after plantation, depending on the density of pathogen propagules in the soil, the *V. dahliae* pathotype prevailing in the soil, the olive cultivar susceptibility and the environmental conditions (Levin *et al.*, 2003; Navas-Cortés *et al.*, 2008). In the Mediterranean region, over an annual cropping season, disease incidence and symptom severity typically increase from late autumn–early winter to spring and sharply decrease in summer, with no further development until the next autumn; this results in polyetic epidemics over several cropping seasons (Navas-Cortés *et al.*, 2008).

V. dahliae can be found in agricultural soils as resistant survival structures called 'microsclerotia' that are stimulated to germinate by root exudates (Schreiber and Green, 1963) and favorable soil environmental conditions, forming hyphae that penetrate into the plant roots and grow into their tissues until they reach the xylem vessels. The rapid upward spread of the pathogen in vascular tissues occurs primarily through conidia transported with the transpiration stream (Talboys, 1962; Garber and Houston, 1966; Presley *et al.*, 1966; Emechebe *et al.*, 1975). This enables the pathogen to spread

throughout the aerial parts of its host within one growing season. The net effect of pathogen infection is a reduction in water flow that induces water stress and is thought to be mainly responsible for the vascular wilt syndrome caused by *V. dahliae* and other wilt pathogens (Ayres, 1978; DeVay, 1989; Van Alfen, 1989).

Water stress in plants caused by either *V. dahliae* infection or drought-induced stomatal closure reduces the transpiration rate. In turn, this decreases evaporative cooling and increases leaf temperature. Early detection of water stress using remote sensing has been successfully achieved in the past using thermal infrared radiation (Jackson *et al.*, 1977, 1981; Idso *et al.*, 1978, 1981; Jackson and Pinter, 1981). Thermal remote sensing of water stress has been fulfilled using spectrometers at ground level (Jackson *et al.*, 1977, 1981; Idso *et al.*, 1978, 1981), thermal sensors at image level (Leinonen and Jones, 2004; Cohen *et al.*, 2005; Sepulcre-Cantó *et al.*, 2006, 2007; Berni *et al.*, 2009b; Zarco-Tejada *et al.*, 2012) and satellite thermal imagery (Sepulcre-Cantó *et al.*, 2009). Working with hand-held infrared thermometers on herbaceous crops, Jackson and co-workers (Idso *et al.*, 1978; Jackson *et al.*, 1981) developed the Crop Water Stress Index (CWSI), which became a popular thermal-based stress indicator. The CWSI is based on the normalization of differences between canopy (Tc) and air temperature (Ta) with evaporative demand (by means of the vapor pressure deficit). Apart from the progress made in water-stress detection using the thermal region, the visible part of the spectrum has also been useful for early water stress detection. This involves using indices focused on bands located at specific wavelengths where photosynthetic pigments are affected by stress conditions. Two spectral indicators of water stress, spanning initial through severe disease symptoms, are widely used. One is the Photochemical Reflectance Index (PRI) (Gamon *et al.*, 1992). This index is sensitive to the epoxidation state of the xanthophyll cycle pigments and to photosynthetic efficiency, serving as a proxy for water stress detection (Thenot *et al.*, 2002; Peguero-Pina *et al.*, 2008; Suárez *et al.*, 2008, 2009, 2010). Another indicator of water stress is solar-induced chlorophyll fluorescence emission (Flexas *et al.*, 1999, 2000, 2002; Moya *et al.*, 2004; Zarco-Tejada *et al.*, 2009, 2012), because of the strong correlation found between steady-state chlorophyll fluorescence and the reduced assimilation caused by water stress conditions. The PRI has been used to assess pre-visual water stress at leaf level (Thenot *et al.*, 2002; Winkel *et al.*, 2002), at canopy level (Evain *et al.*, 2004; Dobrowsky *et al.*, 2005; Peguero-Pina *et al.*, 2008; Sun *et al.*, 2008) and using airborne imaging spectroscopy (Suárez *et al.*, 2008, 2009, 2010). Chlorophyll fluorescence is associated with photosynthesis and other physiological processes, as demonstrated consistently in laboratory studies (e.g., Papageorgiu, 1975; Krause and Weis, 1984). Over the last five years, scientific interest in steady-state chlorophyll fluorescence (Fs) obtained under natural outdoor conditions has increased due to its potential development using remote sensing methods (Soukupová *et al.*, 2008). Although the contribution of fluorescence to the vegetation's radiance signal is estimated to be 2-3%, methods have been developed to extract the signal (Meroni *et al.*, 2004, 2008a,

2008b, 2009; Moya *et al.*, 2004), proving the feasibility of the fluorescence retrieval using the O_2-A absorption feature at 760 nm.

Remote sensing has been used to detect, monitor and quantify a range of diseases in different crops. Comprehensive reviews on the application of remote sensing to the detection of plant diseases are available (e.g., Jackson, 1986; Hatfield and Pinter, 1993; Nilsson, 1995; West *et al.*, 2003; Sankaran *et al.*, 2010; Barton, 2012). Most studies have focused on foliar pathogens in annual crops, where disease symptoms are mainly characterized by distinct color changes in the aerial parts of the plant. However, this technology also has shown potential for detecting root diseases in several crops (e.g., Raikes and Burpee, 1998; Wang *et al.*, 2004; Reynolds *et al.*, 2012). Canopy temperature has shown to be particularly useful to detect root impairment caused by soil-borne pathogens that lead to water stress symptoms, as mentioned above. In fact, Pinter *et al.* (1979) found foliar temperatures 3-4°C higher than those of healthy plants in sugar beet and cotton. Other examples of the use of leaf temperature for the detection of diseases caused by soil-borne pathogens include beans infected with *Fusarium solani*, *Pythium ultimum* or *Rhizoctonia solani* (Tu and Tan, 1985); soybeans affected by brown stem rot caused by *Phialophora gregata* (Mengistu *et al.*, 1987); the flag leaf temperature of cereals with root and vascular diseases, such as barley infected by *Pyrenophora graminea* and wheat infected with *Cephalosporium gramineum* (Nilsson, 1995); and wheat with moderate take-all symptoms caused by *Gaeumannomyces graminis* var. *tritici* (Nilsson, 1991).

Other approaches have included the use of multispectral and hyperspectral imagery, as well as airborne digital color or video imagery, to detect crop diseases. Multispectral imagery enabled the detection of head blight in winter wheat (Dammer *et al.*, 2011), assessment of severity of soybean root rot (Wang *et al.*, 2004) and to evaluate *Rhizoctonia* blight in creeping bentgrass (Raikes and Burpee, 1998). Hyperspectral canopy reflectance was used to quantify *Rhizoctonia* crown and root rot in sugar beet (Reynolds *et al.*, 2012) and to detect the co-infection of sugar beet with this pathogen and the plant parasitic nematode *Heterodera schachatii* (Hillnhütter *et al.*, 2011) as well as *Fusarium* head blight in wheat (Bauriegel *et al.*, 2011).

Some research has been conducted on remote detection of diseases caused by *V. dahliae*. Nilsson (1995) reported that oilseed rape plants infected with *V. dahliae* exhibited leaf temperatures 5-8°C higher than non-infected plants. Chen *et al.* (2008, 2011) reported the application of hyperspectral reflectance to identify cotton canopy affected by VW. They found that the spectral characteristics of infected plants changed gradually with the increase in the visible region with disease severity, while a reduction occurred in the near-infrared region. Yet, to our knowledge remote sensing physiological indices and fluorescence indicators have not been used to study olive tree diseases.

The main objective of this research was to evaluate the use of high-resolution thermal imagery and physiological indices calculated from multispectral and hyperspectral imagery as indicators of VW infection and severity in olive orchards. Time series of airborne thermal, multispectral and hyperspectral imagery were acquired in three consecutive campaigns and related to VW severity at the time of the flight. The hypothesis is that thermal and hyperspectral indices acquired from the airborne imagery are sensitive to physiological changes induced by the infection and colonization by *V. dahliae*.

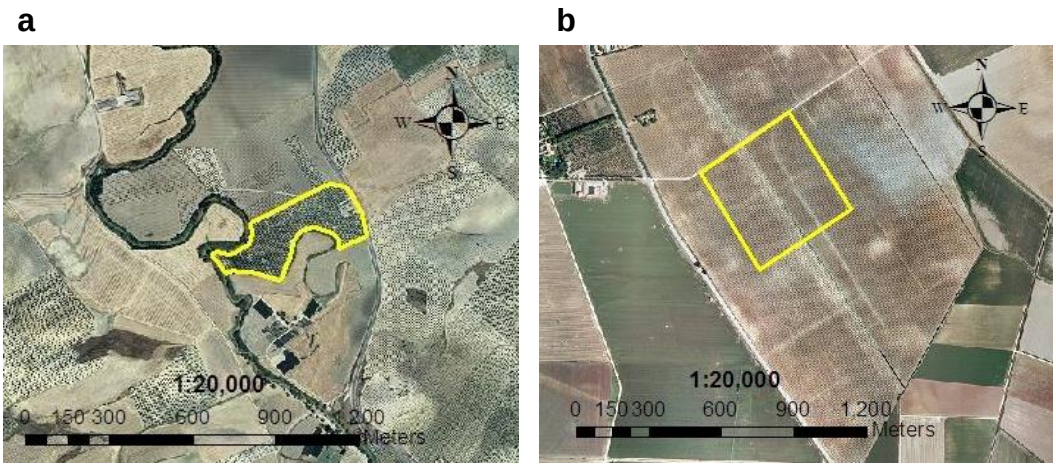

Figure 4.1. Overview of the two study sites in southern Spain used in this study: (a) 7 ha commercial olive orchard in Castro del Rio (Cordoba province); (b) 10-ha commercial olive orchard in Utrera (Seville province).

4.2. Materials and Methods

4.2.1. Study site description

The experimental areas were located in Andalucia, in southern Spain, a region of Mediterranean climate characterized by warm and dry summers and cool and wet winters, with an average annual rainfall of over 550 mm. Two study sites were selected in the Cordoba and Seville provinces, respectively, to account for differences in weather conditions, crop age and tree-crown size, olive cultivars with different reactions to VW and VW incidence and severity. The first study site was located in Castro del Rio (Cordoba province, Spain) (37° 42′ 20″ N, 4° 30′ 45″ W) in a 7-ha commercial orchard planted in 2001 with the olive cultivar (cv.) Picual at a spacing of 6 × 4 m (Fig. 4.1a). Cv. Picual has been found to be highly susceptible to D and susceptible to ND *V. dahliae*, under controlled conditions in artificial inoculation tests (López-Escudero *et al.*, 2004). The initial VW incidence (i.e., percentage of VW symptomatic trees) was estimated in

12%. The second study site was located in Utrera (Seville province, Spain) (37° 4′ 42″ N, 5° 50° 58″ W), in a 10-ha commercial orchard planted in 2006 with cv. Arbequina (Fig. 4.1b). Cv. Arbequina has been shown to be susceptible to D and moderately resistant to ND *V. dahliae*, under controlled conditions in artificial inoculation tests (López-Escudero *et al.*, 2004). The olive trees were planted at a spacing of 6 × 3 m. The initial VW incidence was estimated in 30%. Both orchards were drip irrigated and managed using no-tillage practices; weed control was achieved with herbicide treatments between rows.

4.2.2. Verticillium wilt assessment

Incidence and severity of VW symptoms were assessed in both plots in spring and summer of 2009, 2010 and 2011 in coincidence with airborne campaigns. Severity of the disease was assessed by visual observation of foliar symptoms in each individual tree and assessment on a 0 to 4 rating scale according to the percentage of foliage with disease symptoms, where: 0 = 0%, 0.2 and 0.5 = initial symptoms, 1 = 1 to 33%, 2 = 34 to 66%, 3 = 67 to 100%, and 4 = dead plant. *V. dahliae* infection was confirmed in a sample from each experimental plot by isolating six stem fragments sampled from each of four young symptomatic branches per symptomatic tree as previously described (Navas-Cortés *et al.*, 2008). Identification of *V. dahliae* isolates was based on the morphology of conidiophores and microsclerotia and confirmed by molecular typing through PCR assay using primers DB19/ DB22/espdef01 (Mercado-Blanco *et al.*, 2003); this method yielded a polymorphic amplicon of 523 or 539 bp specific to *V. dahliae*. PCR amplification and gel electrophoresis were conducted as described previously (Mercado-Blanco *et al.*, 2003).

4.2.3. Field measurements

Leaf and near-canopy field measurements were conducted in the olive orchard located in Castro del Rio (Cordoba) during the summer of 2011 to take: a) diurnal measurements throughout the day to monitor the diurnal variation of crown temperature (Tc – Ta) and stomatal conductance (G) in trees covering a gradient in severity levels; and b) leaf and crown measurements at midday to monitor the variation along the VW severity levels of Tc – Ta, leaf chlorophyll fluorescence, leaf Photochemical Reflectance Index (PRI_{570}) (Gamon *et al.*, 1992) and leaf stomatal conductance (G). Eight trees showing different VW severity levels were selected to record pure crown temperature (Tc) with the objective of monitoring its diurnal variation. These measurements were conducted from 7:00 to 17:00 GMT at 5-minute intervals in two dataloggers (model CR10X, Campbell Sci., Logan, UT, USA) with infrared temperature (IRT) sensors (22° half-angle FOV) (model IRR-P, Apogee, Logan, UT, USA) placed 1 m above trees. The

single-band infrared temperature (IRT) sensors covered the 6.5-14 μm range and were evaluated both in the laboratory and in field conditions to characterize the IRT response to diurnal temperature variation (Sepulcre-Cantó *et al.*, 2006). The results yielded errors within the accuracy limits of the instrument (±0.4°C) over a 5° to 40°C range. The instruments were calibrated in the laboratory using a uniform calibration body (integrating sphere, CSTM-USS-2000C Uniform Source System, LabSphere, NH, USA) at two different levels of illumination. This procedure has been reported to be successful in other studies focused on monitoring crown temperature as an indicator of water stress (Berni *et al.*, 2009b; Sepulcre-Cantó *et al.*, 2006; Zarco-Tejada *et al.*, 2012). Air temperature (Ta) and relative humidity (RH) were measured above the canopy with a portable weather station (Model WXT510, Vaisala, Finland) placed 1 m above the canopy (approx. 6 m above the ground). In each of the eight monitored trees, leaf stomatal conductance was measured from 7:00 to 17:00 GMT at 2-hour intervals with a leaf porometer (model SC-1, Decagon Devices, Washington, DC, USA) to monitor the diurnal variation of crown stomatal conductance for the different VW severity levels. A total of five illuminated leaves per tree were measured at each time interval.

In addition to the diurnal measurements conducted for temperature and stomatal conductance, 25 trees covering a gradient in severity levels from asymptomatic to severely affected trees were chosen to monitor the variation of Tc – Ta, leaf chlorophyll fluorescence, leaf PRI_{570} and leaf G between 10:00 and 13:00 GMT on 27 and 28 July 2011. Leaf chlorophyll fluorescence measurements taken under natural sunlight conditions were conducted using the PAM-2100 Pulse-Amplitude Modulated Fluorometer (Heinz Walz GMBH, Effeltrich, Germany). This device measured steady-state Fs and Fm' fluorescence parameters in 25 illuminated leaves per tree. Leaf PRI_{570} measurements calculated as $(R_{570} - R_{531}) / (R_{570} + R_{531})$ (Suárez *et al.*, 2008, 2009, 2010; Zarco-Tejada *et al.*, 2012) were taken in 25 illuminated leaves per tree with a PlantPen instrument custom designed to measure the R_{531} and R_{570} bands (Photon System Instrument, Brno, Czech Republic). Leaf G was measured in five illuminated leaves per tree with the leaf porometer previously used.

4.2.4. Airborne campaigns and remote sensing indices

Imagery in the three years of experiments was acquired from both study sites using narrow-band multispectral, hyperspectral and thermal cameras. The multispectral and thermal cameras were used in airborne campaigns conducted twice per crop season in spring (April/May) and summer (July) of 2009 and 2010. In addition, the thermal camera was flown twice in June 2011. The multispectral and thermal imagery was always acquired at similar sun angles at 10:30 and 12:00 GMT respectively to minimize differences due to sun angle effects between airborne campaigns. Hyperspectral and

thermal images were acquired from the Castro del Rio site on 23 June 2011 at 9:00 GMT using a hyperspectral imager concurrently with the thermal camera operated in 2009 and 2010.

The flights were conducted with two different unmanned aerial vehicles (UAVs) operated by the Spanish Laboratory for Research Methods in Quantitative Remote Sensing (Quantalab, IAS-CSIC, Spain) (Zarco-Tejada *et al.*, 2008, 2012; Berni *et al.*, 2009b). The UAV used for the multispectral and thermal acquisition had a 2-m wingspan for a fixed-wing platform at 5.8 kg take-off weight (TOW) (mX-SIGHT, UAV Services and Systems, Germany) capable of 1-hour endurance. Hyperspectral images were acquired with a larger UAV with a 5-m wingspan for a fixed-wing platform having 13.5 kg take-off weight (TOW) (Viewer, ELIMCO, Seville, Spain) capable of 3-hour endurance. This larger platform was required when operating the hyperspectral imager due to the heavier payload. Both UAV platforms were controlled by an autopilot system (AP04, UAV Navigation, Madrid, Spain) that provided autonomous navigation based on coordinates programmed during the mission planning.

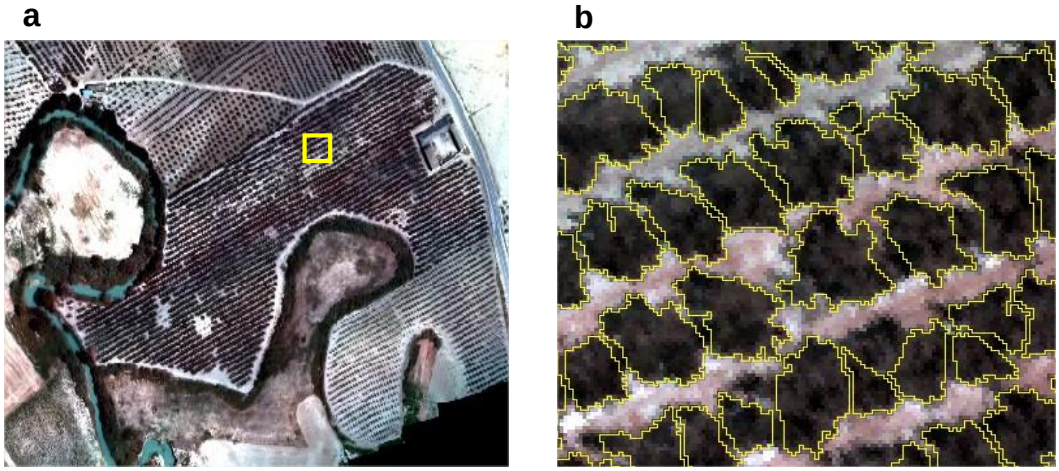

Figure 4.2. Multispectral scene (a) obtained with the multispectral camera on board the UAV platform at 20-cm resolution, showing the Castro del Rio orchard study site (Córdoba province). (b) Automatic object-based crown detection applied to the multispectral imagery to identify pure olive crowns. Yellow square (a) shown in detail in (b).

The multispectral sensor consisted of a 6-band multispectral camera (MCA-6, Tetracam, Inc., California, USA) flying at 250 m above ground level (AGL). The camera was equipped with six independent image sensors and optics with 25-mm diameter filters of 10-nm full width at half-maximum (FWHM) bandwidth (Berni *et al.*, 2009b; Zarco-Tejada *et al.*, 2009). Image resolution was 2592 × 1944 pixels with 10-bit radiometric resolution and an optical focal length of 8.4 mm, yielding an angular field of view (FOV)

of 38.04° × 28.53° and a spatial resolution of 20 cm at 250 m altitude (Fig. 4.2a). The band sets used in each study site included centered wavelengths at 450, 490, 530, 570, 670 and 800 nm.

The hyperspectral imager (Micro-Hyperspec VNIR model, Headwall Photonics, MA, USA) was flown in 2011 at Castro del Río site in the spectral mode with 260 bands at 1.85 nm/pixel at 12-bit radiometric resolution. It yielded a 3.2-nm FWHM with a 12-micron slit and a 6.4-nm FWHM with a 25-micron slit. Data acquisition and storage on board the UAV was set to 50 fps with 18-ms integration time. The 8-mm optical focal length yielded an IFOV of 0.93 mrad and an angular FOV of 49.82°, obtaining a swath of 522 m at 53 × 42 cm resolution, resampled to 40 cm (Fig. 4.3a) for a flight conducted at 550 m AGL altitude and 75 km/h ground speed (Zarco-Tejada *et al.*, 2012).

The multispectral and hyperspectral images were radiometrically calibrated with a uniform light source system (integrating sphere, CSTM-USS-2000C Uniform Source System, LabSphere, NH, USA) at four different levels of illumination and six different integration times. Atmospheric correction was performed with the SMARTS simulation model developed by the National Renewable Energy Laboratory, US Department of Energy (Gueymard, 1995, 2001). This was done using aerosol optical depth measured at 550 nm with a Micro-Tops II sunphotometer (Solar LIGHT Co., Philadelphia, PA, USA). This radiative transfer model has been used in previous studies to perform the atmospheric correction of both narrow-band multispectral and hyperspectral imagery (Berni *et al.*, 2009a, 2009b; Suárez *et al.*, 2010; ZarcoTejada *et al.*, 2012).

A miniaturized inertial measurement unit (IMU) installed on board the UAV and synchronized with the hyperspectral imager acquired altitude data at 100 Hz frequency. The imagery was later orthorectified using PARGE software (ReSe Applications Schläpfer, Wil, Switzerland) (Fig. 4.3a). The mean radiance and reflectance spectra calculated for the six spectral bands obtained by the multispectral camera and the 260 spectral bands acquired by the hyperspectral imager were then used to calculate several spectral indices related to: i) tree crown structure; ii) epoxidation state of the xanthophyll cycle; iii) chlorophyll a+b concentration; iv) blue/green/red ratio indices; v) carotenoid concentration; vi) chlorophyll fluorescence and vii) spectral disease indices (Table 4.1).

The chlorophyll fluorescence retrieval method used was based on the FLD principle (Plascyk, 1975) using three bands as in Maier *et al.* (2003) (see Zarco-Tejada *et al.*, 2012 for fluorescence quantification in a citrus crop using this same hyperspectral imager). Previous results demonstrated the feasibility of retrieving the chlorophyll fluorescence signal using this hyperspectral imager (Zarco-Tejada *et al.*, 2012, 2013). For this reason, the FLD principle could be applied to the hyperspectral imagery to estimate the fluorescence signal, using a total of three bands required for the FLD3 method, where the band inside the O_2-A feature (the "in" wavelength indicates the radiance at L763 nm) and

the radiances (L750 nm; L780 nm) determined at two wavelengths outside and on either side of the O_2-A feature, referred to as the "out" bands.

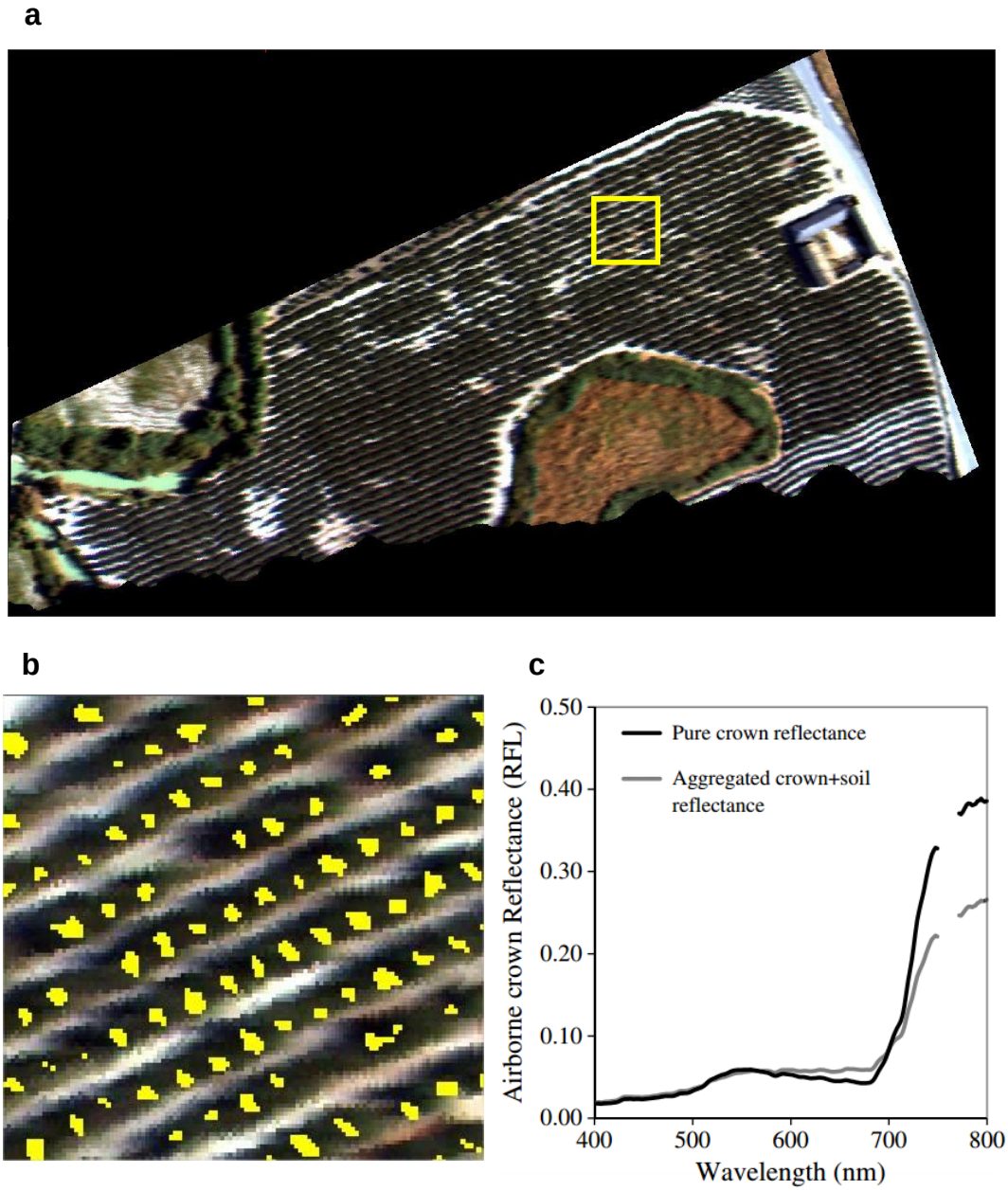

Figure 4.3. Hyperspectral scene (a) obtained with the hyperspectral imager on board the UAV platform at 40-cm resolution. Automatic object-based crown detection applied to the hyperspectral imagery to identify pure olive crowns (b). The methodology enabled the separation of pure olive crowns from shaded and sunlit soil reflectance, observing the effects of pixel aggregation (c). Yellow square (a) shown in detail in (b).

Table 4.1. Overview of the vegetation indices used in this study and their formulations.

Vegetation indices	Equation	Reference
Structural indices		
Normalized Difference Vegetation Index	$NDVI = (R_{800} - R_{670})/(R_{800} + R_{670})$	Rouse *et al.* (1974)
Renormalized Difference Vegetation Index	$RDVI = (R_{800} - R_{670})/\sqrt{(R_{800} + R_{670})}$	Rougean & Breon (1995)
Optimized Soil-Adjusted Vegetation Index	$OSAVI = ((1 + 0.16) \cdot (R_{800} - R_{670})/(R_{800} + R_{670} + 0.16))$	Rondeaux *et al.* (1996)
Triangular Vegetation Index	$TVI = 0.5 \cdot [120 \cdot (R_{750} - R_{550}) - 200 \cdot (R_{670} - R_{550})]$	Broge & Leblanc (2000)
Modified Triangular Vegetation Index	$MTVI = 1.2 \cdot [1.2 \cdot (R_{800} - R_{550}) - 2.5 \cdot (R_{670} - R_{550})]$	Haboudane *et al.* (2004)
Simple Ratio	$SR = R_{800}/R_{670}$	Jordan (1969)
Modified Simple Ratio	$MSR = \frac{R_{800}/R_{670} - 1}{(R_{800}/R_{670})^{0.5} + 1}$	Chen (1996)
Xanthophyll indices		
Photochemical Reflectance Index (570)	$PRI_{570} = (R_{570} - R_{531})/(R_{570} + R_{531})$	Gamon *et al.* (1992)
Photochemical Reflectance Index (515)	$PRI_{515} = (R_{515} - R_{531})/(R_{515} + R_{531})$	Hernández-Clemente *et al.* (2011)
Chlorophyll a+b indices		
RedEdge	$ZM = R_{750}/R_{710}$	Zarco-Tejada *et al.* (2001)
Vogelmann	$VOG1 = R_{740}/R_{720}$	Vogelmann *et al.* (1993)
Gitelson &Merzlyak indices	$GM1 = R_{750}/R_{550}$	Gitelson & Merzlyak (1997)
	$GM2 = R_{750}/R_{700}$	Gitelson & Merzlyak (1997)
Pigment Specific Simple Ratio Chlorophyll a	$PSSRa = R_{800}/R_{675}$	Blackburn (1998)
Pigment Specific Simple Ratio Chlorophyll b	$PSSRb = R_{800}/R_{650}$	Blackburn (1998)
Modified Chlorophyll-Absorption-Integral	$mCAI = \frac{(R_{545} + R_{752})}{2} \cdot (752 - 545) - \sum_{R_{545}}^{R_{752}} (R \cdot 1.158)$	Laudien *et al.* (2003)
Transformed Chlorophyll Absorption in Reflectance Index	$TCARI = 3 \cdot [(R_{700} - R_{670}) - 0.2 \cdot (R_{700} - R_{550}) \cdot (R_{700}/R_{670})]$	Haboudane *et al.* (2002)
Transformed Chlorophyll Absorption in Reflectance Index/ Optimized Soil-Adjusted Vegetation Index	$\frac{TCARI}{OSAVI} = \frac{3 \cdot [(R_{700} - R_{670}) - 0.2 \cdot (R_{700} - R_{550}) \cdot (R_{700}/R_{670})]}{((1 + 0.16) \cdot (R_{800} - R_{670})/(R_{800} + R_{670} + 0.16))}$	Haboudane *et al.* (2002)
R/G/B indices		
Redness index	$R = R_{700}/R_{670}$	Gitelson *et al.* (2000)
Greenness index	$G = R_{570}/R_{670}$	This study
Blue index	$B = R_{450}/R_{490}$	This study
Blue/green indices	$BGI1 = R_{400}/R_{550}$	Zarco-Tejada *et al.* (2005)
	$BGI2 = R_{450}/R_{550}$	Zarco-Tejada *et al.* (2005)
Blue/red indices	$BRI1 = R_{400}/R_{690}$	Zarco-Tejada *et al.* (2012)
	$BRI2 = R_{450}/R_{690}$	Zarco-Tejada *et al.* (2012)
Lichtenhaler index	$LIC3 = R_{440}/R_{740}$	Lichtenhaler *et al.* (1996)
Carotenoid indices		
Structure-Intensive Pigment Index	$SIPI = (R_{800} - R_{445})/(R_{800} + R_{680})$	Peñuelas *et al.* (1995)
Pigment Specific Simple Ratio Carotenoids	$PSSRc = R_{800}/R_{500}$	Blackburn (1998)
R_{520}/R_{500}	R_{520}/R_{500}	Zarco-Tejada *et al.* (2012)
R_{515}/R_{570}	R_{515}/R_{570}	Zarco-Tejada *et al.* (2012)
R_{515}/R_{670}	R_{515}/R_{670}	Zarco-Tejada *et al.* (2012)
Fluorescence		
FLD	$FLD3\ (747; 762; 780)$	Plascyk (1975) Maier *et al.* (2003) Zarco-Tejada *et al.* (2005)
Plant disease index		
Healthy-index	$HI = \frac{R_{534} - R_{698}}{R_{534} + R_{698}} - \frac{1}{2} \cdot R_{704}$	Mahlein *et al.* (2013)
Crop water stress index		
CWSI	$CWSI = \frac{\gamma \cdot (1 + r_c/r_a) - \gamma^*}{\Delta + \gamma \cdot (1 + r_c/r_a)}$	Jackson *et al.* (1981)

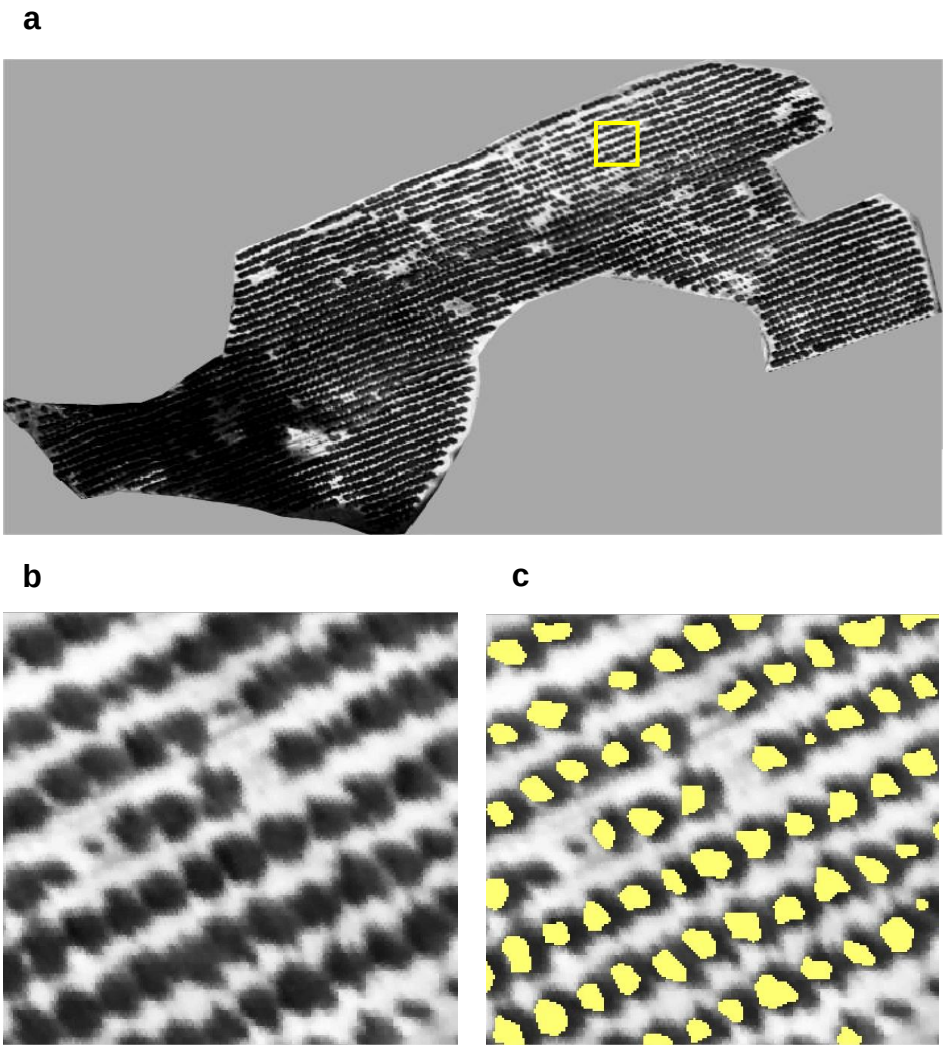

Figure 4.4. Thermal scene (a) of the Castro del Rio site (Córdoba province) obtained with the thermal camera on board the UAV platform at 20-cm resolution, enabling pure olive crown identification (b). Automatic object-based crown detection applied to the thermal imagery to identify pure olive crowns (c). Yellow square (a) shown in detail in (b; c).

The thermal camera (MIRICLE 307, Thermoteknix Systems Ltd, Cambridge, UK) installed on board the two UAVs operated in this study was flown over the experimental sites at altitudes ranging between 150 m and 250 m AGL in 2009 and 2010, and at 550 m AGL when flown together with the hyperspectral imager in 2011 in the morning (~ 9:00 GMT). This camera had a 14.25 mm f1.3 lens connected to a computer via a USB 2.0 protocol. The image sensor was a Focal Plane Array (FPA) based on uncooled microbolometers with a spectral range of 8-12 μm, yielding a 25 μm pixel size. The

camera delivered raw images with a 640 × 480 pixel resolution and 14-bit at-sensor uncalibrated radiance. The camera was radiometrically calibrated in the laboratory using blackbodies at varying target and ambient temperatures to develop radiometric calibration algorithms along with an internal calibration for non-uniformity correction (NUC). Thermal images were acquired at 20 cm pixel resolution, enabling the retrieval of "pure crown" average temperature from each tree studied (Fig. 4.4a). Local atmospheric conditions were determined by air temperature, relative humidity and barometric pressure at the time of flight using a portable weather station (Model WXT510, Vaisala, Finland).

The high-resolution imagery acquired over the orchards enabled single tree identification for field validation purposes (Fig. 4.4b), successfully separating pure crown from soil pixels (Fig. 4.3c). Each single pure tree crown in the entire orchard was identified using automatic object-based crown detection algorithms (Figs. 4.2b; 4.3b; 4.4c). The algorithms applied to the thermal, multispectral and hyperspectral imagery enabled calculation of mean temperature and multispectral and hyperspectral reflectance at pure-crown level for the entire scenes acquired with the unmanned vehicles. The Crop Water Stress Index (CWSI) was calculated for each single tree crown using the high-resolution airborne thermal imagery acquired as described in Berni *et al.* (2009a), with the inputs detailed in Table 4.2.

Table 4.2. Inputs used to calculate the Crop Water Stress Index (CWSI) from high resolution airborne thermal imagery acquired in June 2011 in the Castro del Rio site. The CWSI was calculated as described in Berni *et al.* (2009a).

Inputs	Values	
	2 June 2011	15 June 2011
Air temperature (ºC)	22.93	29.58
Relative humidity (%)	30.31	30.14
Wind speed (m/s)	1	1
Wind measurement height (m)	5	5
Atmospheric pressure (kPa)	99.45	99.60
Cloudiness	0.2	0.2
Latitude (ºN)	37.7058	37.7058
Longitude (ºE)	-4.5117	-4.5117
Altitude (m)	236	236
Solar time (decimal hour)	12.05	12.35
DOY	153	166
Canopy temperature (ºC)	From image	From image
Canopy height (m)	4	4
Frontal LAI	1	1
Canopy emissivity ε	0.98	0.98

4.3. Results and Discussion

4.3.1. Verticillium wilt symptom development

VW symptoms developed extensively in both study sites from early autumn to early winter, reaching their maximum expression during the spring. In the Utrera study site, characterized by 3-year-old cv. Arbequina olive trees, the symptoms consisted mainly of an extensive early drop of infected leaves that were still green; in most cases, this caused a complete defoliation and necrosis of affected branches. In the more established Castro del Rio study site, characterized by 10-yr old cv. Picual olive trees, affected plants mainly exhibited a quick dieback of olive twigs and branches where leaves turned light brown, rolled back toward the abaxial side and dried up, but typically remained attached to the symptomatic shoots. In both experimental sites, if the first VW symptoms developed in the spring, the trees underwent flower mummification and necrosis of both inflorescences and leaves of affected shoots, which usually fell. The type of VW symptoms and temporal dynamics of VW epidemics observed in both study sites were similar to those described in olive orchards affected by VW in southern Spain (Navas-Cortés *et al.*, 2008).

In May 2009, 13.7 and 32.2% of trees were affected by VW in the Castro del Rio and Utrera study sites, respectively (Fig. 4.5a,c), with a mean disease severity in symptomatic trees of 1.26 and 1.19 (0-4 rating scale), respectively. These figures were determined from 41.4% that showed initial disease severity (DS) symptoms ($0 > DS \leq 0.5$), 37.5% had low disease severity symptoms ($0.5 > DS \leq 1.5$), 12.7% had moderate disease severity symptoms ($1.5 > DS \leq 2.5$) and 8.4% of symptomatic trees had severe ($DS \geq 3$) disease symptoms at Castro del Rio. At Utrera, 32.7, 43.0, 17.7 and 6.6% of trees showed these same severity levels, respectively (Fig. 4.5). During the spring of 2009, the disease progressed in both study sites to reach a global incidence of 15.9 and 39.3% in summer at Castro del Rio and Utrera, respectively (Fig. 4.5b,d); however, a similar frequency of trees remained in the three severity classes indicated above. In the 2010 season, overall disease incidence increased to 17.3 and 44.7% at Castro del Rio and Utrera, respectively (Fig. 4.5b,d), but mean disease severity decreased to 1.10 and 1.05 in both sites, respectively. However, minor differences were observed between both sites and the two assessment dates regarding the frequency of affected trees in the three severity classes. The overall frequency of trees at Castro del Rio in the four severity classes ranged from initial (47.3-53.9%), to low (35.6-31.4%), moderate (7.8-1.1%) and severe (9.3-1.6%) disease symptoms (Fig. 4.5b,d).

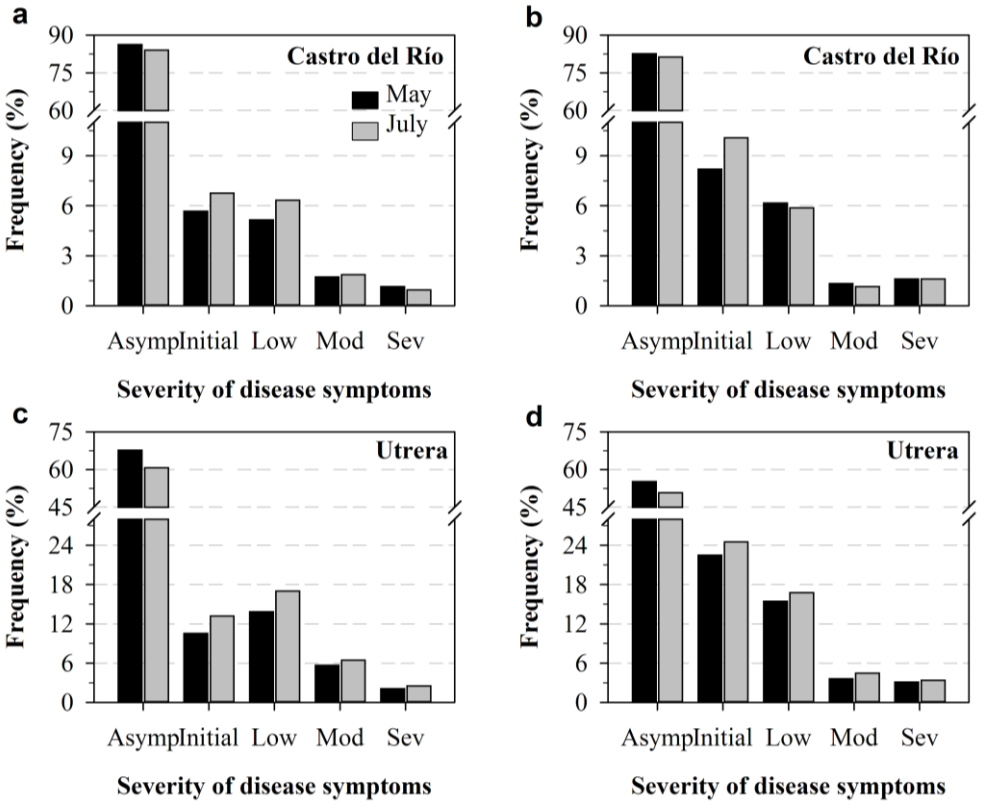

Figure 4.5. Frequency (%) of olive trees showing Verticillium wilt (VW) symptoms at the different severity values in Castro del Rio (Córdoba province) (a,b) and Utrera (Seville province) (c,d) study sites assessed in May and July of 2009 (a,c) and 2010 (b,d). VW severity was assessed by visual inspection of each individual tree using a 0-4 rating scale according to percentage of foliage with disease symptoms, where: 0 = 0%, IS=initial symptoms, 1 = 1 to 33%, 2 = 34 to 66%, 3 = 67 to 100% and 4 = dead plant. Severity of disease symptoms were grouped in asymptomatic (DS=0), initial (0.2≤DS≤0.5), low (1≤DS≤1.5), moderate (2≤DS≤2.5) and severe (3≤DS≤4) disease symptoms.

4.3.2. Field measurement results

Diurnal crown measurements were conducted with the IRT sensors on trees selected to represent asymptomatic trees and those showing initial, low, moderate and severe disease symptoms. Results revealed that midday (i.e., 10:00 to 14:00 GMT) was the best time period to maximize differences in Tc − Ta values. In fact, Tc − Ta values at midday increased with the rise in disease severity level (Fig. 4.6), showing up to 7 K temperature differences between asymptomatic trees (DS = 0) and severely affected trees (DS ≥ 3). Moreover, Tc − Ta values were able to discriminate asymptomatic trees from those affected at early stages of disease development (DS ≤ 1.5), which showed Tc − Ta values from 1 to 2.5 K higher. These results showing lower Tc − Ta values in asymptomatic than

in symptomatic diseased olive trees are in agreement with other studies. Thus, Nilsson (1995) reported higher leaf temperatures in oil seed plants infected with *V. dahliae*. The leaf stomatal conductance (G) data measured on the same trees consistently showed a decrease in stomatal conductance values as crown temperature and disease severity levels increased (Fig. 4.7). These results are in agreement with Berni *et al.* (2009b) and Sepulcre-Cantó *et al.* (2006), who assessed the relationship between stomatal conductance and water stress levels due to deficit irrigation practices in olive trees using thermal sensors and a leaf porometer. A greater difference in stomatal conductance between healthy asymptomatic trees and VW-affected trees was recorded in the morning, with G differences up to 900 mmol/m^2/s between trees with extreme DS values (i.e., DS = 0 vs. DS $\geq$ 3). These differences decreased to a maximum of 700 mmol/m^2/s at midday and declined to 500 mmol/m^2/s after sunset. In addition, our results showed that stomatal conductance was able to discriminate between healthy trees and those at early stages of disease development, which had G values at least 300-500 mmol/m^2/s lower than those of healthy trees.

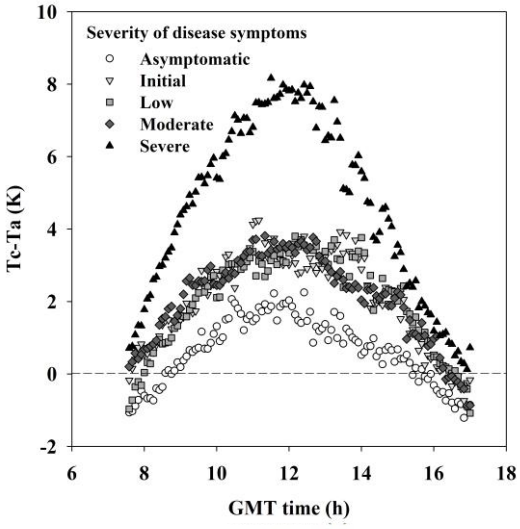

Figure 4.6. Diurnal mean crown temperature (Tc-Ta) measured from 7:00 to 17:00 GMT at 5-minute intervals and obtained with the IRT sensors from trees showing different Verticillium wilt severity levels in the Castro del Rio site (Córdoba province) in the summer of 2011.

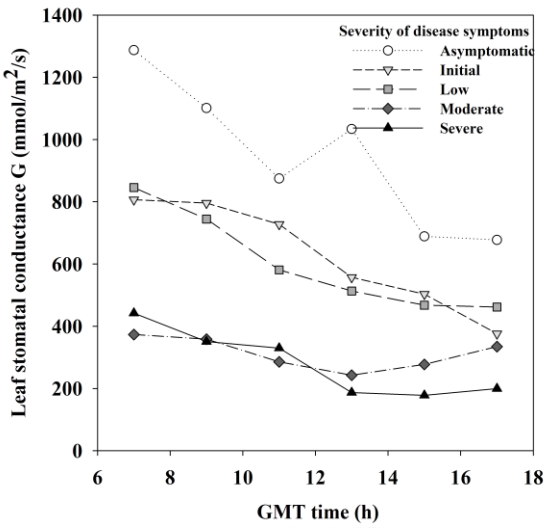

Figure 4.7. Diurnal mean leaf stomatal conductance G measured from 7:00 to 17:00 GMT at 2-hour intervals and obtained with the leaf porometer from trees showing different Verticillium wilt severity levels (n=5 per tree at each measuring time) in the Castro del Rio site (Córdoba province) in the summer of 2011.

Data on crown temperature (Tc − Ta), leaf stomatal conductance (G), leaf PRI_{570} and fluorescence (Fs) acquired between 10:00 and 13:00 GMT in July 2011 were analyzed in trees with different VW severity levels (Fig. 4.8). Crown temperature data (Tc − Ta) measured at midday with IRT sensors in VW affected trees was significantly ($P < 0.05$) higher than that measured in asymptomatic trees, being highest for trees affected by severe VW symptoms (Fig. 4.8a). By contrast, stomatal conductance G showed a negative trend as VW severity increased, showing significant ($P < 0.05$) changes from asymptomatic trees at those showing moderate and severe symptoms (DS ≥ 2) (Fig. 4.8b). Moreover, PRI_{570} was lowest ($P < 0.05$) in asymptomatic trees, and increased steadily with the increase in VW severity (Fig. 4.8c). These results are consistent with that obtained by Suárez *et al.* (2008, 2009) in water-stressed trees. Leaf chlorophyll fluorescence measurements of Fs (Fig. 4.8d) showed a downward trend as VW severity level increased as previously found for trees under water stress (Pérez-Priego *et al.*, 2005; Zarco-Tejada *et al.*, 2009, 2012).

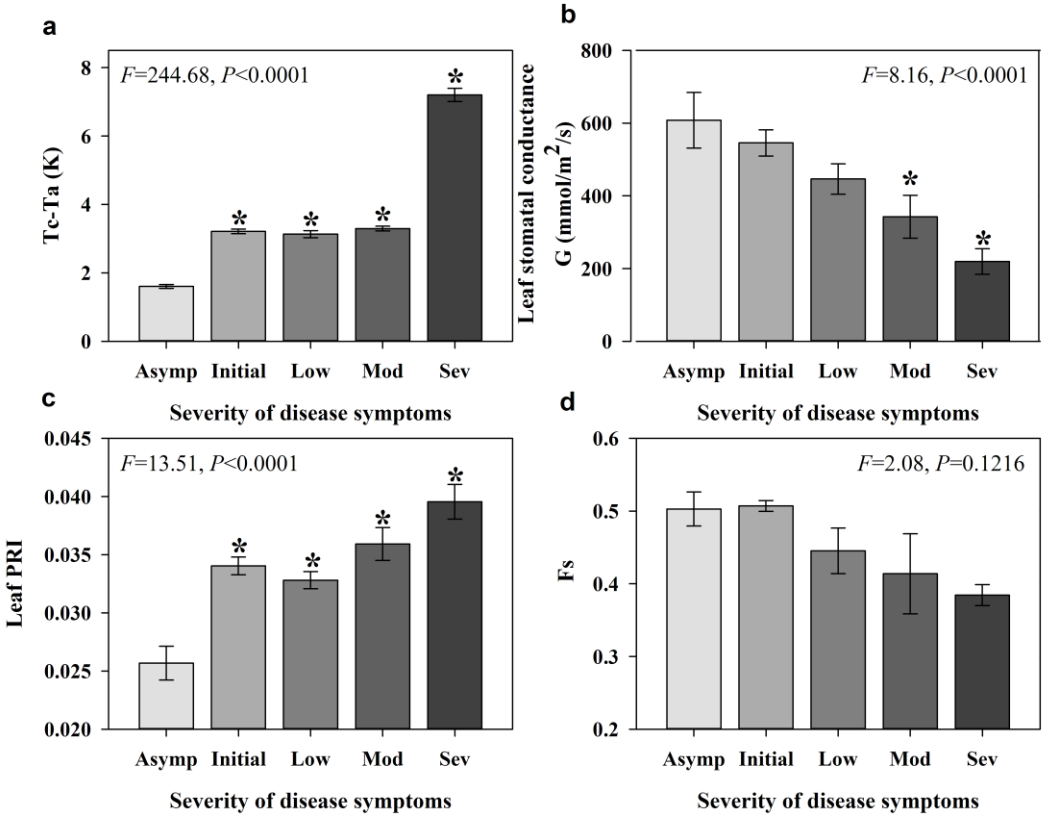

Figure 4.8. Mean measurements of crown temperature (Tc-Ta) (a), leaf stomatal conductance (G) (b), leaf PRI_{570} (c) and leaf Fs (d) for every Verticillium wilt severity level. Analysis of variance of each index was conducted and asterisks indicate significant differences from the asymptomatic plants according to Dunnett's two-tailed test at $P < 0.05$. Error bars indicate standard errors.

Leaf-level measurements conducted for temperature, stomatal conductance, fluorescence and the PRI_{570} in healthy and VW symptomatic trees showed that Tc − Ta and PRI_{570} were sensitive to *V. dahliae* infection and subsequent fungal colonization of affected trees and not simply influenced by structural effects driven by water stress. However, leaf G showed significantly lower values than asymptomatic trees in those affected by moderate or severe VW symptoms, while no significant differences in leaf Fs existed due to *V. dahliae* infection (Fig. 4.8).

4.3.3. Airborne hyperspectral, multispectral and thermal imagery results

4.3.3.1. Tree crown temperature (Tc − Ta) and CWSI

Crown temperature (Tc − Ta) extracted from the airborne thermal imagery in the summer of 2011 was compared against leaf stomatal conductance (G) and leaf PRI_{570} data measured in 25 trees affected by VW (Fig. 4.9). Crown temperature (Tc − Ta) was significantly and linearly correlated with both the decrease of leaf G (R^2 = 0.76, P = 0.002; Fig. 4.9a) and the increase of PRI_{570} (R^2 = 0.51, P = 0.032; Fig. 4.9b). Furthermore, leaf G showed an inverse linear correlation to the leaf PRI_{570} (R^2 = 0.52, P = 0.028; Fig. 4.9c). Crown temperature (Tc − Ta) tended to increase as VW severity level increased (Fig. 4.10). VW affected trees showed up to 2 K higher Tc − Ta than that measured in healthy asymptomatic trees and were consistent in all measurements taken in April and July in both study sites. Indeed, symptomatic trees showed significantly ($P < 0.05$) higher Tc − Ta values than asymptomatic trees at any disease severity level at Castro del Rio, or at low or higher disease severity at Utrera. These results showed similar trends as those presented in Fig. 4.8a, with significant ($P < 0.05$) increases in Tc − Ta at leaf and canopy levels.

As expected, the CWSI estimated from the high-resolution airborne thermal imagery acquired on 2 June 2011 in the Castro del Rio site showed significantly ($P < 0.05$) lower values for asymptomatic trees, with an upward trend as VW severity level increased (Fig. 4.11a). CWSI derived from the thermal imagery on 15 June 2011 decreased linearly and significantly as a function of G obtained on 27 and 28 July 2011 (R^2 = 0.83; $P < 0.001$) (Fig. 4.11b). These results indicate that the CWSI obtained from high spatial resolution thermal imagery can be used to detect the lower transpiration rates induced by *V. dahliae* infection, as could be expected according to previous results (Berni *et al.*, 2009a) showing the usefulness of the CWSI as a water stress indicator. CWSI values estimated on the two different assessment dates in June 2011 were significantly ($P < 0.05$) lower for healthy trees than for those affected by the disease. At early stages of disease development (DS ≤ 1.5), CWSI ranged from 0.21 to 0.35 on 2 June 2011, and from 0.36 to 0.48 on 15 June 2011. At more advanced stages of VW development for trees affected by moderate or

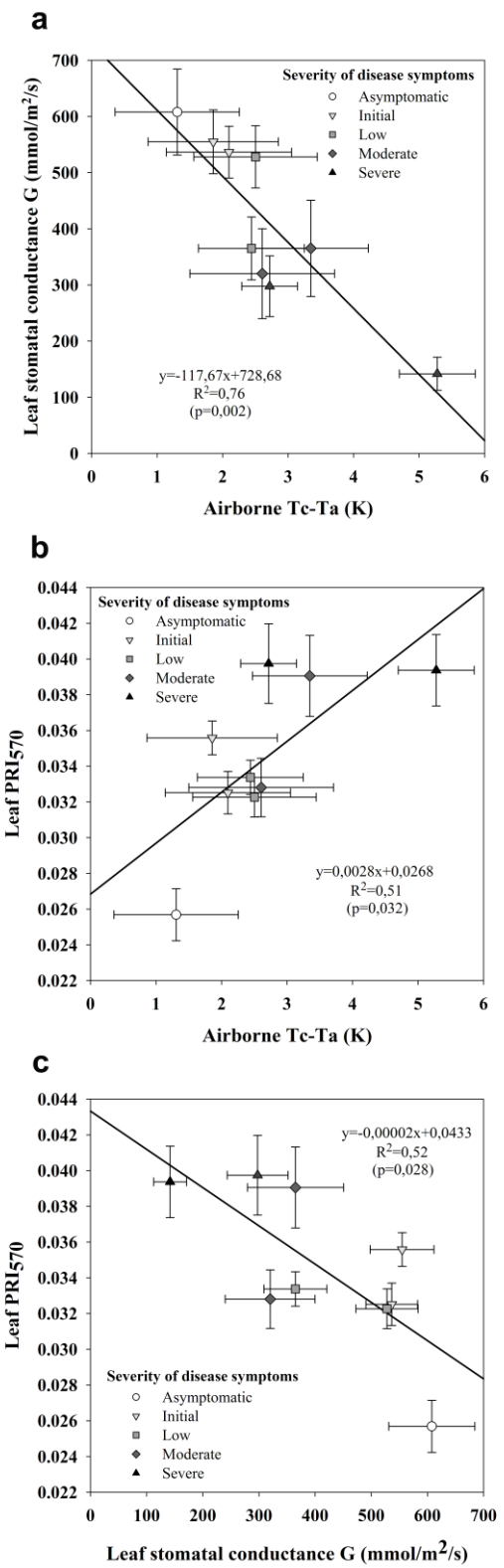

Figure 4.9. Relationship between crown temperature extracted from the thermal imagery and leaf stomatal conductance (G) (a) and leaf PRI_{570} measurements (b) taken on olive trees showing different Verticillium wilt severity levels, and relationship between leaf G and leaf PRI_{570} (c). Thermal imagery was obtained at 11:00 GMT on 15 June 2011 and leaf measurements were obtained between 10:00 and 13:00 GMT on 27 and 28 July 2011 from crowns with different VW severity levels in the Castro del Rio study site (Córdoba province). Error bars indicate standard errors.

severe symptoms, CWSI values tended to increase, ranging from 0.35 to 0.76 on 2 June 2011 and from 0.48 to 0.71 on 15 June 2011.

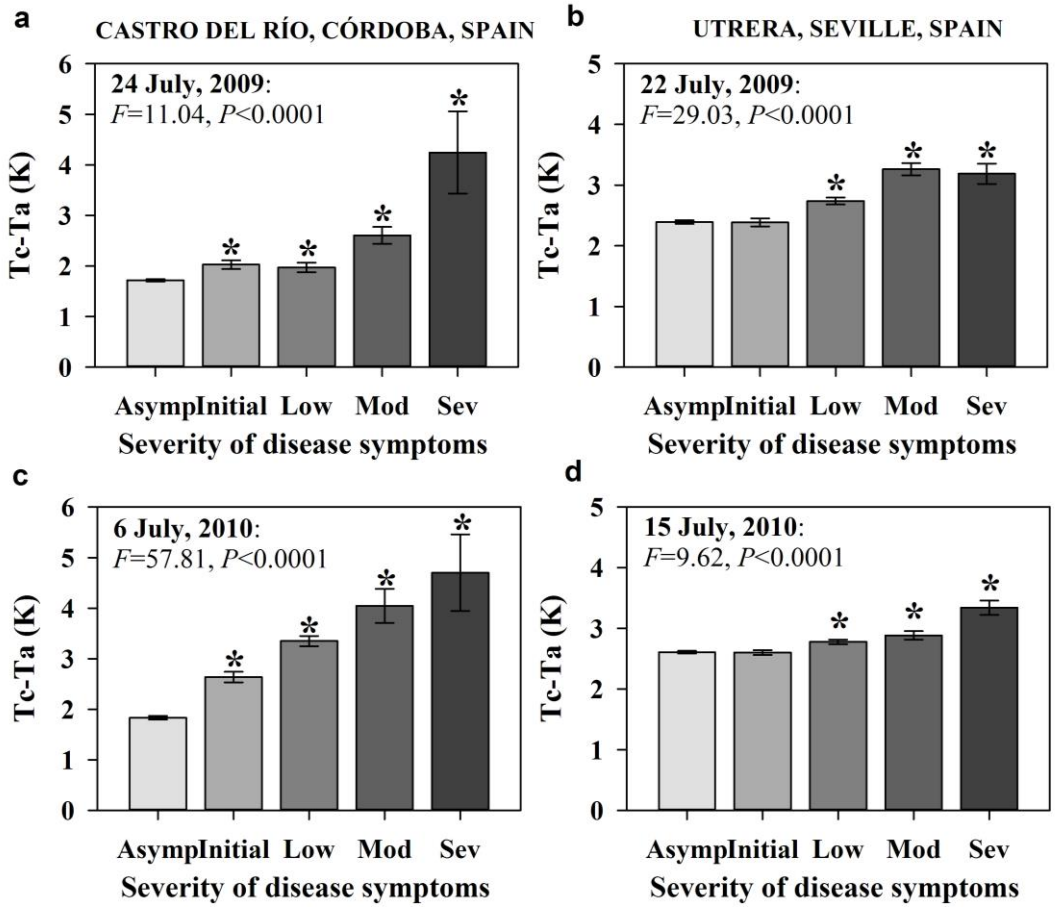

Figure 4.10. Mean measurements of crown temperature (Tc-Ta) for every Verticillium wilt severity level. Tc-Ta was calculated from thermal imagery obtained in summer of two consecutive years (2009 and 2010) for the two study sites, Castro del Rio (Córdoba province) (a, c) and Utrera (Seville province) (b, d). Analysis of variance was conducted and asterisks indicate significant differences from the asymptomatic plants according to Dunnett's two-tailed test at $P < 0.05$. Error bars indicate standard errors.

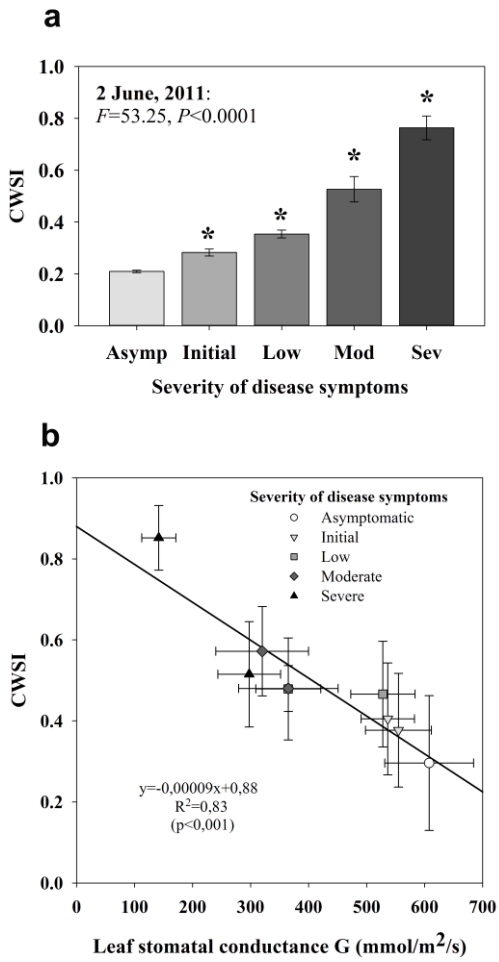

Figure 4.11. (a) Mean values of Crop Water Stress Index (CWSI) for every Verticillium wilt severity level on 2 June 2011 in the Castro del Rio study site (Córdoba province). Analysis of variance was conducted and asterisks indicate significant differences from the asymptomatic plants according to Dunnett's two-tailed test at $P < 0.05$. Error bars indicate standard errors. (b) Relationship between leaf stomatal conductance (G) and the CWSI in trees with different VW severity levels. Leaf stomatal conductance measurements were obtained between 10:00 and 13:00 GMT on 27 and 28 July 2011 and the CWSI was calculated from the thermal imagery obtained at 11:00 GMT on 15 June 2011 in the Castro del Rio study site. Error bars indicate standard errors.

4.3.3.2. Structural indices

The effects of VW on the canopy structure were captured by structural indices such as the NDVI (Fig. 4.12a), RDVI, OSAVI, TVI, MTVI, SR and MSR, that showed higher values for asymptomatic trees except for TVI and MTVI which showed an increase at early stages of disease development. Thus, moderate and severe VW wilt symptoms induced significantly ($P < 0.05$) lower values of NDVI, OSAVI, SR and MSR indices than those estimated in asymptomatic trees (Table 4.3). Furthermore, TVI and MTVI

showed an increase ($P < 0.05$) in trees showing initial symptoms (Table 4.3). These results demonstrate the consistency of structural indices as VW damage indicator due to the expected effects on crown density at moderate or advanced stages of disease development.

4.3.3.3. Physiological indices

The revised xanthophyll indices were calculated based on PRI formulations using R_{570} as the reference band (PRI_{570}) (Fig. 4.12b) and the new formulation using band R_{515} as a reference to minimize structural canopy effects, PRI_{515} (Fig. 4.12c). These indices showed an upward trend as VW severity level increased. The PRI_{515} index was more sensitive to VW than PRI_{570}, and showed significantly ($P < 0.05$) lower values when trees were affected by moderate or severe symptoms (Table 4.3). This result confirms those obtained by Hernández-Clemente *et al.* (2011) in forest canopies and those of Stagakis *et al.* (2012) in orange and mandarin orchards, which demonstrated the robustness of the PRI_{515} to structural effects. Both, airborne-derived (Table 4.3) and leaf-level PRI_{570} (Fig. 4.8c) showed similar positive trend with disease severity, however only at leaf-level resulted in significant differences between healthy and VW affected trees. The chlorophyll indices TCARI (Fig. 4.12d) and TCARI/OSAVI showed an upward trend at early stages of the disease, reaching a maximum of 0.058 and 0.103 units at the low disease severity level, respectively, compared to 0.004 (TCARI) and 0.007 (TCARI/OSARI) observed for healthy trees. These results could indicate a decrease in chlorophyll a+b content (Ca+b) at early stages of *V. dahliae* infection (reducing stomatal conductance and photosynthesis rate). At advanced stages of the disease, the TCARI and TCARI/OSAVI inverted their trends due to the sharp leaf area index (LAI) drop associated with VW severity, showing significantly ($P < 0.05$) lower values at severe disease symptoms with 0.022 and 0.025 value drops between moderate and severely affected trees, respectively. The chlorophyll red edge index, VOG1, GM1, GM2, PSSRa and PSSRb showed significantly ($P < 0.05$) lower values on moderately and severely affected trees compared with values estimated on asymptomatic trees. The mCAI reached a significantly ($P < 0.05$) higher value at trees showing initial symptoms but steadily decreased in trees affected by moderate and severe symptoms.

The Greenness, red index and the blue/green ratio BG2 were not able to detect *V. dahliae* infection, since no significant ($P > 0.05$) changes were detectable when compared with healthy trees (Table 4.3). Interestingly, the blue index (Fig. 4.12e) could discriminate between healthy trees and those affected at any of the disease severity levels that reached significantly lower values ($P < 0.05$). Similarly, the blue/green ratio BG1 presented a significant ($P < 0.05$) decrease at early stages of disease development, but increased slightly at advanced stages, probably due to structural changes occurring in

Table 4.3. Sensitivity of hyperspectral indices to Verticillium wilt symptoms in olive trees. Vegetation indices were calculated from the hyperspectral imagery obtained on 23 June 2011 in the Castro del Rio site (Córdoba province, Spain).

Vegetation indices	F[a]	P[a]	Severity of disease symptoms[b]			
			I	L	M	S
Structural indices						
NDVI	21.66	<0.001			**X**	**X**
RDVI	9.02	<0.001				**X**
OSAVI	11.52	<0.001			**X**	**X**
TVI	7.80	<0.001		**X**		**X**
MTVI	7.27	<0.001		**X**		**X**
SR	14.35	<0.001			**X**	**X**
MSR	16.49	<0.001			**X**	**X**
Xanthophyll indices						
PRI_{570}	2.98	0.0183				
PRI_{515}	11.30	<0.001			**X**	**X**
Chlorophyll a+b indices						
RedEdge	15.95	<0.001			**X**	**X**
VOG1	22.56	<0.001			**X**	**X**
GM1	10.99	<0.001			**X**	**X**
GM2	13.93	<0.001			**X**	**X**
PSSRa	14.70	<0.001			**X**	**X**
PSSRb	14.35	<0.001			**X**	**X**
mCAI	5.26	0.0003		**X**		
TCARI	6.72	<0.001				**X**
TCARI/OSAVI	3.30	0.0105				**X**
R/G/B indices						
R	12.27	<0.001				
G	16.51	<0.001				
B	16.01	<0.001	**X**	**X**	**X**	**X**
BG1	6.41	<0.001	**X**	**X**		
BG2	2.25	0.0611				
BR1	12.01	<0.001	**X**	**X**	**X**	
BR2	13.68	<0.001		**X**	**X**	**X**
LIC3	5.72	<0.001				**X**
Carotenoid indices						
SIPI	12.43	<0.001			**X**	**X**
PSSRc	9.73	<0.001			**X**	**X**
R_{520}/R_{500}	3.67	0.0055				
R_{515}/R_{570}	3.08	0.0152				
R_{515}/R_{670}	14.06	<0.001				
Fluorescence index						
FLD3	4.66	0.0010	**X**	**X**		
Plant disease indices						
HI	9.54	<0.001		**X**	**X**	**X**

[a] F statistic and p-value obtained from the standard analysis of variance (ANOVA).

[b] Significant changes in vegetation indices from asymptomatic plants according to Dunnett's two tailed test at $P < 0.05$ are indicated with X for initial (I) ($0.2 \leq DS \leq 0.5$), low (L) ($1 \leq DS \leq 1.5$), moderate (M) ($2 \leq DS \leq 2.5$) and severe (S) ($3 \leq DS \leq 4$) Verticillium wilt symptoms.

trees severely damaged by the pathogen. The blue/red ratios BR1 and BR2 showed downward trends with the increase in disease severity that resulted in significantly lower values at the initial, low and moderate symptom severity in BR1 (Fig. 4.12f) and low, moderate and severe in BR2. The LIC3 index showed a slightly decrease at early stages of the disease, followed by a significant ($P < 0.05$) increase on severely affected trees. The indices SIPI and PSSRc were inversely correlated with disease severity, showing significantly ($P < 0.05$) lower values at moderate and severe stages of disease development. The R_{520}/R_{500}, R_{515}/R_{570}, and R_{515}/R_{670} ratios were not useful for the detection of VW as no significant differences were detected between asymptomatic and VW affected trees.

The chlorophyll fluorescence signal estimated from the hyperspectral imagery with the FLD method showed a significant ($P < 0.05$) increase at initial and low stages of disease symptom severity (2.677 $W \cdot m^{-2} \cdot \mu m^{-1} \cdot sr^{-1}$), slightly decreasing to 2.019 $W \cdot m^{-2} \cdot \mu m^{-1} \cdot sr^{-1}$ at the severe VW severity level (Fig. 4.12g). This result may indicate that the photosynthetic apparatus of the plant remains undamaged being able to dissipate the excess of energy by fluorescence that could not be maintained when the reduction in photosynthesis occurred at severely stressed plants, causing a decrease in the chlorophyll fluorescence rate. These results are in agreement with the studies conducted by Pérez-Priego *et al.* (2005) and Zarco-Tejada *et al.* (2009, 2012) in citrus and olive orchards under water stress conditions. Comparable results were obtained in airborne (Table 4.3) and leaf-derived chlorophyll fluorescence (Fig. 4.8d) that in both cases reached lower values in trees affected by moderate or severe symptoms. However, a significant ($P < 0.05$) increase in fluorescence occurred in trees at the early stage of disease development only at canopy level (Table 4.3). Finally, the health index (HI) developed to discriminate between healthy and diseased sugar beet leaves affected by different foliar pathogens showed in this study lower values ($P < 0.05$) as the VW disease severity level increases to low, moderate or severe symptoms, respectively (Table 4.3; Fig. 4.12h).

4.4. Conclusions

The present study assessed remote sensing methods for early detection of Verticillium wilt in two olive orchards of different agronomic characteristics. It applied techniques based on the detection of the effects of *V. dahliae* infection and colonization on water flow that eventually cause water stress effects, assessed with thermal, multispectral and hyperspectral domains. It demonstrated that canopy temperature and physiological hyperspectral indices (i.e., PRI and chlorophyll fluorescence) are related with physiological stress caused by VW. Moreover, structural indices (i.e., NDVI) were more related to structural damage caused by VW. Field measurements showed large differences in temperature (Tc − Ta) and stomatal conductance (G) across VW severity

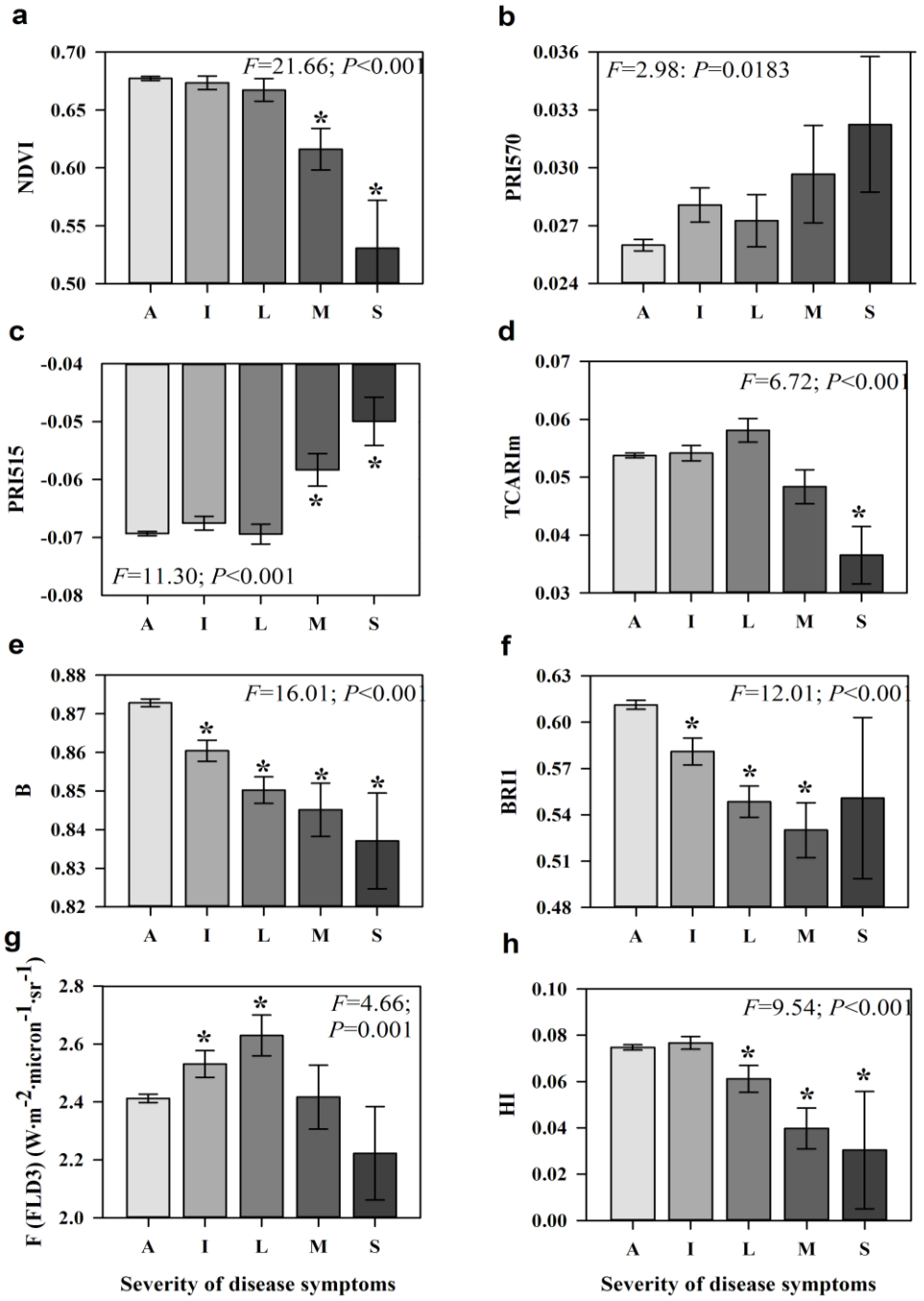

Figure 4.12. Mean measurements of NDVI (a), PRI_{570} (b), PRI_{515} (c), TCARI (d), Blue index (B) (e), B/R index (BR1) (f), chlorophyll fluorescence FLD3 (g) and healthy-index (HI) (h) for every Verticillium wilt severity level. Analysis of variance of each index was conducted and asterisks indicate significant differences from the asymptomatic plants according to Dunnett's two-tailed test at $P < 0.05$. Error bars indicate standard errors.

levels, with higher Tc − Ta and lower G as severity level increased. This allowed identifying trees at the early stages of disease development. At leaf level, the reduction in transpiration and G caused by VW infection was associated with a significant ($P < 0.05$) increase in the PRI_{570} and a decrease in fluorescence. The flights conducted with thermal, multispectral and hyperspectral cameras enabled VW detection by using crown temperature (Tc − Ta; CWSI), assessing structural indices (NDVI, RDVI, OSAVI, TVI, MTVI, SR, MSR), the PRI_{515} index, chlorophyll indices (red edge, VOG1, GM1, GM2, PSSRa, PSSRb, mCAI, TCARI, TCARI/OSAVI), R/G/B indices (B, BG1, BR1, BR2, LIC3), carotenoid (SIPI and PSSRc), fluorescence, and the healthy index (HI). This study proved the potentials for the early detection of *V. dahliae* infection and discrimination among VW severity levels in olive crops using thermal, multispectral and hyperspectral imagery acquired with an unmanned aerial vehicle. Crown temperature, CWSI, B, BG1, BR1 and FLD3 were identified as the best indicators to detect VW at early stages of disease development, while NDVI, PRI_{515}, HI, and chlorophyll and carotenoid indices proved to be good indicators to detect the presence of moderate to severe damage.

Acknowledgments

Financial support from the Spanish Ministry of Education and Science for project AGL2009-13105 and from the Regional Government of Andalusia and the European Social Fund for project P08-AGR-03528 is gratefully acknowledged. R. Calderón is a recipient of research fellowship BES-2010-035511 from the Spanish Ministry of Education and Science. V. González-Dugo, J.A.J. Berni, D. Notario, A. Vera, A, Hornero, R. Romero and K. Gutierrez are acknowledged for their support during the field and airborne campaigns. M. Montes-Borrego, J.L. TraperoCasas and G. León-Ropero are acknowledged for their technical support in Verticillium wilt assessments.

References

Ayres, P.G. (1978). Water relations of diseased plants. In Kozlowski, T.T. (Eds.), *Water Deficits and Plant Growth* (vol.5, pp. 1-60). London, United Kingdom: Academic Press.

Barton, C. (2012). Advances in remote sensing of plant stress. *Plant Soil* 354:41-44.

Bauriegel, E., Giebel, A., Geyer, M., Schmidt, U., & Herppich, W.B. (2011). Early detection of *Fusarium* infection in wheat using hyper-spectral imaging. *Comput. Electron. Agr.* 75:304-312.

Berni, J.A.J., Zarco-Tejada, P.J., Sepulcre-Cantó, G., Fereres, E., & Villalobos, F.J. (2009a). Mapping canopy conductance and CWSI in olive orchards using high resolution thermal remote sensing imagery. *Remote Sens. Environ.* 113:2380-2388.

Berni, J.A.J., Zarco-Tejada, P.J., Suárez, L., & Fereres, E. (2009b). Thermal and narrow-band multispectral remote sensing for vegetation monitoring from an unmanned aerial vehicle. *IEEE T. Geosci. Remote.* 47:722-738.

Blackburn, G.A. (1998). Spectral indices for estimating photosynthetic pigment concentrations:a test using senescent tree leaves. *Int. J. Remote Sens.* 19(4):657-675.

Blanco-López, M.A., Jiménez-Díaz, R.M., & Caballero, J.M. (1984). Symptomatology, incidence and distribution of Verticillium wilt of olive trees in Andalucia. *Phytopathol. Mediterr.* 23:1-8.

Broge, N.H., & Leblanc, E. (2000). Comparing prediction power and stability of broadband and hyperspectral vegetation indices for estimation of green leaf area index and canopy chlorophyll density. *Remote Sens. Environ.* 76:156-172.

Chen, B., Li, S.K., Wang, K.R., Wang, J., Wang, F.Y., Xiao, C.H., Lai, J.C., & Wang, N. (2008). Spectrum characteristics of cotton canopy infected with Verticillium wilt and applications. *Agr. Sci. China* 7:561-569.

Chen, B., Li, S., Wang, K., Zhou, G., & Bai, J. (2011). Evaluating the severity level of cotton *Verticillium* using spectral signature analysis. *Int. J. Remote Sens.* 33:2706-2724.

Chen, J. (1996). Evaluation of vegetation indices and modified simple ratio for boreal applications. *Can. J. Remote Sens.* 22 :229-242.

Cohen, Y., Alchanatis, V., Meron, M., Saranga, Y., & Tsipris, J. (2005). Estimation of leaf potential by thermal imagery and spatial analysis. *J. Exp. Bot.* 56:1843-1852.

Dammer, K.H., Möller, B., Rodemann, B., & Heppner, D. (2011). Detection of head blight (*Fusarium* ssp.) in winter wheat by color and multispectral image analyses. *Crop Prot.* 30:420-428.

DeVay, J.E. (1989). Selection, characterization, pathogenicity and virulence of pectinase-deficient mutants of *Verticillium albo-atrum*. In Tjamos, E.C., & Beckman, C.H. (Eds.), *Vascular Wilt Diseases of Plants* (pp. 197-217). Berlin, Germany: Springer.

Dobrowsky, S.Z., Pushnik, J., Zarco-Tejada, P.J., & Ustin, S.L. (2005). Simple reflectance indices track heat and water stress induced changes in steady-state chlorophyll fluorescence at the canopy scale. *Remote Sens. Environ.* 97 :403-414.

Emechebe A.M., Leaky C.L.A., & Banage, W.B. (1975). Verticillium wilt of cacao in Uganda: incidence and progress of infection in relation to time. *E. Afr. Agr. Forestry J.* 41:184-186.

Evain, S., Flexas, J., & Moya, I. (2004). A new instrument for passive remote sensing: 2. Measurement of leaf and canopy reflectance changes at 531 mm and their relationship with photosynthesis and chlorophyll fluorescence. *Remote Sens. Environ.* 91:175-185.

Falkenberg, N.R., Piccinni, G., Cothren, J.T., Leskovar, D.I., & Rush, C.M. (2007). Remote sensing of biotic and abiotic stress for irrigation management of cotton. *Agr. Water Manage.* 87:23-31.

Flexas, J., Briantais, J.M., Cerovic, Z., Medrano, H., & Moya, I. (2000). Steady-state and maximum chlorophyll fluorescence responses to water stress in grapevine leaves: A new remote sensing system. *Remote Sens. Environ.* 73:282-297.

Flexas, J., Escalona, J.M., & Medrano, H. (1999). Water stress induces different levels of photosynthesis and electron transport rate regulation in grapevine. *Plant Cell Environ.* 22:39-48.

Flexas, J., Escalona, J.M., Evain, S., Gulias, J., Moya, I., Osmond, C.B., & Medrano, H. (2002). Steady-state chlorophyll fluorescence (Fs) measurements as a tool to follow variations of net CO_2 assimilation and stomatal conductance during water-stress in C-3 plants. *Physiol. Plantarum* 114(2):231-240.

Gamon, J.A., Peñuelas, J., & Field, C.B. (1992). A narrow-wave band spectral index that tracks diurnal changes in photosynthetic efficiency. *Remote Sens. Environ.* 41:35-44.

Garber, R.H., & Houston, B.R. (1966). Penetration and development of *Verticillium alboatrum* in the cotton plant. *Phytopathology* 56:1121-1126.

Gil-Pérez, B., Zarco-Tejada, P.J., Correa-Guimaraes, A., Relea-Cangas, E., Navas-Gracia, L.M., Hernández-Navarro, S., Sanz-Requena, J.F., Berjón, A., & Martín-Gil, J. (2010). Remote sensing detection of nutrient uptake in vineyards using narrow-band hyperspectral imagery. *Vitis* 49:167-173.

Gitelson, A.A., & Merzlyak, M.N. (1997). Signature analysis of leaf reflectance spectra: Algorithm development for remote sensing of chlorophyll. *Int. J. Remote Sens.* 18:2691-2697.

Gitelson, A.A., Yacobi, Y.Z., Schalles, J.F., Rundquist, D.C., Han, L., Stark, R., & Etzion, D. (2000). Remote estimation of phytoplankton density in productive waters. *Arch. Hydrobiol. - Special Issues in Advances in Limnology* 55:121-136.

Gueymard, C.A. (1995). SMARTS, a simple model of the atmospheric radiative transfer of sunshine: Algorithms and performance assessment. *Technical report no. FSEC-PF-270-95*. Cocoa, FL, USA: Florida Solar Energy Center.

Gueymard, C.A. (2001). Parameterized transmittance model for direct beam and circumsolar spectral irradiance. *Sol. Energy* 71:325-346.

Haboudane, D., Miller, J.R., Pattey, E., Zarco-Tejada, P.J., & Strachan, I. (2004). Hyperspectral vegetation indices and novel algorithms for predicting green LAI of crop canopies: Modeling and validation in the context of precision agriculture. *Remote Sens. Environ.* 90(3):337-352.

Haboudane, D., Miller, J.R., Tremblay, N., Zarco-Tejada, P.J., & Dextraze, L. (2002). Integrated narrow-band vegetation indices for prediction of crop chlorophyll content for application to precision agriculture. *Remote Sens. Environ.* 84:416-426.

Hatfield, P.L., & Pinter, P.J. (1993). Remote sensing for crop protection. *Crop Prot.* 12:403-413.

Hernández-Clemente, R., Navarro-Cerrillo, R.M., Suárez, L., Morales, F., & Zarco-Tejada, P.J. (2011). Assessing structural effects on PRI for stress detection in conifer forests. *Remote Sens. Environ.* 115:2360-2375.

Hillnhütter, C., Mahlein, A.-K., Sikora, R.A., & Oerke, E.-C. (2011). Remote sensing to detect plant stress induced by *Heterodera schachtii* and *Rhizoctonia solani* in sugar beet fields. *Field Crops Res.* 122:70-77.

Idso, S.B., Jackson, R.D., & Reginato, R. (1978). Extending the "degree day" concept of phenomenological development to include water stress effects. *Ecology* 59:431-433.

Idso, S.B., Jackson, R.D., Pinter, P.J., Reginato, R.J., & Hatfield, J.L. (1981). Normalizing the stress-degree-day parameter for environment variability. *Agric. Forest Meteorol.* 24:45-55.

Jackson, R.D. (1986). Remote sensing of biotic and abiotic plant stress. *Annual Review of Phytopathology* 24:265-287.

Jackson, R.D., & Pinter, P.J., Jr. (1981). Detection of water stress in wheat by measurement of reflected solar and emitted thermal IR radiation. In *Proc. Intern. Colloquium on spectral signatures of objects in remote sensing* (pp. 399-406). Versalle, France: Institut National de la Reserche Agronomique.

Jackson, R.D., Idso, S.B., Reginato, R.J., & Ehrler, W.L. (1977). Crop temperature reveals stress. *Crop Soils* 29:10-13.

Jackson, R.D., Idso, S.B., Reginato, R.J., & Pinter, P.J., Jr. (1981). Canopy temperature as a crop water stress indicator. *Water Resour. Res.* 17:1133-1138.

Jiménez-Díaz, R.M., Cirulli, M., Bubici, G., Jiménez-Gasco, L.M., Antoniou, P.P., & Tjamos, E.C. (2012). Verticillium wilt, a major threat to olive production: Current status and future prospects for its management. *Plant Dis.* 96(3):304-329.

Jiménez-Díaz, R.M., Olivares-García, C., Landa, B.B., Jiménez- Gasco, M.M., & Navas-Cortés, J.A. (2011). Region-wide analysis of genetic diversity in *Verticillium dahliae* populations infecting olive in southern Spain and agricultural factors influencing the distribution and prevalence of vegetative compatibility groups and pathotypes. *Phytopathology* 101:304-315.

Jing, X., Huang, W.J., Wang, J.H., Wang, J.D., & Wang, K.R. (2009). Hyperspectral inversion models on Verticillium wilt severity of cotton leaf. *Spectrosc. Spect. Anal.* 29(12):3348-3352.

Jordan, C.F. (1969). Derivation of leaf area index from quality of light on the forest floor. *Ecology* 50:663-666.

Krause, G.H., & Weis, E. (1984). Chlorophyll fluorescence as a tool in plant physiology. II. Interpretation of fluorescence signals. *Photosynth. Res.* 5:139-157.

Laudien, R., Bareth, G., & Doluschitz, R. (2003). Analysis of hyperspectral field data for detection of sugar beet diseases. In *Proceedings of the EFITA Conference* (pp. 375-381), Debrecen, Hungary, July 5-9, 2003.

Leinonen, I., & Jones, H.G. (2004). Combining thermal and visible imagery for stimulating canopy temperature and identifying plant stress. *J. Exp. Bot.* 55:1423-1431.

Levin, A.G., Lavee, S., & Tsror, L. (2003). Epidemiology of *Verticillium dahliae* on olive (cv. Picual) and its effects on yield under saline conditions. *Plant Pathol.* 52:212-218.

Lichtenhaler, H.K., Lang, M., Sowinska, M., Heisel, F., & Mieh, J.A. (1996). Detection of vegetation stress via a new high resolution fluorescence imaging system. *J. Plant Physiol.* 148:599-612.

López-Escudero, F.J., del Rio, C., Caballero, J.M., & Blanco-López, M.A. (2004). Evaluation of olive cultivars for resistance to *Verticillium dahliae*. *Eur. J. Plant Pathol.* 110:79-85.

Mahlein, A.-K., Rumpf, T., Welke, P., Dehne, H.-W., Plümer, L., Steiner., U., & Oerke, E.-C. (2013). Development of spectral indices for detecting and identifying plant diseases. *Remote Sens. Environ.* 128:21-30.

Maier, S.W., Günther, K.P., & Stellmes, M. (2003). Sun-Induced Fluorescence: A New Tool for Precision Farming. In McDonald, M., Schepers, J., Tartly, L., van Toai, T., & Major, D. (Eds.), *Digital Imaging and Spectral Techniques: Applications to Precision Agriculture and Crop Physiology* (pp. 209-222). Madison, WI, USA: ASA Special Publication.

Meggio, F., Zarco-Tejada, P.J., Núñez, L.C., Sepulcre-Cantó, G., González, M.R., & Martin, P. (2010). Grape quality assessment in vineyards affected by iron deficiency chlorosis using narrow-band physiological remote sensing indices. *Remote Sens. Environ.* 114:1968-1986.

Mengistu, A., Tachibana, H., Epstein, A.H., Bidne, K.G., & Hatfield, J.D. (1987). Use of leaf temperature to measure the effect of brown stem rot and soil moisture stress and its relation to yields of soybeans. *Plant Dis.* 71:632-634.

Mercado-Blanco, J., Rodríguez-Jurado, D., Parrilla-Araujo, S., & Jiménez-Díaz, R.M. (2003). Simultaneous detection of the defoliating and nondefoliating *Verticillium*

dahliae pathotypes in infected olive plants by duplex, nested polymerase chain reaction. *Plant Dis.* 87:1487-1494.

Meroni, M., Colombo, R., & Cogliati, S. (2004). High resolution leaf spectral signature for the detection of solar induced chlorophyll fluorescence. In *Proceedings of the 2nd ESA workshop on remote sensing of solar induced vegetation fluorescence*, Montreal, Canada, November 17-19, 2004.

Meroni, M., Picchi, V., Rossini, M., Cogliati, S., Panigada, C., Nali, C., Lorenzini, G., & Colombo, R. (2008a). Leaf level early assessment of ozone injuries by passive fluorescence and PRI. *Int. J. Remote Sens.* 29(17-18):5409-5422.

Meroni, M., Rossini, M., Guanter, L., Alonso, L., Rascher, U., & Colombo, R. (2009). Remote sensing of solar-induced chlorophyll fluorescence: Review of methods and applications. *Remote Sens. Environ.* 113 :2037-2051.

Meroni, M., Rossini, M., Picchi, V., Panigada, C., Cogliati, S., Nali, C., & Colombo, R. (2008b). Assessing steady-state fluorescence and PRI from hyperspectral proximal sensing as early indicators of plant stress: The case of ozone exposure. *Sensors* 8:1740-1754.

Navas-Cortés, J.A., Landa, B.B., Mercado-Blanco, J., Trapero-Casas, J.L., Rodríguez-Jurado, D., & Jiménez-Díaz, R.M. (2008). Spatiotemporal analysis of spread of infections by *Verticillium dahliae* pathotypes within a high tree density olive orchard in southern Spain. *Phytopathology* 98:167-180.

Nilsson, H.E. (1991). Hand-held radiometry and IR-thermography of plant diseases in field plot experiments. *Int. J. Remote Sens.* 12:545-557.

Nilsson, H.E. (1995). Remote sensing and image analysis in plant pathology. *Annu. Rev. Phytopathol.* 15:489-527.

Papageorgiu, G. (1975). Chlorophyll fluorescence; an intrinsic probe of photosynthesis. In Govindjee (Eds.), *Bioenergetics of photosynthesis* (pp. 319-371). New York, NY, USA: Academic Press.

Peguero-Pina, J.J., Morales, F., Flexas, J., Gil-Pelegrín, E., & Moya, I. (2008). Photochemistry, remotely sensed physiological reflectance index and de-epoxidation state of the xanthophyll cycle in *Quercus coccifera* under intense drought. *Oecologia* 156(1):1-11.

Peñuelas, J., Baret, F. & Filella, I. (1995). Semi-empirical indices to assess carotenoids/chlorophyll a ratio from leaf spectral reflectance. *Photosynthetica* 31:221-230.

Pérez-Priego, O., Zarco-Tejada, P.J., Sepulcre-Cantó, G., Miller, J.R., & Fereres, E. (2005). Detection of water stress in orchard trees with a high-resolution spectrometer through chlorophyll fluorescence in-filling of the O_2-A band. *IEEE T. Geosci. Remote* 43:2860-2869.

Pinter, P.J., Stanghellini, M.E., Reginato, R.J., Idso, S.B., Jenkins, A.D., & Jackson, R.D. (1979). Remote detection of biological stresses in plants with infrared thermometry. *Science* 205:585-587.

Plascyk, J.A. (1975). MK II Fraunhofer Line Dicsriminator (FLD-II) for airborne and orbital remote sensing of solar-stimulated luminescence. *Opt. Eng.* 14(4):339-346.

Presley, J.T., Carns, H.R., Taylor, E.E., & Schnathorst, W.C. (1966). Movement of conidia of *Verticillium albo-atrum* in cotton plants. *Phytopathology* 56:375.

Raikes, C., & Burpee, L.L. (1998). Use of multispectral radiometry for assessment of Rhizoctonia blight in creeping bentgrass. *Phytopathology* 88:446-449.

Reynolds, G.J., Windels, C.E., MacRae, I.V., & Laguette, S. 2012. Remote sensing for assessing Rhizoctonia crown and root rot severity in sugar beet. *Plant Dis.* 96:497-505.

Rondeaux, G., Steven, M., & Baret, F. (1996). Optimization of soil-adjusted vegetation indices. *Remote Sens. Environ.* 55:95-107.

Rougean, J.-L., & Breon, F.M. (1995). Estimating PAR absorbed by vegetation from bidirectional reflectance measurements. *Remote Sens. Environ.* 51:375-384.

Rouse, J.W., Haas, R.H., Schell, J.A., Deering, D.W., & Harlan, J.C. (1974). Monitoring the vernal advancement and retrogradation (greenwave effect) of natural vegetation. *NASA/GSFC Type III Final Report*. Greenbelt, MD, USA: College station Texas A and M University.

Sánchez Hernández, M.E., Ruiz Dávila, A., Pérez De Algaba, A., Blanco López, M.A., & Trapero Casas, A. (1998). Occurrence and etiology of death of young olive trees in southern Spain. *Eur. J. Plant Pathol.* 104:347-357.

Sankaran, S., Mishra, A., Ehsani, R., & Davis, C. (2010). A review of advanced techniques for detecting plant diseases. *Comput. Electro. Agr.* 72:1-13.

Schreiber, L.R., & Green, R.J., Jr. (1963). Effect of root exudates on germination of conidia and microsc1erotia of *Verticillium albo-atrum* inhibited by the soil fungistatic principle. *Phytopathology* 53:260-264.

Sepulcre-Cantó, G., Zarco-Tejada, P.J., Jiménez-Muñoz, J.C., Sobrino, J.A., de Miguel, E., *et al.* (2006). Within-field thermal variability detection as function of water stress in *Olea europea* L. orchards with high resolution spatial remote sensing imagery. *Agric. Forest Meteorol.* 136:31-44.

Sepulcre-Cantó, G., Zarco-Tejada, P.J., Jiménez-Muñoz, J.C., Sobrino, J.A., Soriano, M. A., Fereres, E., Vega, V., & Pastor, M. (2007). Monitoring yield and fruit quality parameters in open-canopy tree crops under water stress. Implications for ASTER. *Remote Sens. Environ.* 107:455-470.

Sepulcre-Cantó, G., Zarco-Tejada, P.J., Sobrino, J.A., Berni, J.A.J., Jiménez-Muñoz, J.C., *et al.* (2009). Discriminating irrigated and rainfed olive orchards with thermal ASTER imagery and DART 3D simulations. *Agric. Forest Meteorol.* 149:962-975.

Soukupová, J., Cséfalvay, L., Urban, O., Kosvancová, M., Marek, M., Rascher, U., & Nedbal, L. (2008). Annual variation of the steady-state chlorophyll fluorescence emission of evergreen plants in temperate zone. *Funct. Plant Biol.* 35:63-76.

Stagakis, S., González-Dugo, V., Cid, P., Guillén-Climent, M.L., & Zarco-Tejada, P.J. (2012). Monitoring water stress and fruit quality in an orange orchard under regulated deficit irrigation using narrow-band structural and physiological remote sensing indices. *ISPRS J. Photogramm.* 71:47-61.

Suárez, L., Zarco-Tejada, P.J., Berni, J.A.J., González-Dugo, V., & Fereres, E. (2009). Modelling PRI for water stress detection using radiative transfer models. *Remote Sens. Environ.* 113:730-740.

Suárez, L., Zarco-Tejada, P.J., González-Dugo, V., Berni, J.A.J., Sagardoy, R., Morales, F., & Fereres, E. (2010). Detecting water stress effects on fruit quality in orchards with time-series PRI airborne imagery. *Remote Sens. Environ.* 114:286-298.

Suárez, L., Zarco-Tejada, P.J., Sepulcre-Cantó, G., Pérez-Priego, O., Miller, J.R., Jiménez-Muñoz, J.C., & Sobrino, J. (2008). Assessing canopy PRI for water stress detection with diurnal airborne imagery. *Remote Sens. Environ.* 112:560-575.

Sun, P., Grignetti, A, Liu, S., Casacchia, R., Salvatori, R., Pietrini, F., Loreto, F., & Centritto, M. (2008). Associated changes in physiological parameters and spectral reflectance indices in olive (*Olea europaea* L.) leaves in response to different levels of water stress. *Int. J. Remote Sens.* 29(6):1725-1743.

Talboys, P.W. (1962). Systemic movement of some vascular pathogens. *T. Brit. Mycol. Soc.* 45:280-281.

Thenot, F., Méthy, M., & Winkel, T. (2002). The photochemical reflectance index (PRI) as a water-stress index. *Int. J. Remote Sens.* 23(23):5135-5139.

Tsror, L. (Lahkim) (2011). Review: Epidemiology and control of *Verticillium* wilt on olive. *Israel J. Plant Sci.* 59:59-69.

Tu, J.C. & Tan, C.S. (1985). Infrared thermometry for determination of root rot severity in bean. *Phytopathology* 75:840-844.

Van Alfen, N.K. (1989). Reassessment of plant wilt toxins. *Annu. Rev. Phytopathol.* 27:533-550.

Vogelmann, J.E., Rock, B.N., & Moss, D.M. (1993). Red edge spectral measurements from sugar maple leaves. *Int. J. Remote Sens.* 14:1563-1575.

Wang, D., Kurle, J.E., Estevez de Jensen, C., & Percich, J.A. (2004). Radiometric assessment of tillage and seed treatment effect on soybean root rot caused by *Fusarium* spp. in central Minnesota. *Plant Soil* 258:319-331.

West, J.S., Bravo, C., Oberti, R., Lemaire, D., Moshou, D., & McCartney, H.A. (2003). The potential of optical canopy measurement for targeted control of field crop diseases. *Annu. Rev. Phytopathol.* 41:593-614.

Winkel, T., Méthy, M., & Thénot, F. (2002). Radiation use efficiency, chlorophyll fluorescence, and reflectance indices associated with ontogenic changes in water-limited *Chenopodium quinoa* leaves. *Photosynthetica* 40(2):227-232.

Zarco-Tejada, P.J., Berjón, A., López-Lozano, R., Miller, J.R., Marin, P., Cachorro, V., *et al.* (2005). Assessing vineyard condition with hyperspectral indices: Leaf and canopy reflectance simulation in a row-structured discontinuous canopy. *Remote Sens. Environ.* 99:271-287.

Zarco-Tejada, P.J., Berni, J.A.J., Suárez, L., & Fereres, E. (2008). A new era in remote sensing of crops with unmanned robots. *SPIE Newsroom*, doi:10.1117/2.1200812.1438.

Zarco-Tejada, P.J., Berni, J.A.J., Suárez, L., Sepulcre-Cantó, G., Morales, F., & Miller, J.R. (2009). Imaging chlorophyll fluorescence from an airborne narrow-band multispectral camera for vegetation stress detection. *Remote Sens. Environ.* 113:1262-1275.

Zarco-Tejada, P.J., Miller, J.R., Mohammed, G.H., Notlamd, T.L.L., & Sampson, P.H. (2001). Scaling-up and model inversion methods with narrow-band optical indices for chlorophyll content estimation in closed forest canopies with hyperspectral data. *IEEE T. Geosci. Remote* 39:1491-1507.

Zarco-Tejada, P.J., Catalina, A., González, M.R., Martín, P. (2013). Relationships between net photosynthesis and steady-state chlorophyll fluorescence retrieved from airborne hyperspectral imagery. *Remote Sens. Environ.* 136:247-258.

Zarco-Tejada, P.J., González-Dugo, V., & Berni, J.A.J. (2012). Fluorescence, temperature and narrow-band indices acquired from a UAV for water stress detection using a hyperspectral imager and a thermal camera. *Remote Sens. Environ.* 117:322-337.

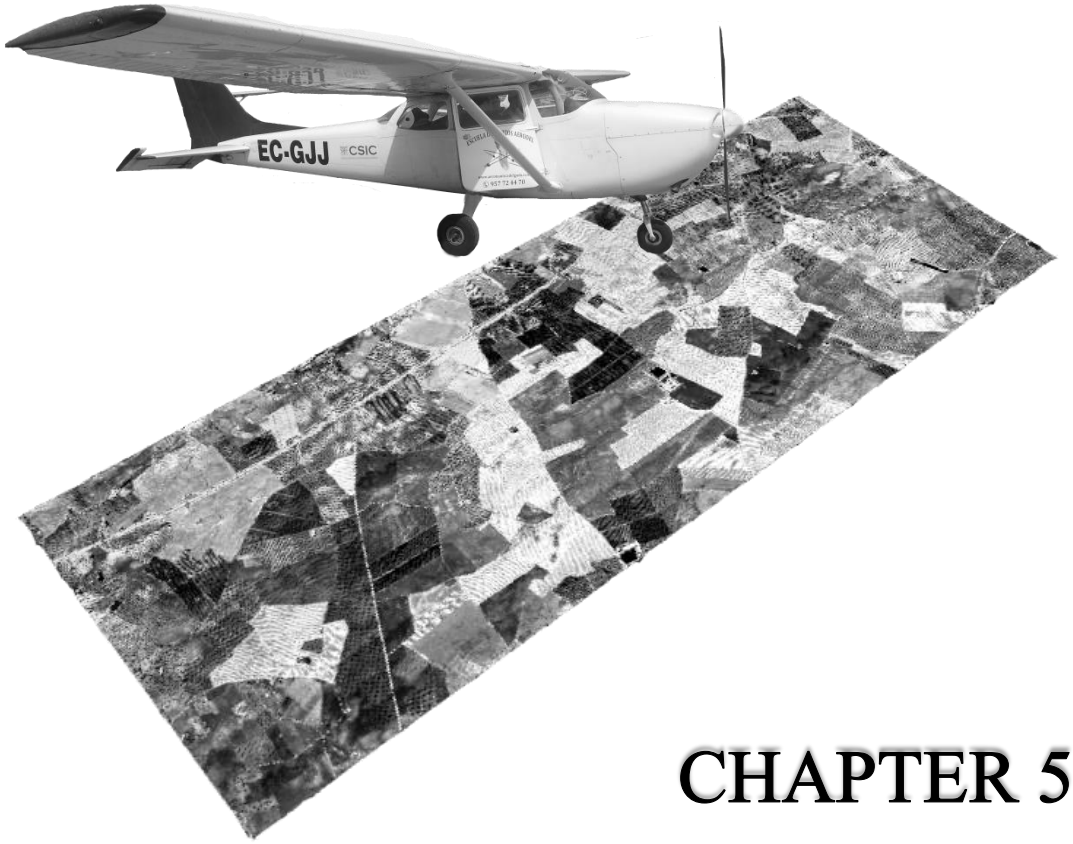

CHAPTER 5

Early detection and quantification of Verticillium wilt in olive using hyperspectral and thermal imagery over large areas

Authors: Calderón, R., Navas-Cortés, J.A., & Zarco-Tejada, P.J.

Instituto de Agricultura Sostenible (IAS), Consejo Superior de Investigaciones Científicas (CSIC), Córdoba, Spain

Published in: *Remote Sensing* 7(5):5584-5610

DOI: 10.3390/rs70505584

CHAPTER 5: Early detection and quantification of Verticillium wilt in olive using hyperspectral and thermal imagery over large areas

Resumen

Los métodos automáticos para una detección temprana de enfermedades de plantas (i.e., síntomas visibles en etapas tempranas del desarrollo de la enfermedad) usando teledetección son cruciales para la protección de cultivos. La Verticilosis (VW) del olivo causada por *Verticillium dahliae* puede controlarse sólo si es detectada en etapas tempranas de su desarrollo. Los métodos de clasificación, análisis lineal discriminante (LDA) y support vector machine (SVM), fueron aplicados para clasificar la severidad de *V. dahliae* usando teledetección a gran escala. Imágenes térmicas e hiperespectrales de alta resolución se adquirieron con una plataforma tripulada que voló un área de olivar comercial de 3,000-ha. LDA alcanzó una precisión en la clasificación global de 59.0% y un κ de 0.487 mientras que SVM obtuvo una mayor precisión en la clasificación, 79.2% con un κ similar, 0.495. Sin embargo, LDA clasificó mejor los árboles en niveles de severidad inicial y bajo, alcanzado precisiones de 71.4% y 75.0%, respectivamente, en comparación con el 14.3% y 40.6% obtenidos por SVM. La temperatura de cubierta normalizada, fluorescencia clorofílica, índices estructurales, de xantofilas, clorofila, carotenos y enfermedad fueron los mejores indicadores de etapas tempranas y avanzadas de la infección por VW. Estos resultados demuestran que los métodos desarrollados en otros estudios a escala de parcela son válidos para vuelos en mayores áreas que constan de varias parcelas de olivar que difieren en características de manejo de suelo y cultivo.

Palabras clave: Verticilosis, detección temprana, hiperespectral, térmico, support vector machine, análisis discriminante lineal.

Abstract

Automatic methods for an early detection of plant diseases (i.e., visible symptoms at early stages of disease development) using remote sensing are critical for precision crop protection. Verticillium wilt (VW) of olive caused by *Verticillium dahliae* can be controlled only if detected at early stages of development. Linear discriminant analysis (LDA) and support vector machine (SVM) classification methods were applied to classify *V. dahliae* severity using remote sensing at large scale.

High-resolution thermal and hyperspectral imagery were acquired with a manned platform which flew a 3,000-ha commercial olive area. LDA reached an overall accuracy of 59.0% and a κ of 0.487 while SVM obtained a higher overall accuracy, 79.2% with a similar κ, 0.495. However, LDA better classified trees at initial and low severity levels, reaching accuracies of 71.4% and 75.0%, respectively, in comparison with the 14.3% and 40.6% obtained by SVM. Normalized canopy temperature, chlorophyll fluorescence, structural, xanthophyll, chlorophyll, carotenoid and disease indices were found to be the best indicators for early and advanced stage infection by VW. These results demonstrate that the methods developed in other studies at orchard scale are valid for flights in large areas comprising several olive orchards differing in soil and crop management characteristics.

Keywords: Verticillium wilt, early detection, hyperspectral, thermal, support vector machine, linear discriminant analysis.

Received: 7 January 2015 / Accepted: 24 April 2015 / Published: 4 May 2015

5.1. Introduction

Olive (*Olea europaea* L.) is one of the most important crops in the Mediterranean Basin, representing 95% of the world production. Spain is the leading olive-producing country with 25% of the world acreage and nearly 39% of the production (FAOSTAT, 2012). Verticillium wilt (VW), caused by the fungus *Verticillium dahliae* Kleb., is the main soil-borne disease threatening this crop worldwide (Jiménez-Díaz *et al.*, 2012). In Spain, VW is of increasing concern for olive production because of its rapid spread and increasing severity associated with recent changes in cropping practices implemented to increase olive yields (Jiménez-Díaz *et al.*, 2011, 2012). These changes include use of self-rooted planting stocks to establish high-tree-density, drip irrigation, reduced or no tillage and high inputs of fertilizers in newly cultivated soils or fertile soils (Villalobos *et al.*, 2006) previously grown with susceptible crops to *V. dahliae*, such as cotton (Jiménez-Díaz *et al.*, 2011).

Currently, no control measure applied singly is fully effective for the management of VW of olive, however, an integrated disease management strategy is the best way to manage the disease, combining the use of preventive, pre-planting and post-planting control measures (Tjamos and Jiménez-Díaz, 1998). Post-planting control measures include: cultural practices (e.g., irrigation managing, weed control and tillage practice), soil solarization and organic or biological amendments. Post-planting VW control measures would be more efficient if VW-affected trees patches within fields are identified at early stages of disease development (i.e., visible symptoms) in order to mitigate the

spread of the pathogen and successive infections to neighboring trees (Navas-Cortés *et al.*, 2008). However, visual inspection of disease symptoms at early stages of development in the field is time-consuming and expensive (Steiner *et al.*, 2008). Remote sensing for the detection of damage caused by soil-borne plant pathogens has proved to be the best-fit technology for optimization of integrated pest management. These methods are rapid and reliable, allowing real-time plant disease monitoring for disease control and management (Sankaran *et al.*, 2010; Mahlein *et al.*, 2012).

V. dahliae infects the plant through the roots and colonizes its vascular system, blocking water flow and eventually inducing wilt symptoms (Van Alfen, 1989). This damage results in a significant reduction in leaf transpiration rate which finally leads to leaf chlorosis and defoliation, causing a change of spectral reflectance (Hillnhütter *et al.*, 2010). Chlorophyll content tends to decrease in infected plants, showing a higher reflectance in the visible (VIS) green (550 nm) and red-edge (650-720 nm) regions. Stressed plants also show a drop in canopy density and leaf area that leads to a decrease of spectral reflectance in the near-infrared (NIR) range (680-800 nm). In addition, the thermal-infrared (TIR) region (8000-15,000 nm) is highly suitable for the detection of *V. dahliae* infection due to the decrease in transpiration rate which induces stomata closure, reducing evaporative cooling and increasing canopy temperature. Considering these changes in the spectrum of infected plants, disease symptoms could be remotely detected in the VIS, red edge, NIR and TIR regions.

Recent work on VW in olive trees demonstrated the success of high-resolution thermal and hyperspectral imagery acquired with an unmanned aerial vehicle to early detect *V. dahliae* infection in two olive commercial orchards in southern of Spain (Calderón *et al.*, 2013). Normalized canopy temperature (Tc − Ta), chlorophyll fluorescence and blue ratios B/BG/BR were found to be the best indicators of early stage infection by VW while the Photochemical Reflectance Index (PRI), structural, chlorophyll and carotenoid indices detected only moderate to severe *V. dahliae* infection. These results obtained at the canopy level using airborne imagery were confirmed by those obtained by Calderón *et al.* (2014) at leaf level under controlled conditions. SPAD readings (as an indicator of leaf chlorophyll content), leaf chlorophyll fluorescence and normalized leaf temperature were demonstrated to be early VW indicators while the ethylene production and PRI detected only advanced stages of VW development.

Up to now, the remote sensing methods discussed above have only been used to detect VW successfully at local scales, in particular, in olive orchards of no more than 10 hectares using small unmanned aircraft. Under these small-scale conditions, unmanned aerial platforms obtain high resolution imagery in short flights of 10 to 40 minutes that avoid large ambient temperature variations, large changes in illumination levels or atmospheric differences during the flight. In addition, the methods were tested in olive

orchards with homogeneous tree structural and crown shape characteristics as well as with a generally uniform background types, understory and soil types across the field. The collection of very high-resolution hyperspectral and thermal imagery over large areas is only possible using manned aircraft or high endurance unmanned aerial systems (UAS) flying over long periods to cover extensive areas at the optimum resolution (i.e. 30-50 cm pixel size) generating mosaics comprising several fields of very different structural and architectural characteristics (i.e., planting patterns, crown shapes and sizes, and background / soil types). Therefore, it is critical to assess methods to detect VW incidence and severity over large areas in order to design VW control strategies at large scale. In this way, the indices identified as indicators for the early and advanced VW detection at local scale (Calderón *et al.*, 2013) should be tested at larger scales to demonstrate their robustness and accuracy over orchards of varying types and conditions.

When acquiring hyperspectral imagery, large amounts of data are obtained and calculated from each single tree, therefore the analysis is complex and different approaches can be used to obtain satisfactory results (Sankaran *et al.*, 2010). In this study, large hyperspectral (50 cm) and thermal (62 cm) mosaics were obtained (ca. 3,000 hectares) comprising a total of 130 fields in order to test different methods for the successful detection among VW severity levels using two different supervised classification approaches: linear and non-linear classification methods. On the one hand, linear classification tries to find linear functions that separate the observations into the different classes. Several linear classification methods have been used to successfully classify remote sensing data for disease detection, such as linear discriminant analysis (LDA) (Delwiche and Kim, 2000), principal component analysis (PCA) (Qin *et al.*, 2008) and logistic regression analysis (LRA) (Delalieux *et al.*, 2007). For the data analyzed in this study, we selected LDA rather than LRA because LDA is a more powerful and efficient analytic strategy when the assumptions of multivariate normality of the independent variables within each class are met, the dependent variable has more than two groups and not all classes have large sample size (Grimm and Yarnold, 1995). Moreover, LDA is superior to PCA in classifying remote sensing data because PCA changes the shape and location of the original data when transformed to a different space whereas LDA only tries to provide more class separability and draw a decision region between the given classes (Balakrishnama and Ganapathiraju, 1998). The classification criterion of LDA (Fisher, 1936) is based on the pooled covariance matrix yielding a linear function and each observation is placed in the class from which it has the smallest generalized squared distance. On the other hand, when classes are not separable by linear boundary, non-linear classification methods are more appropiate. For disease detection from remote sensing data, artificial neural networks (NN) (Moshou *et al.*, 2004) and support vector machines (SVM) (Rumpf *et al.*, 2010) have been the most used non-linear classification methods. SVM methods have been selected in this study because of the

superior performance shown, particularly with respect to the classification of hyperspectral remote sensing data (Camp-Valls *et al.*, 2004). The advantages of SVM over NN (Zanaty, 2012) are: i) the solution achieved by SVM is global and unique due to quadratic programming; ii) computational complexity of SVM does not depend on the dimensionality of the input space so it is usually much quicker for large data sets; iii) SVM is less prone to overfitting; iv) SVM has few parameters to consider; and v) has good generalization capability with few training samples. SVM is based on statistical learning theory (Vapnik, 1998) which aims determine a hyperplane that optimally separates two classes. The optimum hyperplane works in the manner that maximizes the margin between classes.

This study describes an automatic procedure to classify VW infection and severity in olive growing areas with a special focus on the early detection to design focalized VW control strategies at large scale. Because VW is related to several physiological modifications which are reflected in spectral changes, a method based on the combination of various vegetation indices calculated from high-resolution hyperspectral and thermal imagery was applied using LDA and SVM classification methods to fully exploit their combined information.

5.2. Material and Methods

5.2.1. Study site description

The study site is located in Écija (Seville province, southern Spain) (37º 40’ 46’’N, 4º 59’ 41’’ W) and consisted of a 3,000-ha commercial olive area (Fig. 5.1). Within this area several olive orchards were selected differing in soil and crop management characteristics that are shown in Table 5.1 and Figure 5.1. All plots were drip-irrigated.

The climate of the area is Mediterranean characterized by warm and dry summers and cool and wet winters with an average annual rainfall of 550 mm, concentrated from autumn to spring climate (De León *et al.*, 1989).

Table 5.1. Agronomic characteristics of olive plots assessed in this study.

Plot	Olive cultivar	Plant age (years)	Plant density (trees per ha.)	Soil management
1	Picual	30	204	Non tillage
2	Hojiblanca	20	204	Tillage
3	Picual	20	204	Tillage
4	Hojiblanca	15	204	Tillage
5	Picual	20	204	Tillage
6	Picual	15	357	Tillage
7	Hojiblanca	30	123	Non tillage
8	Picual	20	204	Tillage
9	Picual	30	204	Non tillage

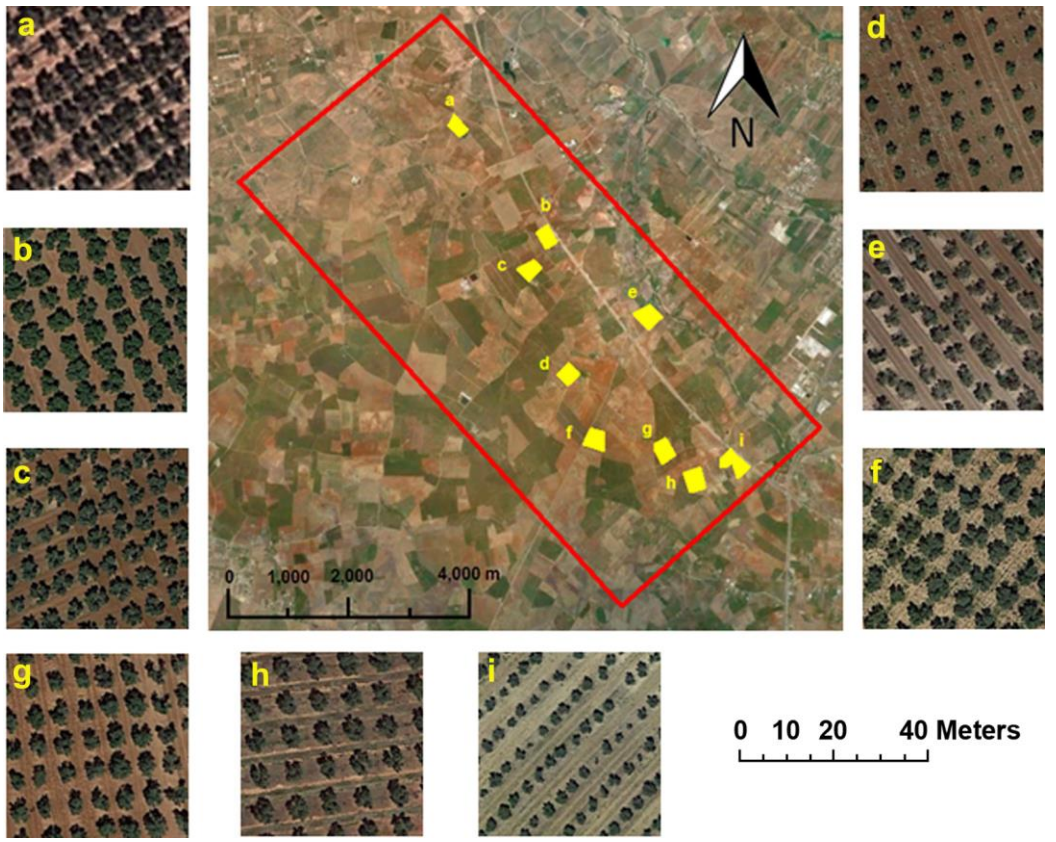

Figure 5.1. Overview of the olive area flown with the manned platform located in Écija (Seville province). Verticillium wilt severity was assessed in the plots which are shown in yellow. High-resolution detail of each individual olive plot assessed in this study was shown with lettering (a-i) in agreement with the plot lettering (a-i) in central image. Note differences in soil and crop management among plots.

5.2.2. Verticillium wilt assessment

Incidence and severity of VW symptoms were assessed in the summer of 2013 in nine selected plots spatially distributed throughout the study site, collecting data for 5,352 olive trees. Disease severity (DS) was assessed by visual inspection of every tree for foliar symptoms and assessment on a 0 to 4 rating scale according to the percentage of foliage with disease symptoms, where: 0 = 0%, 0.2 and 0.5 = initial symptoms, 1 = 1 to 33%, 2 = 34 to 66%, 3 =67 to 100%, and 4 = dead plant (Calderón *et al.*, 2013). These VW severity levels were then regrouped in five VW severity classes: asymptomatic (DS = 0), initial ($0.2 \leq DS \leq 0.5$), low ($1 \leq DS \leq 1.5$), moderate ($2 \leq DS \leq 2.5$) and severe ($3 \leq DS \leq 4$) symptoms (Figure 5.2). *V. dahliae* infection was confirmed by isolating six stem fragments sampled from each of four young symptomatic branches per symptomatic tree as previously described (Navas-Cortés *et al.*, 2008). Identification of *V. dahliae* isolates was based on the morphology of conidiophores and microsclerotia and confirmed by molecular typing through PCR assay using primers DB19/DB22/espdef01 (Mercado-Blanco *et al.*, 2003). This method yielded a polymorphic amplicon of 523 or 539 bp specific to *V. dahliae*. PCR amplification and gel electrophoresis were conducted as previously described (Mercado-Blanco *et al.*, 2003).

5.2.3. Airborne hyperspectral and thermal imagery acquisition

Imagery was acquired from the whole study site on 12 June 2013 using a hyperspectral sensor and a broad-band thermal camera on board a Cessna aircraft operated by the Laboratory for Research Methods in Quantitative Remote Sensing of the Consejo Superior de Investigaciones Científicas (QuantaLab, IAS-CSIC, Spain). Both cameras were flown at 500 m above ground level (AGL). Hyperspectral and thermal images were acquired between 10:30 and 12:00 GMT at 50 cm and 62 cm pixel resolution, respectively.

The hyperspectral sensor flown was the visible and near-infrared (VNIR) micro-hyperspectral imager (Micro-Hyperspec VNIR model, Headwall Photonics, MA, USA) configured in the spectral mode of 260 bands at 1.85 nm/pixel and 12-bit radiometric resolution. It yielded a 6.4 nm full-width at half-maximum (FWHM) with a 25-micron slit in the 400-885 nm region. Data acquisition and storage rate on board the manned platform was set to 50 fps (frames per second) with 18-ms integration time. The 8-mm optical focal length lens yielded an instantaneous field of view (IFOV) of 0.93 mrad and an angular field of view (FOV) of 49.82°.

Radiometric calibration and atmospheric correction methods were applied to the imagery to calculate the spectral reflectance, as described Zarco-Tejada *et al.* (2012). The

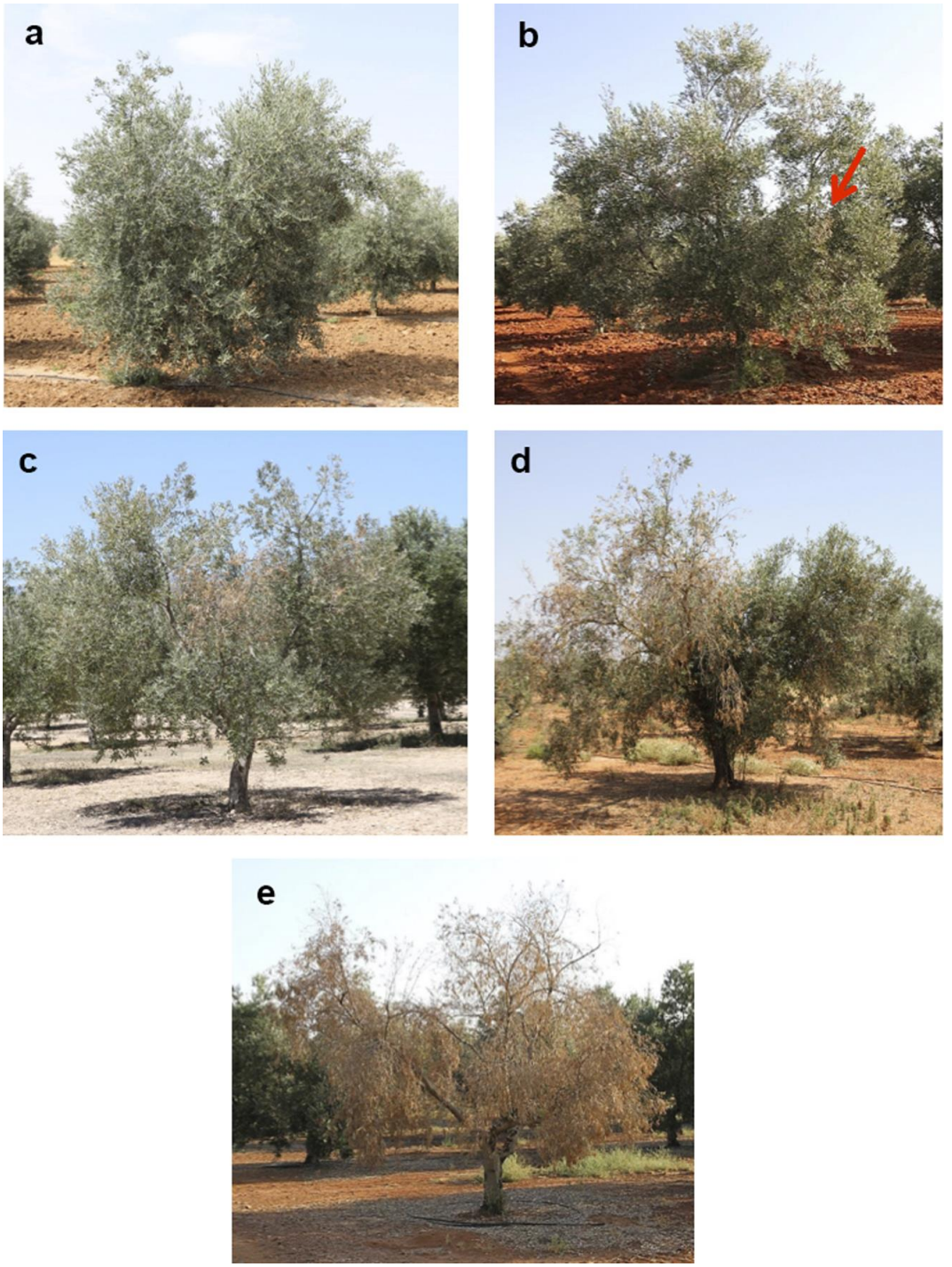

Figure 5.2. RGB images showing olive trees with the five different Verticillium wilt severity classes: (a) asymptomatic, (b) initial, (c) low, (d) moderate and (e) severe disease symptoms.

hyperspectral images were radiometrically calibrated in the laboratory using derived coefficients with a uniform light source system (integrating sphere, CSTM-USS-2000C Uniform Source System, LabSphere, North Sutton, NH, USA) at four levels of illumination and six integration times. Radiance values were converted to reflectance using total incoming irradiance simulated with SMARTS model (Gueymard, 1995, 2001) and aerosol optical depth measured at 550 nm with Micro-Tops II sunphotometer (Solar LIGHT Co., Philadelphia, PA, USA) at the study site at the time of the flight (Berni *et al.*, 2009a,b). This model has been previously used in other studies to perform the atmospheric correction of hyperspectral imagery, such as in Zarco-Tejada *et al.* (2012) and Calderón *et al.* (2013).

Bidirectional reflectance effects are prominent for airborne sensors operating with wide FOV (e.g., in this study the FOV of hyperspectral sensor was 49.82º). Effects are most pronounced in the angular range higher than ±30º from nadir (Beisl, 2001). To minimize directional effects, the flight was conducted in the solar plane, trying to keep the assessed olive orchards as close as possible to the nadir within angular range ±30º from nadir. Hyperspectral reflectance from each training tree was acquired within a range in view angle between -21.6º and +18.6º from nadir. These data ensured that training trees were not affected by off-nadir pixels acquired on each single frame. Ranges in view angles between training trees from the same olive orchard were between 9.3º and 31.4º range. Moreover, due to the large along- and cross-track overlap achieved during the flight (>70%), the resulting hyperspectral mosaic was not affected by pixels falling on the edge of the imagery.

Ortho-rectification of the hyperspectral imagery was conducted using PARGE (ReSe Applications Schläpfer, Wil, Switzerland). This was done using input data acquired with a miniaturized inertial measuring unit (IMU) (MTiG model, Xsens, The Netherlands) installed on-board and synchronized with the micro-hyperspectral imager. The mean radiance and reflectance spectra calculated from the 260 spectral bands obtained by the hyperspectral imager were used to calculate several narrow-band hyperspectral indices in agreement to the study conducted by Calderón *et al.* (2013), where their ability to detect Verticillium wilt at early and/or advanced stage of disease development was demonstrated. The indices that contribute most to the model conducted in this study are shown in Table 5.2 with regard to: (i) tree crown structure; (ii) epoxidation state of the xanthophyll cycle; (iii) chlorophyll a+b concentration; (iv) blue/green/red ratio indices; (v) carotenoid concentration; (vi) chlorophyll fluorescence and (vii) spectral disease indices.

Table 5.2. Overview of the vegetation indices that contribute most to the model conducted in this study and their formulations.

Vegetation indices	Equation	Reference
Structural indices		
Normalized Difference Vegetation Index	$NDVI = (R_{800} - R_{670})/(R_{800} + R_{670})$	Rouse *et al.* (1974)
Renormalized Difference Vegetation Index	$RDVI = (R_{800} - R_{670})/\sqrt{(R_{800} + R_{670})}$	Rougean & Breon (1995)
Enhanced Vegetation Index	$EVI = 2.5 \cdot (R_{800} - R_{670})/(R_{800} + 6 \cdot R_{670} - 7.5 \cdot R_{400} + 1)$	Liu & Huete (1995)
Optimized Soil-Adjusted Vegetation Index	$OSAVI = ((1 + 0.16) \cdot (R_{800} - R_{670})/(R_{800} + R_{670} + 0.16))$	Rondeaux *et al.* (1996)
Triangular Vegetation Index	$TVI = 0.5 \cdot [120 \cdot (R_{750} - R_{550}) - 200 \cdot (R_{670} - R_{550})]$	Broge & Leblanc (2000)
Modified Triangular Vegetation Index	$MTVI = 1.2 \cdot [1.2 \cdot (R_{800} - R_{550}) - 2.5 \cdot (R_{670} - R_{550})]$	Haboudane *et al.* (2004)
Modified Simple Ratio	$MSR = \frac{R_{800}/R_{670} - 1}{(R_{800}/R_{670})^{0.5} + 1}$	Chen (1996)
Xanthophyll indices		
Photochemical Reflectance Index (570)	$PRI_{570} = (R_{570} - R_{531})/(R_{570} + R_{531})$	Gamon *et al.* (1992)
Chlorophyll a+b indices		
Vogelmann	$VOG1 = R_{740}/R_{720}$	Vogelmann *et al.* (1993)
Gitelson &Merzlyak indices	$GM1 = R_{750}/R_{550}$	Gitelson & Merzlyak (1997)
Pigment Specific Simple Ratio Chlorophyll b	$PSSRb = R_{800}/R_{650}$	Blackburn (1998)
Transformed Chlorophyll Absorption in Reflectance Index	$TCARI = 3 \cdot [(R_{700} - R_{670}) - 0.2 \cdot (R_{700} - R_{550}) \cdot (R_{700}/R_{670})]$	Haboudane *et al.* (2002)
Transformed Chlorophyll Absorption in Reflectance Index/ Optimized Soil-Adjusted Vegetation Index	$\frac{TCARI}{OSAVI} = \frac{3 \cdot [(R_{700} - R_{670}) - 0.2 \cdot (R_{700} - R_{550}) \cdot (R_{700}/R_{670})]}{((1 + 0.16) \cdot (R_{800} - R_{670})/(R_{800} + R_{670} + 0.16))}$	Haboudane *et al.* (2002)
R/G/B indices		
Redness index	$R = R_{700}/R_{670}$	Gitelson *et al.* (2000)
Blue/green indices	$BGI1 = R_{400}/R_{550}$	Zarco-Tejada *et al.* (2005)
Lichtenhaler index	$LIC3 = R_{440}/R_{740}$	Lichtenhaler *et al.* (1996)
Carotenoid indices		
Pigment Specific Simple Ratio Carotenoids	$PSSRc = R_{800}/R_{500}$	Blackburn (1998)
R_{515}/R_{570}	R_{515}/R_{570}	Zarco-Tejada *et al.* (2012)
R_{515}/R_{670}	R_{515}/R_{670}	Zarco-Tejada *et al.* (2012)
Fluorescence		
FLD	$FLD3\ (747; 762; 780)$	Plascyk (1975) Maier *et al.* (2003) Zarco-Tejada *et al.* (2005)
Plant disease index		
Healthy-index	$HI = \frac{R_{534} - R_{698}}{R_{534} + R_{698}} - \frac{1}{2} \cdot R_{704}$	Mahlein *et al.* (2013)

The Fraunhofer Line Depth (FLD) principle calculated from a total of three bands (FLD3) was applied to the hyperspectral radiance imagery to quantify the fluorescence signal as described by Zarco-Tejada *et al.* (2012). The bands required for the FLD3 method were the band inside de O_2-A feature (the "in" wavelength indicates the radiance at L762 nm) and the radiances at two wavelengths outside and on either side of the O_2-A feature, referred as the "out" bands (L750 and L780 nm). Previous studies demonstrated successful results in retrieving the chlorophyll fluorescence signal using the micro-hyperspectral imager due to the large spectral oversampling (1.85-nm sampling interval) and 6.4 nm bandwidths (Zarco-Tejada *et al.*, 2012, 2013; Calderón *et al.*, 2013).

The thermal camera (FLIR SC655, FLIR Systems, USA) delivered 640 x 480 pixel resolution and was equipped with a 24.5 mm f1.0 lens, connected to a computer via USB 2.0 protocol. This camera operates with a thermoelectric (TE) cooling stabilization, giving us high sensitivity below 50 mK. The spectral response was in the range of 7.5-13 μm. Radiometric calibration was conducted in the laboratory using a blackbody (model P80P, Land Instruments, Dronfield, UK) at varying target and ambient temperatures and through

vicarious calibrations using surface temperature measurements. Surface temperature was obtained applying atmospheric correction methods to thermal imager data based on MODTRAN radiative transfer code, which models the atmospheric transmissivity and longwave upwelling thermal radiation. Downwelling thermal radiation was measured in the field with a thermal sensor (LaserSight, Optris, Germany). Since only vegetation temperature is retrieved, surface emissivity is considered as 0.98 as an accepted value for natural vegetation (Berni *et al.*, 2009b). Local atmospheric conditions such as air temperature, relative humidity and barometric pressure were measured at the time of the flight with a portable weather station (Model WXT510, Vaisala, Finland) (Table 5.3) and used as input into MODTRAN model. Atmospheric correction methods conducted with single-band thermal cameras were shown to provide successful estimation of vegetation surface temperature (Berni *et al.*, 2009b). Canopy temperature (Tc), extracted from thermal imagery, minus air temperature (Ta) was calculated as a water stress indicator of olive trees (Tc − Ta).

Table 5.3. Local atmospheric conditions measured by a portable weather station during the flight at 30-min interval.

GMT time (h)	Air temperature (ºC)	Relative humidity (%)	Air VPD (KPa)	Wind speed (m/s)	Solar radiation (W/m^2)
10:30	32.4	27.3	3.5	0.7	989
11:00	33.0	26.9	3.7	0.6	984
11:30	33.3	27.8	3.7	0.8	967
12:00	33.8	24.9	4.0	0.9	938

Single tree crown temperature and reflectance were extracted from high-resolution thermal and hyperspectral imagery (Figure 5.3a; 5.4a), respectively, using an automated object-based method. Image segmentation was automatically conducted using Fiji package of ImageJ software (National Institutes of Health, Bethesda, USA, http://www.fiji.sc) to split the digital image into multiple regions that made possible to identify single pure tree crowns (Figure 5.3b; 5.4b). Algorithms developed at the QuantaLab/IAS-CSIC were applied afterwards using GRASS GIS software (GRASS Development Team, http://grass.osgeo.org/) to extract feature for each object, calculating temperature and reflectance's mean statistics of all the pixels composing each whole crown (Figure 5.3c; 5.4c).

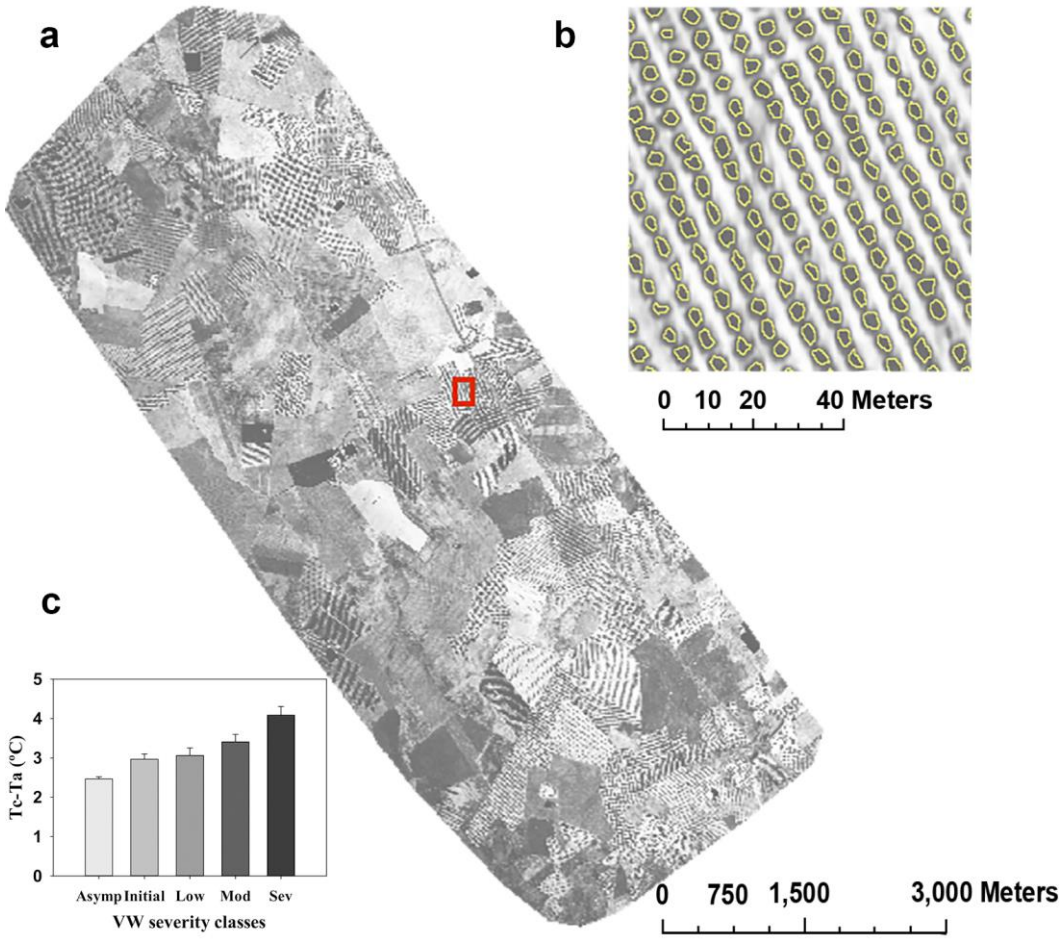

Figure 5.3. Thermal mosaic (a) obtained with the thermal camera on board the manned platform at 63-cm resolution, enabling pure olive crown identification (b). Pure olive crowns were identified using automatic object-based crown detection. Mean crown normalized temperature (Tc-Ta) calculated from thermal imagery is shown for every Verticillium wilt severity class in (c). Mean values of Tc-Ta were supported by the data of the 9 plots, consisting of 510, 98, 64, 46 and 38 olive trees which correspond to asymptomatic, initial, low, moderate and severe severity classes, respectively. Error bars indicate standard errors. Red square (a) is shown in detail in (b).

5.2.4. Data analyses

Multivariate analyses were used to develop models that detected VW infection and severity. The strength of association among normalized canopy temperature (Tc − Ta) and vegetation indices and the VW severity classes was assessed by LDA and SVM methods. Every olive tree assessed was designated with the presence of VW infection and severity of symptoms, as well as Tc − Ta and vegetation indices calculated from the thermal and hyperspectral imagery, respectively.

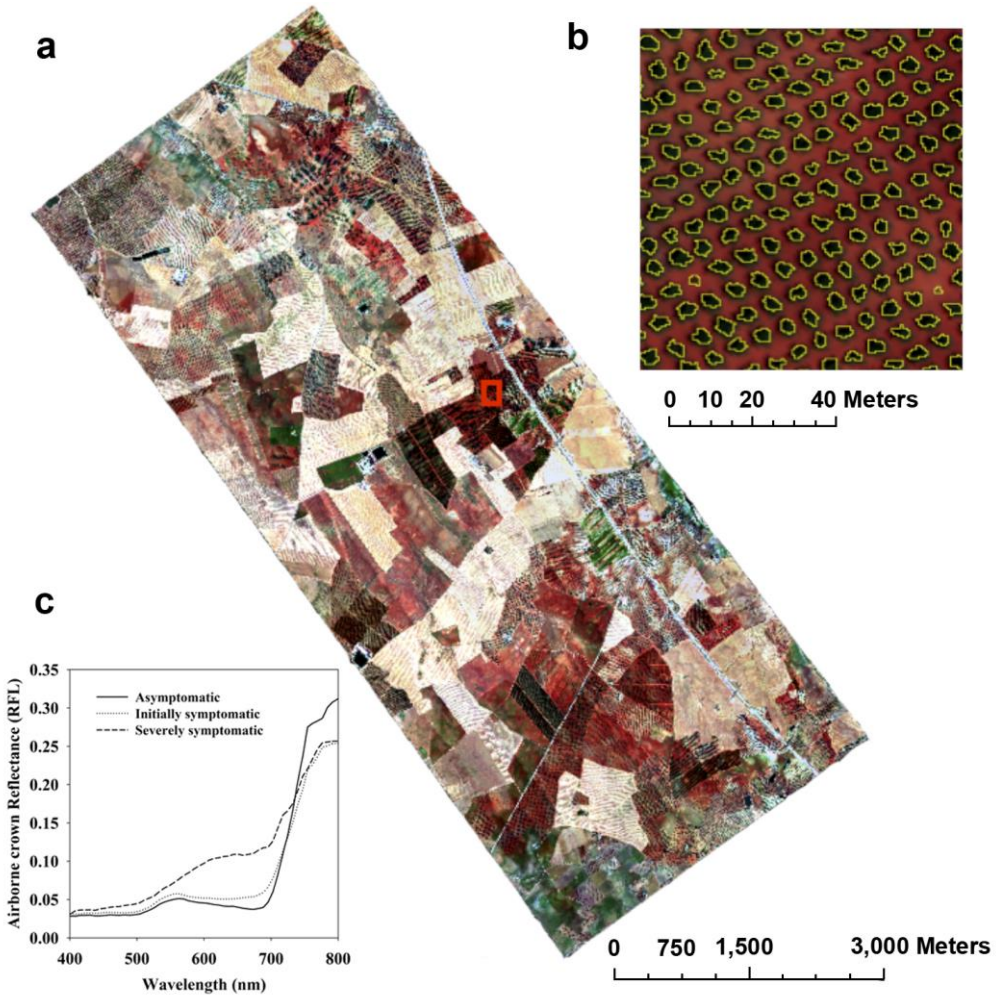

Figure 5.4. Hyperspectral mosaic (a) obtained with the hyperspectral sensor on board the manned platform at 50-cm resolution. Pure olive crowns were identified using automatic object-based crown detection (b). Sample crown reflectance obtained by the hyperspectral imagery from Verticillium wilt asymptomatic, initially symptomatic and severely symptomatic olive trees is shown in (c). Red square (a) is shown in detail in (b).

First, the STEPDISC procedure of SAS software (version 9.4; SAS Institute, Cary, NC, USA) was used to eliminate variables within the model that did not provide additional information or were redundant as determined by the Wilk's lambda method, as well as to add variables outside the model that contribute most to the model (Khattree and Naik, 2000). The DISCRIM procedure of SAS was then used to generate a discriminant function capable of determining the classification accuracy of the dataset, based on the pooled covariance matrix and the prior probabilities of the classification groups. Due to the fact that the data were not normally distributed, a non-parametric discriminant

analysis was conducted specifying a k-value for the k-nearest-neighbour rule. In this study we used a k-value of 4, so each observation is classified into a VW severity class focusing on the information from its four nearest neighbours. A dataset of 756 olive trees was created by randomly selecting the 10% of the asymptomatic trees and including all the trees belonged to the symptomatic VW severity classes. This set was used to run the STEPDISC selected model and then DISCRIM for classifying VW severity groups. Then the classification accuracy of the selected model was evaluated by calculating the overall accuracy value and the kappa (κ) coefficient, which gives an overall accuracy assessment for the classification based on commission and omission error for all classes. The data obtained from the stepwise analysis were further subjected to a canonical discriminant analysis using the CANDISC procedure of SAS to separate classification variables (VW severity classes) based on linear combinations of the quantitative variables (Tc − Ta and vegetation indices). The linear combinations of variables (canonical variates) were then correlated with the original VW severity classes. Canonical variates means (centroid values) were calculated for each classification variable and significance between means was determined using Mahalanobis distance (Khattree and Naik, 2000). Individual values for each canonical variate were plotted in a bi-plot for the first and second canonical variables and for the first and third ones.

SVM analysis calculations were conducted using R software, version 3.1.1 (R Foundation for Statistical Computing, http://www.R-project.org/) with the *e1071* (Meyer *et al.*, 2014) package which provides an interface to the open source machine learning library *libsvm* (Chang and Lin, 2014). For multiclass classification with k classes, *libsvm* uses the one-against-one approach, in which k(k-1)/2 binary classifiers are trained and the appropriate class is found by a voting scheme. SVM conducted non-linear classifications using kernel functions and introducing a cost parameter C to quantify the penalty of misclassification errors. The radial basis function kernel was used in this study because it has fewer parameter values to predefine and yet has been found at least as robust as other kernel types (Joachims, 1998; Huang *et al.*, 2002). As shown in the equation 1 of this kernel, the only parameter that needs to be predefined is γ:

$$K(x_i, x_j) = e^{-\gamma \cdot \|x_i - x_j\|^2} \quad [5.1]$$

In order to specify the best radial basis function and to find an appropriate factor for penalizing classification errors, the parameter C and γ have to be optimized. In this respect, we applied a grid search method using cross validation approach as recommended by Hsu *et al.* (2010). The main idea behind the grid search method is that different pairs of parameters are tested (C and γ in this case) and the one with the highest cross validation accuracy is selected.

5.3. Results

In the summer of 2013, 4.94% of the trees assessed at the field level were infected by VW, with a mean DS in symptomatic trees of 1.41 (0-4 rating scale). Taking account symptomatic trees, 40.08% showed initial DS symptoms, 25.92% had low DS symptoms, 18.62% had moderate DS symptoms and 15.38% of symptomatic trees had severe DS symptoms.

In the forward stepwise discriminant analysis 22 out of 34 indices were selected (Table 5.4). In this model, Tc − Ta and the indices calculated from the thermal and hyperspectral imagery, respectively, that contributed most (partial R-square > 0.05) to discriminate among VW severity classes were OSAVI, LIC3 and normalized canopy temperature (Tc − Ta), followed (partial R-square > 0.03 < 0.05) by GM1, R_{515}/R_{570}, PRI_{570}, red index (R) and TCARI/OSAVI. HI, FLD3, VOG, PSSRb and RDVI showed the lowest contribution (partial R-square < 0.015) to the discriminant function (Table 5.4). Use of LDA allowed classifying the sampled olive trees in a given VW severity class. 71.4%, 75.0%, 78.3% and 76.3% of the initial, low, moderate and severe VW affected trees were correctly classified, respectively (Table 5.5). Interestingly, all symptomatic trees were correctly classified and 55.5% of the asymptomatic plants that were considered symptomatic in the analysis were classified as plants with initial symptoms, the lowest severity class. Overall, the classification accuracy of the model was 59.0% (Table 5.5) and the κ value 0.487 (95% confident interval 0.437 – 0.536). The degree to which the five VW severity categories are separated is measured by the Mahalanobis distance between centroid values for each VW severity category (Table 5.6). As expected, all pairwise distances between the five VW severity categories were statistically significant ($P < 0.005$).

Tc − Ta and vegetation indices, that were part of the discriminant model shown in Table 5.4, were used in a canonical discriminant analysis. In this analysis, three canonical functions (variates) showing significant differences ($P < 0.0001$) among VW severity classes were created. The first canonical variate significantly accounted for 42.3% of the variation while the second and the third ones only accounted for 13.8% and 9.5% of the variation, respectively. The structural indices (i.e., OSAVI, RDVI, MTVI1 and MSR) dominated the three variates. In addition, the first canonical variate was also dominated by positive loadings from Tc − Ta, TCARI, GM1, PSSRb, PRI_{570}, R_{515}/R_{570} and HI and negative loadings from FLD3. In the second canonical variate positive loadings from PSSRb, VOG, TCARI/OSAVI, BGI1, LIC3 and R_{515}/R_{670} were found. The third canonical variate was dominated by positive loadings from PSSRc and negative loadings from GM1, PSSRb and R (Table 5.7). According to canonical loadings, the asymptomatic trees were detected mainly at low Tc − Ta, GM1, PSSRb, PRI_{570}, R_{515}/R_{570} and HI, and

Table 5.4. Variables selected from normalized canopy temperature (Tc-Ta) and vegetation indices in the forward stepwise discriminant analysis to determine the severity of *Verticillium dahliae* infection in olive trees.

Source	Wilks' Lambda	Partial R-square	*F* value	Pr > *F*	Pr <Lambda
OSAVI	0.833	0.1666	37.52	<0.0001	<0.0001
LIC3	0.718	0.1385	30.13	<0.0001	<0.0001
Tc-Ta	0.676	0.0585	11.63	<0.0001	<0.0001
GM1	0.586	0.0397	7.71	<0.0001	<0.0001
R_{515}/R_{570}	0.610	0.0375	7.26	<0.0001	<0.0001
PRI_{570}	0.565	0.0349	6.74	<0.0001	<0.0001
R	0.654	0.0321	6.20	<0.0001	<0.0001
TCARI/OSAVI	0.634	0.0304	5.86	0.0001	<0.0001
EVI	0.501	0.0295	5.61	0.0002	<0.0001
TCARI	0.549	0.0289	5.52	0.0002	<0.0001
MTVI1	0.464	0.0288	5.43	0.0003	<0.0001
R_{515}/R_{670}	0.455	0.0200	3.73	0.0051	<0.0001
NDVI	0.516	0.0198	3.73	0.0052	<0.0001
BGI1	0.483	0.0191	3.58	0.0066	<0.0001
PSSRc	0.447	0.0183	3.42	0.0088	<0.0001
TVI	0.492	0.0165	3.08	0.0156	<0.0001
MSR	0.435	0.0156	2.90	0.0213	<0.0001
HI	0.534	0.0148	2.77	0.0262	<0.0001
FLD3	0.526	0.0143	2.68	0.0310	<0.0001
VOG	0.542	0.0132	2.49	0.0421	<0.0001
PSSRb	0.442	0.0103	1.91	0.1067	<0.0001
RDVI	0.478	0.0098	1.81	0.1250	<0.0001

Table 5.5. Confusion matrix for Verticillium wilt severity classes using the linear discriminant classification based on the indices selected by the forward stepwise discriminant analysis.

	Ground truth					
Prediction	Asymptomatic	Initial	Low	Moderate	Severe	*Class precision*
Asymptomatic	263	0	0	0	0	100%
Initial	137	70	5	1	1	32.7%
Low	48	15	48	2	4	41.0%
Moderate	37	6	6	36	4	40.5%
Severe	25	7	5	7	29	76.3%
Class recall	51.6%	71.4%	75.0%	78.3%	76.3%	59.0%

high structural indices and FLD3 values. As the VW severity increased, the values of Tc − Ta, TCARI, GM1, PSSRb, PRI_{570}, R_{515}/R_{570} and HI were higher, and structural indices and FLD3 were lower. Furthermore, the ranges of the indices values became higher as the VW severity level increased. In contrast, blue/green/red indices (BGI1, R and LIC3), chlorophyll (TCARI/OSAVI and VOG) and carotenoid indices (R_{515}/R_{670} and PSSRc) were not able to detect differences among asymptomatic, initial and low severity levels but could discriminate among asymptomatic, moderate and severe levels (Figure 5.5).

Table 5.6. Squared Mahalanobis distances for Verticillium wilt severity classes obtained in a forward stepwise discriminant analysis.

	Squared Mahalanobis distance				
VW severity class	Asymptomatic	Initial	Low	Moderate	Severe
Asymptomatic	-	3.102	7.032	9.704	18.410
Initial	3.102	-	2.385	5.545	11.067
Low	7.032	2.385	-	3.614	8.761
Moderate	9.704	5.545	3.614	-	5.569
Severe	18.410	11.067	8.761	5.569	-

	F values				
VW severity class	Asymptomatic	Initial	Low	Moderate	Severe
Asymptomatic	-	3.102***	7.032***	9.704***	18.410***
Initial	3.102***	-	2.385**	5.545***	11.067***
Low	7.032***	2.385**	-	3.614***	8.761***
Moderate	9.704***	5.545***	3.614***	-	5.570***
Severe	18.410***	11.067***	8.761***	5.570***	-

** $P < 0.0005$
*** $P < 0.0001$

SVM classification was also conducted for the differentiation among VW severity classes using the vegetation indices selected in the forward stepwise discriminant analysis showed in Table 5.4. Table 5.8 summarizes the results of the SVM model, which classified every olive tree assessed at field level in a given VW severity class. The overall classification accuracy was 79.2% and the κ value 0.495 (95% confident interval 0.433 – 0.557), that was slightly higher than that obtained by LDA. 99.4% of asymptomatic trees were correctly classified in the asymptomatic class and the 14.3%, 40.6%, 67.4% and 55.3% of the initial, low, moderate and high severity infected VW trees were correctly classified, respectively. In contrast to LDA results, SVM was very effective in correctly

identifying asymptomatic trees but showed lower power to identify symptomatic trees. Mostly, this classification method failed in separating between plants infected at early stages of VW development. Thus, 63.2% and 56.3% of trees showing initial or low VW severity were considered as asymptomatic (Table 5.8). The maps generated in Figure 5.6 represent the spatial pattern of VW severity classes assessed at field level and the severity classes predicted by LDA and SVM. Such maps showed an overestimation of VW symptomatic classes by LDA while SVM revealed an underestimation of these classes.

Table 5.7. Standardized canonical coefficients (SCCs) and correlation coefficients (CCCs) of discriminant canonical functions of canopy normalized canopy temperature (Tc-Ta) and vegetation indices selected by the forward stepwise discriminant analysis that determine Verticillium wilt severity levels.

	SCCs			**CCCs**		
Source	**Variate 1**	**Variate 2**	**Variate 3**	**Variate 1**	**Variate 2**	**Variate 3**
OSAVI	-5.773	23.593	-14.241	-0.614	-0.050	0.270
LIC3	-0.262	0.775	0.206	-0.585	-0.090	-0.297
Tc-Ta	0.384	0.214	0.118	0.471	0.032	0.089
GM1	3.326	-0.100	-6.922	-0.565	-0.143	0.164
R_{515}/R_{570}	1.282	-0.022	0.009	0.339	-0.059	-0.001
PRI_{570}	1.149	1.137	0.035	0.342	0.080	0.142
R	1.083	0.760	-2.353	0.324	0.187	0.166
TCARI/OSAVI	-0.736	1.567	-0.348	-0.274	0.360	0.119
EVI	-3.119	-9.210	-2.857	-0.584	-0.072	0.256
TCARI	2.036	-1.356	1.153	-0.459	0.163	0.142
MTVI1	-6.244	9.113	-14.574	-0.559	-0.016	0.285
R_{515}/R_{670}	-0.961	2.189	1.139	-0.327	-0.009	-0.100
NDVI	-1.867	-3.687	1.187	-0.618	-0.054	0.196
BGI1	0.230	0.824	0.470	-0.054	-0.010	-0.150
PSSRc	-1.626	0.499	7.490	-0.396	-0.126	0.260
TVI	-1.418	1.260	5.868	-0.527	0.044	0.319
MSR	-6.167	-9.539	0.776	-0.530	-0.111	0.130
HI	3.354	-1.410	1.030	-0.471	-0.024	-0.146
FLD3	-0.340	-0.271	0.262	-0.379	-0.156	0.137
VOG	-1.017	1.486	-0.067	-0.598	-0.084	0.143
PSSRb	4.601	6.268	-2.450	-0.496	-0.145	0.116
RDVI	15.945	-18.906	24.147	-0.592	-0.049	0.317

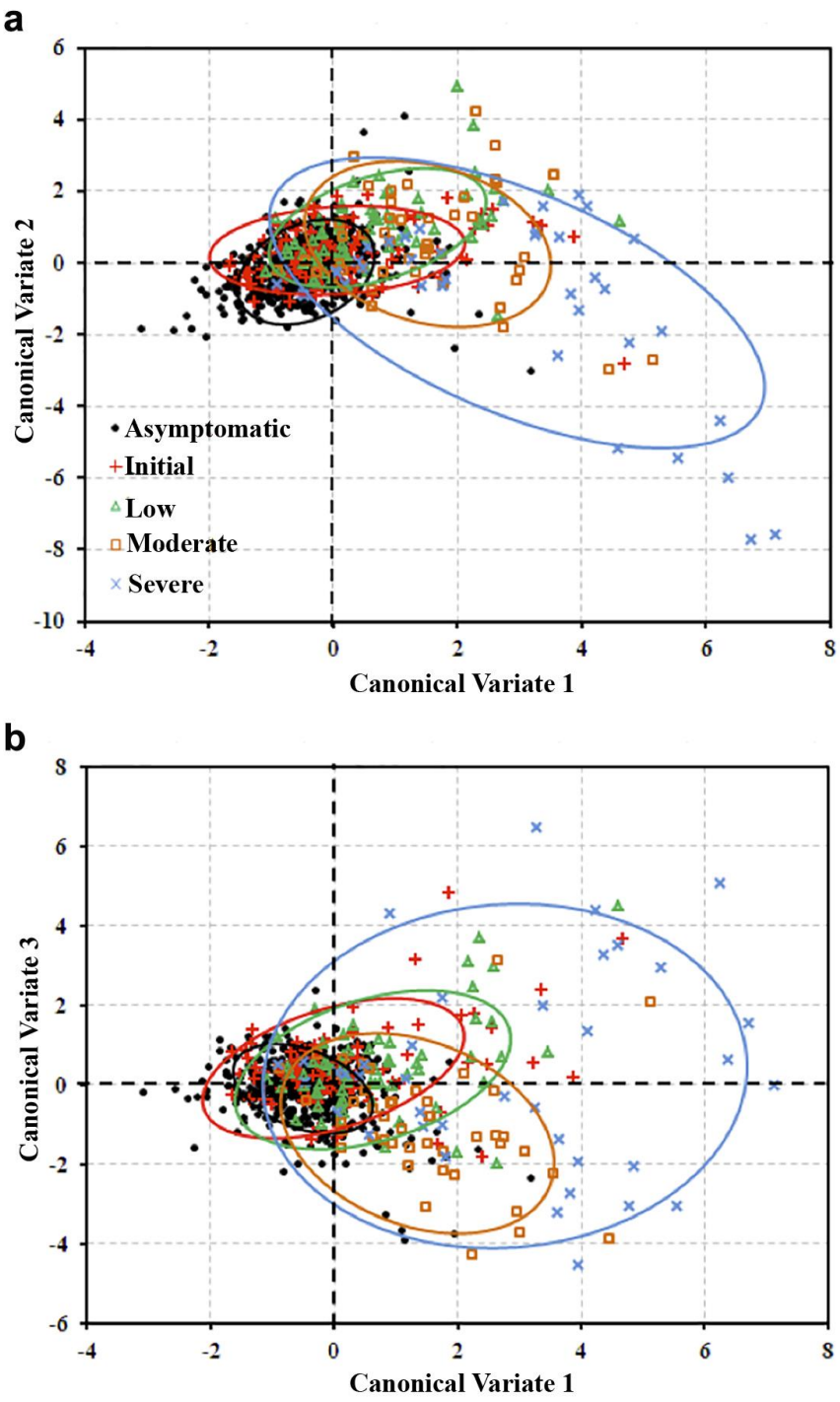

Figure 5.5. Classification of 756 olive trees assessed in Ecija into five Verticillium wilt severity classes based on (a) the first and second canonical variates and (b) the first and third canonical variates, from the canonical discriminant analysis.

Table 5.8. Confusion matrix for Verticillium wilt severity classes using the support vector machine classification based on the indices selected by the forward stepwise discriminant analysis.

	Ground truth					
Prediction	Asymptomatic	Initial	Low	Moderate	Severe	*Class precision*
Asymptomatic	507	79	36	15	11	78.2%
Initial	0	14	1	0	0	93.3%
Low	3	3	26	0	3	74.3%
Moderate	0	2	1	31	3	83.8%
Severe	0	0	0	0	21	100%
Class recall	99.4%	14.3%	40.6%	67.4%	55.3%	79.2%

Table 5.9. Overall accuracy and kappa obtained from the linear discriminant analysis (LDA) and the support vector machine (SVM) classification methods to detect Verticillium wilt severity levels for the individual olive plots assessed and for the all the plots together.

	LDA		**SVM**	
Plot	**Overall accuracy**	**Kappa**	**Overall accuracy**	**Kappa**
1	0.600	0.486	0.862	0.712
2	0.796	0.761	0.880	0.788
3	0.684	0.543	0.785	0.230
4	0.753	0.766	0.685	0.538
5	0.600	0.382	0.825	0.250
6	0.732	0.593	0.902	0.787
7	0.600	0.523	0.911	0.785
8	0.829	0.808	0.927	0.798
9	0.613	0.415	0.793	0.555
All plots	0.590	0.487	0.792	0.495

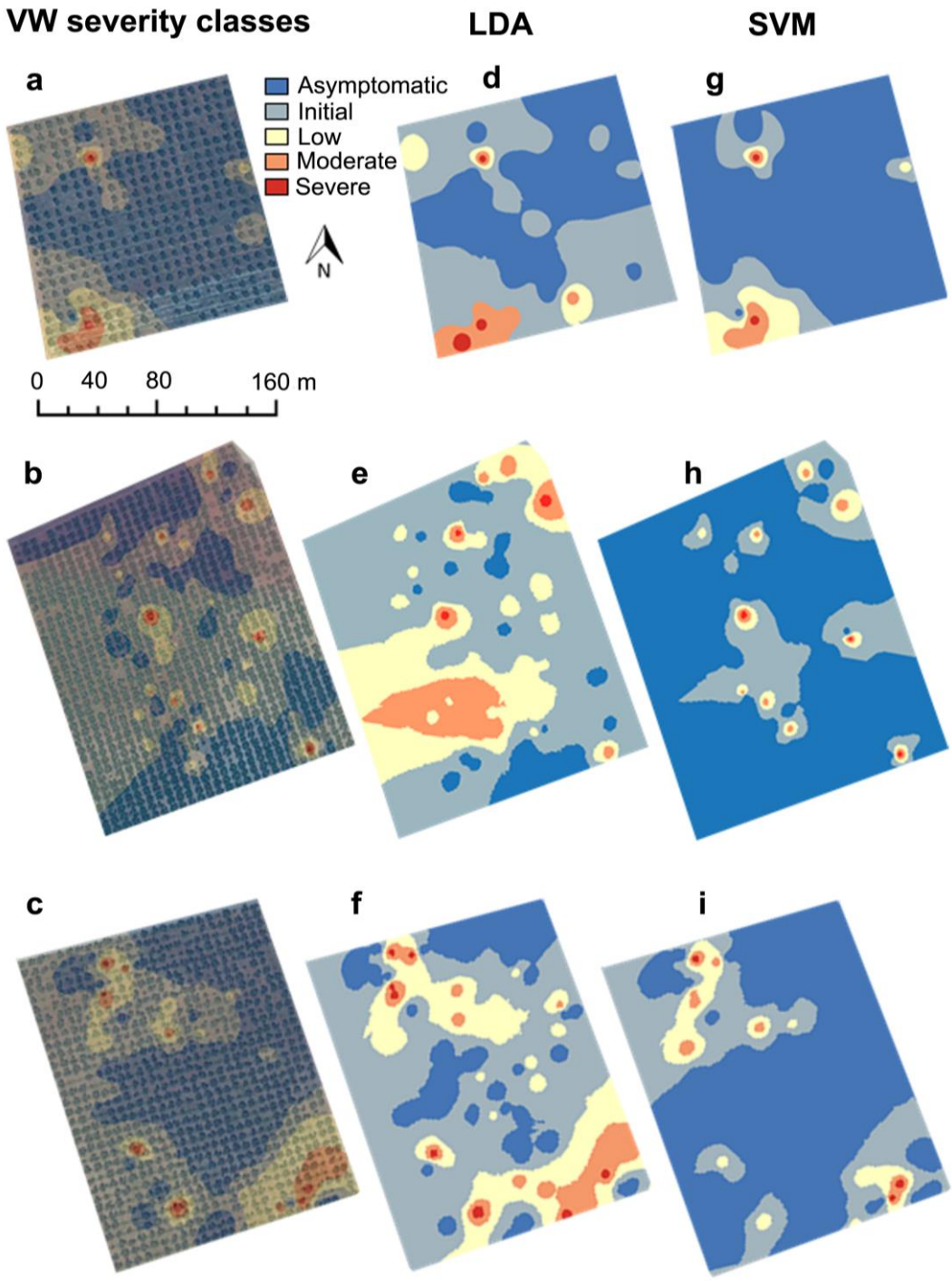

Figure 5.6. Spatial distribution of Verticillium wilt severity classes assessed at field level (a, d, g) and the severity classes predicted by the linear discriminant analysis (LDA) (b, e, h) and support vector machine (SVM) methods (c, f, i) in three different plots.

When analyzing the different plots separately, LDA model reached classification accuracies between 60.0% and 82.9% and κ ranging from 0.382 to 0.808 (Table 5.9). On the other hand, SVM model showed better classification accuracies between 68.5% and 92.7% and slightly lower κ ranging from 0.230 to 0.798. Applying the forward stepwise discriminant analysis to each plot separately, the indices which contributed most to discriminate among VW severity classes for the global model were selected in the majority of plots. Interestingly, Tc − Ta, was selected in all plots, R in seven plots and TCARI/OSAVI in six plots. In addition, structural indices were selected in no more than three plots in contrast to the high discrimination power showed in the global model (Table 5.10).

Table 5.10. Variables selected in the forward stepwise discriminant analysis to distinguish among Verticillium wilt severity levels for each individual plot assessed.

	Plot								
Source	1	2	3	4	5	6	7	8	9
OSAVI		X		X					
LIC3	X	X				X		X	X
Tc-Ta	X	X	X	X	X	X	X	X	X
GM1		X	X			X			X
R_{515}/R_{570}		X		X		X	X	X	
PRI_{570}				X					
R		X		X	X	X	X	X	X
TCARI/OSAVI	X	X	X	X		X		X	
EVI	X	X			X				
TCARI				X				X	X
MTVI1									
R_{515}/R_{670}				X					
NDVI		X	X					X	
BGI1		X	X						
PSSRc			X	X					
TVI		X		X					
MSR									
HI			X	X				X	
FLD3		X		X			X	X	X
VOG		X				X			
PSSRb		X		X					
RDVI		X							

5.4. Discussion

Remote sensing has been demonstrated to be a useful decision support system for crop management (Sankaran *et al.*, 2010; Mahlein *et al.*, 2012). In combination with powerful data analysis methods, remote sensing becomes an essential tool for integrated disease management. In particular, the detection of olive trees infected by *V. dahliae* would be of importance for the management of VW, particularly at early stages of *V. dahliae* infection. The early detection of *V. dahliae* infection would help to avoid the spread of the pathogen to new areas, especially if they are free of *V. dahliae*, and to improve the use of available control measures (Tjamos, 1993; Navas-Cortés *et al.*, 2008; Jiménez-Díaz *et al.*, 2012). A recent study has demonstrated early detection of VW using high-resolution thermal and hyperspectral imagery in two commercial olive orchards (Calderón *et al.*, 2013). *V. dahliae* penetrates into the plant roots, blocking water flow and reducing the transpiration rate which induced the stomata closure. Consequently, evaporative cooling is reduced and canopy temperature increases. Moreover, the reduction in photosynthesis caused by *V. dahliae* infection leads to an increase of the dissipation of energy by fluorescence. Considering these changes, several studies showed the feasibility of VW detection of olive trees at leaf and local scale even before characteristic disease symptoms were visible using normalized temperature, chlorophyll content, chlorophyll fluorescence and blue B/BG/BR indices (Calderón *et al.*, 2013, 2014). However, to our knowledge no studies have explored the robustness of these methods using narrow-band indices and thermal imagery for the early detection of VW in larger olive growing areas (i.e. thousands of hectares) characterized by large differences in crop age, tree-crown size, olive cultivars, crop managements and classes of disease severity. Therefore, the main objective of this study was to develop a robust and accurate method to detect the stress caused by *V. dahliae* infection and severity in olive growing areas to design localized VW control strategies at large scale.

In our study, thermal and hyperspectral imagery were obtained from the study area, obtaining the data for each individual tree of normalized canopy temperature (Tc − Ta,) and 260 spectral bands. As the number of spectral bands increases, the analysis of the data becomes more limited and complex so a dimensional reduction is required without losing important information (Chang, 2013). Thus, the calculation of vegetation indices results in a reduction of the data dimension, which may be also useful in effective data analysis for disease discrimination (Sankaran *et al.*, 2010). Since vegetation indices commonly used in remote sensing of vegetation are disease-specific indices, in this study we used the indices that Calderón *et al.* (2013) proved to be good indicators of VW at early and advanced stages of disease development. Then, these indices were introduced in a forward stepwise discriminant analysis to select the ones contributing the most to the discriminatory power among VW severity classes, so that the spectral dimensionality was

further reduced. Results of this work demonstrates that Tc − Ta,, structural (OSAVI, MTVI1, NDVI, TVI, MSR and RDVI), chlorophyll (GM1, TCARI/OSAVI, TCARI, VOG and PSSRb), carotenoid (PSSRc), blue/green BGI1, blue/red LIC3, FLD3 and HI indices were robust VW indicators in agreement with Calderón *et al.* (2013). However, chlorophyll indices (ZM (Zarco-Tejada *et al.*, 2001), GM2 (Gitelson and Merzlyak, 1997), PSSRa (Blackburn, 1998), mCAI (Laudien *et al.*, 2003)), SIPI (Peñuelas *et al.*, 1995), PRI_{515} (Hernández-Clemente *et al.*, 2011), blue (B) (Calderón *et al.*, 2013) and the blue/red ratios BR1 and BR2 (Zarco-Tejada *et al.*, 2012) were not good indicators in the present study, demonstrating to be influenced by the variation of agronomic characteristics within large olive areas. By contrast, indices that were not robust in Calderon *et al.* (2013), such as PRI_{570}, red (R), R_{515}/R_{570}, R_{515}/R_{670}, were demonstrated to be useful for VW detection in this study. At large scale, these indices may work better detecting VW at advanced stages where crown structural and density changes due to disease stress are more differentiated as the variation in agronomic characteristics within the study area is bigger. When applying the forward stepwise discriminant analysis to individual plots, the indices selected in the analysis including all plots demonstrated their robustness for each plot analyzed separately, with the exception of structural indices. The non-inclusion of structural indices by the stepwise discriminant analysis may be due to the lower within plot variability on crown structure and density according to the presence of fewer differences on agronomic characteristics.

In remote sensing for plant disease detection, different classification methods have been used in order to maximize information obtained from imagery. In this study, two different supervised classification methods were used for data analysis, the LDA and the non-linear SVM methods. Both classification methods have shown good results for detecting plant diseases at small scale (Delwiche and Kim, 2000; Naidu *et al.*, 2009; Rumpf *et al.*, 2010; Römer *et al.*, 2011) but to our knowledge have not been used previously for the detection of plant diseases at large scale, such as the one of this study. For the whole dataset, LDA reached an overall accuracy of 59.0% and a κ of 0.487 while SVM showed a higher overall accuracy, 79.2%, and a slightly higher κ, 0.495. LDA correctly classified the 51.6% of the asymptomatic trees while SVM classified the 99.4%. However, LDA was more efficient in classifying the trees at initial and low VW severity levels, reaching accuracies of 71.4 and 75.0%, respectively, in comparison with the 14.3 and 40.6% obtained by SVM. Both classification methods showed an increase of the class accuracy (class recall) as the VW severity level increased. It is due to the higher differences found in Tc − Ta, and vegetation indices values with the increase in VW severity level when is compared to the asymptomatic class (Calderón *et al.*, 2013). When considering individual olive orchards, the overall classification accuracy reached by both classification methods were generally higher than that attained with the whole dataset.

The lower within plot variability on agronomic characteristics could be responsible for this effect. In addition, SVM obtained higher overall accuracies and κ than LDA.

Recently, there has been growing interest in exploring the potential of SVM for early detection of plant diseases. Thus, Rumpf *et al.* (2010) used this approach to discriminate between healthy sugar beet leaves from that infected with various foliar pathogens that included *Cercospora beticola*, *Uromyces beate* and *Erysiphe betae* at early stages of pathogenesis based on hyperspectral data. Similarly, Römer *et al.* (2011) detected wheat leaf rust at a pre-symptomatic stage using UV-light induced fluorescence data analysed by SVM classification methods. Nevertheless, in our study, although SVM reached the highest overall accuracy, LDA classified olive trees better at the initial and low VW severity levels with accuracies of 71.4% and 75.0%, respectively, in comparison with the 14.3% and 40.6% obtained by SVM. After LDA, a canonical discriminant analysis was conducted to reduce the dimensionality of the variables included in the model. Thus, three canonical variates were derived accounting for 42.3%, 13.8% and 9.5% of the variation, respectively. The first canonical variate allowed the discrimination between the asymptomatic and symptomatic VW severity classes, particularly at the initial and low levels. This variate was dominated by Tc − Ta,, structural indices (RDVI, MTVI1, MSR, OSAVI and EVI), PRI_{570}, FLD3, HI, chlorophyll (TCARI, GM1, PSSRb) and carotenoid (R_{515}/R_{570}) indices, whose value ranges increased as the severity level increased. The second and third canonical variates were able to distinguish between asymptomatic and VW severity levels at advanced stages of disease development. These variates were dominated by the blue/green/red (BGI1, R and LIC3), structural (OSAVI, RDVI, NDVI, EVI, TVI, RDVI, MTVI1 and MSR), chlorophyll (TCARI/OSAVI, PSSRb, GM1 and VOG) and carotenoid indices (R_{515}/R_{670} and PSSRc).

Canopy temperature has proven to be useful to detect root impairment caused by *V. dahliae* in several studies. Nilsson (1995) reported that oilseed rape plants infected with *V. dahliae* showed leaf temperatures 5-8ºC higher than non-infected plants. In addition, normalized leaf and canopy temperature were identified as early indicators of *V. dahliae* infection in olive trees (Calderón *et al.*, 2013, 2014), showing up to 2ºC higher in VW infected trees. Hyperspectral reflectance differences were also demonstrated to identify VW in cotton and olive crops. Chen *et al.* (2008, 2011) confirmed that the spectral characteristics of cotton infected plants changed gradually with the increase in the visible region with disease severity, while a reduction occurred in the near-infrared region. Moreover, results obtained in this study at canopy level confirmed those obtained at leaf level under controlled conditions by Calderón *et al.* (2013), who identified SPAD readings (chlorophyll content) and chlorophyll fluorescence as early VW indicators. In addition, these results were also in agreement with the study carried out by Calderón *et al.* (2013) at canopy level in two olive commercial orchards, proving the potential for early detection of *V. dahliae* infection in olive crops using hyperspectral imagery acquired with

an unmanned aerial vehicle. In that study, FLD3, B, BGI1 and BRI1 were determined as VW indicators at initial stages of disease development. Moreover, Calderón *et al.* (2013) proved structural, chlorophyll, carotenoid and HI indices to be good VW indicators at advanced stages of disease development. In conclusion, Tc − Ta, calculated from thermal imagery and chlorophyll fluorescence estimated with the FLD3 in-filling retrieval method from the hyperspectral imagery allowed identifying olive trees at the early stages of disease development as much at orchard scale as at larger scale. Thus, the use of Tc − Ta, and FLD3 as early indicators of Verticillium wilt is not influenced by the variation of agronomic characteristics within the study area. However, it is not the case for blue/blue-green/blue-red (B, BG1 and BR1) ratios which were found good indicators of Verticillium wilt at initial and low severity levels at orchard scale but only detected moderate and advanced severity levels at larger scale. Structural, xanthophyll, chlorophyll, carotenoid and disease indices and green/red ratios calculated from hyperspectral imagery proved to be good indicators to detect the presence of moderate to severe damage caused by Verticillium wilt as much at orchard scale as at larger scale.

5.5. Conclusions

In the present study, a procedure to develop a robust and accurate method for the automatic classification of *V. dahliae* infection and severity using remote sensing was assessed at large scale. This study completed the one conducted by Calderón *et al.* (2013) at orchard scale, extrapolating the methods to larger areas comprising several olive orchards differing in soil and crop management characteristics. High-resolution imagery was acquired with a thermal and a hyperspectral camera installed on board a manned platform which flew a 3,000-ha commercial olive area. We calculated narrowband hyperspectral indices and normalized canopy temperature (Tc − Ta,) from the hyperspectral and thermal imagery and used linear discriminant analysis (LDA) and support vector machine (SVM) methods to discriminate among VW severity classes exploiting the combined information of these indices and Tc − Ta,. For the whole dataset, LDA reached an overall accuracy of 59.0% and a κ of 0.487 while SVM obtained a higher overall accuracy, 79.2%, and a similar κ, 0.495. However, LDA classified better the trees at initial and low severity levels, reaching accuracies of 71.4% and 75.0%, respectively, in comparison with the 14.3% and 40.6% obtained by SVM. Tc − Ta,, structural indices (RDVI, MTVI1, MSR, OSAVI and EVI), PRI_{570}, FLD3, HI, chlorophyll (TCARI, GM1, PSSRb) and carotenoid (R_{515}/R_{570}) indices detected VW at early and advanced stages of disease development, while the structural (NDVI and TVI), blue/green/red (BGI1, R and LIC3), chlorophyll (TCARI/OSAVI and VOG) and carotenoid indices (R_{515}/R_{670} and PSSRc) were good indicators of VW at advanced stages. Comparing with the results obtained by Calderón *et al.* (2013), Tc − Ta, and FLD3 allowed identifying olive trees at

the early stages of disease development as much at orchard scale as at larger scale, being not influenced by the variation of agronomic characteristics within the study area. Structural, xanthophyll, chlorophyll, carotenoid and disease indices and blue/green/red ratios proved to be good indicators to detect the presence of moderate to severe damage caused by VW. These results demonstrate that the methods developed at orchard scale are validated for flights in large areas consisting of olive orchards with different characteristics.

Acknowledgments

Financial support for this research was provided by Project P08-AGR-03528 from ‘‘Consejería de Economía, Innovación y Ciencia’’ of Junta de Andalucía and the European Social Fund, and projects AGL-2012-37521 and AGL2012-40053-C03-01 from the Spanish ‘‘Ministerio de Economía y Competitividad’’ and the European Social Fund. R. Calderón is a recipient of research fellowship BES-2010-035511 from the Spanish ‘‘Ministerio de Ciencia e Innovación’’. D. Notario, A. Vera, A. Hornero, A. Gómez and R. Romero are acknowledged for their support during the airborne campaign and the image processing. G. León-Ropero is acknowledged for his technical support in Verticillium wilt assessments.

Author Contributions

Conceived and designed the experiments: R.C., J.A.N.C. and P.J.Z.T. Performed the experiments: R.C., J.A.N.C. and P.J.Z.T. Analyzed the data: R.C., J.A.N.C. and P.J.Z.T. Contributed reagents/materials/analysis tools: J.A.N.C. and P.J.Z.T. Wrote the paper: R.C., J.A.N.C. and P.J.Z.T.

References

Balakrishnama, S., & Ganapathiraju, A. (1998). *Linear Discriminant Analysis - A Brief Tutorial*. Mississippi, MS, USA: Institute for Signal and Information Processing, Department of Electrical and Computer Engineering, Mississippi State University.

Beisl, U. (2001). *Correction of Bidirectional Effects in Imaging Spectrometer Data*, Remote Sensing Series No. 37. Zurich, Switzerland: Remote Sensing Laboratories.

Berni, J.A.J., Zarco-Tejada, P.J., Sepulcre-Cantó, G., Fereres, E., & Villalobos, F.J. (2009a). Mapping canopy conductance and CWSI in olive orchards using high resolution thermal remote sensing imagery. *Remote Sens. Environ.* 113:2380-2388.

Berni, J.A.J., Zarco-Tejada, P.J., Suárez, L., & Fereres, E. (2009b). Thermal and narrow-band multispectral remote sensing for vegetation monitoring from an unmanned aerial vehicle. *IEEE T. Geosci. Remote.* 47:722-738.

Blackburn, G.A. (1998). Spectral indices for estimating photosynthetic pigment concentrations: a test using senescent tree leaves. *Int. J. Remote Sens.* 19(4):657-675.

Broge, N.H., & Leblanc, E. (2000). Comparing prediction power and stability of broadband and hyperspectral vegetation indices for estimation of green leaf area index and canopy chlorophyll density. *Remote Sens. Environ*. 76:156-172.

Calderón, R., Lucena, C., Trapero-Casas, J.L., Zarco-Tejada, P.J., & Navas-Cortés, J.A. (2014). Soil Temperature Determines the Reaction of Olive Cultivars to *Verticillium dahliae* Pathotypes. *PLoS ONE* 9(10):e110664. doi:10.1371/journal.pone.0110664

Calderón, R., Navas-Cortés, J.A., Lucena, C., & Zarco-Tejada, P.J. (2013). High-resolution airborne hyperspectral and thermal imagery for early detection of *Verticillium* wilt of olive using fluorescence, temperature and narrow-band spectral indices. *Remote Sens. Environ.* 139:231-245.

Camps-Valls, G., Gomez-Chova, L., Calpe-Maravilla, J., Martin-Guerrero, J.D., Soria-Olivas, E., Alonso-Chorda, L., & Moreno, J. (2004). Robust support vector method for hyperspectral data classification and knowledge discovery. *IEEE T. Geosci. Remote* 42 (7):1530-1542.

Chang, C.C., & Lin, C.J. (2014). LIBSVM: A Library for Support Vector Machines. http://www.csie.ntu.edu.tw/~cjlin/libsvm/

Chang, C.-I. (2013). *Data Dimensionality Reduction, in Hyperspectral Data Processing: Algorithm Design and Analysis*. Hoboken, NJ, USA: John Wiley & Sons, Inc.

Chen, B., Li, S., Wang, K., Zhou, G., & Bai, J. (2011). Evaluating the severity level of cotton Verticillium using spectral signature analysis. *Int. J. Remote Sens.* 33:2706-2724.

Chen, B., Li, S.K., Wang, K.R., Wang, J., Wang, F.Y., *et al.* (2008). Spectrum characteristics of cotton canopy infected with Verticillium wilt and applications. *Agric. Sci. China* 7:561-569.

Chen, J. (1996). Evaluation of vegetation indices and modified simple ratio for boreal applications. *Can. J. Remote Sens.* 22:229-242.

De León, A., Arriba, A., & De La Plaza, M.C. (1989). *Caracterización agroclimática de la provincia de SEVILLA*. Madrid, Spain: Ministerio de Agricultura, Pesca y Alimentación.

Delalieux, S., van Aardt, J., Keulemans, W., Schrevens, E., & Coppin, P. (2007). Detection of biotic stress (*Venturia inaequalis*) in apple trees using hyperspectral data: Non-parametric statistical approaches and physiological implications. *Eur. J. Agron.* 27(1):130-143.

Delwiche, S.R., & Kim, M.S. (2000). Hyperspectral imaging for detection of scab in wheat. In *Proceedings SPIE* Vol. 4203, Biological Quality and Precision Agriculture II (pp. 13-20), Boston, MA, USA, December 2000.

FAOSTAT (2012). The Statistical Database (FAOSTAT), Rome. http://faostat.fao.org/

Fisher, R.A. (1936). The Use of Multiple Measurements in Taxonomic Problems. *Ann. Eugenic.* 7:179-188.

Gamon, J.A., Peñuelas, J., & Field, C.B. (1992). A narrow-wave band spectral index that tracks diurnal changes in photosynthetic efficiency. *Remote Sens. Environ.* 41:35-44.

Gitelson, A.A., & Merzlyak, M.N. (1997). Signature analysis of leaf reflectance spectra: Algorithm development for remote sensing of chlorophyll. *Int. J. Remote Sens.* 18:2691-2697.

Gitelson, A.A., Yacobi, Y.Z., Schalles, J.F., Rundquist, D.C., Han, L., Stark, R., & Etzion, D. (2000). Remote estimation of phytoplankton density in productive waters. *Archives in Hydrobiology - Special Issues in Advances in Limnology* 55:121-136.

Grimm, L.G., & Yarnold, P.R. (Eds.) (1995). *Reading and understanding multivariate statistics*. Washington, DC, USA: American Psychological Association.

Gueymard, C.A. (1995). SMARTS, a simple model of the atmospheric radiative transfer of sunshine: Algorithms and performance assessment. *Technical report no. FSEC-PF-270-95*. Cocoa, FL, USA: Florida Solar Energy Center.

Gueymard, C.A. (2001). Parameterized transmittance model for direct beam and circumsolar spectral irradiance. *Sol. Energy* 71:325-346.

Haboudane, D., Miller, J.R., Pattey, E., Zarco-Tejada, P.J., & Strachan, I. (2004). Hyperspectral vegetation indices and novel algorithms for predicting green LAI of crop canopies: Modeling and validation in the context of precision agriculture. *Remote Sens. Environ.* 90(3):337-352.

Haboudane, D., Miller, J.R., Tremblay, N., Zarco-Tejada, P.J., & Dextraze, L. (2002). Integrated narrow-band vegetation indices for prediction of crop chlorophyll content for application to precision agriculture. *Remote Sens. Environ.* 84:416-426.

Hernández-Clemente, R., Navarro-Cerrillo, R.M., Suárez, L., Morales, F., & Zarco-Tejada, P.J. (2011). Assessing structural effects on PRI for stress detection in conifer forests. *Remote Sens. Environ.* 115:2360-2375.

Hillnhütter, C., Schweizer, A., Kühnhold, V., & Sikora, R.A. (2010). Remote sensing for the detection of soil-borne plant parasitic nematodes and fungal pathogens. In Oerke, E.-C., Gerhards, R., Menz, G., & Sikora, R.A. (Eds.), *Precision Crop Protection – the Challenge and Use of Heterogeneity* (pp.151-165). New York, NY, USA: Springer.

Hsu, C.W., Chang, C.C., & Lin, C.J. (2010). A practical guide to support vector classification. http://www.csie.ntu.edu.tw/~cjlin/papers/guide/guide.pdf

Huang, C., Davis, L.S., & Townshend, J.R.G. (2002). An assessment of support vector machines for land cover classification. *Int. J. Remote Sens.* 23:725-749.

Jiménez-Díaz, R.M., Cirulli, M., Bubici, G., Jiménez-Gasco, L.M., Antoniou, P.P., & Tjamos, E.C. (2012). Verticillium wilt, a major threat to olive production: Current status and future prospects for its management. *Plant Dis.* 96: 304-329.

Jiménez-Díaz, R.M., Olivares-García, C., Landa, B.B., Jiménez-Gasco, M.M., & Navas-Cortés, J.A. (2011). A region-wide analysis of genetic diversity in *Verticillium dahliae* infecting olive in southern Spain and agricultural factors influencing the distribution and prevalence of vegetative compatibility groups and pathotypes. *Phytopathology* 101:304-315.

Joachims, T. (1998). Text Categorization with Support Vector Machines: Learning with Many Relevant Features. In Nédellec, C., & Rouveirol, C. (Eds.), *Machine Learning: ECML 1998* (vol. 1398; pp. 137-142). Heidelberg, Germany: Springer.

Khattree, R., & Naik, D.N. (2000). *Multivariate Data Reduction and Discrimination with SAS Software*. Cary, NC, USA: SAS Institute Inc.

Laudien, R., Bareth, G., & Doluschitz, R. (2003). Analysis of hyperspectral field data for detection of sugar beet diseases. In *Proceedings of the EFITA Conference* (pp. 375-381), Debrecen, Hungary, July 2003.

Lichtenhaler, H.K., Lang, M., Sowinska, M., Heisel, F., & Mieh, J.A. (1996). Detection of vegetation stress via a new high resolution fluorescence imaging system. *J. Plant Physiol.* 148:599-612.

Liu, H.Q., & Huete, A.R. (1995). A feedback based modification of the NDVI to minimize canopy background and atmospheric noise. *IEEE T. Geosci. Remote* 33:457-465.

Mahlein, A.-K., Oerke, E.-C., Steiner, U., & Dehne, H.-W. (2012). Recent advances in sensing plant diseases for precision crop protection. *Eur. J. Plant Pathol.* 133:197-209.

Mahlein, A.-K., Rumpf, T., Welke, P., Dehne, H.-W., Plümer, L., Steiner., U., & Oerke, E.-C. (2013). Development of spectral indices for detecting and identifying plant diseases. *Remote Sens. Environ.* 128:21-30.

Maier, S.W., Günther, K.P., & Stellmes, M. (2003). Sun-Induced Fluorescence: A New Tool for Precision Farming. In McDonald, M., Schepers, J., Tartly, L., van Toai, T., & Major, D. (Eds.), *Digital Imaging and Spectral Techniques: Applications to Precision Agriculture and Crop Physiology* (pp. 209-222). Madison, WI, USA: American Society of Agronomy.

Mercado-Blanco, J., Rodríguez-Jurado, D., Parrilla-Araujo, S., & Jiménez-Díaz, R.M. (2003). Simultaneous detection of the defoliating and nondefoliating *Verticillium dahliae* pathotypes in infected olive plants by duplex, nested polymerase chain reaction. *Plant Dis.* 87:1487-1494.

Meyer, D., Dimitriadou, E., Hornik, K., Weingessel, A., Leisch, F., Chang, C. C., & Lin, C. C. (2014). *Misc Functions of the Department of Statistics (e1071)*, TU Wien. R package version 1.6-4.

Moshou, D., Bravo, C., West, J., Wahlen, S., McCartney, A., & Ramon, H. (2004). Automatic detection of 'yellow rust' in wheat using reflectance measurements and neural networks. *Comput. Electron. Agr.* 44(3):173-188.

Naidu, R.A., Perry, E.M., Pierce, F.J., & Mekuria, T. (2009). The potential of spectral reflectance technique for the detection of Grapevine leafroll-associated virus-3 in two red- berried wine grape cultivars. *Comput. Electron. Agr.* 66:38-45.

Navas-Cortés, J.A., Landa, B.B., Mercado-Blanco, J., Trapero-Casas, J.L., Rodríguez-Jurado, D., & Jiménez-Díaz, R.M. (2008). Spatiotemporal analysis of spread of infections by *Verticillium dahliae* pathotypes within a high tree density olive orchard in southern Spain. *Phytopathology* 98:167-180.

Nilsson, H.E. (1995). Remote sensing and image analysis in plant pathology. *Annu. Rev. Phytopathol.* 15:489-527.

Peñuelas, J., Baret, F., & Filella, I. (1995). Semi-empirical indices to assess carotenoids/chlorophyll a ratio from leaf spectral reflectance. *Photosynthetica* 31:221-230.

Plascyk, J.A. (1975). MK II Fraunhofer Line Dicsriminator (FLD-II) for airborne and orbital remote sensing of solar-stimulated luminescence. *Opt. Eng.* 14(4):339-346.

Qin, J., Burks, T.F., Kim, M.S., Chao, K., & Ritenour, M.A. (2008). Citrus canker detection using hyperspectral reflectance imaging and PCA-based image classification method. *Sens, Instrum. Food Qual. Saf.* 2:168-177.

Römer, C., Bürling, K., Hunsche, M., Rumpf, T., Noga, G., & Plümer, L. (2011). Robust fitting of fluorescence spectra for pre-symptomatic wheat leaf rust detection with Support Vector Machines. *Comput. Electron. Agr.* 79:180-188.

Rondeaux, G., Steven, M., & Baret, F. (1996). Optimization of soil-adjusted vegetation indices. *Remote Sens. Environ.* 55:95-107.

Rougean, J.-L., & Breon, F.M. (1995). Estimating PAR absorbed by vegetation from bidirectional reflectance measurements. *Remote Sens. Environ.* 51:375-384.

Rouse, J.W., Haas, R.H., Schell, J.A., Deering, D.W., & Harlan, J.C. (1974). Monitoring the vernal advancement and retrogradation (greenwave effect) of natural vegetation, *NASA/GSFC Type III Final Report*. Greenbelt, MD, USA: College Station Texas A and M University.

Rumpf, T., Mahlein, A.-K., Steiner, U., Oerke, E.-C., & Plümer, L. (2010). Early detection and classification of plant diseases with support vector machines based on hyperspectral reflectance. *Comput. Electron. Agric.* 74(1):91-99.

Sankaran, S., Mishra, A., Ehsani, R., & Davis, C. (2010). A review of advanced techniques for detecting plant diseases. *Comput. Electron. Agric.* 72:1-13.

Steiner, U., Buerling, K., & Oerke, E.-C. (2008). Sensor use in plant protection. *Gesunde Pflanz.* 60(4):131-141.

Tjamos, E.C. (1993). Prospects and strategies in controlling Verticillium wilt of olive. In *Bulletin OEPP/EPPO Bulletin 23* (pp. 505-512).

Tjamos, E.C., & Jiménez Díaz, R.M. (1998). Management of disease. In Hiemstra, J.A., & Harris, D.C. (Eds.), *A Compendium of Verticillium Wilt in Tree Species* (pp. 55-57). Wageningen, the Netherlands: Posen and Looijen.

Van Alfen, N.K. (1989). Reassessment of plant wilt toxins. *Annu. Rev. Phytopathol.* 27:533-550.

Vapnik, V. (1998). *Statistical Learning Theory*. New York, NY, USA: Wiley-Interscience.

Villalobos, F.J., Testi, L., Hidalgo, J., Pastor, M., & Orgaz, F. (2006). Modelling potential growth and yield of olive (*Olea europaea* L.) canopies. *Eur. J. Agron.* 24:296-303.

Vogelmann, J.E., Rock, B.N., & Moss, D.M. (1993). Red edge spectral measurements from sugar maple leaves. *Int. J. Remote Sens.* 14:1563-1575.

Zanaty, E.A. (2012). Support Vector Machines (SVMs) versus Multilayer Perception (MLP) in data classification. *Egypt. Informatics J.* 13(3):177-183.

Zarco-Tejada, P.J., Berjón, A., López-Lozano, R., Miller, J.R., Marin, P., Cachorro, V., *et al.* (2005). Assessing vineyard condition with hyperspectral indices: Leaf and

canopy reflectance simulation in a row-structured discontinuous canopy. *Remote Sens. Environ.*, 99:271-287.

Zarco-Tejada, P.J., Catalina, A., González, M.R., & Martín, P. (2013). Relationships between net photosynthesis and steady-state chlorophyll fluorescence retrieved from airborne hyperspectral imagery. *Remote Sens. Environ.* 136:247-258.

Zarco-Tejada, P.J., González-Dugo, V., & Berni, J.A.J. (2012). Fluorescence, temperature and narrow-band indices acquired from a UAV for water stress detection using a hyperspectral imager and a thermal camera. *Remote Sens. Environ.* 117:322-337.

Zarco-Tejada, P.J., Miller, J.R., Mohammed, G.H., Notlamd, T.L.L., & Sampson, P.H. (2001). Scaling-up and model inversion methods with narrow-band optical indices for chlorophyll content estimation in closed forest canopies with hyperspectral data. *IEEE T. Geosci. Remote* 39:1491-1507.

CHAPTER 6

CONCLUSIONS

CHAPTER 6: CONCLUSIONS

6.1. Conclusions of the Research Published Papers

From the Research Article: Calderón, R., Lucena, C., Trapero-Casas, J. L., Zarco-Tejada, P. J., & Navas-Cortés, J. A. (2014). **Soil Temperature Determines the Reaction of Olive Cultivars to *Verticillium dahliae* Pathotypes.** *PLoS ONE* 9(10):e110664.

I. Verticillium wilt development in olive plants infected by the D pathotype was faster and more severe on cv. Picual than on cv. Arbequina. Cv. Picual plants were more susceptible to the D than to the ND pathotype.

II. The optimal soil temperature range for the D pathotype development was 16 to 24ºC for cv. Picual and 20 to 24ºC for cv. Arbequina. For the ND pathotype, a range of 16 to 20ºC was estimated as the most favorable for infection. Soil temperatures higher than 28ºC showed a drastic reduction of Verticillium wilt symptom development.

III. Stress-related parameters measured at leaf level (temperature, steady-state chlorophyll fluorescence Fs, Photochemical Reflectance Index PRI, chlorophyll content and ethylene production) were able to detect the physiological stress caused by *V. dahliae* infection and severity in olive plants, applying a multinomial logistic regression analysis and a tree classification which correctly classified 73.40 and 76.60% of the cases, respectively.

IV. Chlorophyll content, Fs and leaf temperature were identified as the best indicators to detect Verticillium wilt at early stages of disease development, while ethylene production and PRI were good indicators to detect Verticillium wilt at advanced stages.

From the Research Article: Calderón, R., Navas-Cortés, J. A., Lucena, C., & Zarco-Tejada, P. J. (2013). **High-resolution airborne hyperspectral and thermal imagery for early detection of Verticillium wilt of olive using fluorescence, temperature and narrow-band spectral indices.** *Remote Sensing of Environment* 139:231-245.

V. High-resolution thermal, multispectral and hyperspectral imagery acquired with an unmanned aerial vehicle (UAV) demonstrated its potential for the early detection of *V. dahliae* infection and discrimination among Verticillium wilt severity levels at orchard scale.

VI. Field measurements at leaf and crown-level validated the results obtained from imagery, confirming that these results are due to the stress caused by Verticillium

wilt and not simply influences by structural effects driven by the water stress induced by *V. dahliae* infection. The reduction in transpiration and stomatal conductance caused by Verticillium wilt was associated with significant increases ($P < 0.05$) in leaf PRI and crown temperature and a decrease in leaf Fs.

VII. Canopy temperature and Crop Water Stress Index (CWSI) calculated from the thermal imagery and blue/blue-green/blue-red (B, BG1 and BR1) ratios and chlorophyll fluorescence (FLD3) calculated from the hyperspectral imagery were identified as the best indicators to detect Verticillium wilt at early stages of disease development. Structural indices (i.e., NDVI), PRI, disease index (HI), chlorophyll and carotenoid indices and the red/green ratios calculated from hyperspectral imagery were good indicators to detect the presence of moderate to severe damage caused by Verticillium wilt.

From the Research Article: Calderón, R., Navas-Cortés, J. A., & Zarco-Tejada, P. J. (2015). **Early detection and quantification of Verticillium wilt in olive using hyperspectral and thermal imagery over large areas.** *Remote Sensing* 7(5):5584-5610.

VIII. The study conducted in the previous Research Article at orchard scale was validated over larger olive areas which comprise several olive orchards differing in soil and crop management characteristics.

IX. Linear discriminant analysis (LDA) and support vector machine (SVM) methods were applied for the automatic classification of *V. dahliae* infection and severity in large olive areas. LDA reached an overall accuracy of 59.00% and a κ of 0.487 while SVM obtained a higher overall accuracy, 79.20%, and a similar κ, 0.495.

X. LDA classified better the trees at initial and low severity levels, reaching accuracies of 71.42 and 75.00%, respectively, in comparison with the 14.29 and 40.63% obtained by SVM.

XI. When considering individual olive orchards, the overall classification accuracies reached by LDA and SVM were higher than those attained with the whole dataset due to the lower within variability on agronomic characteristics.

XII. Canopy temperature, structural indices (RDVI, MTVI1, MSR, OSAVI and EVI), PRI, FLD3, HI, chlorophyll (TCARI, GM1, PSSRb) and carotenoid (R_{515}/R_{570}) indices detected Verticillium wilt at early and advanced stages of disease development, while the structural (NDVI and TVI), blue/green/red (BGI1, R and LIC3), chlorophyll (TCARI/OSAVI and VOG) and carotenoid indices (R_{515}/R_{670} and PSSRc) were good indicators of Verticillium wilt only at advanced stages.

6.2. General Conclusions

I. The optimal soil temperature range for the D pathotype development was 16 to 24ºC for cv. Picual and 20 to 24ºC for cv. Arbequina. For the ND pathotype, a range of 16 to 20ºC was estimated as the most favorable for infection. Soil temperatures higher than 28ºC showed a drastic reduction of Verticillium wilt symptom development. These results will be useful to better understand the differential geographic distribution of *V. dahliae* pathotypes and to assess the potential effect of climate change on the development of Verticillium wilt of olive under future climate change scenarios.

II. At leaf level, Verticillium wilt was associated with an increase of temperature and reflectance in the visible green region due to a drop in chlorophyll content and a decrease of Fs because of a reduction in photosynthesis rate, even from early stages of disease development. *V. dahliae* infection was also detected by an increase of ethylene production and PRI, but only at advanced stages of disease development.

III. Canopy temperature and physiological indices calculated from high-resolution thermal and hyperspectral imagery were able to detect the stress caused by *V. dahliae* infection in olive trees, with special focus on the early detection to design focalized Verticillium wilt control strategies at orchard and larger scale.

IV. Canopy temperature and CWSI calculated from thermal imagery and chlorophyll fluorescence estimated with the FLD3 *in-filling* retrieval method from the hyperspectral imagery allowed identifying olive trees at the early stages of disease development as much at orchard scale as at larger scale. Thus, the use of canopy temperature, CWSI and FLD3 as early indicators of Verticillium wilt are not influenced by the variation of agronomic and crop management characteristics within the study area. However, it is not the case for blue/blue-green/blue-red (B, BG1 and BR1) ratios which were found good indicators of Verticillium wilt at initial and low severity levels at orchard scale but only detected moderate and advanced severity levels at larger scale.

V. Structural, xanthophyll, chlorophyll, carotenoid and disease indices and green/red ratios calculated from hyperspectral imagery proved to be good indicators to detect the presence of moderate to severe damage caused by Verticillium wilt as much at orchard scale as at larger scale.

APPENDIX:

SCIENTIFIC PRODUCTION

APPENDIX: Scientific production

Other scientific contributions derived from this Doctoral Thesis are listed below

Peer reviewed publications in international journals

Calderón, R., Montes-Borrego, M., Landa, B.B., Navas-Cortés, J.A. & Zarco-Tejada, P.J. (2014). **Detection of downy mildew of opium poppy using high-resolution multispectral and thermal imagery acquired with an unmanned aerial vehicle**. *Precision Agriculture* 15(6):639-661.

Oral communications at conferences

Calderón, R., Navas-Cortés, J.A., Lucena, C. & Zarco-Tejada, P.J. (2013). **Teledetección aerotransportada hiperespectral y térmica de alta resolución para la detección temprana de Verticilosis en olivar usando fluorescencia, temperatura e índices espectrales**. In *XV Congreso de la Asociación Española de Teledetección* (pp. 414-417), INTA, Torrejón de Ardoz (Madrid), Spain, October 22-23, 2013. Madrid, Spain: Asociación Española de Teledetección.

Calderón, R., Navas-Cortés, J.A., Montes-Borrego, M., Landa, B.B., Lucena, C., & Zarco-Tejada, P.J. (2014). **Detection of Verticillium wilt of olive trees and downy mildew of opium poppy using hyperspectral and thermal UAV imagery**. In *European Geosciences Union General Assembly 2014*, Vienna, Austria, April 27 - May 4, 2014.

Calderón, R., Navas-Cortés, J.A., & Zarco-Tejada, P.J. (2014). **Early detection and quantification of Verticillium wilt in olive using UAV and manned platforms to acquire hyperspectral and thermal imagery at local and regional scale**. In *Proceedings of the 2nd International Conference on Robotics, Associated High-Technologies and Equipment for Agriculture and Forestry* (pp. 309-318), Madrid, Spain, May 21-23, 2014. Madrid, Spain: RHEA Consortium.

Calderón, R., Navas-Cortés, J.A., & Zarco-Tejada, P.J. (2014). **Early detection and quantification of Verticillium wilt in olive using hyperspectral and thermal imagery acquired by manned platforms at regional scale**. In *Programme and Abstract Book of the 4th International Symposium: Recent Advances in Quantitative Remote Sensing* (pp. 70-71), Torrent (Valencia), Spain, September 22-26, 2014. Valencia, Spain: University of Valencia.

Poster communications at conferences and courses

Calderón, R., Navas-Cortés, J.A., Lucena, C. & Zarco-Tejada, P.J. (2013). **High-resolution hyperspectral and thermal imagery acquired from UAV platforms for early detection of Verticillium wilt using fluorescence, temperature and narrow-band indices**. In *Proceedings of the Workshop on UAV-based Remote Sensing Methods for Monitoring Vegetation* (pp. 7-14), Cologne, Germany, September 9-10. Cologne, Germany: University of Cologne.

Calderón, R., Navas-Cortés, J.A., & Zarco-Tejada, P.J. (2014). **Soil temperature effects in Verticillium wilt development. Assessment using spectral indices and canopy temperature**. In *5th ESA Advanced Training Course on Land Remote Sensing 2014*, Valencia, Spain, September 8-12, 2014.